SECTION A

JOURNAL OF RESEARCH

of the NATIONAL BUREAU OF STANDARDS

JNBAAR 80A (1), 1-141 (Jan.-Feb. 1976)

U.S. DEPARTMENT OF COMMERCE / National Bureau of Standards

Physics and Chemistry

Journal of Research

of the

National Bureau of Standards

A. Physics and Chemistry

Jan.–Feb. • 1976

VOLUME • 80A

NUMBER • 1

Associate Editor: D. D. Wagman

Publication dates:
Feb. 1, Apr. 1, June 1, Aug. 1, Oct. 1, Dec. 1, 1976

J. Res. Nat. Bur. Stand. (U.S.), A

JOURNAL OF RESEARCH

The National Bureau of Standards Journal of Research reports research and development in the fields of activity shown at right. Also included from time to time are survey articles on topics closely related to the Bureau's scientific and technical program.

The Journal is published in two separate sections as follows:

A. Physics and Chemistry

Contains papers of interest primarily to scientists working in these fields. Issued six times a year. Annual subscription: domestic, $17.00; foreign, $21.25. Single copy, varies.

B. Mathematical Sciences

Presents studies and compilations designed mainly for the mathematician and the theoretical physicist. Issued quarterly. Annual subscription: domestic, $9.00; foreign, $11.25. Single copy, $2.25.

NATIONAL BUREAU OF STANDARDS

The National Bureau of Standards[1] was established by an act of Congress March 3, 1901. The Bureau's overall goal is to strengthen and advance the Nation's science and technology and facilitate their effective application for public benefit. To this end, the Bureau conducts research and provides: (1) a basis for the Nation's physical measurement system, (2) scientific and technological services for industry and government, (3) a technical basis for equity in trade, and (4) technical services to promote public safety. The Bureau consists of the Institute for Basic Standards, the Institute for Materials Research, the Institute for Applied Technology, the Institute for Computer Sciences and Technology, and the Office for Information Programs.

THE INSTITUTE FOR BASIC STANDARDS provides the central basis within the United States of a complete and consistent system of physical measurement; coordinates that system with measurement systems of other nations; and furnishes essential services leading to accurate and uniform physical measurements throughout the Nation's scientific community, industry, and commerce. The Institute consists of the Office of Measurement Services, the Office of Radiation Measurement and the following Center and divisions:

Applied Mathematics — Electricity — Mechanics — Heat — Optical Physics — Center for Radiation Research: Nuclear Sciences; Applied Radiation — Laboratory Astrophysics[2] — Cryogenics[2] — Electromagnetics[2] — Time and Frequency[2].

THE INSTITUTE FOR MATERIALS RESEARCH conducts materials research leading to improved methods of measurement, standards, and data on the properties of well-characterized materials needed by industry, commerce, educational institutions, and Government; provides advisory and research services to other Government agencies; and develops, produces, and distributes standard reference materials. The Institute consists of the Office of Standard Reference Materials, the Office of Air and Water Measurement, and the following divisions:

Analytical Chemistry — Polymers — Metallurgy — Inorganic Materials — Reactor Radiation — Physical Chemistry.

THE INSTITUTE FOR APPLIED TECHNOLOGY provides technical services to promote the use of available technology and to facilitate technological innovation in industry and Government; cooperates with public and private organizations leading to the development of technological standards (including mandatory safety standards), codes and methods of test; and provides technical advice and services to Government agencies upon request. The Institute consists of the following divisions and Centers:

Standards Application and Analysis — Electronic Technology — Center for Consumer Product Technology: Product Systems Analysis; Product Engineering — Center for Building Technology: Structures, Materials, and Life Safety; Building Environment; Technical Evaluation and Application — Center for Fire Research: Fire Science; Fire Safety Engineering.

THE INSTITUTE FOR COMPUTER SCIENCES AND TECHNOLOGY conducts research and provides technical services designed to aid Government agencies in improving cost effectiveness in the conduct of their programs through the selection, acquisition, and effective utilization of automatic data processing equipment; and serves as the principal focus within the executive branch for the development of Federal standards for automatic data processing equipment, techniques, and computer languages. The Institute consists of the following divisions:

Computer Services — Systems and Software — Computer Systems Engineering — Information Technology.

THE OFFICE FOR INFORMATION PROGRAMS promotes optimum dissemination and accessibility of scientific information generated within NBS and other agencies of the Federal Government; promotes the development of the National Standard Reference Data System and a system of information analysis centers dealing with the broader aspects of the National Measurement System; provides appropriate services to ensure that the NBS staff has optimum accessibility to the scientific information of the world. The Office consists of the following organizational units:

Office of Standard Reference Data — Office of Information Activities — Office of Technical Publications — Library — Office of International Relations — Office of International Standards.

[1] Headquarters and Laboratories at Gaithersburg, Maryland, unless otherwise noted; mailing address Washington, D.C. 20234.
[2] Located at Boulder, Colorado 80302.

U.S. DEPARTMENT OF COMMERCE
Elliot L. Richardson, Secretary

NATIONAL BUREAU OF STANDARDS
Ernest Ambler, Acting Director

Order all publications from the Superintendent of Documents
U.S. Government Printing Office, Washington, D.C. 20402.

The Secretary of Commerce has determined that the publication of this periodical is necessary in the transaction of the public business required by law of this Department. Use of funds for printing this periodical has been approved by the Director of the Office of Management and Budget through June 30, 1976.

JOURNAL OF RESEARCH of the National Bureau of Standards—A. Physics and Chemistry
Vol. 80A, No. 1, January–February 1976

Line Strengths and Lifetimes of Levels in Neutral Uranium

Charles H. Corliss

Institute for Basic Standards, National Bureau of Standards, Washington, D.C. 20234

(October 29, 1975)

Relative intensities of 549 U I lines observed in a dc copper arc are used to derive transition probabilities and oscillator strengths. Upper limits to lifetimes for 65 levels in neutral uranium atoms are determined.

Key words: Lifetimes in U I: oscillator strengths for U I: transition probabilities for U I: uranium spectrum.

1. Introduction

Separation of isotopes by excitation of excited states through absorption of laser radiation is a relatively new development that has particular application in separation of uranium isotopes. Knowledge of approximate values for oscillator strengths of U I lines and lifetimes of corresponding upper levels is useful in that work. This paper reports such values for 549 lines and 65 levels of U I.

2. Derivation of Oscillator Strengths

The observations from which the oscillator strengths reported here are derived were taken from the NBS Tables of Spectral-Line Intensities by Meggers, Corliss, and Scribner [1961]. Those intensities were measured in a 10 A dc arc between copper electrodes containing one atom of uranium for every 1000 atoms of copper. In 1962 Corliss and Bozman published oscillator strengths for 326 lines of U I. They used an arc temperature of 5100 K to obtain a relative scale which was then adjusted to an absolute scale by comparison with other elements for which absolute oscillator strengths were then known.

In the 13 years that have elapsed since then, much more accurate work on determination of oscillator strengths has been reported. The number of papers published on the subject now amounts to nearly 2400, whereas in 1962 it was only 600. This greatly expanded and also improved knowledge of oscillator strengths has given us a better understanding of the population distribution of excited levels of atoms in the copper arc of Meggers, Corliss, and Scribner. According to the study made by Corliss in 1962, the best oscillator strengths then available indicated that the level population of atoms in our copper arc declined by a factor of 17 for every 10 000 cm^{-1} rise in level value. Recent measurements of oscillator strengths show that the arc is in fact hotter, so that the corresponding decline in level populations is more nearly a factor of 10. This factor of 10 is used in the present work to calculate relative oscillator strengths in U I.

Since about 1964 there have been many measurements of lifetimes of atomic levels by means of beam-foil spectroscopy and since 1956, by the method of delayed coincidence. These new measurements make conversion of relative scales to absolute scales much more certain than previously. The method of delayed coincidence has been used recently by Klose [1975] to measure the lifetime of the U I level at 27887 cm^{-1} above the ground state. I have equated his value for this level, 7.3 ns, to the reciprocal of the sum of the transition probabilities of the two principal transitions (at 3584.88 and 4620.23 Å) from the level to adjust the relative values to the absolute scale.

3. Accuracy of Results

The standard deviation of an individual determination of the intensity from Meggers, Corliss and Scribner is about 32 percent. Klose's uncertainty in the lifetime is about 15 percent. These two uncertainties affect all of the normalized transition probabilities equally. The log of the uncertainty in the value adopted for the rate of decline of population of levels of U I in the arc plasma is estimated to be ± 0.1 for every 10 000 cm^{-1} that the upper level departs from the level of normalization at 27 887 cm^{-1}. A line with an upper level separated about 5000 cm^{-1}, for example, from that level would have an uncertainty in the log gf of ± 0.05 arising from the population uncertainty. The corresponding uncertainties of 0.12 in the intensity and 0.06 in the lifetime when combined quadratically with the chosen example of uncertainty in population brings the total

error to 0.14 (an error of 38 percent in this case. More than half of the U I lines reported here arise from levels that lie within 5000 cm^{-1} of the normalized level.

Recently Voigt [1975] has measured oscillator strengths for 22 lines of U I. His results are systematically different from the values reported here. His values are smaller than mine below 4240 Å and larger at longer wavelengths. It can also be said that his values are smaller than mine for upper energy levels above 24 000 cm^{-1} and larger at lower energy levels. Whether the wavelength or the energy level is significant for the discrepancy is not clear.

The uncertainties in the level lifetimes calculated from the transition probabilities can be determined from the uncertainties of these transition probabilities but there remains an additional error arising from unobserved transitions from each level not included in the summation. The existence of this error requires that the lifetimes be regarded as upper limits. If, however, calculation of lifetimes is restricted to only those levels involving relatively strong lines, the error due to faint lines will be small. In this paper we have restricted the calculation of lifetimes to upper levels for which the sum of the intensities of downward transitions given in Meggers, Corliss, and Scribner is 20 or larger on their scale. Since the faintest observed lines are between 0.3 and 7 on that scale, depending on the spectral region, there is some assurance that the given upper limit will not be far above the correct lifetime.

As an example, we show below the lifetimes for three levels from unpublished measurements obtained by a method of laser excitation and subsequent isotope separation by Janes, Itzkan, Pike, Levy, and Levin [1975] compared with our intensity summations and corresponding derived lifetimes. Note that the lifetime for the case where the $\Sigma I > 20$ is in much better agreement than the cases involving only faint lines.

Level cm^{-1}	Lifetime *ns* (J, I, P, L&L)	ΣI	Lifetime *ns* (Corliss)
23572	60	33	66
23433	155	4	490
23212	170	4.6	320

This limited comparison tends to support our reasoning.

4. Tables of Results

Table 1 lists the wavelength in Angstroms; the lower and upper levels in cm^{-1}; *gA*, the weighted transition probability in units of 10^8 transitions per second; *gf*, the weighted oscillator strength, and log *gf* (base ten). The wavelengths are from Harrison's MIT Wavelength Tables [1939] or from unpublished measurements of Kiess, Humphreys, and Laun [1946]. The levels are from a thesis by Guyon [1972].

TABLE 1. *Transition probabilities for lines of* U I

Wavelength Å	Energy levels cm^{-1}	gA 10^8/s	gf	log gf	Wavelength Å	Energy levels cm^{-1}	gA 10^8/s	gf	log gf
2855.96	0–35004	3.2	.39	−.41	3431.14	4276–33412	2.6	.46	−.33
2926.13	0–34164	1.8	.23	−.64	3433.90	7645–36758	5.7	1.0	.00
2951.93	620–34486	2.4	.32	−.50	3434.61	0–29107	.82	.15	−.84
2998.36	0–33341	1.9	.25	−.59	3435.20	3800–32902	2.3	.42	−.38
3027.66	620–33640	4.1	.56	−.25	3435.49	0–29099	3.9	.70	−.16
3048.64	620–33412	4.7	.65	−.19	3442.95	0–29036	1.8	.32	−.50
3114.54	0–32098	2.1	.30	−.52	3448.78	0–28987	.96	.17	−.77
3147.09	620–32386	3.5	.52	−.28	3458.17	3800–32709	3.8	.68	−.17
3214.70	0–31098	.73	.11	−.95	3459.92	0–28894	2.4	.42	−.37
3263.12	0–30637	1.1	.18	−.75	3462.21	0–28875	2.0	.37	−.44
3293.56	0–30353	.63	.10	−.99	3463.54	620–29484	3.4	.62	−.21
3319.21	3868–33987	2.9	.48	−.32	3466.30	0–28840	4.1	.73	−.14
3345.56	0–29881	.76	.13	−.89	3469.49	3800–32615	2.2	.40	−.40
3345.89	620–30499	1.3	.22	−.65	3469.78	0–28811	.78	.14	−.85
3360.00	0–29753	1.1	.19	−.72	3473.43	3800–32582	4.8	.86	−.06
3368.98	0–29673	.55	.094	−1.03	3480.36	5762–34486	8.5	1.5	.19
3378.20	4453–34046	1.5	.26	−.59	3489.37	0–28650	9.8	1.8	.25
3390.39	620–30107	6.1	1.1	.02	3493.99	620–29233	2.4	.44	−.36
3390.97	3800–33282	2.1	.36	−.44	3497.26	3800–32386	2.1	.39	−.41
3395.52	0–29442	2.1	.36	−.44	3500.07	0–28563	3.8	.71	−.15
3397.19	4275–33703	1.4	.24	−.62	3501.00	4453–33008	1.2	.23	−.65
3405.72	3800–33154	1.6	.29	−.54	3502.24	3868–32413	3.6	.66	−.18
3407.87	3800–33136	2.5	.43	−.37	3504.00	3800–32331	4.6	.84	−.08
3414.32	4453–33733	1.4	.25	−.61	3504.93	0–28523	.88	.16	−.79
3418.39	620–29866	.58	.10	−.99	3507.05	620–29126	1.7	.31	−.51
3430.18	3868–33013	.80	.14	−.85	3507.34	0–28504	4.7	.86	−.06

TABLE 1. *Transition probabilities for lines of* U I—Continued

Wavelength Å	Energy levels cm^{-1}	gA $10^8/s$	gf	log gf	Wavelength Å	Energy levels cm^{-1}	gA $10^8/s$	gf	log gf
3511.44	0–28470	1.5	.27	−.57	3620.08	0–27616	1.6	.31	−.50
3513.68	620–29072	2.2	.40	−.40	3622.04	0–27600	.37	.072	−1.14
3514.61	0–28444	9.4	1.7	.24	3622.70	4275–31871	4.2	.83	−.08
3516.85	3868–32294	2.1	.39	−.41	3634.56	3868–31374	1.5	.29	−.54
3522.67	3800–32180	2.0	.38	−.42	3635.30	3801–31301	1.7	.34	−.47
3525.65	0–28355	1.4	.26	−.58	3637.51	5991–33474	3.3	.66	−.18
3531.64	620–28927	1.6	.30	−.52	3638.20	3801–31279	14.	2.7	.43
3534.33	0–28286	1.8	.34	−.47	3638.65	8118–35593	5.4	1.1	.03
3535.84	620–28894	.48	.091	−1.04	3642.44	4275–31722	2.8	.57	−.25
3537.28	0–28262	1.4	.26	−.58	3644.24	620–28053	3.3	.65	−.18
3538.23	620–28875	.80	.15	−.82	3649.58	5762–33154	2.2	.44	−.36
3539.65	3800–32044	3.3	.62	−.21	3651.53	3800–31178	11.	2.1	.33
3542.57	4276–32496	4.8	.90	−.05	3652.07	4275–31649	8.7	1.7	.24
3543.73	7326–35536	3.7	.69	−.16	3653.21	3801–31166	2.2	.45	−.35
3545.44	4275–32472	3.7	.69	−.16	3654.89	3868–31221	2.3	.45	−.34
3545.67	4453–32648	3.8	.72	−.14	3659.16	620–27941	7.4	1.5	.17
3546.13	620–28811	1.6	.30	−.52	3659.59	620–27938	1.3	.27	−.57
3548.62	4275–32447	2.2	.41	−.38	3667.13	0–27261	.69	.14	−.86
3550.17	5762–33921	3.1	.58	−.24	3669.18	5762–33008	3.0	.60	−.22
3552.95	4453–32590	1.1	.21	−.67	3670.53	7645–34881	9.2	1.9	.27
3553.44	3800–31934	1.9	.37	−.43	3674.13	620–27829	1.4	.29	−.53
3555.32	0–28119	3.8	.72	−.14	3677.39	3801–30986	4.1	.82	−.09
3557.84	0–28099	2.2	.41	−.39	3679.38	620–27791	1.8	.37	−.43
3560.31	5991–34070	3.2	.60	−.22	3680.88	4275–31435	4.2	.85	−.07
3561.41	3800–31871	4.2	.79	−.10	3682.46	0–27148	.90	.18	−.74
3561.80	0–28067	6.4	1.2	.09	3685.78	620–27744	1.4	.29	−.54
3563.66	0–28053	2.1	.41	−.39	3697.13	3800–30841	3.7	.75	−.12
3564.18	620–28669	.77	.15	−.83	3702.62	4276–31276	4.9	1.0	.01
3565.05	4276–32318	2.1	.41	−.39	3703.27	620–27616	2.1	.44	−.36
3566.60	620–28650	15.	2.8	.44	3704.09	7326–34315	9.9	2.0	.31
3571.16	620–28614	.92	.18	−.76	3707.29	3800–30767	4.4	.91	−.04
3574.11	7005–34976	5.2	1.0	.00	3707.95	3868–30829	2.1	.43	−.36
3574.76	0–27966	1.7	.33	−.48	3709.87	5762–32709	3.2	.67	−.18
3577.92	0–27941	2.0	.38	−.42	3713.56	0–26921	2.8	.58	−.24
3578.33	0–27938	1.3	.25	−.60	3715.47	4275–31182	4.9	1.0	.00
3580.25	620–28543	1.2	.23	−.64	3716.14	3800–30702	2.0	.42	−.37
3582.62	4275–32180	2.8	.53	−.27	3719.29	620–27499	.99	.20	−.69
3584.88	0–27887	17.	3.3	.51	3720.39	3800–30672	4.3	.90	−.05
3585.84	620–28499	1.5	.29	−.54	3722.68	7191–34046	9.4	1.9	.29
3587.78	4453–32318	1.8	.34	−.46	3731.45	0–26792	.74	.15	−.81
3589.66	620–28470	1.5	.29	−.54	3731.77	7645–34434	4.8	1.0	.00
3589.79	3800–31649	3.1	.59	−.23	3732.26	3801–30587	4.3	.89	−.05
3591.74	620–28454	2.4	.46	−.34	3733.58	6249–33025	7.4	1.6	.19
3592.97	620–28444	.74	.14	−.84	3742.35	7005–33719	7.2	1.5	.18
3593.20	4276–32098	3.4	.66	−.18	3751.18	5762–32412	17.	3.5	.55
3593.68	5762–33580	2.4	.46	−.34	3751.72	620–27267	2.1	.45	−.35
3600.29	620–28387	.88	.17	−.77	3758.36	4276–30876	9.7	2.1	.31
3601.19	8118–35879	2.4	.47	−.33	3763.27	7006–33571	12.	2.5	.41
3602.48	3801–31552	1.8	.35	−.45	3765.35	0–26550	2.0	.43	−.37
3603.36	0–27744	.76	.15	−.83	3766.89	4453–30993	8.9	1.9	.28
3603.74	4276–32017	1.7	.33	−.49	3773.44	6249–32742	17.	3.5	.55
3605.28	0–27729	2.4	.47	−.33	3776.48	4275–30747	5.8	1.2	.09
3610.69	4453–32141	2.1	.41	−.39	3781.75	7645–34080	5.1	1.1	.04
3611.40	0–27682	.37	.073	−1.14	3786.84	6249–32648	7.3	1.6	.20
3615.54	0–27650	.74	.15	−.84	3788.16	5991–32381	5.4	1.2	.06
3616.33	3801–31445	3.8	.75	−.12	3792.41	4275–30636	2.3	.50	−.30
3617.49	7103–34739	1.9	.37	−.43	3793.28	6249–32604	11.	2.4	.39
3617.62	3800–31435	.88	.17	−.76	3796.20	3868–30203	4.2	.91	−.04

TABLE 1. *Transition probabilities for lines of* U I—Continued

Wavelength Å	Energy levels cm^{-1}	gA $10^8/s$	gf	log gf	Wavelength Å	Energy levels cm^{-1}	gA $10^8/s$	gf	log gf
3797.77	11308–37631	18.	3.9	.59	4160.95	0–24026	.31	.081	−1.09
3798.84	11308–37624	23.	5.0	.69	4162.43	3801–27818	2.7	.69	−.16
3801.15	620–26921	2.0	.43	−.37	4166.64	620–24613	.36	.093	−1.03
3808.93	6249–32496	11.	2.4	.38	4169.06	8119–32098	4.7	1.2	.09
3810.10	3868–30107	1.6	.35	−.46	4186.96	4276–28153	2.3	.59	−.23
3812.00	0–26226	13.	2.9	.46	4191.94	0–23849	.24	.064	−1.20
3818.06	5762–31945	4.2	.92	−.04	4198.22	620–24433	.69	.18	−.74
3819.25	4276–30451	2.2	.49	−.31	4201.13	7645–31442	2.4	.63	−.20
3821.95	3801–29958	4.0	.88	−.06	4213.87	11308–35032	7.8	2.1	.32
3822.35	10347–36501	8.9	2.0	.29	4214.28	7645–31367	2.0	.54	−.27
3829.79	0–26104	.83	.18	−.74	4219.97	4275–27965	.78	.21	−.68
3831.86	4275–30365	4.4	.97	−.01	4222.36	3801–27478	3.6	.97	−.01
3835.22	0–26066	.82	.18	−.74	4231.67	7646–31270	5.3	1.4	.15
3839.62	3801–29838	20.	4.3	.64	4236.04	620–24220	.80	.21	−.67
3846.24	7005–32997	4.0	.89	−.05	4246.26	0–23544	1.1	.29	−.53
3846.55	3801–29791	3.9	.86	−.07	4266.32	0–23433	.22	.061	−1.22
3854.22	0–25938	4.1	.92	−.04	4267.94	6249–29672	.93	.25	−.60
3863.09	3868–29747	1.9	.43	−.37	4288.84	6249–29559	3.4	.94	−.03
3871.04	0–25826	9.6	2.2	.33	4306.82	0–23212	.11	.030	−1.53
3876.13	0–25792	1.6	.35	−.45	4313.13	3801–26979	1.4	.39	−.41
3879.53	4453–30222	4.3	.97	−.01	4335.73	0–23058	.47	.13	−.88
3894.12	0–25672	3.1	.70	−.16	4354.55	3800–26758	1.2	.35	−.46
3899.27	4275–29914	4.0	.92	−.04	4355.75	620–23572	1.9	.54	−.27
3906.46	3868–29459	5.7	1.3	.11	4362.05	0–22919	1.6	.46	−.33
3908.32	4453–30032	2.1	.48	−.32	4371.76	8119–30986	2.2	.64	−.19
3917.25	8119–33640	9.5	2.2	.34	4372.76	0–22862	.25	.072	−1.14
3926.22	0–25463	2.0	.45	−.34	4383.27	3801–26608	.47	.14	−.86
3928.83	0–25445	.73	.17	−.77	4393.60	0–22754	1.2	.34	−.47
3943.82	0–25349	7.2	1.7	.22	4426.94	0–22583	.24	.070	−1.15
3948.45	0–25319	1.7	.41	−.39	4440.74	3801–26313	.34	.10	−1.00
3951.48	4453–29753	1.5	.36	−.44	4469.32	0–22368	.18	.055	−1.26
3955.38	7103–32378	7.2	1.7	.23	4516.73	620–22754	.25	.077	−1.11
3959.20	7005–32255	3.5	.82	−.09	4551.98	620–22583	.17	.053	−1.27
3964.22	6249–31467	8.5	2.0	.30	4563.95	13127–35032	3.4	1.1	.02
3967.47	620–25818	.81	.19	−.72	4576.64	620–22464	.19	.060	−1.22
3974.90	7645–32796	4.0	.94	−.03	4620.23	6249–27887	3.7	1.2	.07
3980.80	5762–30876	2.6	.61	−.21	4631.62	0–21585	.68	.22	−.66
3997.09	3800–28811	1.6	.39	−.41	4663.75	620–22056	.18	.058	−1.24
3999.18	3801–28799	1.6	.38	−.41	4715.68	10208–31408	1.3	.45	−.35
4005.21	620–25580	2.7	.66	−.18	4743.53	6249–27324	.45	.15	−.82
4005.70	620–25577	1.2	.29	−.54	4756.80	620–21637	.50	.17	−.77
4034.50	4453–29233	3.2	.78	−.11	4768.66	620–21585	.12	.042	−1.38
4039.75	7645–32392	2.0	.50	−.30	4778.10	10347–31270	1.1	.38	−.41
4042.76	620–25349	6.1	1.5	.18	4780.19	10081–30994	1.1	.36	−.44
4047.62	620–25319	2.4	.60	−.22	4785.91	3868–24757	.25	.087	−1.06
4061.35	620–25235	.48	.12	−.92	4790.06	7645–28516	.70	.24	−.62
4064.16	5991–30589	2.2	.54	−.27	4810.90	3801–24581	.25	.085	−1.07
4091.64	0–24433	.54	.14	−.87	4842.48	620–21265	.15	.054	−1.27
4101.91	8118–32490	6.4	1.6	.21	4868.86	3801–24334	.23	.083	−1.08
4103.12	7326–31690	5.0	1.3	.10	4885.15	0–20464	.11	.041	−1.39
4108.36	0–24334	.33	.084	−1.08	4910.35	6249–26608	.53	.19	−.72
4116.88	3868–28151	.63	.16	−.79	4928.44	4276–24560	.29	.11	−.97
4132.02	4275–28470	1.7	.44	−.36	4933.06	3801–24067	.15	.054	−1.26
4133.50	0–24186	.96	.25	−.61	4955.78	7646–27818	.62	.23	−.64
4141.86	620–24757	.37	.094	−1.03	4967.33	3801–23927	.25	.094	−1.03
4146.61	7326–31435	1.4	.35	−.46	5011.42	620–20569	.068	.026	−1.59
4153.97	0–24067	4.1	1.1	.02	5027.38	0–19885	.44	.17	−.78
4156.66	620–24671	2.0	.52	−.28	5063.77	3801–23544	.20	.078	−1.11

TABLE 1. *Transition probabilities for lines of* U I—Continued

Wavelength Å	Energy levels cm^{-1}	gA $10^8/s$	gf	log gf	Wavelength Å	Energy levels cm^{-1}	gA $10^8/s$	gf	log gf
5088.29	0–19648	.050	.020	−1.71	5813.83	5991–23187	.072	.036	−1.44
5164.14	8119–27478	.85	.34	−.47	5814.41	3868–21062	.035	.018	−1.75
5272.00	7646–26608	.20	.083	−1.08	5816.79	10288–27475	.19	.097	−1.01
5280.38	0–18933	.15	.062	−1.21	5819.01	7006–24186	.072	.037	−1.43
5308.54	3801–22633	.20	.086	−1.07	5836.03	10347–27478	.77	.39	−.41
5315.27	7646–26454	.22	.094	−1.03	5852.01	4453–21536	.050	.025	−1.59
5319.38	10081–28874	.43	.18	−.73	5898.78	6249–23197	.13	.069	−1.16
5329.26	0–18759	.084	.036	−1.45	5902.50	3868–20805	.085	.044	−1.35
5382.94	620–19192	.027	.012	−1.93	5915.40	0–16900	.35	.18	−.74
5385.54	13127–31690	.46	.20	−.69	5925.47	7646–24517	.20	.10	−.98
5389.83	10347–28895	.39	.17	−.77	5929.33	3801–20662	.074	.039	−1.41
5400.90	10288–28798	.72	.32	−.50	5933.82	620–17468	.028	.015	−1.83
5410.24	4276–22754	.073	.032	−1.50	5942.77	5762–22584	.058	.031	−1.52
5423.35	5762–24195	.084	.037	−1.43	5948.57	7646–24452	.12	.063	−1.20
5459.27	620–18933	.041	.018	−1.74	5956.86	3868–20651	.074	.040	−1.40
5496.43	4276–22464	.17	.078	−1.11	5971.50	620–17362	.098	.052	−1.28
5500.69	620–18794	.035	.016	−1.80	5976.32	3801–20529	.36	.19	−.71
5510.41	13127–31270	1.3	.59	−.23	5986.10	3868–20569	.10	.055	−1.26
5511.49	620–18759	.099	.045	−1.35	5997.31	6249–22919	.28	.15	−.82
5513.39	7326–25458	.16	.073	−1.14	5997.96	4276–20943	.062	.034	−1.47
5531.26	7864–25938	.18	.082	−1.08	5999.41	3801–20464	.080	.043	−1.37
5557.87	620–18607	.048	.022	−1.65	6000.19	11308–27969	.40	.22	−.67
5564.17	3801–21768	.30	.14	−.86	6008.87	10254–26892	.31	.17	−.77
5573.07	10347–28286	.27	.12	−.91	6010.86	10347–26979	.32	.17	−.76
5573.59	6249–24186	.087	.040	−1.39	6014.07	14845–31468	.89	.48	−.32
5608.86	15720–33544	.89	.42	−.38	6016.73	5762–22378	.056	.030	−1.52
5610.89	6249–24067	.42	.20	−.70	6017.57	6249–22862	.12	.068	−1.17
5616.58	8119–25918	.16	.074	−1.13	6019.19	4453–21062	.064	.035	−1.46
5620.78	620–18406	.12	.055	−1.26	6028.13	3868–20452	.080	.044	−1.36
5621.51	3801–21585	.12	.057	−1.24	6035.54	7191–23755	.051	.028	−1.56
5632.47	10069–27818	.24	.11	−.94	6039.60	8119–24671	.19	.10	−.99
5634.38	7646–25389	.29	.14	−.86	6050.48	3868–20392	.032	.017	−1.76
5636.78	7005–24741	.080	.038	−1.42	6050.67	7326–23849	.070	.038	−1.42
5640.30	5762–23486	.090	.043	−1.37	6056.80	0–16506	.023	.013	−1.90
5648.38	10557–28256	.18	.085	−1.07	6057.07	6249–22754	.095	.052	−1.28
5658.26	3868–21536	.077	.037	−1.43	6062.30	4276–20766	.069	.038	−1.42
5669.42	620–18254	.057	.027	−1.56	6077.29	620–17070	.15	.082	−1.08
5680.37	6249–23849	.098	.047	−1.32	6089.19	3801–20219	.054	.030	−1.53
5685.19	4453–22038	.065	.031	−1.50	6101.77	6249–22633	.11	.059	−1.23
5705.66	10819–28341	.23	.11	−.95	6127.77	8119–24433	.14	.079	−1.10
5709.49	7103–24613	.098	.048	−1.32	6129.72	620–16930	.045	.026	−1.59
5716.87	4453–21941	.096	.047	−1.33	6132.61	11308–27609	.37	.21	−.67
5722.23	13535–31005	.42	.21	−.68	6138.54	10685–26971	.14	.081	−1.09
5736.38	7006–24433	.19	.093	−1.03	6152.25	4275–20525	.033	.019	−1.73
5750.54	8856–26241	.26	.13	−.89	6164.50	7326–23544	.058	.033	−1.48
5758.14	0–17362	.038	.019	−1.73	6171.85	7646–23844	.31	.18	−.75
5758.35	4276–21637	.050	.025	−1.60	6175.38	4276–20464	.12	.070	−1.15
5761.88	16244–33595	.61	.31	−.51	6215.37	3801–19885	.051	.029	−1.53
5763.59	7103–24449	.048	.024	−1.63	6234.30	4276–20312	.056	.033	−1.49
5763.66	7326–24671	.050	.025	−1.60	6246.53	5762–21766	.078	.046	−1.34
5765.41	8118–25458	.12	.060	−1.22	6268.66	8119–24067	.11	.067	−1.17
5767.43	5991–23325	.074	.037	−1.44	6292.03	8133–24022	.11	.067	−1.17
5771.05	6249–23572	.078	.039	−1.41	6295.32	620–16506	.030	.018	−1.74
5777.77	12362–29665	.31	.16	−.80	6298.53	4275–20148	.062	.037	−1.43
5780.59	6249–23544	.47	.23	−.63	6359.28	0–15721	.036	.022	−1.66
5796.51	17091–34338	.92	.46	−.34	6372.43	3801–19489	.17	.10	−.99
5802.11	8119–25349	.41	.21	−.68	6372.97	5762–21448	.026	.016	−1.79
5805.20	5991–23212	.072	.036	−1.44	6383.59	4453–20114	.027	.017	−1.78

TABLE 1. *Transition probabilities for lines of* U I—Continued

Wavelength Å	Energy levels cm^{-1}	gA $10^8/s$	gf	log gf	Wavelength Å	Energy levels cm^{-1}	gA $10^8/s$	gf	log gf
6389.77	5991–21637	.11	.068	−1.17	7164.87	4453–18406	.059	.046	−1.34
6392.74	0–15638	.035	.022	−1.67	7172.10	14845–28784	.32	.25	−.61
6395.42	0–15632	.11	.069	−1.16	7194.63	10685–24581	.24	.19	−.72
6397.14	7006–22633	.11	.068	−1.16	7196.66	10081–23972	.11	.083	−1.08
6411.59	7326–22919	.060	.037	−1.43	7205.42	10686–24560	.12	.095	−1.02
6430.93	5991–21536	.038	.024	−1.63	7210.28	6249–20114	.071	.055	−1.26
6449.17	620–16122	.16	.099	−1.00	7254.44	7645–21426	.21	.17	−.78
6465.00	7326–22790	.22	.14	−.86	7371.95	5991–19552	.040	.032	−1.49
6481.72	5762–21185	.020	.013	−1.89	7390.99	10208–23734	.10	.085	−1.07
6488.35	13535–28943	.24	.15	−.82	7392.11	13127–26652	.20	.17	−.78
6503.62	4276–19648	.050	.032	−1.50	7396.98	4453–17969	.083	.068	−1.17
6518.94	6249–21585	.078	.050	−1.30	7416.57	10081–23560	.10	.082	−1.08
6520.98	8133–23464	.034	.022	−1.66	7425.50	0–13463	.050	.041	−1.39
6526.08	7645–22964	.046	.029	−1.53	7517.39	16040–29339	.38	.32	−.49
6527.04	5762–21079	.020	.013	−1.89	7528.70	19103–32381	1.5	1.3	.11
6542.98	10347–25626	.11	.073	−1.14	7533.91	3801–17070	.23	.20	−.71
6552.75	7326–22583	.021	.014	−1.87	7550.23	10685–23926	.28	.24	−.63
6555.01	3868–19119	.038	.025	−1.61	7590.52	5762–18933	.036	.031	−1.51
6582.78	7864–23051	.024	.015	−1.81	7595.04	10686–23849	.11	.095	−1.02
6601.39	7646–22790	.030	.019	−1.71	7600.27	16040–29194	.30	.26	−.59
6603.98	7326–22464	.062	.041	−1.39	7609.16	7326–20464	.10	.088	−1.06
6620.52	620–15721	.037	.024	−1.61	7619.34	7646–20766	.19	.17	−.78
6625.29	5762–20852	.048	.032	−1.50	7631.72	3801–16900	.056	.049	−1.31
6628.65	11677–26758	.11	.073	−1.14	7634.74	7326–20420	.080	.070	−1.15
6647.79	3800–18839	.024	.016	−1.79	7639.54	4276–17362	.075	.066	−1.18
6656.81	620–15638	.012	.0078	−2.11	7653.62	8878–21940	.057	.050	−1.30
6683.38	3801–18759	.054	.036	−1.44	7748.19	16040–28943	.57	.51	−.29
6691.21	10686–25627	.058	.039	−1.41	7754.18	7326–20219	.078	.070	−1.15
6727.96	5762–20621	.019	.013	−1.90	7759.87	7646–20529	.084	.076	−1.12
6736.80	0–14839	.017	.012	−1.93	7761.84	7006–19885	.11	.10	−.99
6754.93	8119–22919	.047	.032	−1.49	7784.13	620–13463	.031	.028	−1.55
6768.64	7864–22634	.030	.020	−1.69	7816.32	13128–25918	.29	.26	−.58
6780.62	8118–22862	.031	.021	−1.67	7832.02	14845–27609	.19	.17	−.77
6782.70	3868–18607	.012	.0081	−2.09	7835.71	5991–18749	.018	.016	−1.79
6782.85	4453–19192	.013	.0093	−2.03	7844.71	16040–28784	.70	.64	−.19
6790.30	7646–22368	.14	.096	−1.02	7868.75	3801–16506	.063	.059	−1.23
6812.98	4453–19127	.0067	.0046	−2.33	7875.36	11308–24002	.35	.33	−.48
6813.75	11677–26349	.035	.024	−1.62	7881.94	6249–18933	.41	.38	−.42
6813.81	11633–26305	.034	.024	−1.62	7900.43	4276–16930	.047	.044	−1.36
6818.29	3868–18531	.029	.020	−1.69	7904.28	8119–20766	.079	.074	−1.13
6820.76	4276–18933	.11	.078	−1.11	7907.96	7006–19648	.061	.057	−1.24
6824.45	7103–21753	.073	.051	−1.29	7918.80	4276–16900	.047	.044	−1.36
6826.93	0–14644	.17	.12	−.93	7959.96	7326–19885	.065	.062	−1.21
6832.71	7006–21637	.036	.025	−1.60	7963.96	10081–22634	.26	.25	−.61
6846.25	6249–20852	.050	.035	−1.46	7970.46	8119–20662	.22	.21	−.68
6869.07	19761–34315	2.7	1.9	.28	7975.08	11308–23843	.23	.22	−.66
6887.74	8119–22633	.090	.064	−1.19	7975.47	18933–31468	.46	.44	−.36
6902.55	4276–18759	.031	.022	−1.65	7991.30	6249–18759	.050	.048	−1.32
6915.31	5762–20219	.052	.037	−1.43	7998.60	13128–25627	.35	.33	−.48
6917.05	3801–18254	.069	.050	−1.30	8012.96	4453–16930	.017	.016	−1.80
7015.70	8119–22368	.086	.064	−1.20	8019.38	7006–19472	.051	.049	−1.31
7030.69	620–14839	.016	.011	−1.94	8034.79	10347–22790	.18	.18	−.76
7033.84	10347–24560	.30	.22	−.66	8055.61	8119–20529	.076	.074	−1.13
7074.78	4276–18406	.15	.11	−.96	8065.47	10069–22464	.17	.16	−.78
7101.61	4453–18531	.18	.14	−.86	8065.84	3800–16195	.014	.014	−1.86
7128.89	620–14644	.088	.067	−1.18	8097.62	8118–20464	.11	.11	−.98
7130.05	5762–19783	.041	.031	−1.51	8126.23	10081–22383	.10	.099	−1.00
7147.87	10347–24334	.40	.31	−.51	8137.21	10347–22633	.12	.12	−.91

TABLE 1. *Transition probabilities for lines of* U I—Continued

Wavelength Å	Energy levels cm^{-1}	gA $10^8/s$	gf	log gf	Wavelength Å	Energy levels cm^{-1}	gA $10^8/s$	gf	log gf
8153.71	13128–25389	.23	.23	−.63	8496.09	8119–19885	.079	.086	−1.07
8174.30	4276–16506	.077	.077	−1.11	8504.53	11457–23212	.17	.18	−.74
8175.84	16040–28268	.45	.45	−.34	8540.19	5762–17468	.072	.078	−1.11
8230.83	5762–17908	.043	.043	−1.36	8542.32	10254–21958	.064	.070	−1.16
8240.51	5762–17894	.021	.022	−1.66	8557.32	10686–22368	.14	.15	−.81
8262.05	8119–20219	.21	.21	−.67	8567.71	4453–16122	.034	.037	−1.43
8310.69	11457–23486	.18	.18	−.74	8570.51	8119–19783	.17	.19	−.73
8318.34	4275–16294	.075	.077	−1.11	8574.59	6249–17908	.051	.056	−1.25
8329.74	7645–19647	.064	.067	−1.17	8607.96	0–11614	.13	.14	−.84
8346.74	5991–17969	.078	.082	−1.09	8641.12	16040–27609	.59	.66	−.18
8357.07	3868–15831	.027	.028	−1.55	8659.57	10208–21753	.12	.14	−.86
8381.86	7006–18933	.16	.17	−.78	8691.28	0–11502	.037	.042	−1.37
8387.19	4275–16195	.034	.035	−1.45	8710.77	5991–17468	.12	.13	−.88
8389.16	5991–17908	.078	.082	−1.09	8753.68	10347–21768	.31	.36	−.44
8441.20	7646–19489	.16	.17	−.78	8757.77	620–12035	.059	.068	−1.17
8445.35	3801–15638	.15	.16	−.80	8816.56	7191–18530	.075	.088	−1.06
8450.02	3801–15632	.074	.080	−1.10					

TABLE 2. *Upper limits to lifetimes for levels in* U I

Level cm^{-1}	J	g	Lifetime ns	n	Level cm^{-1}	J	g	Lifetime ns	n
16900.385	7	15	330.	3	28562.631	5	11	29.	1
18932.762	5	11	120.	6	28650.295	5	11	4.5	2
19885.513	7	15	200.	5	28811.960	6	13	33.	3
21584.692	6	13	130.	4	28840.936	5	11	27.	1
22754.057	6	13	81.	4	28874.930	6	13	40.	3
22918.552	7	15	75.	4	29099.578	5	11	28.	1
23543.504	7	15	83.	4	29232.652	5	11	20.	2
23572.082	6	13	66.	2	29459.910	4	9	16.	1
24066.562	7	15	31.	4	29837.646	7	15	7.7	1
24433.256	6	13	83.	4	30107.096	4	9	12.	2
24671.385	6	13	58.	3	30747.892	7	15	26.	1
25319.272	5	11	26.	2	30875.581	6	13	11.	2
25348.976	6	13	9.5	3	30986.296	8	17	27.	2
25462.659	6	13	66.	1	30993.006	5	11	12.	1
25580.748	6	13	47.	1	31178.758	8	17	16.	1
25672.464	7	15	49.	1	31270.334	9	19	25.	3
25825.562	6	13	14.	1	31279.130	8	17	12.	1
25938.231	6	13	30.	2	31435.401	7	15	23.	3
26225.568	6	13	9.8	1	31467.623	6	13	15.	1
26550.427	6	13	65.	1	31649.690	6	13	11.	2
26920.718	5	11	23.	2	31871.569	6	13	15.	2
27477.553	8	17	32.	3	32098.168	7	15	15.	3
27615.796	6	13	35.	2	32412.827	6	13	7.7	1
27818.491	8	17	48.	3	32495.736	5	11	6.9	2
27886.992	7	15	7.3	2	32604.071	5	11	9.7	1
27938.049	5	11	42.	2	32648.876	5	11	9.9	2
27941.251	6	13	14.	2	32742.570	5	11	6.6	1
28053.058	6	13	24.	2	33570.669	7	15	13.	1
28067.646	5	11	17.	1	33639.564	6	13	9.6	2
28118.841	7	15	39.	1	34046.448	3	7	6.5	2
28444.515	5	11	11.	2	34315.658	8	17	13.	2
28470.179	6	13	28.	3	34486.486	5	11	10.	2
28503.449	5	11	24.	1					

Table 2 lists the upper levels in cm^{-1}, the J-value of the level, the statistical weight $(2J+1)$, the upper limit of the lifetime in nanoseconds (10^{-9} s), and the number of transitions in the summation. All of these levels are of even parity.

5. References

Corliss, C. H. [1962], J. Res. Nat. Bur. Stand. (U.S.), **66A** (Phys. and Chem.), No. 1, 5–12 (Jan.–Feb. 1962).

Corliss, C. H. and Bozman, W. R. [1962], Experimental Transition Probabilities for Spectral Lines of Seventy Elements, NBS Mono. No. 53.

Guyon, F. [1972], Thesis, Univ. de Paris-Sud, Orsay.

Harrison, G. R. [1939], M.I.T. Wavelength Tables (John Wiley & Sons, New York).

James, G. S., Itzkan, I., Pike, C. T., Levy, R. H., and Levin, L. [1975], IEEE/OSA Conference on Laser Engineering and Applications (Post-Deadline Paper).

Klose, J. [1975], Phys. Rev. A **11**, 1840.

Meggers, W. F., Corliss, C. H., and Scribner, B. F. [1961], Tables of Spectral-Line Intensities, NBS Mono. 32, Pt. I.

Voigt, P. A. [1975], Phys. Rev. A **11**, 1845.

(Paper 80A1–875)

JOURNAL OF RESEARCH of the National Bureau of Standards—A. Physics and Chemistry
Vol. 80A, No. 1, January–February 1976

Optical Properties of Nuclear Matter

J. S. O'Connell

Institute for Basic Standards, National Bureau of Standards, Washington, D.C. 20234

(September 18, 1975)

The index of refraction and absorptive properties are estimated in nuclear matter consisting of protons and neutrons and in nuclear matter charge neutralized by electrons.

Key words: Absorption cross section; index of refraction; nuclear matter; optical properties; photon; plasma frequency.

1. Introduction

Nuclear matter is a hypothetic substance consisting of interacting neutrons and protons in large enough numbers that the system can be considered infinite. The properties of this medium are determined by the nucleon-nucleon potential (usually with the Coulomb forces between the protons omitted to avoid the infinite Coulomb potential). Two properties, the equilibrium density and binding energy per nucleon, can be derived from measurements on finite nuclei because the conditions at the center of a very large nucleus approximate those of nuclear matter.

The purpose of this investigation is to study the important interaction mechanisms of photons in nuclear matter as a function of frequency in order to estimate the photon propagation characteristics in the medium. In the next section we review some of the basic facts of nuclear matter. In section 3 the photon-nucleon cross sections for various processes are computed. These processes are then reexamined in section 4 for the case where electrons are added to the medium causing net charge neutralization. Finally, a discussion of the results and conclusions are presented in section 5.

2. Nuclear Matter

The charge density distribution of finite nuclei as determined by elastic electron scattering indicates the nucleon density of heavy nuclei is fairly constant in the interior of the nucleus with a value

$$\rho = 0.170 \text{ nucleons/fm}^3.$$

We shall adopt this value for infinite nuclear matter. The total binding energy of finite nuclei as expressed in a semiempirical mass formula can be extrapolated to an infinite number of nucleons (half protons, half neutrons). The average binding energy per nucleon in nuclear matter (i.e., the coefficient of the term linear in number of nucleons) is

$$B = -15.68 \text{ MeV/nucleon}.$$

It is the goal of nuclear matter theory to reproduce these "observed" properties, ρ and B, starting from a potential $V(\mathbf{r})$ between two nucleons. A review of these calculations is given by Bethe [1][1]. The Reid soft-core potential, one of the better phenomenological nucleon-nucleon potentials, yields $\rho_{\text{RSC}} = 0.20$ fm^{-3} and $B_{\text{RSC}} = -11.25$ MeV in a calculation of the two-body contributions. Estimates of higher order contributions seem to account for discrepancies between the Reid potential predictions and the observables.

Nuclear matter is usually discussed within the framework of the Fermi gas model. For no interactions among nucleons ($V(\mathbf{r}) = 0$) the individual nucleon wave function is a plane wave of momentum $\mathbf{k}$

$$\psi(r) = e^{i\mathbf{k}\cdot\mathbf{r}}.$$

These functions are normalized in a unit volume and are subject to antisymmetrization for identical nucleons. Our units are chosen to have $\hbar = c = 1$.

The distribution of nucleon momentum in the Fermi gas model is uniform from $k = 0$ to $k = k_F$ (the Fermi momentum). The maximum momentum k_F is related to the nucleon density by

$$k_F^3 = \frac{3\pi^2}{2}\rho$$

which gives $k_F = 1.36$ fm^{-1}. This value of the Fermi momentum is also in agreement with inelastic electron

[1] Figures in brackets indicate the literature references at the end of this paper.

scattering in the quasielastic region. This value corresponds to a maximum kinetic energy per particle of

$$\frac{k_F^2}{2M} = 37 \text{ MeV}$$

and an average kinetic energy of 22 MeV. These plane waves form the basis set used in the solution of the problem of interacting nucleons.

In nuclear matter the Schrödinger equation for the wave function $\psi(r)$ of two nucleons with relative momentum $\mathbf{k} = \mathbf{k}_1 - \mathbf{k}_2$ interacting through a potential $V(\mathbf{r})$ is modified by a term which takes into account the fact that nucleons cannot scatter into momentum states already occupied by other nucleons. The modification as derived by Bethe and Goldstone for a s-wave potential is

$$\left(\frac{d^2}{dr^2} + k^2\right) u(r) = MV(r)\, u(r) - \frac{1}{\pi}\int_0^\infty \chi(r,r')\, V(r')\, u(r')\, dr'$$

where $u(r) = kr\,\psi(r)$ and

$$\chi(r,r') = \frac{\sin k_F(r-r')}{r-r'} - \frac{\sin k_F(r+r')}{r+r'}.$$

The solution of the Bethe-Goldstone equation can be written as a free wave minus a defect part

$$u(r) = \sin kr - \Delta u(r).$$

Figure 2 shows the defect function [2] for the Reid soft-core potential. The function $\Delta u/k$ is not sensitive to either the relative momentum, $\mathbf{k}$, or the total momentum $\mathbf{k}_1 + \mathbf{k}_2$. An important feature of $\Delta u(r)$ is that it is small by the time r approaches the average internucleon separation distance, $\rho^{-1/3} = 1.8$ fm. This means that for subsequent collisions nucleons approach each other in relatively pure plane-wave states.

The defect function normalization is such that

$$\kappa = \frac{3}{8}\rho \int_0^\infty |\Delta u(r)|^2 dr$$

is the probability that a s-wave pair of particles is outside the Fermi sea. For the Reid soft-core potential $\kappa = 0.14$ summed over all partial waves.

The Pauli exclusion principle which prevented nucleon-nucleon scattering to occupied momentum states will also modify photon-nucleon interactions. If in free space a photon process imparts a momentum transfer q to a nucleon, the cross section in nuclear matter will be reduced by a factor

$$R(q) = \frac{3}{4}\frac{q}{k_F}\left[1 - \frac{1}{12}\left(\frac{q}{k_F}\right)^2\right], \qquad q < 2k_F$$

because only a fraction R of the nucleons will have an initial momentum $\mathbf{k}$ such that the final momentum will exceed the Fermi momentum $|\mathbf{k}+\mathbf{q}| > k_F$. The expression is derived by calculating the excluded volume of the initial and final Fermi momentum spheres shown in figure 1.

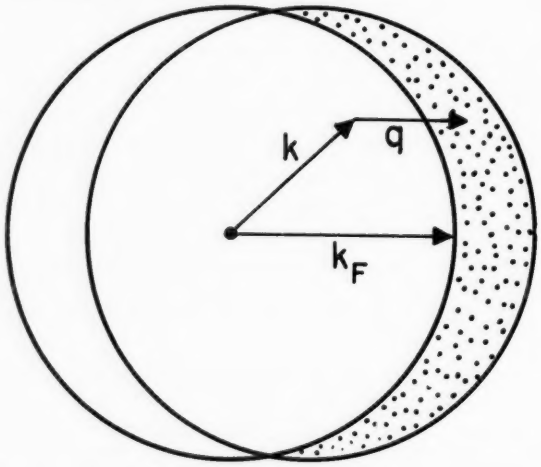

FIGURE 1. *Initial (left sphere) and final (right sphere) momentum distributions in a Fermi gas model in which a momentum* q *is to be given each nucleon.*

Only those nucleons for which $|\mathbf{k}+\mathbf{q}| > k_F$ are allowed to make the transition. The fraction $\mathbf{R}(q)$ is the ratio of excluded volume (shaded) to the total $(4/3\pi\ k_F^3)$.

3. Photon Interactions

Consider a photon of frequency ω incident on a semi-infinite slab of nuclear matter. The index of refraction (ratio of wavelength in vacuum to that in the material) is related to the forward elastic scattering amplitude $f(\omega)$ by

$$n^2(\omega) = 1 + \frac{4\pi\rho f(\omega)}{\omega^2}.$$

In general both f and n are complex numbers. The imaginary part of f is related to the absorption cross section through the optical theorem

$$4\pi \text{ Im } f(\omega) = \omega\sigma(\omega).$$

The real part of f can be calculated from the imaginary part by the use of a dispersion relation, but we will not make use of this approach in our estimates. We now examine the photon interaction mechanisms [3].

3.1. Thomson Scattering

Electromagnetic waves scatter from the free proton (mass M, charge e) with an amplitude

$$f = -\frac{e^2}{M} = -1.54 \times 10^{-3} \text{ fm},$$

which is independent of frequency. The forward amplitude is the same in nuclear matter because no momentum is transferred to the proton. It is convenient to introduce a quantity called the plasma frequency

$$\omega_0^2 = 4\pi\rho_P \frac{e^2}{M},$$

which for $\rho_P = 0.085$ protons/fm^3 has the value $\omega_0 = 8.0$ MeV. The index of refraction due to Thomson scattering can be written as

$$n^2(\omega) = 1 - \frac{\omega_0^2}{\omega^2}.$$

Note that for $\omega < 8$ MeV the index n is imaginary which means an incident photon will be reflected as it tries to enter the medium. This phenomenon is analogous to the reflection of light waves from the surface of a metal due to Thomson scattering by the conduction electrons.

Within the medium the photon intensity falls off exponentially and the $1/e$ penetration depth is given by

$$d_{\text{Thomson}} = (\omega_0^2 - \omega^2)^{-1/2}.$$

For $\omega << \omega_0$ this distance is 25 fm.

Above the plasma frequency $n(\omega)$ is real and the photons propagate freely with the index approaching unity from below.

3.2. Proton Compton Effect

Photon scattering by the proton's charge is inelastic at angles other than 0° and therefore absorptive. The differential cross section for scattering by a free proton is given by the Klein-Nishina formula

$$\frac{d\sigma^{\text{free}}_{\text{Compton}}}{d\Omega} = \left(\frac{e^2}{M}\right)^2 \frac{1}{2}\left(\frac{\omega'}{\omega}\right)^2 \left[\frac{\omega'}{\omega} + \frac{\omega}{\omega'} - \sin^2\theta\right]$$

where the scattered photon energy is

$$\omega' = \omega\left(1 + \frac{\omega}{M}(1 - \cos\theta)\right)^{-1}.$$

For incident photon energies small compared to the proton mass, $\omega << M = 938$ MeV, the photon energy loss $\omega - \omega'$ is small and the free cross section can be approximated by

$$\frac{d\sigma^{\text{free}}_{\text{Compton}}}{d\Omega} \simeq \left(\frac{e^2}{M}\right)^2 \frac{1}{2}(1 + \cos^2\theta).$$

In nuclear matter this cross section must be multiplied by the Pauli reduction factor. The momentum transfer to the proton is

$$q = 2\omega \sin\frac{1}{2}\theta.$$

The total Compton cross section for a noninteracting Fermi gas is then

$$\sigma^{NM(\omega)}_{\text{Compton}} \simeq \int \frac{3}{4}\frac{q}{k_F}\left(\frac{d\sigma^{\text{free}}}{d\Omega}\right) d\Omega = \frac{276}{105}\pi\left(\frac{e^2}{M}\right)^2 \frac{\omega}{k_F}.$$

For example, $\sigma^{NM}_{\text{Compton}}(100\text{ MeV}) = 0.73 \times 10^{-31}$ cm^2.

3.3. Pair Production

An important absorption mechanism is the conversion of the photon to an electron-positron pair in the Coulomb field of the proton. The free proton cross section for $\omega >> m_e$ is given by

$$\sigma^{\text{free}}_{\text{pair}} = \left(\frac{e^2}{m_e}\right)^2 \left[\frac{28}{9}\ln\frac{2\omega}{m_e} - \frac{218}{27}\right]$$

where m_e is the mass of the electron. The proton is required to take up an average momentum transfer of $\bar{q} \cong m_e$. Thus, the nuclear matter cross section per proton is

$$\sigma^{\text{NM}(\omega)}_{\text{pair}} = \frac{3}{4}\frac{m_e}{k_F}\sigma^{\text{free}(\omega)}_{\text{pair}}.$$

A $1/e$ absorption length can be computed using

$$d = (\rho_P \sigma)^{-1}.$$

Typical values are:

ω (MeV)	$\sigma^{\text{NM}}_{\text{pair}}$ ($\times 10^{-27}$ cm^2)	$\text{Im}f_{\text{pair}}$ ($\times 10^{-3}$ fm)	d_{pair} (fm)
10.	0.38	0.15	306.
30.	0.77	0.93	153.
100.	1.19	4.80	99.

The imaginary part of the forward scattering amplitude exceeds the real Thomson aplitude above 50 MeV.

3.4. Absorption on Correlated Neutron-Proton Pairs

Single particle ejection, which is an important photoabsorption mechanism in finite nuclei, is not possible in a noninteracting system in which the nucleon has definite linear momentum because energy and momentum cannot be simultaneously conserved. However, in an interacting Fermi gas the defect wave function has a spread of momentum components that allows two nucleons to absorb a photon and be ejected from the Fermi sea.

An estimate of the absorption cross section of this process can be made by considering the electric dipole transition of a correlated neutron-proton pair using the s-wave defect wave function as the initial state and a free p-wave for the final state

$$do = (2\pi)^2 \frac{e^2}{M^2\omega} |\mathcal{M}(p)|^2 \frac{dn}{d\omega}.$$

The density of final two-nucleon states is a function of the final relative momentum **p**

$$\frac{dn}{d\omega} = \frac{d^3p}{(2\pi)^3 d\omega} = \frac{1}{(2\pi)^3} \frac{Mp}{2} d\Omega_p.$$

The $E1$ matrix element is calculated from the momentum space wave functions as

$$\mathcal{M}(p) = \int \psi_f \hat{\epsilon} \cdot \mathbf{k}\, \psi_i d^3k$$

where $\hat{\epsilon}$ is the photon polarization vector.

A properly normalized initial state is

$$\psi_i(k) = (3\rho/8)^{1/2} \cdot \Delta\psi(k)$$

where for convenience we use the Fourier transform of the defect wave function

$$\Delta\psi(k) = \frac{1}{(2\pi)^{3/2}} \int e^{i\mathbf{k}\cdot\mathbf{r}} \frac{\Delta u(r)}{kr} d^3k.$$

The final state with both particles outside the Fermi momentum sphere is

$$\psi_f = (2\pi)^{3/2}\, \delta^3(\mathbf{p}-\mathbf{k}).$$

The matrix element is simply evaluated as

$$\mathcal{M}(p) = (3\rho/8)^{1/2}\, (2\pi)^{3/2}\, \hat{\epsilon} \cdot \mathbf{p} \Delta\psi(p).$$

The total cross section averaged over photon polarization is then

$$\sigma(\omega) = \pi^3 \frac{e^2}{M} \rho \left(\frac{p^3}{\omega}\right) |\Delta\psi(p)|^2.$$

We take the threshold for the reaction to be twice the average single particle binding energy, 16 MeV. Thus, photon energy and final relative momentum are related by

$$\omega = \frac{p^2}{M} + 32 \text{ MeV}.$$

The resulting cross section is plotted in figure 2. At the peak $\omega = 100$ MeV the nuclear matter cross section is about 13 percent of the free deuteron cross section.

3.5. Pion Production

At photon energies greater than the mass of the pion $\omega > m_\pi = 140$ MeV the reaction

$$\gamma + N \rightarrow N + \pi$$

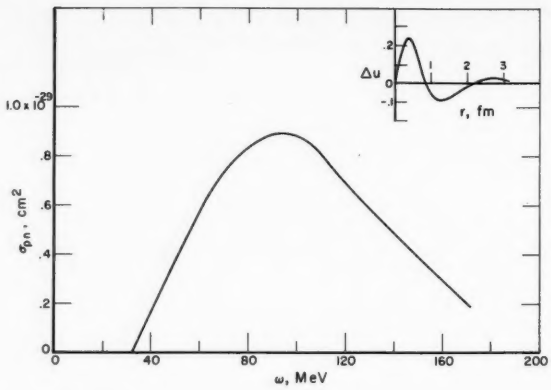

FIGURE 2. *Upper right insert shows s-wave defect wave function for a soft-core nucleon-nucleon potential.*

The curve σ_{pn} is the cross section per nucleon for the absorption of a photon by a correlated neutron-proton pair calculated using Δu.

occurs for both neutrons and protons. The cross section for free nucleons reaches a peak at $\omega = 300$ MeV of 0.5×10^{-27} cm^2 (the 3, 3 resonance). After a few smaller resonances the cross section is essentially constant between 2 GeV and 20 GeV at 0.1×10^{-27} cm^2. One might expect that the nuclear matter cross section would be the free cross section modified by the Pauli reduction factor $R(q)$ where the nucleon recoil momentum is

$$q = \left[\frac{2m_\pi M}{M + m_\pi} (\omega - m_\pi)\right]^{1/2}.$$

However, the A dependence of the high energy absorption cross section for finite nuclei

$$\frac{\sigma_{\gamma A}}{\sigma_{\gamma N}} = \begin{cases} A^{0.75}, & \omega = 0.14 \text{ to } 2 \text{ GeV} \\ A^{0.91}, & \omega > 2 \text{ GeV} \end{cases}$$

indicates [4] a shadowing phenomenon which is more complicated than the incoherent sum of individual nucleon events in nuclear matter. Present theories contend that a high energy photon spends a fraction of the time as a spin-one meson (vector dominance model). Mesons propagating in nuclear matter have a large and complex index of refraction [5]. For our purposes, however, it is probably safe to assume that the photo pion absorption cross section per nucleon is no larger than that of the free nucleon at the same photon energy. In this case, the high energy absorption will be dominated by the ever-increasing e^+e^- production process.

4. Photon Interactions in Charge Neutralized Nuclear Matter

If electrons are added to the proton-neutron matter to achieve charge neutrality ($\rho_e = \rho_P = 0.085$ fm^{-3}) the optical properties are drastically changed. Müller

and Rafelski [6] argue that charge neutralization occurs spontaneously when the Coulomb potential exceeds $[k_F^2 + m_e]^{1/2} \simeq k_F = 268$ MeV. This occurs for finite nuclei which have more than 10^4 protons.

The plasma frequency of the electrons is much higher than that of the protons because of the smaller electron mass,

$$\omega_0^{\text{electron}} = (4\pi \rho_e e^2/m_e)^{1/2} = 342 \text{ MeV},$$

with an associated penetration depth less than a fm. As a consequence, any photons with energy less than 342 MeV will be reflected from the surface of a semi-infinite slab of this material.

Photon propagation in the medium becomes possible again for $\omega > 342$ MeV. Pair production in the Coulomb fields of the electrons and protons is influenced by the requirement that the e^- which is produced must have a momentum greater than k_F. Thus, the threshold for pair production is raised from $2m_e$ to k_F and the $\ln \frac{2\omega}{m_e}$ term in the high energy cross section formula becomes $\ln \frac{2\omega}{k_F}$. In the threshold region the e^+ and e^- energies are not shared symmetrically and there will be mutual screening of the electron and proton Coulomb fields. An estimate of the combined pair production cross section can only be made for $\omega > 2$ GeV, viz.,

$$\sigma_{\text{pair}}^{epn}(\omega) \simeq \frac{3}{2}\frac{m_e}{k_F}\left(\frac{e^2}{m_e}\right)^2\left[\frac{28}{9}\ln\frac{2\omega}{k_F} - \frac{218}{27}\right].$$

The photo pion absorption cross section is unaffected by the electron component of nuclear matter. Above 2 GeV the pair cross section is larger than $\sigma_{\gamma\pi}$, but the reverse is probably true between 342 MeV and 2 GeV. Compton scattering on the electrons is smaller than both these cross sections.

5. Discussion and Conclusions

The main results are displayed in figure 3. Proton-neutron matter is dominated by reflective Thomson scattering below 8 MeV and pair production above the proton plasma frequency. All real nuclei are too small to exhibit the low frequency imaginary index of refraction expected of *np* matter since the largest diameter (14 fm) is still small compared to the penetration depth (25 fm). Also, pair production on finite nuclei occurs coherently in the intense Coulomb field at the edge of the nucleus rather than from individual protons in the interior.

Electron-proton-neutron matter has a much higher plasma frequency so that photons do not penetrate the medium until $\omega > 342$ MeV. Pion production from the protons and neutrons dominates the absorption up to about 2 GeV, then pair production becomes more important; however, both these processes are difficult to calculate accurately.

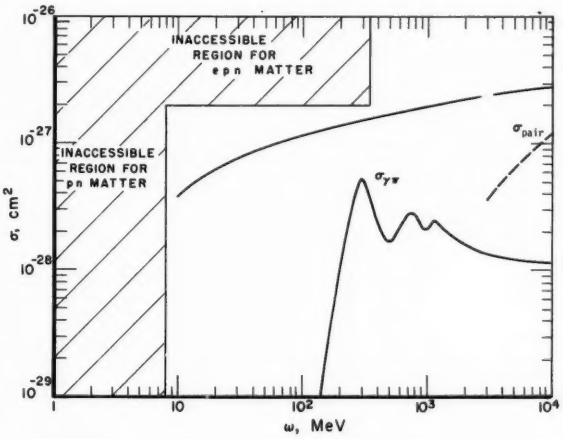

FIGURE 3. *Cross sections for dominant photoabsorption processes in nuclear matter.*

The vertical line at $\omega = 8$ MeV marks the frequency below which photons will not propagate in matter composed of protons and neutrons. The line at $\omega = 342$ MeV is the limiting energy for matter composed of electrons, protons, and neutrons. The solid curve labeled σ_{pair} is the absorption cross section per proton for e^+e^- production in *pn* matter: the dashed curve for *epn* matter. The curve labeled $\sigma_{\gamma\pi}$ is the free nucleon photo pion absorption cross section. This cross section is probably an upper limit to the process in nuclear matter Other photon interaction cross sections, Compton scattering, and nucleon pair absorption, are less that 10^{-29} cm² at all energies.

6. References

[1] Bethe, H. A., Theory of Nuclear Matter *in* Annual Review of Nuclear Science, Vol. **21**, 1971.

[2] Siemens, P. J., Nucl. Phys. **A141**, 225 (1970).

[3] Roy, R. R., and Reed, R. O., Interactions of Photons and Leptons with Matter (Academic Press, 1968).

[4] Weise, W., Hadronic Aspects of Photon-Nucleus Interactions, Physics Reports **136**, No. 2 (1974).

[5] Johnson, M., LAMPF Summer School on Pion-Nucleus Scattering, 1973, LA-5443-C.

[6] Müller, B., and Rafelski, J., Phys. Rev. Lett. **34**, 349 (1975).

(Paper 80A1-876)

JOURNAL OF RESEARCH of the National Bureau of Standards—A. Physics and Chemistry
Vol. 80A, No. 1, January–February 1976

A Study of the Polarization of Fluorescence of Ordered Systems With Application to Ordered Liquid Crystals

E. D. Cehelnik* and K. D. Mielenz

Institute for Materials Research, National Bureau of Standards, Washington, D.C. 20234

and

R. B. Cundall

Chemistry Department, The University of Nottingham, Nottington, NG72RD, England

(October 28, 1975)

The fluorescence polarization of uniaxial molecules dissolved in an ordered medium is studied. A theoretical model is developed which relates the polarization of the fluorescence emission to molecular structure, orientation of absorption and emission dipole oscillators and the degree of ordering. This theory was tested experimentally using all trans 1,6-diphenyl-1,3,5-hexatriene dissolved in an ordered liquid crystal.

Key words: 1,6-Diphenyl-1,3,5-hexatriene; fluorescence; linear dichroism; liquid crystals; polarization; spectrofluorimetry.

1. Introduction

In continuation of previous polarization studies of ordered liquid crystal [1, 2][1] and isotropic liquid systems [2, 3, 4], this work is concerned with the polarization of fluorescence by molecules dissolved in an ordered liquid crystal. A general theoretical model is developed that can be used with various linearly dichroic systems, such as streaming solutions or stretched polymer films, molecular crystals or membranes. The model is verified experimentally for the case of a fluorescent dye dissolved in an ordered nematic liquid crystal.

The liquid crystal solvent used here was a mixture of cholesteryl chloride and cholesteryl laurate [5, 2, 1]. These mixtures are normally cholesteric with a helical arrangement of the molecules. However, at a definite composition and temperature, T_{nem}, a nematic state results [5]. In the "unordered" nematic state of the mesophase the molecules are parallel within domaines. These domaines are oriented randomly with respect to each other thus giving the characteristic cloudiness and opacity of nematic liquid crystals. When an electric field is applied the domaines orient in such a way that the solvent molecules are parallel to the electric field [5].

The liquid crystal mixture (L.C.M.) changes from an opaque to a clear state within a few seconds, this change being reversible once the field is turned off. This ordering phenomenon can be used to order solute molecules which are dissolved in the L.C.M. at low concentrations. The L.C.M. used was a 1.95/1 by weight ratio of cholesteryl chloride to cholesteryl laurate, which is nematic at $T_{nem} = 30$ °C [5, 2, 1]. Ordering was achieved by application of an electric field of the order of 40 kV/cm.

*Present address: College of Environmental and Applied Science, Governor State University, Park Forest South, Illinois 60466.

[1] Figures in brackets indicate the literature references at the end of this paper.

The solute molecule used here as well as previously [1, 2] is 1,6-diphenyl-1,3,5-hexatriene (DPH), which is a long "rod like" molecule that absorbs light in the ultraviolet and fluoresces with a blue emission. DPH is fairly soluble in this L.C.M. and is aligned with its long molecular axis parallel to the direction of orientation of the ordered liquid crystal [1, 2].

2. Theory

2.1. Definitions and Outline of Approach

As a theoretical model for the fluorescence polarization of an ordered sample, we consider a collection of uniaxial solute molecules with absorption and emission dipole oscillators that have a fixed orientation with respect to the molecular axis as indicated in figure 1a. This fixed orientation is defined by three angles: ρ and δ, the angles between the unit vector in the direction of the molecular axis, $\mathbf{l}$, and the unit vectors in the directions of the absorption and emission dipole oscillators, $\mathbf{p}_0$ and $\mathbf{q}_0$, respectively; and v, the angle enclosed by the planes $(\mathbf{l}, \mathbf{p}_0)$ and $(\mathbf{l}, \mathbf{q}_0)$. Thus we have, relative to a molecular reference frame consisting of $\mathbf{l}$ and two arbitrarily chosen orthogonal unit vectors $\mathbf{m}$ and $\mathbf{n}$ in the plane perpendicular to $\mathbf{l}$,

$$\mathbf{p}_0 = [\cos \rho, \sin \rho \cos (u), \sin \rho \sin (u)], \tag{1a}$$

$$\mathbf{q}_0 = [\cos \delta, \sin \delta \cos (u+v), \sin \delta \sin (u+v)], \tag{1b}$$

where u is defined in figure 1a. A further angle defined by the molecular structure is θ, the angle between the absorption and emission dipole oscillators. According to eqs (1a, b), it is related to ρ, δ, and v by

$$\begin{aligned} \cos \theta &= \mathbf{p}_0 \cdot \mathbf{q}_0 \\ &= \cos \rho \cos \delta + \sin \rho \sin \delta \cos (v). \end{aligned} \tag{1c}$$

It will be assumed that each molecule can rotate about its molecular axis. Then, different molecules have rotated through different angles u at the time of excitation so that, for the sample as a whole, u is a random variable. The angle v that enters into the theory depends on the relative orientation of the absorption dipole oscillator $\mathbf{p}_0$ *at the time of absorption* with respect to the emission dipole oscillator $\mathbf{q}_0$ *at the time of emission*. Therefore, v becomes equal to the intramolecular angle shown in figure 1a in the borderline case of molecules that do not rotate appreciably during the time interval between absorption and emission, but becomes a random variable for a large number of molecules that rotate fast and have long fluorescence lifetimes. The theory presented here treats the general case in which v falls anywhere within this range.

The ordering of the molecules is produced by an external force, such as an electric or magnetic field, that is applied to the sample. It is assumed that this force hinders the tumbling motion of the individual molecular axes so that, for each molecule, the angle χ between the molecular axis and the direction of the applied force does not change appreciably between the times of absorption and emission. The applied force produces a preferential orientation of the molecular axes with respect to the x axis of the laboratory reference frame in figure 1b. This alinement of the molecules is defined by a distribution function $f(\chi)$, so that $f(\chi) \sin \chi d\chi$ is proportional to the number of molecules with molecular axes that enclose angles between χ and $\chi + d\chi$ with the x axis. The angular distribution of the molecular axes is assumed to be symmetric about the x axis, so that $f(-\chi) = f(\chi)$; and it is also assumed that the probabilities for "upside-up" and "upside-down" alinement of a molecule are the same, so that $f(\chi + \pi) = f(\chi)$. A suitable form for $f(\chi)$ is the quasi-gaussian distribution function used in an earlier paper [1],

$$f(\chi) = e^{\kappa(|\cos \chi| - 1)}, \tag{2a}$$

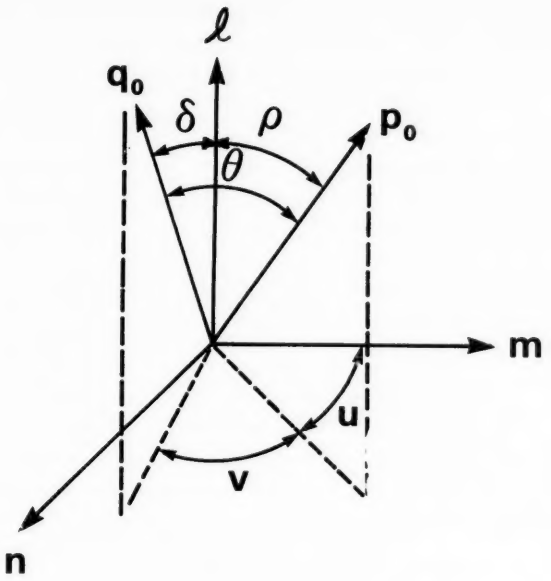

(1a)

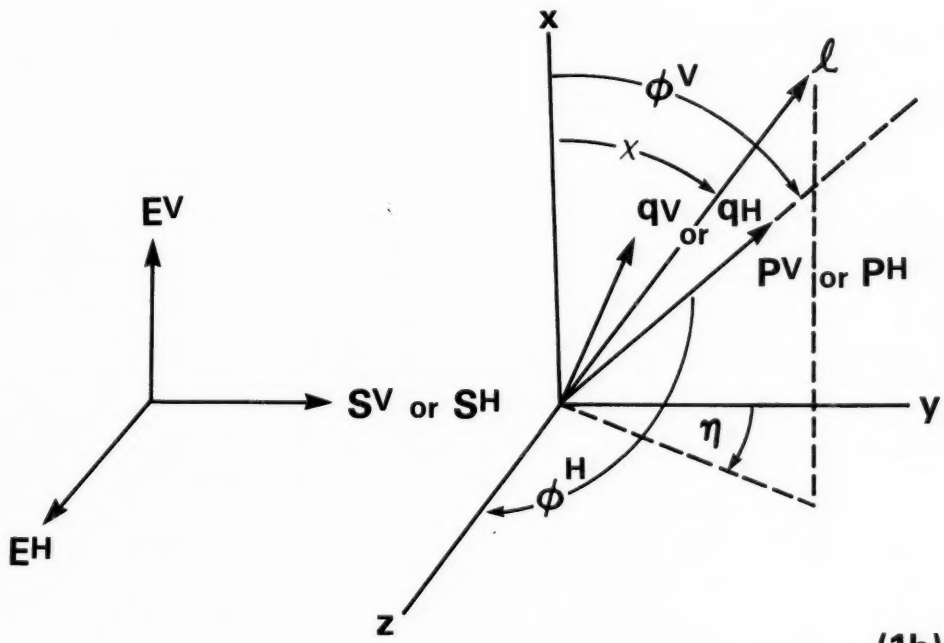

(1b)

FIGURE 1. *Diagrams of the model showing the molecular reference frame (1a) and the laboratory reference frame (1b) where* p *refers to the absorption dipole,* q *refers to the emission dipole and* l *refers to the long molecular axis of the molecule.*

597-633 O - 76 - 2

where $e^{\kappa} = f(0)/f(\pi)$ defines the proportion of molecules oriented parallel and perpendicular to the x axis, respectively. This function $f(\chi)$ leads to the following closed expressions for the averages of $\cos^2\chi$ and $\cos^4\chi$ that will appear in the equations to be developed:

$$N \equiv \overline{\cos^2\chi} \equiv \frac{\int_{-\pi}^{\pi} \cos^2\chi f(\chi) \sin \chi d\chi}{\int_{-\pi}^{\pi} f(\chi) \sin \chi d\chi}$$

$$= \frac{\kappa^2 - 2\kappa + 2(1 - e^{-\kappa})}{\kappa^2(1 - e^{-\kappa})}, \tag{2b}$$

$$M \equiv \overline{\cos^4\chi} \equiv \frac{\int_{-\pi}^{\pi} \cos^4\chi f(\chi) \sin \chi d\chi}{\int_{-\pi}^{\pi} f(\chi) \sin \chi d\chi}$$

$$= \frac{\kappa^4 - 4\kappa^3 + 12\kappa^2 - 24\kappa + 24(1 - e^{-\kappa})}{\kappa^4(1 - e^{-\kappa})}. \tag{2c}$$

A plot of N and M versus κ is reproduced in figure 2. The limits of N are 1/3 for a random distribution of absorbing molecules ($f(\chi) \equiv 1$) and 1.0 for perfect ordering ($f(\chi) \equiv$ Dirac delta func-

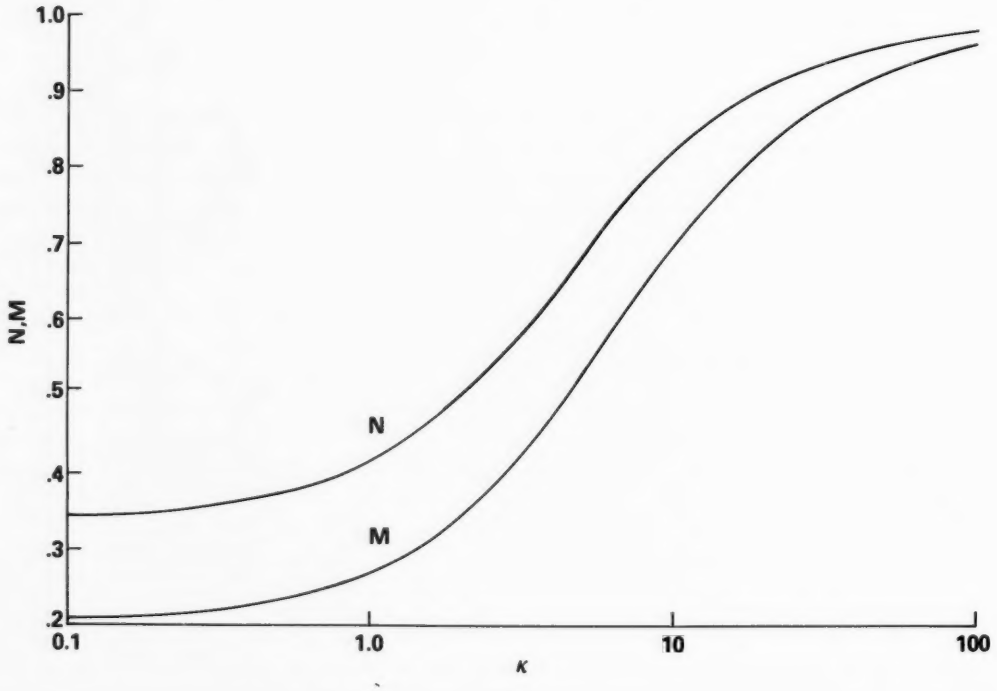

FIGURE 2. *Calculated plots of the two orientation terms* N *and* M *as a function of one adjustable parameter* κ *where the distribution function is assumed to be of the form,* $f(\chi) = e^{\kappa(|\cos\chi|-1)}$.

tion). The corresponding limits for M are 1/5 and 1.0 respectively. The transition between these two borderline cases depends on the specific form of $f(\chi)$.

As also indicated in figure 1b, the exciting radiation is assumed to be incident upon the sample in the y-direction of the laboratory reference frame, and is assumed to be plane polarized with its electric field vector, $\mathbf{E}^V$ or $\mathbf{E}^H$, parallel to the x or z axes. The corresponding photon flux densities of the exciting radiation are denoted by S^V and S^H, respectively. The squared magnitudes of the absorption and emission dipole vectors $\mathbf{p}$ and $\mathbf{q}$ are taken to be equal to the probabilities for absorption and emission by a molecule, so that for excitation with vertically polarized radiation,

$$|\mathbf{p}^V|^2 = S^V\sigma_0\cos^2\phi^V, \quad |\mathbf{q}^V|^2 = Q|\mathbf{p}^V|^2, \tag{3a}$$

and for excitation with horizontally polarized radiation,

$$|\mathbf{p}^H|^2 = S^H\sigma_0\cos^2\phi^H, \quad |\mathbf{q}^H|^2 = Q|\mathbf{p}^H|^2, \tag{3b}$$

where the superscripts V and H denote the polarization of the exciting radiation. Here, ϕ^V and ϕ^H are the respective angles between the absorption oscillator and the exciting electric field, σ_0 is the absorption cross section for absorption oscillators that are parallel to the exciting field, and Q is the fluorescence quantum yield.

The components of the absorption and emission dipole vectors with respect to the laboratory axes can now be calculated as follows. According to figure 1b we have

$$\mathbf{l} = (\cos\chi, \sin\chi\cos\eta, \sin\chi\sin\eta), \tag{4a}$$

where η is a random angle because of the rotation of the molecule about the molecular axis. Then, the two unit vectors

$$\mathbf{m} = (-\sin\chi, \cos\chi\cos\eta, \cos\chi\sin\eta), \tag{4b}$$

$$\mathbf{n} = (0, -\sin\eta, \cos\eta)$$

(not shown in figure 1b) may be taken to represent the other two axes of the molecular reference frame, so that

$$\mathbf{A} = \begin{pmatrix} \cos\chi & -\sin\chi & 0 \\ \sin\chi\cos\eta & \cos\chi\cos\eta & -\sin\eta \\ \sin\chi\sin\eta & \cos\chi\sin\eta & \cos\eta \end{pmatrix} \tag{4d}$$

is a suitable matrix to transform molecular coordinates into laboratory coordinates. Hence, eqs (1a) and (4d) show that the x and z components of the unit vector in the direction of the absorption dipole oscillator $\mathbf{p}$ in figure 1b are

$$(\mathbf{Ap}_0)_x \equiv \cos\phi^V = \cos\chi\cos\rho - \sin\chi\sin\rho\cos(u), \tag{5a}$$

$$(\mathbf{Ap}_0)_z \equiv \cos\phi^H = \sin\chi\sin\eta\cos\rho + \cos\chi\sin\eta\cos(u) + \cos\eta\sin(u)\sin\rho. \tag{5b}$$

Similarly, eqs (1b) and (4d) yield the unit vector $\mathbf{Aq}_0$ in the direction of the emission dipole oscillator $\mathbf{q}$, so that

$$\mathbf{q}^V = \sqrt{\sigma_0 Q S^V}\,(\mathbf{Ap}_0)_x\mathbf{Aq}_0, \tag{6a}$$

$$\mathbf{q}^H = \sqrt{\sigma_0 Q S^H}\,(\mathbf{A}\mathbf{p}_0)_z \mathbf{A}\mathbf{q}_0, \tag{6b}$$

according to eqs (3a, b) and (6a, b). Here,

$$(\mathbf{A}\mathbf{q}_0)_x = \cos\chi\cos\delta - \sin\chi\sin\delta\cos(u+v), \tag{7a}$$

$$(\mathbf{A}\mathbf{q}_0)_y = \sin\chi\cos\eta\cos\delta + [\cos\chi\cos\eta\cos(u+v) - \sin\eta\sin(u+v)]\sin\delta, \tag{7b}$$

$$(\mathbf{A}\mathbf{q}_0)_z = \sin\chi\sin\eta\cos\delta + [\cos\chi\sin\eta\cos(u+v) + \cos\eta\sin(u+v)]\sin\delta. \tag{7c}$$

In order to describe the sample as a whole, these expressions must be replaced by their rms averages for a large number of molecules.

The fluorescence intensity I emitted by the sample into a given viewing direction is proportional to the squared rms components of $\mathbf{q}^V$ and $\mathbf{q}^H$ in the plane perpendicular to the viewing direction, and is polarized in the directions of these components. Therefore, the four intensity readings that are obtained for the four possible combinations of vertical and horizontal setting of a pair of excitation and emission polarizers are, for 90° viewing in the direction of the z axis,

$$R_V^V(90°) = T_V k\,\overline{(q_x^V)^2},\ R_H^V(90°) = T_H k\,\overline{(q_y^V)^2}, \tag{8a}$$

$$R_V^H(90°) = T_V k\,\overline{(q_x^H)^2},\ R_H^H(90°) = T_H k\,\overline{(q_y^H)^2}, \tag{8b}$$

and for 180° viewing in the direction of the y axis,

$$R_V^V(180°) = T_V k\,\overline{(q_x^V)^2},\ R_H^V(180°) = T_H k\,\overline{(q_z^V)^2}, \tag{8c}$$

$$R_V^H(180°) = T_V k\,\overline{(q_x^H)^2},\ R_H^H(180°) = T_H k\,\overline{(q_z^H)^2}, \tag{8d}$$

Here, superscripts and subscripts denote the respective settings of the excitation and emission polarizers, T_V and T_H are the responsivities of the emission detection system for vertically and horizontally polarized light, and k is a geometry factor.

At any other viewing angle, the readings obtained can be expressed as linear combinations of the 90° and 180° readings. For example, for an arbitrary viewing angle α, the reading with both polarizers in the horizontal position is

$$\begin{aligned} R_H^H(\alpha) &= R_H^H(90°)\sin^2(\alpha) + R_H^H(180°)\cos^2(\alpha) \\ &= T_H k\,[(q_y^H)^2\sin^2(\alpha) + (q_z^H)^2\cos^2(\alpha)]. \end{aligned} \tag{8e}$$

2.2. Derivation of Equations

The six vector coordinates that completely define the system are found by combining eqs (5a) and (5b) with eqs (7a), (7b), and (7c) to give

$$(q_x^V)^2 = S^V\sigma_0 Q(\mathbf{A}\mathbf{p}_0)_x(\mathbf{A}\mathbf{q}_0)_x \tag{9a}$$

$$(q_y^V)^2 = S^V\sigma_0 Q(\mathbf{A}\mathbf{p}_0)_x(\mathbf{A}\mathbf{q}_0)_y \tag{9b}$$

$$(q_z^V)^2 = S^V\sigma_0 Q(\mathbf{A}\mathbf{p}_0)_x(\mathbf{A}\mathbf{q}_0)_z \tag{9c}$$

$$(q_x^H)^2 = S^H\sigma_0 Q(\mathbf{A}\mathbf{p}_0)_z(\mathbf{A}\mathbf{q}_0)_x \tag{9d}$$

$$(q_y^H)^2 = S^H \sigma_0 Q (\mathbf{Ap}_0)_z \, (\mathbf{Aq}_0)_y \tag{9e}$$

$$(q_z^H)^2 = S^H \sigma_0 Q (\mathbf{Ap}_0)_z \, (\mathbf{Aq}_0)_y . \tag{9f}$$

In this work, the averaging of these expressions was done in three steps. First the terms were multiplied through and averaged with respect to all possible angles u using

$$\frac{\int_0^{2\pi} \cos u \, du}{\int_0^{2\pi} du} = 0, \qquad \frac{\int_0^{2\pi} \cos^2 u \, du}{\int_0^{2\pi} du} = \frac{1}{2}$$

$$\frac{\int_0^{2\pi} \cos^3 u \, du}{\int_0^{2\pi} du} = 0, \qquad \frac{\int_0^{2\pi} \cos^4 u \, du}{\int_0^{2\pi} du} = \frac{3}{8}, \tag{10}$$

u being a random variable. Next they were averaged over all possible angles η, using analogous equations to eqs (10) since η was also assumed to be a random variable. Finally the terms were collected and expressed as functions of N and M as given by eqs (2b) and (2c). The resultant expressions were found to be

$$\overline{(q_x^V)^2}/S^V \sigma_0 Q = \left(\frac{17M - 10N + 1}{8}\right) AB + \left(\frac{1 - 2N + M}{4}\right) C + 2(N - M)\, D + \left(\frac{6N - 5M - 1}{8}\right) (A + B) + \left(\frac{1 - 2N + M}{4}\right), \tag{11a}$$

$$(q_y^V)^2/S^V \sigma_0 Q = \; (q_z^V)^2/S^V \sigma_0 Q = \left(\frac{10N - 17M - 1}{16}\right) AB + \left(\frac{2N - M - 1}{8}\right) C + (M - N) D + \left(\frac{5M + 6N - 3}{16}\right) A + \left(\frac{5M - 6N + 1}{16}\right) B + \left(\frac{3 - 2N - M}{16}\right), \tag{11b, c}$$

$$\overline{(q_x^H)^2}/S^H \sigma_0 Q = \left(\frac{10N - 17M - 1}{16}\right) AB + \left(\frac{2N - M - 1}{8}\right) C + (M - N)\, D + \left(\frac{5M - 6N + 1}{16}\right) A + \left(\frac{5M + 6N - 3}{16}\right) B + \left(\frac{3 - 2N - M}{16}\right), \tag{11d}$$

$$\overline{(q_y^H)^2}/S^H \sigma_0 Q = \left(\frac{17M + 22N - 15}{64}\right) AB + \left(\frac{M - 10N + 1}{32}\right) C + \left(\frac{2N - M - 1}{4}\right) D + \left(\frac{11 - 30N - 5M}{64}\right) (A + B) + \left(\frac{M + 22N + 1}{64}\right), \tag{11e}$$

$$\overline{(q_z^H)^2}/S^H \sigma_0 Q = \left(\frac{51M - 62N + 19}{64}\right) AB + \left(\frac{3M + 2N + 3}{32}\right) C + \left(\frac{2N - 3M + 1}{4}\right) D + \left(\frac{6N - 15M + 1}{64}\right) (A + B) + \left(\frac{3M + 2N + 3}{64}\right); \tag{11f}$$

where

$$A = \cos^2 \rho$$

$$B = \cos^2 \delta$$

$$C = \sin^2 \rho \sin^2 \delta \cos^2 v$$

$$D = \cos \rho \cos \delta \sin \rho \sin \delta \cos v.$$

The six general expressions can now be expressed in their final form of a contribution due to a dependence on ρ only and composite contributions of ρ, δ, and v.

These are

$$\overline{(q_x^V)^2}/S^V\sigma_0 Q = (a^V + 2b^V) \tag{12a}$$

$$\overline{(q_y^V)^2}/S^V\sigma_0 Q = (q_z^V)^2/S^V\sigma_0 Q = (a^V - b^V) \tag{12b, c}$$

$$\overline{(q_x^H)^2}/S^H\sigma_0 Q = (a^H - b^H + 2c^H) \tag{12d}$$

$$\overline{(q_y^H)^2}/S^H\sigma_0 Q = (a^H - b^H - c^H) \tag{12e}$$

$$\overline{(q_z^H)^2}/S^H\sigma_0 Q = (a^H + 2b^H - c^H) \tag{12f}$$

where

$$a^V = \frac{1}{6}\left[N(3\cos^2 \rho - 1) + \sin^2 \rho\right],$$

$$b^V = \frac{1}{24}\left[(9M - 6N + 1)\cos^2 \rho - (3M - 4N + 1)\right](3\cos^2 \delta - 1)$$

$$+ (N - M)\cos \rho \cos \delta \sin \rho \sin \delta \cos v$$

$$+ \frac{1}{16}(M - 2N + 1)(2\cos^2 v - 1)\sin^2 \rho \sin^2 \delta,$$

$$a^H = \frac{1}{12}\left\{2 - \left[\sin^2 \rho + N(3\cos^2 \rho - 1)\right]\right\},$$

$$b^H = \left(\frac{M - 2N + 1}{48}\right)(3\cos^2 \delta - 1)(3\cos^2 \rho - 1)$$

$$+ \left(\frac{M - 1}{6}\right)\cos \rho \cos \delta \sin \rho \sin \delta \cos v$$

$$+ \left(\frac{M + 6n + 1}{96}\right)(2\cos^2 v - 1)\sin^2 \rho \sin^2 \delta,$$

$$c^H = \frac{1}{96}\left[(5M + 6N - 3) - (15M - 6N - 1)\cos^2 \rho\right](3\cos^2 \delta - 1)$$

$$+ \left(\frac{5M - 6N + 1}{12}\right)\cos \rho \cos \delta \sin \rho \sin \delta \cos v$$

$$+ \left(\frac{18N - 5M - 5}{192}\right)(2\cos^2 v - 1)\sin^2 \rho \sin^2 \delta.$$

The total intensities emitted by the sample for the two types of excitation, vertical and horizontal, are thus,

$$\overline{(q^V)^2}/S^V\sigma_0 Q = [\overline{(q_x^V)^2} + \overline{(q_y^V)^2} + \overline{(q_z^V)^2}]/S^V\sigma_0 Q = 3a^V$$

$$= \frac{N(3\cos^2\rho - 1) + \sin^2\rho}{2} \tag{13a}$$

$$\overline{(q^H)^2}/S^H\sigma_0 Q = [\overline{(q_x^H)^2} + \overline{(q_y^H)^2} + \overline{(q_z^H)}]/S^V\sigma_0 Q = 3a^H$$

$$= \frac{2 - \sin^2\rho - N(3\cos^2\rho - 1)}{4}. \tag{13b}$$

Since the total intensity emitted by the sample is directly proportional to the total intensity absorbed the dichroic ratio for absorption can be given by

$$D_a = \overline{(q^V)^2}/\overline{q^H)^2} = \frac{S^V}{S^H}\frac{2N + (1 - 3N)\sin^2\rho}{(1 - N) + \frac{1}{2}(3N - 1)\sin^2\rho}. \tag{13c}$$

This equation is the same as the one derived in [1] for the absorption of polarized light by molecules oriented in an ordered liquid crystal.

At this point it is desirable to test eqs (12a–f) for two limiting cases of M and N to check the correctness of the derivation.

(a) *Perfect ordering, $N=1.0$, $M=1.0$.* Under these conditions the six expressions reduce to

$$\overline{(q_x^V)_{0r}^2}/S^V\sigma_0 Q = \cos^2\rho\cos^2\delta \tag{14a}$$

$$\overline{(q_y^V)_{0r}^2}/S^V\sigma_0 Q = \overline{(q_z^r)_{0r}^2}/S^V\sigma_0 Q = \frac{1}{2}\cos^2\rho\sin^2\delta \tag{14b, c}$$

$$\overline{(q_x^H)_{0r}^2}/S^H\sigma_0 Q = \frac{1}{2}\cos^2\delta\sin^2\rho \tag{14d}$$

$$\overline{(q_y^H)_{0r}^2}/S^H\sigma_0 Q = \frac{1}{8}\{3(\cos^2\rho - 1)(\cos^2\delta - 1) - 2\sin^2\rho\sin^2\delta\cos^2 v\} \tag{14e}$$

$$\overline{(q_z^H)_{0r}^2}/S^H\sigma_0 Q = \frac{1}{8}\{(\cos^2\rho - 1)(\cos^2\delta - 1) + 2\sin^2\rho\sin^2\delta\cos^2 v\} \tag{14f}$$

These equations show the interplay of the three angles which define the molecule. If these equations are used to calculate the total flux emitted by the sample for the two types of excitation, the following are obtained,

$$\overline{(q^V)^2_{0r}} \equiv \overline{(q^V_x)^2_{0r}} + \overline{(q^V_y)^2_{0r}} + \overline{(q^V_z)^2_{0r}}$$

$$= S^V \sigma_0 Q \cos^2 \rho, \tag{15a}$$

$$\overline{(q^H)^2_{0r}} \equiv \overline{(q^H_x)^2_{0r}} + \overline{(q^H_y)^2_{0r}} + \overline{(q^H_z)^2_{0r}}$$

$$= S^H \sigma_0 Q \frac{1}{2} \sin^2 \rho. \tag{15b}$$

These equations show the correct dependence on ρ and that the dependence on δ and v drops out. Thus if $\rho = 0°$ (absorption dipole oscillator along the long molecular axis), vertically polarized light is absorbed since all the long molecular axes are aligned in the vertical direction (parallel to electric field) and horizontally polarized light is not absorbed.

(b) *Random distribution, $N = 1/3$, $M = 1/5$.* Under these conditions eqs (12a-f) reduce to

$$\overline{(q^V_{x_r})^2}/S^V \sigma_0 Q = \overline{(q^H_{z_r})^2}/S^H \sigma_0 = \frac{1}{15} \{2 \cos^2 \rho \cos^2 \delta + 2 \sin^2 \rho \sin^2 \delta \cos^2 v$$

$$+ 4 \cos \rho \cos \delta \sin \rho \sin \delta \cos v + 1\}$$

$$= \frac{1}{15} (2 \cos^2 \theta + 1) \tag{16a}$$

$$\overline{(q^V_{y_r})^2}/S^V \sigma_0 Q = \overline{(q^V_{z_r})^2}/S^V \sigma_0 Q = \overline{(q^H_{x_r})^2}/S^H \sigma_0 Q = \overline{(q^H_{y_r})^2}/S^H \sigma_0 Q$$

$$= \frac{1}{15} \{2 - [\cos^2 \rho \cos^2 \delta + 2 \cos \rho \cos \delta \sin \rho \sin \delta \cos v + \sin^2 \rho \sin^2 \delta \cos^2 v]\}$$

$$= \frac{1}{15} (2 - \cos^2 \theta) \tag{16b}$$

where eq (1c) has been used to express the results in terms of θ. These equations are the same as the ones obtained in a previous paper on the polarization of fluorescence of a random but frozen distribution of absorbing molecules [3]. Notice that information on θ, the angle between the absorption and emission dipole oscillators, is easily obtained when polarizers are placed in the beams. When eqs (16a, b) are used to calculate the total flux emitted by the sample for vertically and horizontally polarized excitation, one obtains

$$(q^V_r)^2 \equiv \overline{(q^V_{x_r})^2} + \overline{(q^V_{y_r})^2} + \overline{(q^V_{z_r})^2}$$

$$= \frac{1}{3} S^V \sigma_0 Q, \tag{17a}$$

$$(q^H_r)^2 \equiv \overline{(q^H_{x_r})^2} + \overline{(q^H_{y_r})^2} + \overline{(q^H_{z_r})^2}$$

$$= \frac{1}{3} S^H \sigma_0 Q. \tag{17b}$$

This result shows that the sample is an isotropic absorber and that there is no dependence on ρ, as there was in the case of perfect ordering shown by eqs (15a, b).

2.3. Application to the DPH-liquid crystal system

Previous studies have shown [1, 2] that the longest wavelength absorption band of DPH is due to a transition involving the fully conjugated molecule and that the absorption dipole oscillator lies along the long molecular axis; i.e., $\rho = 0°$. Also, the fluorescence emission dipole oscillator is almost parallel to the absorption dipole oscillator [1, 2], and therefore it also lies along the long molecular axis; i.e., $\delta = \theta = v = 0°$. Finally it has been shown that for DPH dissolved in the ordered liquid crystal mixture used here, the excited DPH molecules do not rotate at all during the time interval between absorption and emission [2]. With these conditions, the six expressions given by eqs (12a–f) reduce to

$$\overline{(q_x^V)^2}/S^V\sigma_1 Q = M, \tag{18a}$$

$$\overline{(q_y^V)^2}/S^V\sigma_0 Q = \overline{(q_z^V)^2}/S^V\sigma_0 Q = \overline{(q_x^H)^2}/S^H\sigma_0 Q = \left(\frac{N-M}{2}\right), \tag{18b, c, d}$$

$$\overline{(q_y^H)^2}/S^H\sigma_0 Q = \left(\frac{1-2N+M}{8}\right) \tag{18e}$$

$$\overline{(q_z^H)^2}/S^H\sigma_0 Q = 3\left(\frac{1-2N+M}{8}\right). \tag{18f}$$

The fluorescence intensity readings which one obtains for the two viewing positions, 90° (rt angle) and 180° (straight through), of an ordered DPH sample can now be written with reference to eqs (8a–d) as

$$R_V^V(90°) = R_V^V(180°) = kS^H T_H\, FG\sigma_0 Q\, M, \tag{19a}$$

$$R_H^V(90°) = R_H^V(180°) = kS^H T_H\, F\, \sigma_0 Q\left(\frac{N-M}{2}\right), \tag{19b}$$

$$R_V^H(90°) = R_V^H(180°) = kS^H T_H\, G\, \sigma_0 Q\left(\frac{N-M}{2}\right), \tag{19c}$$

$$R_H^H(90°) = kS^H T_H \sigma_0 Q\left(\frac{1-2N+M}{8}\right), \tag{19d}$$

$$R_H^H(180°) = kS^H T_H \sigma_0 Q\frac{3}{8}(1-2N+M), \tag{19e}$$

where $F \equiv S^V/S^H$ is the polarization ratio of the exciting flux reaching the sample and $G \equiv T_V/T_H$ is the polarization ratio of the emission detection system. As written, F and G are instrumental parameters and, with this liquid crystal system, can be determined easily since the unordered liquid crystal (i.e., no electric field applied to the sample) is cloudy and opaque, and acts as a light scatterer and depolarizer. Thus randomized fluorescence intensity readings, analogous to those given by eqs (19a–e), can be taken with the electric field off, and can be expressed as

$$R_V^V(90°)_r = R_V^V(180°)_r = k_r S^H T_H FG\sigma_0 Q, \tag{20a}$$

$$R_H^V(90°)_r = R_H^V(180°)_r = k_r S^H T_H F \sigma_0 Q, \tag{20b}$$

$$R_V^H(90°)_r = R_V^H(180°)_r = k_r S^H T_H G \sigma_0 Q, \tag{20c}$$

$$R_H^H(90°)_r = R_H^H(180°)_r = k_r S^H T_H \sigma_0 Q. \tag{20d}$$

where k_r differs from k due to the scattering of the unordered crystal.

Taking the following ratios

$$F = \frac{R_V^V(90°)_r}{R_V^H(90°)_r} = \frac{R_H^V(90°)_r}{R_H^H(90°)_r} = \frac{R_V^V(180°)_r}{R_V^H(180°)_r} = \frac{R_H^V(180°)_r}{R_H^H(180°)_r}, \tag{21a}$$

$$G = \frac{R_V^V(90°)_r}{R_H^V(90°)_r} = \frac{R_V^H(90°)_r}{R_H^H(90°)_r} = \frac{R_V^V(180°)_r}{R_H^V(180°)_r} = \frac{R_V^H(180°)_r}{R_H^H(180°)_r}, \tag{21b}$$

gives estimates of F and G for the two different viewing positions. If the sample is a point source emitter, and if the two viewing positions, 90° and 180°, are equivalent in terms of the solid angle of emission collected, then not only should the estimates of F and G at each viewing position agree with one another but also the individual readings, such as $R_V^V(90°)_r$ and $R_V^V(180°)_r$, should agree. These two conditions, as well as the assumption that the solvent does not absorb any of the exciting light are inherent in the derivation of the equations and, as will be shown, must be modified if they do not apply. Nevertheless, corresponding readings of the two sets of data (field on and field off) can always be divided to give

$$VV(90°) = VV(180°) = k'M, \tag{22a}$$

$$VH(90°) = VH(180°) = k'\left(\frac{N-M}{2}\right), \tag{22b}$$

$$HV(90°) = HV(180°) = k'\left(\frac{N-M}{2}\right), \tag{22c}$$

$$HH(90°) = k'\left(\frac{1-2N+M}{8}\right), \tag{22d}$$

$$HH(180°) = k'\frac{3}{8}\left(1-2N+M\right), \tag{22e}$$

where $k' = k/k_r$ and $VV(90°) = R_V^V(90°)/R_V^V(90°)_r$, etc. The first letter of this new notation refers to the mode of the excitation polarizer and the second to the emission polarizer. Ratios of these equations will give information on the values of N and M that the sample exhibits.

3. Experimental Data [6]

Experimental data were taken using two different spectrofluorimeters. Preliminary data were taken using the Nottingham spectrofluorimeter [7], which is a right-angle viewing instrument. Polacoat 105 UV-visible polarizers were used in both the excitation and emission beams. The sample used was a 7.2×10^{-5} g DPH/1.055g L.C.M. mixture where the L.C.M. was also a 1.95/1 by weight mixture of cholesterol chloride to cholesterol laurate [5]. The sample cell consisted of a piece of 7.5 mm diameter Spectrosil tubing with a stationary bottom electrode and an adjustable top electrode with the liquid crystal mixture sandwiched between. A detailed description of this cell is

given in [2]. The cylindrical cell was enclosed in a three-windowed aluminum heating block. The nominal electrode gap used was ~ 4 mm and the temperature of the system was kept at $T_{nem} = 30 \pm 1$ °C.

Additional data, allowing a test of the above theory, were taken using the new NBS goniospectrofluorimeter [8]. This versatile instrument allows viewing of a cylindrical sample from any arbitrary viewing angle from about 20° to 180°. However, the three-windowed aluminum heating block used in study limited the viewing of the liquid crystal sample cell to the 90° and 180° viewing positions. The sample cell used here was similar to the one above except that 3 mm diameter tubing and electrodes were used. Also, a lower concentration of DPH in the L.C.M. was used—1.2×10^{-7} DPH/1.104g L.C.M. This was done to approximate a point source sample by making the cell physically small, and also by keeping the light intensity constant as it propagated through the cell. Glan-Taylor polarizers were used with this instrument with a Corning 7–54 filter placed in the excitation beam and a 1 cm path length cut-off filter (saturated solution of $NaNO_2$ in water) in the emission beam. The filter combination allowed viewing of the sample cell at 180° (straight through) by reducing the amount of scattered and/or nonabsorbed exciting light which reached the detector. Again, the electrode gap used was 4 mm and the temperature of the cell was kept at 30 ± 1 °C.

4. Results and Discussion

4.1. Degree of Polarization as a Function of Applied Electric Field Strength

Using the Nottingham spectrofluorimeter and sample, the excitation wavelength was set at $\lambda_{ex} = 370$ nm and the emission wavelength at $\lambda_{em} = 425$ nm. Without the electric field applied, the four readings $R_V^V(90°)_r$, $R_H^V(90°)_r$, $R_V^H(90°)_r$ and $R_H^H(90°)_r$ were taken. Then the electric field was applied in steps up to 60 kV/cm and the four readings $R_V^V(90°)$, $R_H^V(90°)$, $R_V^H(90°)$ and $R_H^H(90°)$ were taken at each voltage. These readings were then divided by the ones with the field off to give $VV(90°)$, $VH(90°)$, $HV(90°)$ and $HH(90°)$ for each voltage setting. These data are plotted in figure 3 against applied voltage and show that the readings reach steady state values after 30 kV/cm, thus showing that single domain conditions are achieved, and that as long as the voltage is above 30 kV/cm the signal level will remain constant and will be unaffected by small drifts in the electric field strength. Therefore, all further experiments were performed with voltages of 40 kV/cm.

4.2. Polarization as a Function of Wavelength

Again using the Nottingham spectrofluorimeter and sample, the emission wavelength was set at $\lambda_{em} = 425$ nm and the four readings with the electric field on—$R_V^V(90°)$, $R_H^V(90°)$, $R_V^H(90°)$ and $R_H^H(90°)$—were taken as a function of excitation wavelength from 245 to 400 nm. Ratios of these readings were then taken with reference to eqs (19a–e) to give

$$R_V^V(90°)/R_H^V(90°) = G\left(\frac{2M}{N-M}\right), \tag{23a}$$

$$R_V^H(90°)/R_H^H(90°) = G4\left(\frac{N-M}{1-2N+M}\right). \tag{23b}$$

These particular ratios were calculated so as to eliminate the parameter F, which is a function of excitation wavelength. Here, G is constant since the emission wavelength does not change. The two ratios are plotted in figure 4 and show that with excitation into the longest wavelength absorption band, determinations of N and M are wavelength independent thus indicating that there is indeed only one absorption dipole absorbing in this region. The two ratios become wavelength dependent at shorter wavelengths due to increased solvent absorption, and also due to the appearance of other

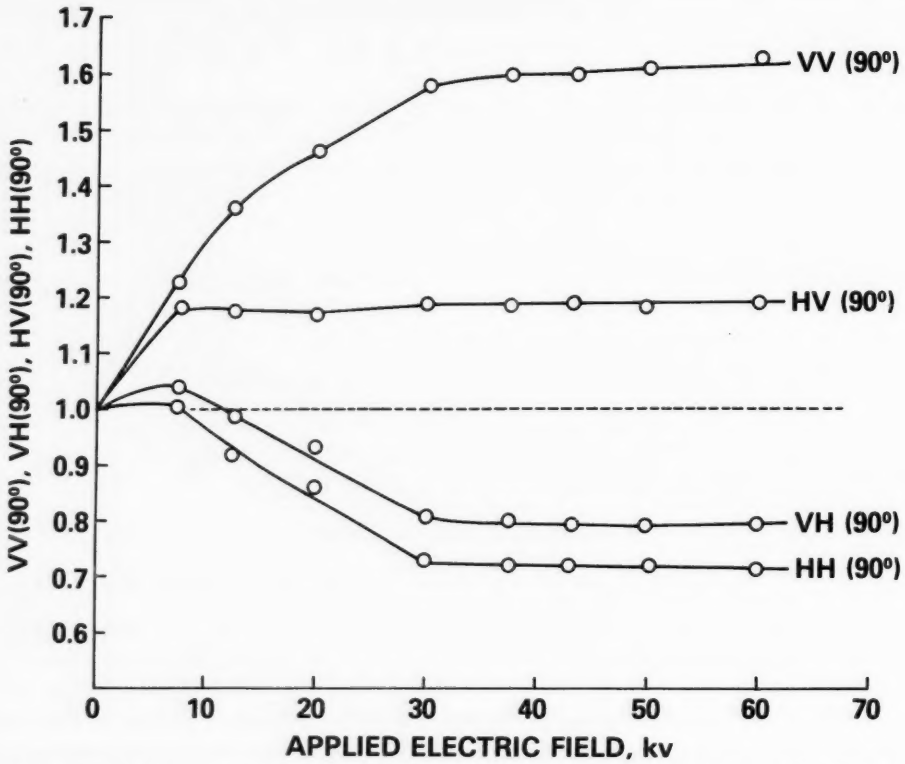

FIGURE 3. *Degree of polarization of an ordered sample as a function of applied electric field strength for the four sets of orthogonal polarizer settings.*

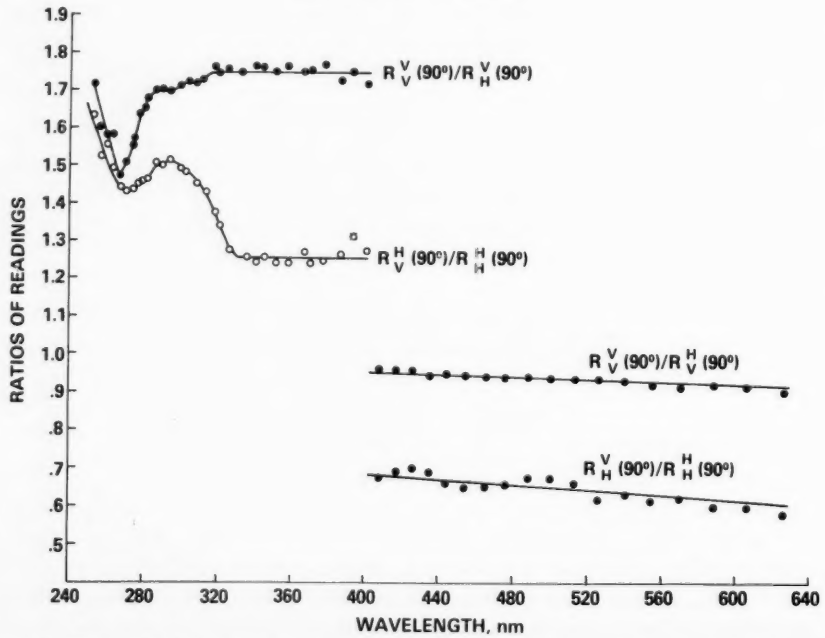

FIGURE 4. *Degree of polarization of an ordered sample as a function of excitation and emission wavelength.*

transitions in the absorption spectrum which have different angles between their absorption dipole oscillators and the long molecular axis [1]. Thus $\lambda_{ex} = 370$ nm was chosen at the optimum excitation wavelength.

With $\lambda_{ex} = 370$ nm, the four readings $R_V^V(90°)$, $R_H^V(90°)$, $R_V^H(90°)$ and $R_H^H(90°)$ were taken as a function of emission wavelength from 408 to 625 nm. The ratios

$$R_V^V(90°)/R_V^H(90°) = F\left(\frac{2M}{N-M}\right) \tag{23c}$$

$$R_H^V(90°)/R_H^H(90°) = 4F\left(\frac{N-M}{1-2N+M}\right) \tag{23d}$$

were then calculated and are also shown in figure 4. The nearly horizontal straight lines show that the degree of polarization of the fluorescence emission is also independent of emission wavelength, as one would expect, and that fluorescence occurs from only one emission dipole oscillator.

4.3. Quantitative Test of Theoretical Model

Using the NBS spectrofluorimeter and sample with the excitation wavelength set at λ_{ex}=370 nm and with the emission wavelength set at $\lambda_{em} = 465$ nm, fluorescence intensity readings were taken with and without the applied electric field at the two viewing positions, $\alpha = 90°$ and 180°. These data are shown in table 1. The readings with the electric field off were divided according to eqs (21a, b) to give the estimates of F and G shown in table 2. The agreement of the individual field off

TABLE 1

Experimental readings taken with and without the applied electric field for the determination of the degree of polarization of the fluorescence emission and for the determination of the correction factor due to the birefringence of the ordered liquid crystal solvent.

$\lambda_{ex} = 370$ nm $\lambda_{em} = 465$ nm	Field OFF		Field ON		Ratio $\frac{\text{ON}}{\text{OFF}}$	
	Volts		Volts		90°	180°
	90°	180°	90°	180°		
R_V^V	0.05295	0.05469	0.08422	0.15763	1.5906	2.8822
R_H^V	.09032	.08732	.06125	.11744	0.67814	1.3449
R_V^H	.09759	.10123	.08657	.15156	.88708	1.4972
R_H^H	.16486	.16176	.09116	.31235	.55295	1.9310
$\lambda_{ex} = 465$ nm						
$\lambda_{em} = 465$ nm						
$R_V^{V'}$	–	.31083	–	.21128		
$R_H^{V'}$	–	.49496	–	.01487		
$R_V^{H'}$	–	.53113	–	.02222		
$R_H^{H'}$	–	.84711	–	.92759		

TABLE 2

Table of instrumental polarization correction factors obtained from the data taken with the electric field off.

	$\lambda_{ex}=370$, $\lambda_{em}=465$		$\lambda_{ex}=465$, $\lambda_{em}=465$
	90°	180°	180°
$F=\frac{R_V^V(\alpha)_r}{R_V^H(\alpha)_r}$	0.543	0.540	0.585
$=\frac{R_H^V(\alpha)_r}{R_H^H(\alpha)_r}$	.548	.540	.584
$G=\frac{R_V^V(\alpha)_r}{R_H^V(\alpha)_r}$	.586	.626	.628
$=\frac{R_V^H(\alpha)_r}{R_H^H(\alpha)_r}$	.592	.626	.627

readings in table 1 for the two viewing positions, 90° and 180°, show that the sample is essentially a point source. The agreement of the values of F in table 2 show that the unordered liquid crystal is acting as a depolarizer. The values of G in table 2 agree for a given viewing angle but change when going from the 90° to the 180° viewing position. This is not surprising since the emission is being detected through two different windows in the heating block.

When the electric field is turned on, the individual polarization readings change from the values they had with the electric field off. However, the data in table 1 indicate that the two viewing positions are no longer equivalent since according to eqs (19a–e) only the R^H reading should have changed in going from 90° to 180° viewing, and then only by a factor of 3 instead of 3.43. Even if the assumed model for the DPH dipoles is in error the $R_V^V(90°)$ and $R_H^V(90°)$ readings should still equal the $R_V^V(180°)$ and $R_H^V(180°)$ readings respectively. Therefore, this discrepancy is attributed to the fact that, with the field on, the sample is no longer a point source. There are two reasons for this. First, the ordered liquid crystal mixture is strongly birefrigent and, therefore, not equivalent to the unordered sample. Thus, the G correction factor estimated from the latter is not quite correct. Secondly, the liquid crystal solvent has been shown to have its own dichroic ratio for absorption when the electric field is on and, therefore, will modify the polarization ratio F of the exciting radiation in wavelength regions of solvent absorption. Thus, the ratio of the field on to field off data as given by eqs (22a–e) should really be written as,

$$VV(\alpha) = k_\alpha(1 - e^{-A(V)})\ T_V'\ M \tag{24a}$$

$$VH(\alpha) = k_\alpha(1 - e^{-A(V)})\ T_H'\left(\frac{N-M}{2}\right) \tag{24b}$$

$$HV(\alpha) = k_\alpha\ (1 - e^{-A(H)})\ T_V'\left(\frac{N-M}{2}\right) \tag{24c}$$

$$HH(90°) = k_{90°}(1 - e^{-A(H)})\ T_H'\left(\frac{1-2N+M}{8}\right) \tag{24d}$$

$$HH(180°) = k_{180°}(1 - e^{-A(H)})\ T_H'\ \frac{3}{8}\ (1-2N+M) \tag{24e}$$

where $\alpha = 90°$ or 180°, $A(V)$ and $A(H)$ are the absorbances for vertically and horizontally polarized exciting light, respectively, T_V' is another responsivity factor for vertically polarized emission due to the birefrigence of the sample, and T_H' is the horizontal responsitivity. The proportionality constants $k_{90°}$ and $k_{180°}$ differ because the sample is no longer a point source.

The best way to eliminate any effect due to the solvent absorption is to obtain ratios only from the readings which have constant excitation polarization and constant viewing angle. Thus, we define the ratios

$$\frac{VV(90°)}{VH(90°)} = \frac{2M}{N-M} G' \tag{25a}$$

$$\frac{HV(90°)}{HH(90°)} = 4\left(\frac{N-M}{1-2N+M}\right) G' \tag{25b}$$

$$\frac{VV(180°)}{VH(180°)} = \frac{2M}{N-M} G' \tag{25c}$$

$$\frac{HV(180°)}{HH(180°)} = \frac{4}{3}\left(\frac{N-M}{1-2N+M}\right) G' \tag{25d}$$

where $G' = T_V'/I_H'$.

4.4. Determination of G'

The polarization ratio, G', due to the birefringence of the ordered liquid crystal solvent was determined experimentally by removing the filter in the excitation beam and setting the excitation monochromator wavelength to $\lambda_{ex} = 465$ nm to match the fluorescence emission wavelength. With the emission detection system set at the 180° viewing position the 465 nm flux was monitored as it propagated through the liquid crystal cell. The four intensity readings – $R_V^{V'}(180°)$, $R_H^{V'}(180°)$, $R_V^{H'}(180°)$ and $R_H^{H'}(180°)$ – were also taken with and without the applied electric field (see table 1). Since neither the liquid crystal solvent nor the DPH absorb at this wavelength the effect of the birefringence can now be determined directly. The readings with the electric field off were then divided according to eqs (21a) and (21b) to give estimates of G and F (465 nm) which are then given in table 2. The estimate of G agrees with the previous estimates derived from the fluorescence intensity readings, but the value of F (465 nm) differs from the value of F (370 nm) determined previously. This is to be expected since F is a function of excitation wavelength. The data obtained with the field on (table 1, bottom) show that the $R_H^{V'}(180°)$ and $R_V^{H'}(180°)$ readings are small compared to the $R_V^{V'}(180°)$ and $R_H^{H'}(180°)$ readings, thus showing that the ordered liquid crystal is not depolarizing the light as it propagates through the solution and any effect is thus due to the way the emission detection system views the birefringent sample. Thus the ratio of the $R_V^{V'}(180°)$ and $R_H^{H'}(180°)$ readings can be written as,

$$\frac{R_V^{V'}(180°)}{R_H^{H'}(180°)} = \frac{S^V T_V' T_V}{S^H T_H' T_H} = F\ (465\ \text{nm})\ G'G. \tag{26}$$

Solving eq (26) for G' using $R_V^V(180°) = 0.2113$, $R_H^H(180°) = 0.9276$, F 465 nm) = 0.5845 and $G = 0.6275$ gives a value of $G' = 0.6210$.

4.5. Determination of M and N

With G' determined, eqs (25a–d) can be rearranged to give

$$\frac{N}{M} = 2\frac{VH(90°)}{VV(90°)}G' + 1, \tag{27a}$$

$$\frac{1}{M} = 4\frac{HH(90°)}{HV(90°)}G'\left(\frac{N}{M} - 1\right) + 2\frac{N}{M} - 1, \tag{27b}$$

$$\frac{N}{M} = 2\frac{VH(180°)}{VV(180°)}G' + 1, \tag{27c}$$

$$\frac{1}{M} = \frac{4}{3}\frac{HH(180°)}{HV(180°)}G'\left(\frac{N}{M} - 1\right) + 2\frac{N}{M} - 1. \tag{27d}$$

Equations (27a) and (27b) can now be solved simultaneously, using the 90° data of the "Ratio" column in table 1 to obtain estimates of M and N. Likewise, eqs (27c) and (27d) with the 180° data in the same column will give estimates of M and N. These are tabulated in table 3a along with a value of κ for each estimate from the curves in figure 2.

In order to check the precision of these results, the measurements were repeated. The electric field was turned off and it was found that after a few minutes the sample returned reversibly to its initial unordered state, as the polarization readings were the same as those obtained before the electric field had been applied the first time. Then a second set of data was taken and processed in the same manner as before. The final results for N, M, and κ are given in table 3b, showing that for each viewing angle the M and N values of table 3a were reproduced to 0.01. Thus the differences of the M values for 90° and 180° viewing are within the experimental uncertainty for both sets of data. The values for N obtained for 180° viewing are, however, consistently higher than the 90° values by about three times the experimental reproducibility. This was also observed from preliminary data taken when the experiment was first being set up. Also the average value of $N = 0.55$ from the data in table 3 is lower than the value of 0.633 obtained previously [1] from a study of the absorption of polarized light by DPH molecules dissolved in the same L.C.M. This may be due to the fact that in this study the cylindrical sample cell has more bulk solution than the thin rectangular cell used in the absorption experiment. Another possibility is that the model of the DPH molecule may not be quite correct as far as the angles of the different dipoles oscillators are concerned. Small variations in angles or molecule movement could cause large changes in the magnitudes of N and M as well as differences of their values as a function of viewing angle as can be seen by examination of eqs (12a–f). The differences in the values of κ as determined from N data compared to M data can be attributed to the type of distribution function used if indeed the average values of N and M are correct.

TABLE 3

Calculated values of the orientation terms N and M evaluated from experimental data taken at two different viewing positions of the liquid crystal-DPH sample. The value of κ for each N and M is determined from the curves in figure 2.

(a) First Experiment

	M	κ	N	κ
90° Data	0.35	2.1	0.53	2.4
180° Data	.36	2.2	.57	2.9

(b) Second Experiment

	M	κ	N	κ
90° Data	0.34	2.0	0.53	2.4
180° Data	.35	2.1	.56	2.8

5. References and Note

[1] Cehelnik, E. D., Cundall, R. B., Timmons, C. J., and Bowley, R. M., Proc. R. Soc. Lond. A. **335,** 387–405 (1973).
Note: Equation V in this reference should read

$$D=\frac{A(\parallel)}{A(\perp)}=\frac{2N+(1-3N)\sin^2\phi}{(1-N)+\frac{1}{2}(3N-1)\sin^2\phi}.$$

Equation III should read

$$\ldots\ldots+\frac{1}{2}\bar{K}_2\,dn\,[2N+(1-3N)\sin^2\phi_2],$$

[2] Cehelnik, E. D., Cundall, R. B., Lockwood, J. R., and Palmer, T. F., J. Chem. Soc. Farad. Trans. II, **70,** 224–252, (1974).
[3] Cehelnik, E. D., Mielenz, K. D., and Velapoldi, R. A., J. Res. Nat. Bur. Stand. (U.S.), **79A** (Phys. and Chem.), No. 1, 1–16 (Jan.–Feb. 1975).
[4] Mielenz, K. D., Cehelnik, E. D., and McKenzie, R. L., Elimination of polarization bias in fluorescence intensity measurements, J. Chem. Phys. **64,** 370, (1976).
[5] Sackman, E., and Rehm, D., Chem. Phys. Letters **4,** 537, (1970).
[6] In order to describe materials and experimental procedures adequately, it is occasionally necessary to identify commercial products by manufacturer's name or label. In no instances does such identification imply endorsement by the National Bureau of Standards, nor does it imply that the particular product or equipment is necessarily the best available for that purpose.
[7] Cundall, R. B., and Evans, G. B., J. Sci. Instr. **1,** 305, (1968).
[8] Mielenz, K. D., to be published, see refs. 3 and 4 for a short description of the instrument.

(Paper 80A1–877)

597-633 O - 76 - 3

JOURNAL OF RESEARCH of the National Bureau of Standards—A. Physics and Chemistry
Vol. 80A, No. 1, January–February 1976

PVT and Vapor Pressure Measurements on Ethane*

G. C. Straty and R. Tsumura**

Institute for Basic Standards, National Bureau of Standards, Boulder, Colorado 80302

(October 15, 1975)

New measurements of the vapor pressures and *PVT* properties of ethane are reported. *PVT* determinations have been made from near the triple point to 320 K at pressures to 33 MPa. The density range investigated extends to more than three times the critical density. The new measurements of the vapor pressures of ethane extend from 160 K to near the critical point.

Key words: Density; ethane; vapor pressure; *PVT*.

1. Introduction

Liquefied fuel gases, such as LNG, are expected to play an increasing role in satisfying future energy requirements. Accurate thermophysical properties data for these liquefied gas mixtures are necessary for the design of liquefaction plants, transport equipment, shipping and receiving terminals, and for custody transfer. The near infinite variations in mixture compositions encountered with these fuel gases rule out completely experimental or strictly computational approaches for determining these properties. Calculation methods, based on accurate, wide range pure component data and selected mixtures data are being developed in a number of laboratories, and appear to offer the only reliable and economical approach for the generation of the necessary thermophysical properties.

This paper reports new measurements of vapor pressures and *PVT* properties of pure ethane. The measurements have been made as part of a comprehensive program to provide the required experimental data and to develop suitable calculation techniques for mixture properties determinations. *PVT* measurements have been made from near the triple point (90.348 K) [1][1] to 320 K at pressures up to 33 MPa. The density range extends to more than three times the critical density. The new measurements of the vapor pressures extend from 160 K to near the critical temperature (305 K).

2. Experimental Detail

To measure single-phase densities, the gas expansion technique was used. A series of pressure-temperature observations are made on a nearly constant density sample of fluid confined in a cell of accurately calibrated volume. When either the maximum pressure or maximum temperature is reached, the fluid is expanded, to low pressure, into large calibrated volumes maintained at an accurately known temperature above room temperature. The density can then be determined from the cell volume and the compressibility factor (PV/RT) of the ethane at the conditions of the expansion volumes.

The ethane used was commercially available research grade with specified minimum purity of 99.98 percent. This purity was verified by chromatographic analysis. Temperatures were measured on the IPTS (1968) with a platinum resistance thermometer calibrated by the National Bureau of Standards. Pressures above about 3 MPa were measured by referencing to oil pressures derived from an oil dead weight gauge accurate to within 0.015 percent. Lower pressures were measured with a precision fused quartz bourdon tube gauge which had been previously calibrated against an air dead weight gauge accurate to within 0.01 percent. The apparatus and procedures were similar to those used previously in this laboratory for measurements on several other cryogenic fluids [2–5] and have been described in detail [6–8]. Slight modification to existing apparatus was necessary because of the higher critical temperature of ethane. Those external parts of the system which contained fluid during a measurement were heated to well above the critical temperature (typically 330 K) in order to reduce the relative density of the fluid residing in these parts, permitting a more accurate adjusted density to be computed.

*This work was carried out at the National Bureau of Standards under the sponsorship of the American Gas Association, Inc.

**Consejo Nacional De Ciencia Y Tecnologia (CONACYT) Mexico City. Currently a guest worker with the Cryogenics Division, National Bureau of Standards, Institute for Basic Standards.

[1] Figures in brackets indicate the literature references at the end of this paper.

3. Results

With the techniques used here, each experimental *PVT* "run" consists of a number of pressure-temperature observations lying along a near-isochoric path. About 50 such runs were made covering a density range of from about 1.5 to over 21.5 mol/l. Each run consisted of from 5 to 16 *PVT* points, depending on the density. Measurements were always made at fixed temperatures to permit direct analysis in terms of isotherms. A total of over 450 *PVT* data points was determined. These data are tabulated along isotherms in table 1.

TABLE 1. PVT *data for ethane*

P (MPa)	ρ (mol/l)
$T=92.00$ K	
0.7928	21.629
$T=93.00$ K	
8.7870	21.682
$T=94.00$ K	
3.5870	21.599
10.4980	21.664
$T=96.00$ K	
6.3091	21.555
14.6217	21.641
$T=98.00$ K	
8.1853	21.503
19.1732	21.625
$T=100.00$ K	
1.7991	21.348
11.3755	21.468
23.8694	21.613
$T=102.00$ K	
4.7964	21.315
15.4890	21.448
28.5382	21.603
$T=104.00$ K	
1.1828	21.198
6.9584	21.269
19.9098	21.434
33.1959	21.594
$T=106.00$ K	
9.0567	21.221
24.4329	21.422
$T=108.00$ K	
1.8227	21.065
6.4514	21.125
12.4806	21.193
29.0045	21.412
$T=110.00$ K	
4.7101	21.034
16.4766	21.176
33.5810	21.403

P (MPa)	ρ (mol/l)
$T=112.00$ K	
1.1911	20.911
6.8417	20.990
11.2851	21.041
20.6898	21.163
$T=114.00$ K	
3.8739	20.882
8.8149	20.942
24.9715	21.152
$T=116.00$ K	
1.9636	20.776
6.3156	20.841
12.0035	20.913
19.0660	21.009
29.2820	21.143
$T=118.00$ K	
8.0478	20.791
15.7492	20.896
23.2017	20.997
$T=120.00$ K	
1.2747	20.621
6.8130	20.702
10.8020	20.757
19.6919	20.883
27.3594	20.988
$T=122.00$ K	
3.8664	20.592
14.2998	20.737
23.7193	20.873
31.5310	20.979
$T=124.00$ K	
6.2436	20.553
11.6827	20.627
18.0492	20.724
27.7606	20.863
$T=126.00$ K	
7.9236	20.505
21.9553	20.712
31.8410	20.855
$T=128.00$ K	
0.6715	20.312
10.4787	20.470
18.8911	20.597
25.8617	20.703
35.9026	20.847

P (MPa)	ρ (mol/l)
$T=130.00$ K	
2.9285	20.287
13.7499	20.450
29.7809	20.694
$T=132.00$K	
5.4980	20.254
17.2765	20.436
26.4639	20.577
33.6963	20.687
$T=134.00$ K	
7.2368	20.209
20.8906	20.425
$T=136.00$ K	
1.3689	20.030
9.2490	20.167
24.5518	20.416
34.0682	20.561
$T=138.00$ K	
3.7831	20.008
12.1243	20.144
28.2309	20.407
$T=140.00$ K	
6.0574	19.972
15.3375	20.129
31.9091	20.400
$T=142.00$ K	
7.6559	19.926
18.7024	20.117
35.5822	20.392
$T=144.00$ K	
0.9387	19.722
9.8460	19.890
22.1094	20.107
$T=148.00$ K	
5.4489	19.667
15.7717	19.856
28.9678	20.091
$T=152.00$ K	
1.2079	19.424
8.9240	19.584
22.1746	19.836
35.8308	20.077

P (MPa)	ρ (mol/l)
$T=156.00$ K	
5.5978	19.369
14.2846	19.545
28.6589	19.820
$T=160.00$ K	
0.4675	19.091
8.9636	19.288
20.2324	19.524
35.1468	19.806
$T=164.00$ K	
4.2580	19.043
14.0474	19.250
26.2885	19.508
$T=168.00$ K	
1.7297	18.817
7.6437	18.969
19.6507	19.230
32.3436	19.495
$T=172.00$ K	
1.2449	18.650
5.7607	18.768
11.8776	18.916
25.3400	19.214
38.3722	19.482
$T=176.00$ K	
1.1073	18.488
5.2091	18.602
8.8759	18.691
16.9907	18.892
31.0365	19.201
$T=180.00$ K	
0.5247	18.295
4.9583	18.442
8.2782	18.525
13.3001	18.655
22.2633	18.876
36.7092	19.189
$T=184.00$ K	
3.9725	18.253
7.9795	18.368
12.4806	18.483
18.2646	18.635
27.5482	18.862

TABLE 1. PVT *data for ethane*—Continued

P (MPa)	ρ (mol/l)
$T = 188.00$ K	
1.9817	18.021
7.2058	18.186
11.9718	18.323
17.2059	18.463
23.3273	18.620
32.8340	18.850
$T = 192.00$ K	
0.9865	17.815
5.5964	17.977
10.6669	18.128
16.5186	18.302
22.0330	18.447
28.3464	18.607
$T = 196.00$ K	
0.4943	17.619
4.4533	17.775
8.4330	17.903
14.9662	18.104
21.1586	18.286
26.8669	18.434
33.3677	18.595
$T = 200.00$ K	
0.6801	17.445
3.5738	17.581
7.3933	17.709
12.2367	17.866
19.4175	18.087
25.8517	18.273
31.6945	18.423
$T = 204.00$ K	
3.7760	17.411
6.7420	17.524
10.6983	17.658
16.4076	17.846
23.9051	18.074
30.2305	18.262
36.4896	18.412
$T = 208.00$ K	
0.5897	17.079
6.8033	17.354
9.6616	17.461
14.6253	17.634
20.6552	17.831
28.3791	18.062
35.0871	18.251
$T = 212.00$ K	
3.4269	17.048
9.6570	17.293
13.3583	17.434
18.6673	17.619
24.9088	17.819
32.8419	18.051

P (MPa)	ρ (mol/l)
$T = 216.00$ K	
2.1043	16.798
6.4050	16.998
13.2349	17.267
17.2225	17.417
22.7370	17.606
29.1542	17.808
$T = 220.00$ K	
1.4301	16.567
5.1249	16.761
8.9985	16.934
16.9669	17.250
21.1113	17.404
26.8053	17.594
33.3471	17.798
$T = 224.00$ K	
4.3322	16.536
7.6124	16.699
12.2714	16.904
20.7255	17.237
25.0127	17.392
30.8565	17.584
$T = 228.00$ K	
1.8552	16.198
6.9228	16.483
10.4762	16.654
15.7164	16.887
24.4895	17.225
28.8946	17.382
34.8859	17.574
$T = 232.00$ K	
1.2667	15.950
4.5825	16.167
9.4583	16.428
13.6904	16.633
19.2025	16.874
28.2402	17.215
32.7523	17.372
$T = 236.00$ K	
3.8508	15.920
7.0049	16.114
12.4747	16.403
16.9765	16.618
22.6904	16.862
31.9811	17.205
$T = 240.00$ K	
1.2548	15.515
2.2021	15.586
6.3368	15.877
9.4209	16.062
15.5972	16.387
20.2787	16.606
26.1772	16.852
35.7046	17.196

P (MPa)	ρ (mol/l)
$T = 244.00$ K	
3.6366	15.487
4.6703	15.556
8.5355	15.817
12.2246	16.039
18.7424	16.375
23.5869	16.595
29.6476	16.842
$T = 248.00$ K	
1.7380	15.078
5.9925	15.449
6.8908	15.508
11.1353	15.788
15.1129	16.023
21.8905	16.364
26.8798	16.586
33.1044	16.833
$T = 252.00$ K	
1.5930	14.311
3.9746	15.056
8.0325	15.392
9.0553	15.457
13.8649	15.771
18.0296	16.011
25.0394	16.354
30.1617	16.577
$T = 256.00$ K	
3.7062	14.790
6.1397	15.018
10.3740	15.358
11.5324	15.433
16.6249	15.758
20.9491	16.000
28.1716	16.345
33.4255	16.568
$T = 260.00$ K	
2.6858	14.414
5.7990	14.757
8.0637	14.963
12.8526	15.340
14.0783	15.417
19.3947	15.747
23.8662	15.990
31.2936	16.336
$T = 264.00$ K	
2.4038	14.085
4.6766	14.389
7.6561	14.705
10.2294	14.931
15.3689	15.327
16.6466	15.405
22.1619	15.737
26.7721	15.981
34.3986	16.328

P (MPa)	ρ (mol/l)
$T = 268.00$ K	
3.0548	13.884
4.2654	14.062
6.5471	14.352
9.6680	14.669
12.5033	14.914
17.8943	15.316
19.2306	15.395
24.9268	15.728
29.6684	15.973
$T = 272.00$ K	
2.0844	1.243
3.6257	13.670
4.8506	13.859
6.0679	14.032
8.2942	14.302
11.8077	14.650
14.8065	14.901
20.4232	15.306
21.8042	15.385
27.6780	15.719
32.5542	15.964
$T = 276.00$ K	
2.1376	1.242
3.2684	13.256
5.3267	13.644
6.5457	13.824
7.7197	13.983
10.2212	14.275
13.9836	14.636
17.1196	14.890
22.9462	15.297
24.3837	15.377
30.4166	15.711
35.4306	15.957
$T = 280.00$ K	
2.1904	1.241
2.9758	12.787
4.8428	13.234
6.9195	13.604
8.1526	13.778
9.4890	13.951
12.2137	14.259
16.1653	14.625
19.4376	14.880
25.4635	15.288
26.9473	15.368
33.1520	15.703
$T = 284.00$ K	
2.2428	1.240
4.3982	12.768
6.3596	13.203
8.4885	13.563
9.8840	13.751
11.3395	13.933
14.2261	14.247
18.3557	14.615
21.7505	14.872
27.9731	15.280
29.4971	15.360
35.8724	15.696

TABLE 1. PVT *data for ethane*—Continued

P (MPa)	ρ (mol/l)
T = 288.00 K	
2.2951	1.239
3.0547	1.955
3.9706	12.194
5.8026	12.745
7.7971	13.160
10.1657	13.540
11.6682	13.735
13.2063	13.920
16.2439	14.237
20.5477	14.607
24.0580	14.863
30.4719	15.273
32.0446	15.353
T = 292.00 K	
2.3466	1.239
3.8113	11.522
5.2158	12.173
7.1396	12.707
9.3105	13.131
11.8771	13.525
13.4688	13.723
15.0863	13.910
18.2640	14.228
22.7394	14.598
26.3645	14.855
32.9673	15.265
T = 296.00 K	
2.3987	1.238
3.2373	1.952
3.8806	2.880
4.3963	11.212
4.8686	11.505
6.4389	12.146
8.4817	12.672
10.8697	13.115
13.6040	13.514
15.2773	13.713
16.9735	13.900
20.2846	14.219
24.8761	14.591
28.6475	14.848
35.4484	15.258

P (MPa)	ρ (mol/l)
T = 300.00 K	
2.4492	1.237
4.0309	2.875
4.6932	10.611
5.3970	11.196
5.9485	11.485
7.6275	12.109
9.8845	12.652
12.4490	13.102
12.4489	13.102
15.3377	13.504
17.0906	13.704
18.8621	13.892
22.3018	14.211
27.0931	14.583
30.9501	14.841
T = 304.00 K	
2.4997	1.237
3.4158	1.950
4.1784	2.873
4.6828	4.325
4.7721	9.097
4.9674	9.788
5.3930	10.298
5.5668	10.596
6.3948	11.173
6.9986	11.455
8.8474	12.082
11.3086	12.638
14.0362	13.092
17.0942	13.495
18.9013	13.696
20.7454	13.884
24.3137	14.204
29.2629	14.576
33.2309	14.833
T = 306.00 K	
4.8094	4.323
4.9441	6.533
5.0757	9.092
5.8014	10.290

P (MPa)	ρ (mol/l)
T = 308.00 K	
2.5499	1.236
4.3236	2.871
4.9341	4.321
5.1434	6.530
5.3872	9.086
5.6969	9.775
6.2111	10.280
6.4452	10.574
7.3779	11.142
8.0352	11.424
10.0940	12.066
12.7418	12.628
15.6258	13.083
18.6310	13.487
20.7132	13.688
22.6296	13.876
26.3246	14.196
31.4261	14.569
35.5024	14.826
T = 312.00 K	
2.5996	1.235
3.5908	1.947
4.4668	2.869
5.1793	4.316
5.5401	6.522
6.0206	9.072
6.4330	9.756
7.0307	10.254
7.3179	10.546
8.3744	11.116
9.1114	11.404
11.3574	12.054
14.1819	12.618
17.2177	13.075
20.5666	13.480
22.5240	13.681
24.5119	13.869
28.3286	14.189
33.5824	14.562

P (MPa)	ρ (mol/l)
T = 316.00 K	
2.6491	1.235
4.6083	2.866
5.4200	4.312
5.9358	6.513
6.6610	9.054
7.1729	9.732
7.8532	10.229
8.1986	10.522
9.3878	11.099
10.1982	11.390
12.6240	12.044
18.8045	13.068
22.3004	13.472
24.3313	13.673
26.3290	13.862
30.3236	14.183
T = 320.00 K	
2.6983	1.234
3.7629	1.945
4.7483	2.864
5.6574	4.307
6.3309	6.503
7.3064	9.032
7.9172	9.710
8.6869	10.211
9.0937	10.506
10.4137	11.087
11.2486	11.380
13.9007	12.036
17.0663	12.602
20.4014	13.060
24.0318	13.466
26.1304	13.667
28.2588	13.855
32.3174	14.176

Although comparison with data from other sources is, in general, impossible without multiple interpolations, the agreement has been deduced by examining the density deviations of the various data sets [9, 10] from densities calculated from an equation of state for ethane due to Goodwin [11]. The agreement is found to be, in general, within the combined experimental error. Maximum difference occur in the critical region where the equation of state representation is expected to be less satisfactory and where the experimental densities are subject to increasing uncertainty. Estimated uncertainty in the experimental densities in this work is typically ±0.1 percent at the lowest temperatures, increasing to ±0.2 percent at higher temperatures and lower densities, becoming as much as ±1.0 percent in the critical region.

New vapor pressure measurements also have been made at 5 K intervals from 160 to 300 K and are given in table 2. At each temperature, the pressure was measured at least twice with some ethane being removed from the cell between measurements. Identical pressure observations indicated that the two-phase condition existed in the cell.

A vapor pressure equation of the form

$$ln(P/P_t) = A\chi + B\chi^2 + C\chi^3 + D\chi^4 + E\chi(1-\chi)^{3/2} \quad (1)$$

was fit to all available data for ethane [12]. Here, $\chi = (1-T_t/T)/(1-T_t/T_c)$, and P and T are the pressure and temperature and t and c refer to the triple and critical points. Coefficients giving the best fit were found to be the following:

$A = 10.67324$
$B = 8.33782$
$C = -3.08489$
$D = -0.65857$
$E = 6.04955$
$P_t = 1.14 \times 10^{-5}$ bar
$T_t = 90.348$ K [Ref 1]
$T_c = 305.330$ K [Ref 10]

TABLE 2

T (K)	P kPa	T (K)	P kPa
160.00	21.502	230.00	700.48
165.00	30.670	235.00	825.96
170.00	42.870	240.00	966.60
175.00	58.636	245.00	1124.4
180.00	78.734	245.00	1124.8
180.00	78.706	250.00	1300.0
185.00	103.84	250.00	1301.9
190.00	134.63	250.00	1302.1
190.00	134.72	250.00	1301.8
195.00	172.21	255.00	1495.0
195.00	172.26	260.00	1670.3
200.00	217.26	265.00	1947.9
200.00	217.32	270.00	2208.0
205.00	270.93	275.00	2493.1
205.00	271.00	275.00	2493.2
210.00	334.13	280.00	2804.6
210.00	334.17	280.00	2806.2
210.00	333.98	285.00	3144.3
210.00	333.99	290.00	3513.5
215.00	407.34	298.15	4190.9
220.00	492.16	298.15	4188.9
225.00	589.73	300.00	4353.5

Deviations of the experimental vapor pressures from those calculated from this equation for the various data sets [9, 10, 13] are shown in figure 1.

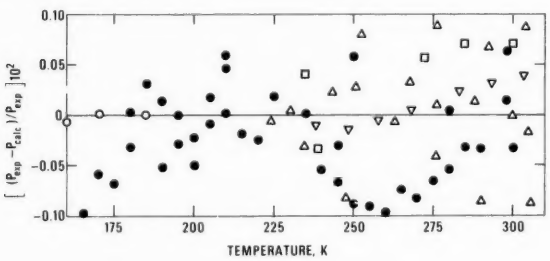

FIGURE 1. *Deviations of vapor pressures from* eq. 1.

● This work; ○ Ziegler et al. (Ref. [13]); △ Pal (Ref. [9]); □ Pope (Ref. [9]); ▽ Douslin and Harrison (Ref. [10]).

4. Summary

We have made new wide-range measurements of the vapor pressures and *PVT* properties of ethane. These are the only data currently available which cover the entire temperature range from the triple point to 320 K. In addition, these data are the only accurate *PVT* data available for the compressed liquid below about 190 K. The data are being used along with other available data to refine the calculation of thermodynamic functions for ethane and as input to, and as a check upon, new calculation methods for predicting liquefied natural (fuel) gas properties being studied in this and other laboratories.

5. References and Notes

[1] Straty, G. C., and Tsumura, R., J. Chem. Phys., **64,** 859 (1976).
[2] Weber, L. A., J. Res. Nat. Bur. Stand. (U.S.), **74A** (Phys. and Chem.), No. 1, 93–129 (Jan.–Feb. 1970).
[3] Prydz R., and Straty, G. C. Nat. Bur. Stand. (U.S.), Tech. Note 392, 197 pages (Revised 1973).
[4] Goodwin, R. D., Nat. Bur. Stand. (U.S.) Tech. Note 653, 280 pages (April 1974).
[5] Weber, L. A., NASA SP–3088/NBSIR 74–374 (1975).
[6] Goodwin, R. D., J. Res. Nat. Bur. Stand. (U.S.), **65C,** (Eng. and Instr.), No. 4, 231–243, (Oct.–Dec. 1961).
[7] Straty, G. C., and Prydz, R., Rev. Sci. Inst. **41,** 1223 (1970).
[8] Goodwin and Prydz, R., J. Res. Nat. Bur. Stand. (U.S.), **76A** (Phys. and Chem.), No. 2, 81–101 (Mar.–Apr. 1972).
[9] Pope G. A., (also reports vapor pressure and *PVT* data of A. K. Pal). Ph.D. Thesis, Dept. of Chemical Engineering, Ric University, Houston, Texas (July 1971).
[10] Douslin, D. R., and Harrison, R. H., J. Chem. Thermo **5,** 491 (1973).
[11] Goodwin, R. D., NBSIR 74–398 (1974). Goodwin has used a nonanalytic equation of state to correlate previously available data on ethane and to calculate provisional thermodynamic functions. Experimental data from this work are being used to fill in gaps in previously published data and to refine the equation of state to permit more accurate calculations of thermodynamic properties to be made. We defer extensive comparisons between data sets and a more elaborate analysis for inclusion in a final report in preparation.
[12] Further refinements in the correlation are expected which will probably alter slightly the final values of the constants. The deviation plot, however, is representative of the agreement among data sets. Coefficients for this equation will be included in the final report. See also reference [8].
[13] Ziegler, W. T., Kirk, B. S., Mullins, J. C., and Berquest, A. R., Tech. Rept. No. 2, Project A–764, Eng. Expt. Sta. Georgia Inst. Tech.; Atlanta, Georgia, December 1964.

(Paper 80A1–878)

JOURNAL OF RESEARCH of the National Bureau of Standards—A. Physics and Chemistry
Vol. 80A, No. 1, January–February 1976

Functional Equations for the Enhancement Factors for CO_2-Free Moist Air

Lewis Greenspan

Institute for Basic Standards, National Bureau of Standards, Washington, D.C. 20234

(October 7, 1975)

Equations are presented which explicitly express the enhancement of water vapor in CO_2-free air from 0.1 to 2 MPa. The equations are approximations to the formulation of Hyland and provide the means of obtaining enhancement with very modest computational facilities. The agreement with Hyland's enhancement values is well within his estimated uncertainty.

Key words: Enhancement factor; moist air; saturated air.

1. Introduction

The effective saturation pressure of water vapor in equilibrium with a plane surface of liquid or solid water in the presence of an admixed gas above its critical temperature differs from the saturation vapor pressure of the pure phase. It is expressed by

$$f = \frac{x_w P}{e_s} \tag{1}$$

where f = the enhancement factor
x_w = the mole fraction of water vapor in the saturated mixture.
P = total pressure above the surface of the condensed phase (liquid or solid)
e_s = the pure phase saturation vapor pressure of water.

In the field of humidity it is important to know both e_s and f in order to determine the quantity of saturated water vapor in a gas. As an example, the mixing ratio of a gas saturated with water vapor is given by

$$r = \frac{\epsilon f e_s}{P - f e_s} \tag{2}$$

where r = the mixing ratio in mass of water vapor per unit mass of associated dry gas.
ϵ = the ratio of the molecular weight of water to the molecular weight of the associated dry gas.

Whereas e_s is and has been known over a fairly wide range of temperature to a high degree of accuracy, accurate values of f have not been available for any gas until Hyland [1][1] recently published values of f for water vapor in CO_2-free air over a wide range of temperatures and pressures. These values are based on experiments from which the approximate theoretical form for the second interaction (cross) virial coefficient for air-water vapor mixtures was obtained. Use of this coefficient in a thermodynamically based equation permits determination of the enhancement factor. This equation, though implicit in f, can be used in an iterative mode to calculate f over fairly wide ranges of temperature and pressure. The equation is complex and implicit in f and therefore requires high speed computer capability for the determination of f at any given temperature and pressure. An alternate and simpler method of obtaining values of f for specific conditions would be by interpolation in tables first obtained by computer from Hyland's equation. Since a two way (temperature and pressure) interpolation of a function nonlinear in two parameters would be required, such interpolation would, at best, be awkward unless the table were close spaced.

By generalizing an equation, originally due to Goff and Gratch [2] and fitting it to values obtained from Hyland's relation, we have obtained simplified explicit equations for f which can be easily programed for a computer or can be calculated with the aid of a pocket calculator.

[1] Figures in brackets indicate the literature references at the end of this paper.

2. Method

Goff and Gratch [2] used the following form of equation for f

$$f = \exp\left[\alpha\left(1 - \frac{e_s}{P}\right) + \beta\left(\frac{P}{e_s} - 1\right)\right] \tag{3}$$

where α and β were obtained from theoretical equa-

tions and presented in a table of α and β for water and ice as a function of temperature. The implication was that α and β were independent of pressure, which is not precisely true, but they are fairly insensitive over modest pressure ranges.

We obtained values of α and β based on the new data given by Hyland. We calculated these values of α and β for water at temperatures from −50 to 100 °C and pressures from 0.101325 MPa (1 atm) to 2.0265 MPa (20 atm) and for ice from −100 to 0 °C over the same pressure range.

α and β were obtained by a least square fit of Hyland's values to equation

$$\frac{P}{P-e}\operatorname{Ln} f=\alpha+\beta\frac{P}{e} \tag{4}$$

at 20 equally spaced values of pressure from 0.101325 MPa to 2.0265 MPa for every 2 deg C.

We then fitted these values of α and β as a function of temperature, a minimum of 26 points being used for any α or β fit. The result was

$$\alpha=\sum_{i=1}^{4} A_i t^{(i-1)} \tag{5}$$

and

$$\beta=\exp\sum_{i=1}^{4} B_i t^{(i-1)} \tag{6}$$

where t is in degrees Celsius IPTS 68.

Table 1 gives the values of A_i and B_i for three conditions at 0.1 to 2 MPa.

TABLE 1. *Coefficients for* f

	Water −50 to 0 °C	Water 0 to 100 °C	Ice −100 to 0 °C
A1	3.62183×10^{-4}	3.53624×10^{-4}	3.64449×10^{-4}
A2	2.60553×10^{-5}	2.93228×10^{-5}	2.93631×10^{-5}
A3	3.86501×10^{-7}	2.61474×10^{-7}	4.88635×10^{-7}
A4	3.82449×10^{-9}	8.57538×10^{-9}	4.36543×10^{-9}
B1	−10.7604	−10.7588	−10.7271
B2	6.39725×10^{-2}	6.32529×10^{-2}	7.61989×10^{-2}
B3	-2.63416×10^{-4}	-2.53591×10^{-4}	-1.74771×10^{-4}
B4	1.67254×10^{-6}	6.33784×10^{-7}	2.46721×10^{-6}

The agreement between these equations and values obtained with the Hyland formulation is shown in table 2.

It is of interest to compare deviations between these formulations and Hyland's formulation with his estimate of the total uncertainty. This comparison is shown in table 3 for the range in which Hyland has given an estimated uncertainty. The deviations nowhere exceed Hyland's estimated uncertainties and in general are more than an order of magnitude less than the uncertainties.

TABLE 2. *Summary of deviations of* f *from Hyland formulation*

Temp °C	Water Deviation, %		Ice Deviations, %	
	Sigma	Max	Sigma	Max
100	0.003	0.004		
90	.002	−0.004		
80	.003	−0.006		
70	.001	−0.003		
60	.002	0.003		
50	.004	0.005		
40	.003	0.004		
30	.002	−0.005		
20	.005	−0.013		
10	.006	−0.014		
0	.008	0.011		
−0	.007	−0.009	0.059	0.008
−10	.006	−0.014	.020	−0.042
−20	.008	−0.015	.038	−0.076
−30	.011	−0.020	.020	−0.046
−40	.014	−0.029	.024	0.033
−50	.019	−0.035	.052	0.068
−60			.051	0.069
−70			.032	−0.060
−80			.083	−0.196
−90			.109	−0.259
−100			.163	0.222

It will be noted that these formulations have been compared with Hyland's formulation in regions where Hyland has declined to assign uncertainties (below −50 °C and above 90 °C as well as in regions where he has published no values (below −80 °C, above 90 °C and for water below 0 °C). Despite the questionable validity of his formulation in these areas, namely the region of supercooled water and the region of ice below −50 °C, there is no formulation for f in these regions that is more valid at this time. It is our suggestion therefore that the Hyland formulation be used for all water-air f factors up to the boiling point. It is for this reason that we have proposed our simplified equations for this wide region.

As can be seen from table 2, the agreement between these formulations is exceedingly good above 0 °C and quite good for water down to −50 °C. Because there does not appear to be any need for f factors for supercooled water below −50 °C, we have terminated our equation at that point.

There is a need for f factors for ice below −50 °C and we have therefore extended our formulation to −100 °C. As can be seen from table 2, the agreement with Hyland is considerably poorer for ice than for water. The agreement can be improved by using two sets of coefficients, one for 0 to −50 °C and the other for −50 to −100 °C, in the same form of the equation. The coefficients, are given in table 4 and the deviations are given in table 5. For the alternate equations, table 3 is not applicable below 0 °C and table 6 is the applicable section of that table.

TABLE 3. *Individual deviations from Hyland formulation*

	T °C							
P	90	70	50	30	10	− 10	− 30	−50
MPa	Deviations, percent							
0.1	0.001 (0.001)	− 0.001 (0.01)	−0.003 (0.01)	− 0.004 (0.01)	− 0.006 (0.03)	− 0.012 (0.04)	− 0.021 (0.05)	− 0.029 (0.06)
.2	0.000 (0.01)	− 0.001 (0.02)	− 0.002 (0.03)	− 0.003 (0.03)	− 0.005 (0.06)	− 0.010 (0.07)	− 0.016 (0.10)	− 0.014 (0.13)
.3	− 0.001 (0.02)	− 0.001 (0.03)	− 0.001 (0.05)	− 0.002 (0.04)	− 0.003 (0.09)	− 0.009 (0.11)	− 0.012 (0.14)	− 0.001 (0.19)
.4	− 0.001 (0.03)	0.000 (0.05)	0.000 (0.06)	− 0.001 (0.05)	− 0.002 (0.11)	− 0.008 (0.15)	− 0.009 (0.19)	0.011 (0.25)
.5	− 0.001 (0.04)	0.000 (0.06)	0.001 (0.08)	0.000 (0.07)	− 0.001 (0.14)	− 0.007 (0.18)	− 0.006 (0.24)	0.022 (0.32)
1.	− 0.001 (0.09)	0.000 (0.13)	0.004 (0.17)	0.002 (0.13)	0.001 (0.29)	− 0.009 (0.37)	− 0.003 (0.48)	0.059 (0.64)
2.	− 0.004 (0.20)	− 0.003 (0.26)	0.003 (0.35)	− 0.005 (0.27)	− 0.014 (0.58)	− 0.042 (0.75)	− 0.046 (0.98)	0.047 (1.30)

Figures in ( ) are Hyland's estimated uncertainties in percent for the same conditions as the deviation above.

TABLE 4. *Coefficients for Ice Equation for* f *(alternative form)*

	− 100 to − 50 °C	− 50 to 0 °C
A1	9.88896×10^{-4}	3.61345×10^{-4}
A2	5.74491×10^{-5}	2.9465×10^{-5}
A3	8.90422×10^{-7}	5.21676×10^{-7}
A4	6.20355×10^{-9}	5.01622×10^{-9}
B1	− 10.4148	− 10.7401
B2	9.11735×10^{-2}	7.36812×10^{-2}
B3	5.14117×10^{-5}	-2.68806×10^{-4}
B4	3.55087×10^{-6}	1.53964×10^{-6}

TABLE 5. *Summary of deviations of* f *from Hyland formulation (alternative form)*

Temp	Ice Deviation, %	
°C	Sigma	Max
0	0.005	− 0.009
− 10	.006	− .013
− 20	.008	− .014
− 30	.010	− .019
− 40	.013	− .027
− 50	.018	− .033
− 60	.024	− .052
− 70	.032	− .059
− 80	.043	− .080
− 90	.060	− .126
− 100	.092	− .148

TABLE 6. *Individual deviations from Hyland formulation (alternative form)*

P	T °C		
MPa	− 10	− 30	− 50
	Deviations, %		
0.1	−0.011 (0.04)	−0.019 (0.05)	−0.033 (0.06)
.2	−0.008 (0.07)	−0.013 (0.10)	−0.022 (0.13)
.3	−0.005 (0.11)	−0.008 (0.14)	−0.013 (0.19)
.4	−0.002 (0.15)	−0.003 (0.19)	−0.004 (0.25)
.5	0.000 (0.18)	0.001 (0.24)	0.003 (0.32)
1.	0.006 (0.37)	0.012 (0.48)	0.021 (0.64)
2.	−0.013 (0.75)	−0.018 (0.98)	−0.028 (1.30)

Figures in ( ) are Hyland's estimated uncertainties in percent for the same conditions as the deviation above.

3. Discussion

We have attempted to present equations that will be useful to a wide range of workers in the field of

humidity measurement. We have used a historical form of the equation which appears to give reasonably adequate results up to 2. MPa.

It should be pointed out that the deviations between the values obtained from these equations and the values obtained from the Hyland formulation are not random. These equations therefore are not an alternative expression of the Hyland formulation, but merely a convenience for obtaining approximate values of Hyland's f factor.

Of course, there are those who have need for Hyland's results above 2 MPa, and those people we have not helped. It is regrettable that we required three equations to cover the desired range (some may feel that the four equations are necessary) and that each of the equations has eight coefficients. We do not suggest that the equations presented here are the optimum equations available, but only that they appear adequate for most purposes and appropriate for adoption where uniform simple computations are desirable. It must also be pointed out that these formulations are based on the 1968 IPTS temperature scale, the Wexler [3] formulation for the vapor pressure of water and the Goff [4] formulation for the vapor pressure of ice, which is completely consistent with the work of Hyland. Were new vapor pressure equations to be used which give values that differ markedly from the referenced equations, these formulations would no longer be acceptable. It is important to be aware that under the same circumstances, the values of f calculated with Hyland's formulation would differ from his published values.

4. References

[1] Hyland, R. W., A Correlation for the second interation virial coefficients and enhancement factors for CO_2-free moist air from −50 to +90 °C, J. Res. Nat. Bur. Stands. (U.S.), **79A,** (Phys. and Chem.), No. 4, 551–560 (July–Aug. 1975).

[2] Goff, J. A., Standardization of Thermodynamic Properties of Moist Air, Heating, Piping and Air Cond. **21,** 118 (1949).

[3] Wexler, A., and Greenspan, L., Vapor pressure equation for water in the range 0 to 100 °C, J. Res. Nat. Bur. Stand. (U.S.), **75A,** (Phys. and Chem.), No. 3, 213–230 (May–June 1971).

[4] Goff, J. A., Saturation Pressure of Water on the New Kelvin Scale, Humidity and Moisture, Vol. **III,** A. Wexler and W. A. Wildhack, Eds. (Reinhold Publishing Corp., New York, 1964), p. 28d.

(Paper 80A1–879)

JOURNAL OF RESEARCH of the National Bureau of Standards — A. Physics and Chemistry
Vol. 80A, No. 1, January–February 1976

Experimental Values for the Elastic Constants of a Particulate-Filled Glassy Polymer

Jack C. Smith

Institute for Materials Research, National Bureau of Standards, Washington, D.C. 20234

(June 20, 1975)

Young's modulus and Poisson's ratio have been measured simultaneously on a series of particulate composites containing volume fractions of filler up to 0.50. The composites consisted of small glass spheres imbedded in a rigid epoxy polymer matrix. The measured values were compared with theoretical values calculated from current theories. A recently generalized and simplified version of van der Poel's theory provided the best agreement. It predicted values of Young's modulus for composites with filler volume fractions up to 0.35. Measured values of Poisson's ratio exhibited scattering, but were consistent with values calculated from van der Poel's theory.

Key words: Composite materials; elastic constants; filled polymers; mechanical properties; particulate composites; Poisson's ratio; Young's modulus.

1. Introduction

It has been known for some time that the addition of a particulate filler to a polymeric material can greatly affect the elastic properties of the resulting composite. The effect is a mechanical one complicated by several superimposed effects of a chemical and physical nature. The pure mechanical effect is best understood. It is accounted for in terms of the local strain distortions due to dissimilarities between the matrix and filler material. Various theories have been propounded to explain it, and reviews of these theories are available [1–3][1].

In order to test these theories good data are needed for a series of macroscopically homogeneous and isotropic composites containing various known amounts of filler. The filler and matrix materials should be isotropic, and the two elastic constants necessary to characterize each of them should be known. These two elastic constants should preferably be obtained by simultaneous measurements on the same specimen in order to minimize effects due to viscoelasticity and specimen variation.

There are a number of physical and chemical effects that must be considered in choosing an appropriate composite system for testing. The rubber-carbon black system for instance is complicated by the following effects [4–6]: The small carbon particles present in large numbers bond to the rubber molecules and significantly increase the degree of crosslinking of the rubber matrix; the carbon particles associate together in long chains thus producing a structure effect; and the filled rubber composite softens after a previous deformation. For these reasons this system does not provide a satisfactory test of theories dealing with the mechanical effect.

In some cases the presence of the filler particle may induce crystallization, crosslinking or other structural changes in the surrounding shell of polymer matrix, thus introducing an additional phase with consequent changes in mechanical properties [7–11]. This effect should be avoided by using a filler which adheres firmly to the matrix, but does not exercise a long-range influence on the matrix structure. In addition the filler particle dimensions should be large enough that the total filler surface area is comparatively small.

The room temperature behavior of a composite formed at elevated temperatures may be affected by frozen-in stresses due to differences in the thermal expansion properties of the matrix and filler material [12]. In cast composites this effect can be reduced by gelling at room temperature, and cooling slowly after any post cure at elevated temperatures.

The shape and orientation of the filler particles may cause the composition to be anisotropic, but this effect is easily avoided by using spherical filler particles.

Previous checks of the theories have met some

[1] Figures in brackets indicate the literature references at the end of this paper.

of the above criteria in various ways. For those composites consisting of a rigid filler imbedded in a rubbery matrix of Poisson's ratio 0.5, the shear modulus of the composite increases as the volume fraction of the filler is increased. This effect is analogous to the increase in viscosity of a suspension of particles in a liquid [13], so that viscosity data such as those provided by Eilers [14] can be used in a partial check of the theories.

Data are also available on composites with a rubbery matrix, but these data are usually incomplete in that only one elastic constant is measured as a function of the volume fraction of filler. In these cases the dependence on filler content of the other constant, that is needed to characterize an isotropic material, cannot be checked. Schwarzl et al. [15] and Waterman [16] however, have provided complete data on a composite system consisting of NaCl crystals imbedded in a rubbery polyurethane matrix, and have compared them with the predictions of van der Poel's theory [17]. Additional data on this material have been provided by Nicholas and Freudenthal [18]. Payne [6] has measured the shear moduli of composites consisting of natural rubber filled with glass spheres, whiting and a "nonstructure" carbon black, and has given a valuable discussion of this system.

When the polymer matrix is in the leathery or glassy state, one can no longer assume as in the rubbery case that Poisson's ratio of the matrix is close to 0.5. Yet, unless two elastic constants are known for the matrix material, and reasonable values of the constants can be assumed for the filler, theoretical predictions for the composite's elastic behavior can only be approximate. In much of the data for glassy-matrix composites the constants of the components are not completely specified, and in most cases only one constant characterizing the composite (i.e. Young's modulus or shear modulus) is measured as a function of filler content. Some useful but usually incomplete data are available [17, 19–22]. More data on glassy-matrix composites are desirable, and for this reason the work reported here was undertaken.

2. Materials

The system of composites studied consisted of glass spheres imbedded in and adhering to a glassy epoxy matrix. A series of such materials was fabricated, each member containing a different volume fraction of glass spheres.

The matrix material was formed from the diglycidyl ether of bisphenol-A (DGEBA) hardened with a stoichiometric amount of triethylenetetramine (TETA). The DGEBA resin used (DER–332, Dow Chemical Co.)[2] was almost pure monomer with an epoxy equivalent weight 172–178. The glass transition temperature of the hardened polymer as determined by dilatometry was 120 °C. The density determined by hydrostatic weighing was 1.187 g/cm^3 for material stored 185 days at 24 °C and 54 percent R.H.

The filler material consisted of glass spheres with a distribution of diameters in the range 1 to 30 μm. The glass was an optical crown glass, soda lime type, with a silica content not less than 60 percent (Standard Class IV Unispheres No. 4000, Cataphote Corp.). The manufacturer specifies an approximate Young's modulus for this glass of 7.6×10^{10} Pa (11×10^6 lb/in^2) as measured on a bulk sample. Poisson's ratio for soda lime glass, given in the literature [23], is 0.23. The density of this glass as determined with a pycnometer is 2.392 g/cm^3.

Before use the glass spheres were cleaned by passing them near the poles of a powerful permanent magnet a number of times to remove iron impurities. They were washed twice in boiling distilled water and twice in boiling isopropanol, and dried overnight under vacuum at 130 °C. The dried spheres were coated with the coupling agent γ-aminopropyltriethoxysilane (A1100, Union Carbide Corp.) as follows: A given weight of spheres was added to an equal weight of freshly prepared 1 percent-solution of A1100 in water. The slurry was stirred for 15 min, filtered, and washed with an equal amount of water. The spheres were then dried overnight under vacuum at 130 °C, and then lightly ground in a mortar to break up agglomerations.

Before use the DGEBA monomer was deaerated in a vacuum oven for at least 1 hour at 60 °C. A weighed amount was transferred to a flask, the glass spheres added, and the slurry stirred under vacuum for an hour to remove air introduced with the spheres. The TETA hardener was added, and the mixture rapidly stirred under vacuum for 5 minutes. The mixture then was carefully poured into a mold formed from clamped glass plates separated by spacers and sealed with rubber tubing. The plates had previously been treated with a mold release a nt.

The mold was sealed and the contents allowed to cure for 16 hours at room temperature. Before gelling occurred the mold was rotated at 1 rpm in order to prevent the glass spheres from settling. The material was post cured in an unclamped mold for 24 hours at 75 °C followed by 8 hours at 150 °C. The oven was then turned off and the cured composite allowed to come to room temperature overnight in the oven. According to reported research on similar materials [24, 25] this should produce an almost completely cured resin with only minimal strains introduced by the molding process.

Several series of composites containing volume fractions of glass spheres up to 0.50 were prepared by this process. The content of glass was determined by hydrostatic weighing and found to be uniform throughout each of the cast samples. Test specimens of dumbbell shape [26] with 5-cm gage length, 1.3-cm

[2] Certain commercial equipment, instruments or materials are identified in this paper in order to provide an adequate description. In no case does such identification imply recommendation or endorsement by the National Bureau of Standards.

gage width and 0.5-cm thickness were prepared from the castings, using a high-speed router. Four specimens were obtained from each cast sample.

3. Procedure

The specimens were tested on a tensile testing machine at 0.05-cm/min rate of extension and 12.5-cm grip separation. The state of strain in the uniform narrow portion of the specimen was monitored with a strain gage extensometer of nominal 5-cm gage length. The exact value of the initial gage length was determined in situ with a cathetometer. A transverse extensometer employing a small linear variable differential transformer was used to obtain simultaneous measurements of the width of the specimen during test. The amplified outputs of the two extensometers and the load-extension curve of the tensile tester were recorded separately. Simultaneous data values were obtained by putting small simultaneous pip marks on the recorder traces by means of a pushbutton operated pulse circuit.

The data were used to plot stress-strain curves and curves of transverse strain versus longitudinal strain for the specimens. The initial slope of the stress-strain curve was taken as Young's modulus of the specimen, and the negative of the initial slope of the transverse strain-longitudinal strain curve was taken as Poisson's ratio. As all of the specimens were subjected to the same low rate of straining during data acquisition, it was believed that the relative effects of viscoelasticity would be small. Therefore viscoelastic effects were not considered in the subsequent analysis.

4. Results

During early stages of the research it was assumed that the samples were fully cured, so that tensile properties could be measured 1 or 2 weeks after preparation. The results of these measurements are given in table 1. Each value listed is the average of measurements on the four specimens obtained from each cast sample, and the variation between specimens is expressed as the probable error of a single observation. The probable errors are of the order of 3 percent of the measured value for both Young's modulus and Poisson's ratio. The variation from sample to sample however was noticeably greater, even though the extra samples of same filler content were made and measured by the same standardized procedure.

A later series of samples made and measured is listed in table 2. These samples were tested 200 days after preparation to see if there was an aging effect. During this time the samples were stored over a saturated solution of $Mg(NO_3)_2 \cdot 6H_2O$ maintained at the laboratory temperature of 24 °C. This provided an environment of 54 percent relative humidity. As a

TABLE 1. *Results for samples tested 1 to 2 weeks after preparation*[a]

Volume fraction of filler	Days to test	Young's modulus	Poisson's ratio
φ		E *GPa*	ν
0.0000	13	3.21 ± 0.09	0.426 ± 0.008
.0000	7	2.74 ± .11	.425 ± .010
.0000	10	2.53 ± .06	.378 ± .003
.0000	13	2.48 ± .05	.370 ± .009
.0482	7	[b]3.35 ± .06	[b].430 ± .012
.0495	10	2.58 ± .03	.336 ± .014
.0498	13	2.83 ± .03	.368 ± .006
.0985	13	3.19 ± .03	.391 ± .018
.1477	14	3.62 ± .13	.384 ± .010
.1965	7	3.74 ± .04	.353 ± .007
.1983	8	4.25 ± .12	.383 ± .012
.1992	13	3.91 ± .03	.370 ± .008
.2486	14	4.59 ± .10	.374 ± .007
.2980	5	5.09 ± .07	.333 ± .003
.2988	12	5.02 ± .11	[b].373 ± .004
.3480	15	6.14 ± .15	.376 ± .010
.4015	8	6.67 ± .15	.318 ± .012
.4513	12	8.17 ± .23	[c].310 ± .005
.4981	14	9.95 ± .90	[b].347 ± .010

[a] Expressed as value ± probable error of a single observation. Each value is the average of measurements on four specimens, except as noted.
[b] Average of three specimens.
[c] Average of two specimens.

TABLE 2. *Results for samples tested approximately 200 days after preparation*[a, b]

Volume fraction of filler	Days to test	Young's modulus	Poisson's ratio
φ		E *GPa*	ν
0.0000	198	2.99 ± 0.11	0.401 ± 0.011
.0000	194	[c]3.00 ± .05	[c].403 ± .021
.0000	190	[d]3.03 ± .05	[d].400 ± .005
.0245	203	3.11 ± .02	.404 ± .008
.0494	197	3.32 ± .11	.385 ± .007
.0701	203	3.41 ± .08	.395 ± .006
.0993	207	3.75 ± .09	.377 ± .019
.1494	208	4.19 ± .14	.366 ± .010
.2251	209	5.08 ± .08	.384 ± .020
.3025	209	6.01 ± .21	.375 ± .017
.3960	208	7.94 ± .12	.354 ± .018
.4960	208	12.09 ± .09	.330 ± .013

[a] Expressed as value ± probable error of a single observation. Each value is the average of measurements on four specimens.
[b] Specimens were stored at 24 °C and 54 percent R.H. before testing, except as noted.
[c] Stored in a vacuum desiccator over anhydrous $CaSO_4$ at 24 °C.
[d] Stored over water at 24 °C.

check on the effect of moisture two extra samples of epoxy matrix material were prepared. One was stored over water, and the other was stored over anhydrous $CaSO_4$ in a vacuum desiccator.

Comparison of the values given in tables 1 and 2 shows that there is an age hardening effect. The Young's moduli tabulated in table 2 are slightly higher than the corresponding moduli in table 1. However the measurement values obtained do not seem to have been affected by the relative humidity of the environment. The Young's moduli for the three samples stored in different environments are not significantly different.

5. Discussion

The data just presented will now be analyzed with the help of a theory due to van der Poel [17], and compared with the predictions of other theories. Let G represent the shear modulus, K bulk modulus, E Young's modulus, and ν Poisson's ratio of the composite; let the subscripts f and m refer to the filler and matrix respectively, and let φ represent the volume fraction of filler. These elastic constants are interrelated by the equations,

$$E=\frac{9KG}{3K+G} \tag{1}$$

$$\nu=\frac{3K-2G}{6K+2G} \tag{2}$$

so that only two constants are required to characterize the initial elastic behavior of an isotropic material. Van der Poel's theory provides two relationships,

$$K=K(G_m, K_f, K_m, \varphi) \tag{3}$$

$$G=G(G_f, G_m, \nu_f, \nu_m, \varphi) \tag{4}$$

and similar relationships are provided by the other theories.

Relation (3) is also used in the theory of Kerner [27], and is the same as Hashin and Shtrikman's equation for the highest lower bound of the bulk modulus [28]. However van der Poel's relation (4) for the shear modulus, as given in the original presentation, was very complicated. A table of values was provided, but this table was limited to materials for which Poisson's ratio of the matrix was 0.5. In addition there was an error in the derivation. Recently van der Poel's method has been reexamined, the error corrected, and the method extended for use with matrix materials having any value for Poisson's ratio [29]. Subsequently the calculation of G has been simplified [30].

If the elastic constants E_m, ν_m, E_f, ν_f of the matrix and filler materials are known, the corresponding values K_m, G_m, K_f, G_f can be calculated by means of relations (1) and (2). K and G for the composite can be calculated as a function of φ, using equations (3) and (4), and the corresponding values of E and ν then can be calculated from relations (1) and (2). It is these calculated values of E and ν that are compared with the experimental data.

In order to determine how well the theories agree with the experimental data it is necessary to have accurate values of E_m and ν_m for use in the theoretical calculations. The average of the measured values of E_m and ν_m was not regarded as sufficiently accurate, so more accurate values were obtained by the following extrapolation procedure: The averages of E_m and ν_m were used as a first approximation, and curves of E versus φ and ν versus φ were calculated using van der Poel's theory. These curves were fitted to the experimental data for values of φ up to 0.15. This was done by shifting the curves mathematically along the E or ν axis to obtain a least squares fit with the experimental data. The shape and slope of the curves was maintained constant during the shifting process. The intercepts of the shifted curves provided new values of E_m and ν_m. The process was repeated until convergence was obtained.

The values of E_m and ν_m obtained by this process are: For the data of table 1, $E_m=2.68\times10^9$ Pa, $\nu_m=0.394$; for data of table 2, $E_m=3.01\times10^9$ Pa, $\nu_m=0.394$. It is apparent from the above values of E_m that age hardening occurred during the time interval between tests at 10 days and 200 days after sample preparation.

Relative moduli E/E_m for the samples are plotted as a function of filler volume fraction in figure 1. Data for the fresh samples (table 1) are plotted as open

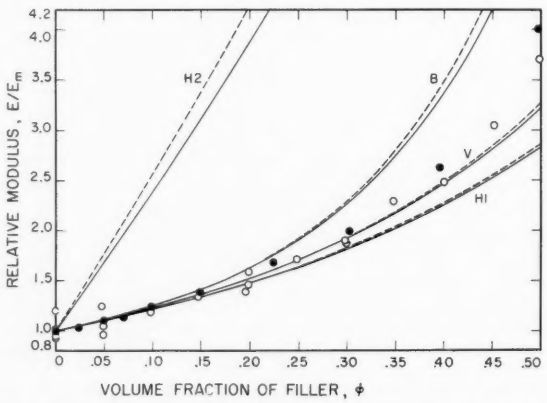

FIGURE 1. *Plot of relative Young's modulus* E/E_m *versus volume fraction of filler, from the data of tables 1 and 2.*

Open circles, data from table 1 using $E_m=2.68\times10^9$ Pa; solid circles, data from table 2 using $E_m=3.01\times10^9$ Pa. Dash curves, theoretical values calculated using $E_m=2.68\times10^9$ Pa; solid curves, theoretical values calculated using $E_m=3.01\times10^9$ Pa. HI, calculated using Hashin and Shtrikman's highest lower bounds for shear and bulk moduli; H2 calculated using Hashin and Shtrikman's least upper bounds for shear and bulk moduli; V, van der Poel's theory; B, Budiansky's theory.

circles, and for the age hardened samples (table 2) as solid circles. Predicted values from the van der Poel and Budiansky [31] theories and the least upper (curve H2) and highest lower bounds H1 of Hashin and Shtrikman's theory are shown as pairs of solid and dashed lines. The dashed lines show predicted values for the fresh samples ($E_m = 2.68 \times 10^9$ Pa), and the solid lines show values for the age hardened samples ($E_m = 3.01 \times 10^9$ Pa). Predicted values of Kerner's widely used theory are the same as those of Hashin and Shtrikman's highest lower bound H1, and have been shown to be approximations to the values calculated using van der Poel's theory [30].

It is apparent from figure 1 that the values of relative modulus E/E_m calculated using van der Poel's theory are in good agreement with the measured values for filler volume fractions up to 0.35, and give slightly better predictions than values calculated using the Kerner or Hashin and Shtrikman lower bound theory. At higher filler volume fractions up to 0.50 measured values exceed the van der Poel predictions, but are less than those of Budiansky.

Poisson's ratios are plotted in figure 2. Values for the fresh samples are plotted as open circles, and values for the age hardened samples as solid circles. Predictions of the van der Poel, Budiansky and Hashin and Shtrikman theories are shown as pairs of solid and dashed lines, where the dashed lines depict values for the fresh samples, and the solid lines depict values for the age hardened samples. Predictions of Kerner's theory are the same as those of the Hashin and Shtrikman curves designated as H1.

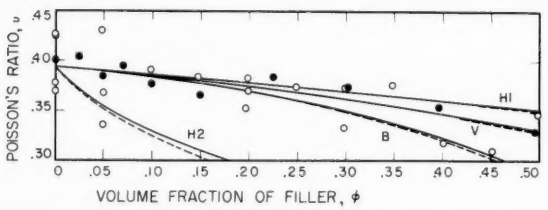

FIGURE 2. *Plot of Poisson's ratio versus volume fraction of filler, from data of tables 1 and 2.*

Open circles, data from table 1; solid circles, data from table 2. Dash curves, theoretical values calculated using $E_m = 2.68 \times 10^9$ Pa; solid curves, theoretical values calculated using $E_m = 3.01 \times 10^9$ Pa. H1, calculated using Hashin and Shtrikman's highest lower bounds for shear and bulk moduli; H2, calculated using Hashin and Shtrikman's least upper bounds for shear and bulk moduli; V, van der Poel's theory; B, Budiansky's theory.

The order of the curves in figure 2 is reversed from the order observed in plots of E/E_m versus φ. Thus curve H2 calculated using Hashin and Shtrikman's values for the least upper bounds on K and G actually becomes a lower bound curve for Poisson's ratio ν, and curve H1 calculated from the highest lower bound values becomes the upper bound curve. Also the curve calculated from Budiansky's theory lies below that calculated from van der Poel's theory. The reversal in the order of these curves is a consequence of the decrease in the value of ν with increasing φ.

Although there is considerable scatter in the data, the curve of values calculated from van der Poel's theory seems to provide the best fit. These results indicate that the generalized van der Poel theory is better than other current theories in predicting the mechanical effect of filler on the elastic properties of a particulate composite. As the calculations involved in the application of this theory have now been simplified [29, 30], it is hoped that the theory will be more frequently used in the interpretation of experimental data.

6. References

[1] Hashin, Z., Appl. Mech. Rev. **17,** 1 (1964).
[2] Reiner, M., Encyclopedia of Physics, S. Flügge, Ed., (Springer-Verlag, 1958), Vol. 6, p. 522.
[3] Nielsen, L. E., J. Comp. Matls. **1,** 100 (1967).
[4] Reinforcement of Elastomers, G. Kraus, Ed., (John Wiley, 1965).
[5] Payne, A. R., J. Appl. Polym. Sci. **6,** 57 (1962).
[6] Payne, A. R., J. Appl. Polym. Sci. **6,** 368 (1962).
[7] Kardos, J. L., J. Adhesion **5,** 119 (1973).
[8] Wang, T. T. and Schonhorn, H., J. Appl. Phys. **40,** 5131 (1969).
[9] Droste, D. H. and DiBenedetto, A. T., J. Appl. Polym. Sci. **13,** 2119 (1969).
[10] Kwei, T. K., J. Polym. Sci. **A3,** 3229 (1965).
[11] Lipatov, Yu. S., Lipatova, T. E., Vasilienko, Ya. P. and Sergeyeva, L. M., Vysokomol. Soyed. **5,** 290 (1963); Polym. Sci. USSR **4,** 920 (1963).
[12] Nielsen, L. E. and Lewis, T. B., J. Polym. Sci. **A2,** 1705 (1969).
[13] Goodier, J. N., Phil. Mag. (7) **22,** 678 (1936).
[14] Eilers, H., Kolloid Z. **97,** 313 (1941).
[15] Schwarzl, F. R., Mechanics and Chemistry of Solid Propellants, Proceedings of the Fourth Symposium on Naval Structural Mechanics, edited by A. C. Eringen, H. Liebowitz, S. L. Koh and J. M. Crowley (Pergamon Press, New York, N.Y., 1967), p. 503.
[16] Waterman, H. A., Rheol. Acta. **5,** 140 (1966); **8,** 22 (1969).
[17] van der Poel, C., Rheol. Acta. **1,** 198 (1958).
[18] Nicholas, T. and Freudenthal, A. M., Rheol. Acta. **7,** 174 (1968).
[19] Mandel, J. and Dantu, P., Annales des Ponts et Chaussées **133,** 115 (1963).
[20] Lewis, T. B. and Nielsen, L. E., J. Appl. Polym. Sci. **14,** 1449 (1970).
[21] Radford, K. C., J. Matls. Sci. **6,** 1286 (1971).
[22] Nicolais, L. and Nicodemo, L., Intern. J. Polym. Matls. **4,** 229 (1974).
[23] Engineering Materials Handbook, C. L. Mantell, Ed. (McGraw-Hill, 1958), table 27-5.
[24] Chaio, T. T., Cummins, A. D. and Moore, R. L., Composites **3,** 10 (1972).
[25] Arridge, R. G. C. and Speake, J. H., Polymer **13,** 443 (1972).
[26] Specimen Type I, ASTM Test Method D638-72, ASTM Standards, Part 27 (1973).
[27] Kerner, E. H., Proc. Phys. Soc. **B69,** 808 (1956).
[28] Hashin, Z. and Shtrikman, S., J. Mech. Phys. Solids **11,** 127 (1963).
[29] Smith, J. C., J. Res. Nat. Bur. Stand. (U.S.), **78A** (Phys. and Chem.), No. 3, 355-361 (May-June 1974).
[30] Smith, J. C., J. Res. Nat. Bur. Stand. (U.S.), **79A** (Phys. and Chem.), No. 2, 419-423 (March-April 1975).
[31] Budiansky, B., J. Mech. Phys. Solids **13,** 223 (1965).

(Paper 80A1-880)

597-633 O - 76 - 4

JOURNAL OF RESEARCH of the National Bureau of Standards—A. Physics and Chemistry
Vol. 80A, No. 1, January–February 1976

Heat Capacities of Polyethylene IV. High Molecular Weight Linear Polyethylene

Shu-Sing Chang

Institute for Materials Research, National Bureau of Standards, Washington, D.C. 20234

(August 27, 1975)

A high molecular weight linear polyethylene sample has been studied by adiabatic calorimetry from 10 to 380 K. Two broad temperature regions of unusual spontaneous temperature drift have been observed. The phenomena occurring around 240 K are similar to that observed in other polyethylene samples studied in this series, and are presumed to be caused by the relaxational processes in the amorphous phase. The weak exothermic behavior occurring around 160 K is presumed to be caused by the stabilization of the quenched sample.

Key words: Glass transition; heat capacity; high molecular weight linear polyethylene; polyethylene; temperature drift; thermodynamic properties.

1. Introduction

The heat capacity behavior of a sample of high molecular weight linear polyethylene has been studied recently by Beatty and Karasz [1, 2].[1] High molecular weight polyethylene is more difficult to crystallize than lower molecular weight polyethylene. Increased amorphous content should provide a stronger indication of the existence of a glass transition in partially crystalline linear polyethylene. A region of rather abrupt change in the heat capacity differences between that high molecular weight sample and a linear polyethylene sample studied by Dainton et al. [3] was noted. For the quenched high molecular weight sample, there was an 8 percent increase in the heat capacity occurring in the temperature region 130 to 190 K. For the annealed sample, there was about 5 percent increase. At higher temperatures a bend in the heat capacity curve was noted similar to Dainton's data. The region near 150 K was assigned as the glass transition temperature of linear polyethylene. Spontaneous temperature drifts under adiabatic conditions, indicative of relaxational processes, were not noted in detail.

A similar high molecular weight linear polyethylene sample from the same manufacturer was studied in this laboratory in the temperature range from 10 to 380 K. Detailed spontaneous temperature drifts were carefully observed on the sample under various thermal treatments. The results and conclusions from this study are somewhat different from the previously mentioned literature.

[1] Figures in brackets indicate the literature references at the end of this paper.

2. Experimental Section

2.1. Calorimetry

Heat capacity measurements on the high molecular weight linear polyethylene sample were made with the same vacuum adiabatic calorimeter [4] that was used in the previous studies [5, 6] on polyethylene samples derived from Standard Reference Materials 1475 and 1476.

2.2. Materials

A sample of high molecular weight polyethylene was furnished by Dr. R. J. Schaffhauser of the Plastics Division, Allied Chemical Corp.,[2] bearing the designation 260–100. This resin was at one time also designated as AC8X, as was Beatty's sample [2]. It was produced by Ziegler-type vapor phase polymerization. Its molecular weight is estimated by the manufacturer as $8–13 \times 10^6$. It has an ash content of 0.04 percent and contains no additives. The molecular weights are estimated in the order of $2.7–3 \times 10^6$ by both viscometry and light scattering measurements from the Polymer Characterization Section of the National Bureau of Standards. Whether the discrepancy in the molecular weights is caused by the degradation of the polymer

[2] Commercial materials are identified in this paper to adequately specify the experimental procedure. Such identification does not imply recommendation or endorsement by the National Bureau of Standards.

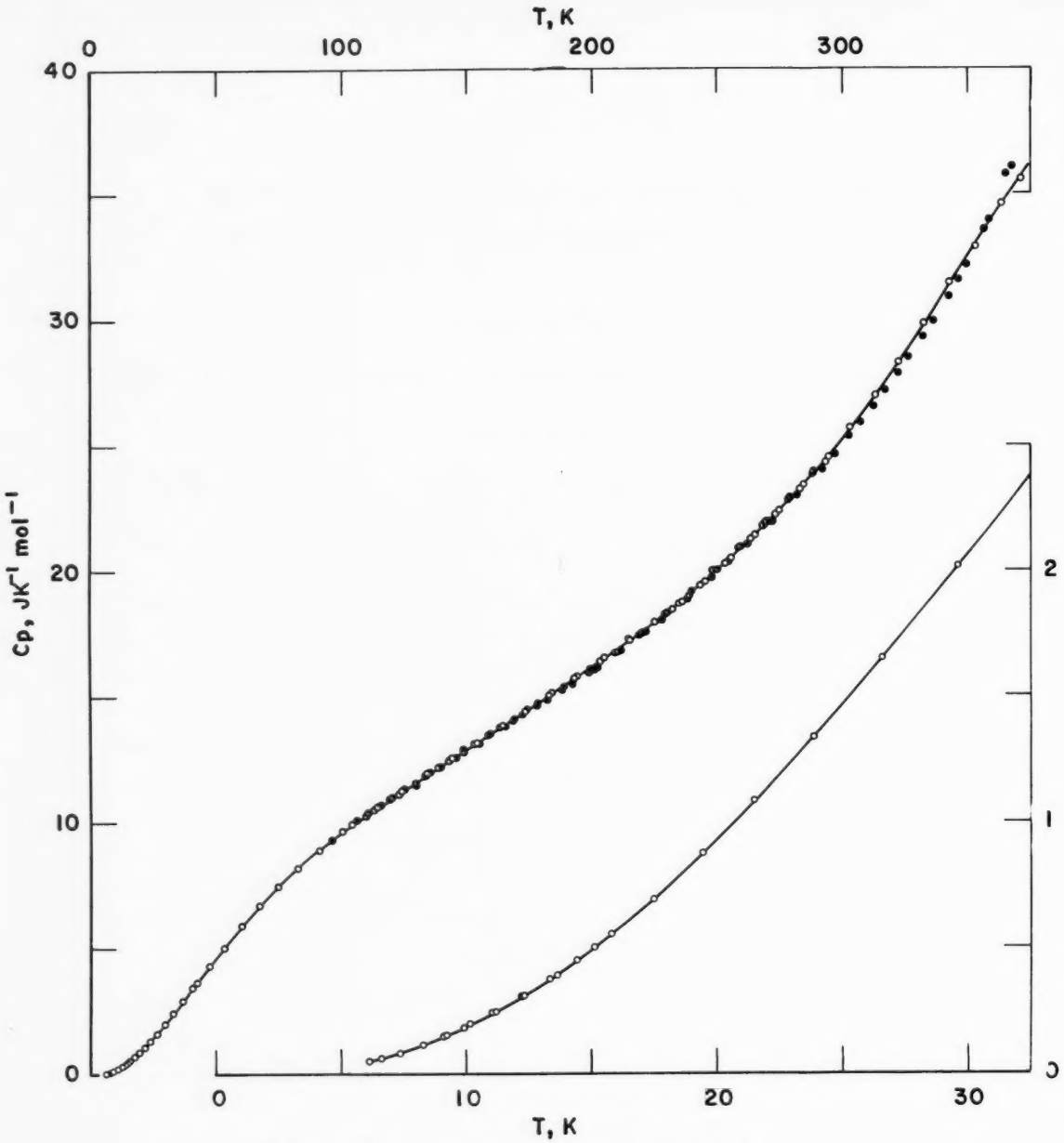

FIGURE 1. *Heat capacity of high molecular weight linear polyethylene.*

◑ Annealed at <300 K, ● annealed at 370 K, ○ quenched.

at high temperatures or by differences in the procedures to estimate the molecular weight was not determined.

The sample was received in the form of a powder. Attempts to fuse the powder together under its own weight in vacuum at 150 °C were not successful due to the high viscosity of the melt. The heating produced a sintered product. In order to avoid degradation of the high molecular weight material at high pressure and temperature, molding was not tried.

The material was pressed into pellets of about 1.27 cm in diameter and about 1 cm in height in a hydraulic press at room temperature. 73.891 g (mass in vacuum) of the material was loaded in the sample container for

at 3.8 cm Hg (5.1 kPa) at room temperature was sealed in to improve thermal conduction within the sample container.

3. Results

The results of the heat capacity measurements are tabulated in table 1 and shown graphically in figure 1. Table 1 is separated into various sections according to the thermal treatment the sample received. Within the section, the data are arranged in the order of increasing initial temperature of a series of heat capacity measurements. The series are numbered in chronological sequence throughout table 1 in order to facilitate the tracing of the thermal history of the sample.

TABLE 1. *Heat capacity data of high molecular weight linear polyethylene*

T, K	C_p, J K^{-1} mol^{-1}	T, K	C_p, J K^{-1} mol^{-1}
Quenched			
SERIES X		SERIES III	
6.13	0.0507	104.82	9.895
6.62	.0623	114.82	10.59
7.38	.0843	124.63	11.24
8.33	.1170	134.58	11.88
9.26	.1558	144.57	12.51
10.18	.1982	154.63	13.16
11.18	.2484	164.68	13.81
12.33	.3130	174.62	14.46
13.64	.3954	184.56	15.11
15.13	.5016	194.64	15.78
SERIES IX		SERIES VIII	
9.11	0.1500	113.50	10.50
9.96	.1875	123.38	11.16
11.06	.2445	133.50	11.81
12.27	.3106	143.76	12.46
13.37	.3773	153.86	13.11
14.48	.4536	163.71	13.74
15.80	.5549	173.57	14.39
17.50	.6963	183.45	15.06
19.45	.8758	193.35	15.69
21.51	1.082	203.39	16.36
23.87	1.335		
26.59	1.649		
29.63	2.015		
32.96	2.437		
36.62	2.916		
40.68	3.453		
SERIES XI		SERIES IV	
42.32	3.663	205.32	16.51
47.20	4.296	215.33	17.21
53.44	5.085	225.29	17.92
60.36	5.906	235.29	18.69
67.54	6.690	245.31	19.55
74.97	7.436	255.21	20.44
82.91	8.171	265.11	21.38
91.40	8.882	274.99	22.37
100.88	9.609	284.83	23.41
		294.73	24.55

TABLE 1. *Heat capacity data of high molecular weight linear polyethylene*—continued

T, K	C_p, J K^{-1} mol^{-1}	T, K	C_p, J K^{-1} mol^{-1}
Quenched			
SERIES V		SERIES XII	
205.41	16.50	303.29	25.70
215.44	17.19	313.08	26.96
225.40	17.92	322.98	28.27
232.41	18.45	332.98	29.80
236.45	18.77	342.96	31.43
243.46	19.40	353.02	32.84
253.42	20.29	363.28	34.56
263.36	21.23	370.79	35.52
273.38	22.21		
283.37	23.26		
293.33	24.35		
Slow-Cooled from 295 K			
SERIES I		SERIES II	
111.21	10.35	201.20	16.06
120.85	10.98	210.86	16.75
130.04	11.57	220.65	17.49
139.42	12.16	230.44	18.30
149.33	12.79	240.24	19.14
159.23	13.41	250.03	20.02
169.02	14.02	259.82	20.95
178.84	14.64	269.70	21.92
188.70	15.26	279.57	22.92
198.69	15.91	289.33	23.96
Quenched and then annealed at 225 K, and 143 K			
SERIES VI		SERIES VII	
110.07	10.27	209.60	16.67
120.01	10.94	219.52	17.42
129.92	11.57	229.35	18.23
139.87	12.20	239.08	19.10
149.65	12.83	248.78	20.03
159.42	13.44	258.62	20.84
169.42	14.07	268.58	21.76
179.44	14.70	278.62	22.76
189.48	15.34	288.71	23.84
199.55	16.00		
Annealed at 370 K			
SERIES XIII		SERIES XIV	
283.27	23.10	340.49	30.54
292.99	24.16	349.78	32.17
302.85	25.33	358.71	33.95
312.75	26.54	367.28	36.05
322.67	27.87		
332.59	29.29		
342.49	30.88		
Slow-Cooled from 370 K			
SERIES XV		SERIES XVII	
96.80	9.29	228.40	18.00
106.83	10.03	238.11	18.84
116.47	10.69	247.90	19.72
126.09	11.31	254.90	20.29
135.86	11.96	262.09	21.01
145.80	12.55	272.14	21.97
155.72	13.17	282.08	22.99
165.63	13.79	292.09	24.05

TABLE 1. *Heat capacity data of high molecular weight linear polyethylene*-continued

T, K	C_p, J K^{-1} mol^{-1}	T, K	C_p, J K^{-1} mol^{-1}
Slow-Cooled from 370 K			
SERIES XVI		SERIES XVIII	
172.39	14.21	297.52	24.63
182.23	14.83	307.32	25.90
192.21	15.45	317.06	27.14
202.23	16.10	326.91	28.46
212.18	16.79	336.84	29.93
222.06	17.52	346.75	31.57
		356.51	33.45
		366.15	35.72

Quenched samples were produced by admitting helium gas to the cryostat while the assembly was submerged in liquid nitrogen. A cooling rate in the order of 4–5 K min^{-1} was achieved. Slow-cooling (rate annealing) rates of 0.5–1 K h^{-1} were often used in conjunction with isothermal annealing (soak annealing) at a particular temperature for a period of days.

The temperature increment for a heat capacity determination may be inferred from the differences in the mean temperatures of the adjacent determinations within the series. Curvature corrections have been added to correct for the effect of the finite temperature increment of a determination. The precision of the measurement above 25 K is in the order of 0.05 percent. Below 25 K, the precision gradually changes to about 1 percent at 5 K. The accuracy over most of the temperature range of the measurement is comparable to the precision as indicated by heat capacity measurements on a Calorimetry Conference standard sample of sapphire [4].

Smoothed heat capacity values representing those of a quenched (5 K min^{-1}) high molecular weight linear polyethylene are listed in table 2. Enthalpy and entropy increments referring to the zero point enthalpy and the residual entropy of the sample are also listed. Since the partially crystalline sample is expected to have undetermined residual entropies at 0 K, Gibbs free energy is not given in table 2.

TABLE 2. *Thermodynamic properties of high molecular weight Linear Polyethylene*

($-CH_2-$=14.027)

T, K	C_p, J K^{-1}mol^{-1}	$H-H_0$, J mol^{-1}	$S-S_0$, J K^{-1} mol^{-1}
5	0.037	0.047	0.012
10	.190	.527	.073
15	.492	2.175	.203
20	.929	5.677	.401
25	1.463	11.63	.664
30	2.062	20.41	.983
35	2.702	32.31	1.349
40	3.360	47.47	1.752
45	4.016	65.91	2.186
50	4.656	87.60	2.642
60	5.862	140.3	3.600
70	6.946	204.4	4.586

TABLE 2. *Thermodynamic properties of high molecular weight Linear Polyethylene*-continued

($-CH_2-$=14.027)

T, K	C_p, J K^{-1}mol^{-1}	$H-H_0$, J mol^{-1}	$S-S_0$, J K^{-1} mol^{-1}
80	7.909	278.8	5.578
90	8.769	362.3	6.560
100	9.545	453.9	7.525
110	10.26	553.0	8.469
120	10.94	659.0	9.391
130	11.59	771.7	10.29
140	12.22	890.7	11.17
150	12.86	1016.	12.04
160	13.50	1148.	12.89
170	14.15	1286.	13.73
180	14.81	1431.	14.55
190	15.47	1582.	15.37
200	16.14	1740.	16.18
210	16.82	1905.	16.99
220	17.52	2077.	17.79
230	18.27	2256.	18.58
240	19.09	2443.	19.38
250	19.96	2638.	20.17
260	20.90	2842.	20.97
270	21.87	3056.	21.78
280	22.89	3280.	22.59
290	24.00	3514.	23.42
300	25.20	3760.	24.25
310	26.51	4019.	25.10
320	27.90	4291.	25.96
330	29.38	4577.	26.84
340	30.91	4877	27.74
350	32.46	5194.	28.66
360	34.00	5526.	29.60
370	35.44	5877.	30.55
380	36.76	6248.	31.51
273.15	22.18	3125.	22.04
298.15	24.97	3714.	24.10

4. Discussion

The crystallinity of 45 percent for this powdery sample was estimated from heat of fusion measurements using a dynamic scanning calorimeter. Heat of fusion of a pressure crystallized linear polyethylene (96% crystallinity) [6] was used as the reference.

Although the high molecular weight sample has lower crystallinity than the SRM 1475 in the condition as received (71% crystallinity) [5], it shows a somewhat lower heat capacity over the temperature range 90 to 310 K. Only at lower and higher temperatures does this sample exhibit the expected higher heat capacity. The heat capacity of this sample is very similar to that of a sample of SRM 1475 slowly cooled from the melt (88% crystallinity) [6] in the temperature range 100 to 220 K.

In a plot of heat capacity differences, figure 2, between the heat capacity of this sample and that extrapolated for crystalline linear polyethylene [6], the changes in the 150 and 240 K regions are not as large as that for the 71 percent crystallinity sample. Beatty's data [2] are also included in figure 2. A relatively rapid heat capacity increase over that of the crystalline linear polyethylene occurs in the tempera-

ture region of 120 to 170 K. Above 200 K, the scattering of the data causes difficulties in the conclusion of either the existence or nonexistence of a subtle heat capacity change. DTA or DSC studies on some other high molecular weight polyethylene samples suggested the occurrence of a step change in the heat capacity around 150 K [7, 8] and indicated a surprisingly constant heat capacity difference between the high molecular weight sample and a high crystallinity sample [8].

The lack of a strong glass-like feature in the heat capacity behavior of this high molecular weight material is in parallel to a recent thermal expansivity study on the same materials. Low temperature thermal expansions of polyethylene samples have been studied on strips of compression molded thin films [9]. The

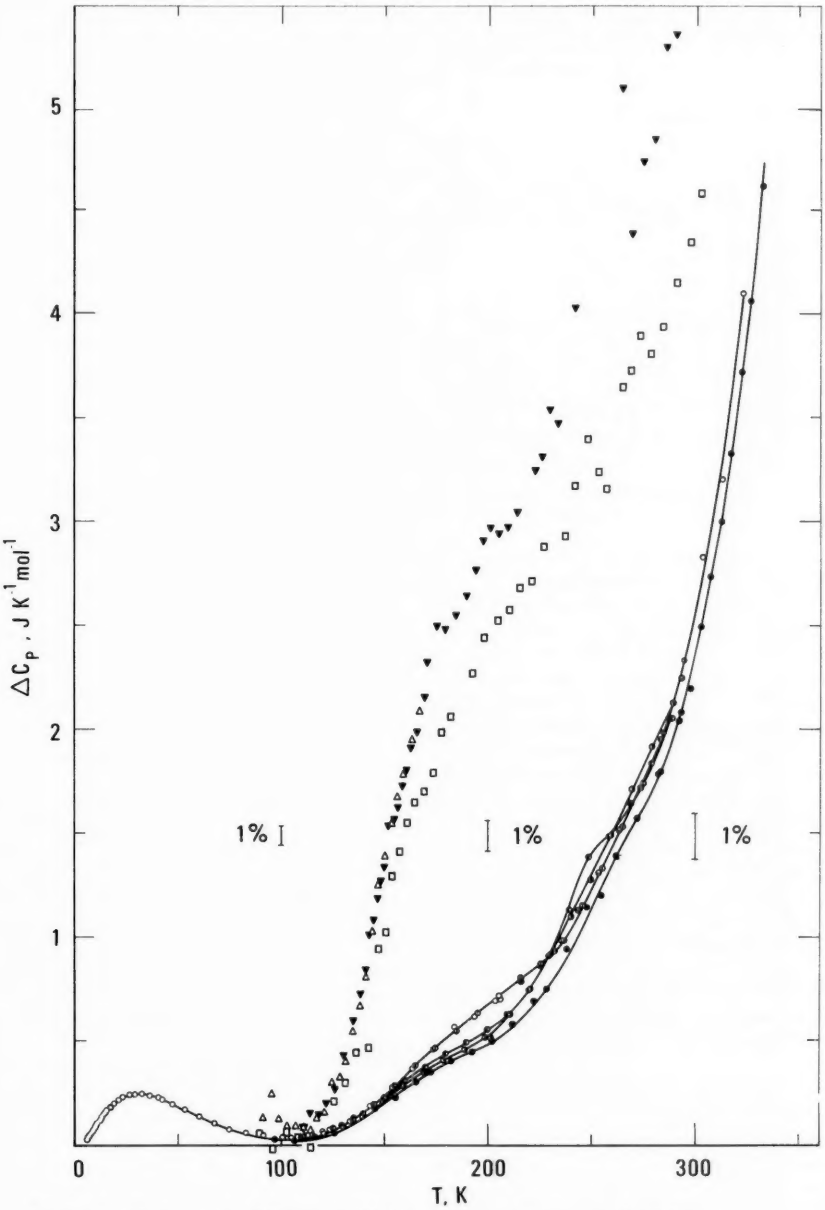

FIGURE 2. *Heat capacity differences of high molecular weight linear polyethylene.*

This research: ◐ and ◑ annealed at < 300 K; ● annealed at 370 K; ○, ⊘ and ⊖ quenched. Beatty [2]: △ run 1; ▼ run 2; □ run 3.

samples included the two Standard Reference Materials 1475 and 1476, used in a previous calorimetric study [5], and the high molecular weight sample used in the present calorimetric work. In all three samples, double peaks in the derivatives of the thermal expansion coefficients at about 110 and 150 K were observed. These peaks are stronger in linear polyethylene than in branched polyethylene. Weaker peaks were observed in the temperature range 180 to 200 K. Above 200 K, there were strong peaks in the branched polyethylene, a weak one in the high molecular weight sample and only a monotonic increase in the ordinary linear polyethylene.

Although the appearance of a discontinuity in the heat capacity behavior is perhaps a necessary condition for a glass transition, it is not a sufficient condition. A broad distribution in the relaxation times may cause the glass transformation to occur over a wide temperature range, thus making a weak heat capacity discontinuity in partially crystalline material even more difficult to assess. Since the glass transition is kinetic in nature, relaxational phenomena should also be observed in the glass transition region. One highly sensitive method to detect the thermal relaxation is the method of observing the spontaneous temperature changes of the sample under adiabatic conditions [10]. The sign and the magnitude of the temperature drift as a function of time and temperature may be correlated with different thermal treatments and histories. Both the discontinuity in the heat capacity behavior and the adiabatic temperature drift are commonly observed in glass transition regions of various materials and also in glass-like transitions in crystals [11].

The drift observations are shown in figure 3. These are the drift rates observed at 20 minutes after the heater energy has been turned off. Because of the geometric arrangement of various components in the sample container [4], the temperature of the thermometer and the heater is slightly higher than that of the sample during the heating period. Therefore, when the energy is turned off, there is an exponential decay of the temperature of the thermometer until a thermal equilibrium is reached between the sample and the sample container assembly. The decay constant depends on the construction of the sample container, the thermal conductivity of the sample and the amount of helium gas sealed in the sample container. The decay constant is about 50 s for this sample container [12] at high temperatures and less at lower temperatures. Therefore up to 10 to 15 minutes may be required for the sample to reach a temperature distribution which is uniform to within 10^{-4} K.

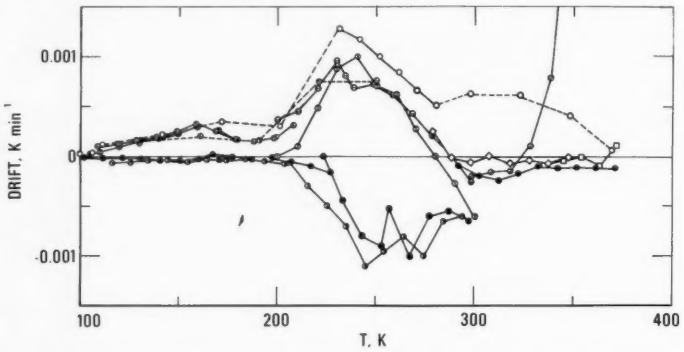

FIGURE 3. *Spontaneous adiabatic temperature drift of high molecular weight linear polyethylene.*

Open circles and squares (quenched): ⦶ Ser. III and IV, ⊖ V, ⊘ VIII, ⊘ XII, ◇ XIII, □ XIV, ○ before Ser. XV and ⊗ before Ser. IX, drift observations only. Filled or half-filled circules (annealed): ◑ I and II, ● XV–XVII.

The drift behavior in the 240 K region for the high molecular weight material occurs in similar temperature range and magnitude as that observed for the as-received SRM 1475 [6, 10] and is presumed to be caused by the relaxational behavior in the amorphous phase. For the quenched sample, i.e., cooling rate is greater than the rate of heat capacity determination of 5–10 K h^{-1}, the drift rate is generally positive (exothermic) with a broad peak around 230 K. There is also a weaker peak at around 160 K. When the sample was heated to 370 K for the first time, large exothermic behavior showed up above 330 K, indicating the onset of further crystallization processes. For the sample either slow-cooled continuously to 100 K or annealed at 225 and 140 K, there is an endothermic peak only around 245 K. No endothermic behavior was observed at temperatures below 210 K for the sample either slow cooled or annealed. Thus the weaker exothermic peak occurring around 160 K for quenched samples is presumed due to some stabilization processes such as the relief of strain.

In the broad temperature region near 240 K, the drift behavior as observed in figure 3 and in other linear polyethylene samples [6, 10] seems to indicate the existence of double peaks. Special thermal treatments were performed in attempts to resolve these peaks. Figure 4 shows the results of the drift observations for two combinations of quenching, annealing and slow cooling treatments. The sample was first annealed at 250 K for 1 day and then quenched from 250 K. Upon

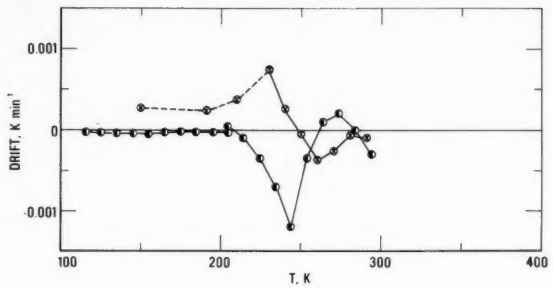

FIGURE 4. *Spontaneous adiabatic temperature drift of high molecular weight linear polyethylene.*

⊗ Annealed at 250 K and then quenched from 250 K (before Ser. IX). ◐ Quenched from 360 K and then annealed at 225 K and 143 K (Ser. VI and VII).

heating the sample, it showed exothermic behavior, similar to that of a quenched sample, at temperatures below 250 K. Above 250 K, endothermic effects similar to an annealed sample were seen.

The sample was quickly cooled (5 K min^{-1}) to 225 K and held there for 4 days, until the drift decreased from an initial value of greater than 1 mK min^{-1} to less than 0.05 mK min^{-1}. It was then slowly cooled (2.5 K h^{-1}) to 143 K and held there for 2 days. An endothermic peak was observed at about 245 K. Above 245 K, a small exothermic peak appeared near 270 K. Apparently annealing at 225 K did not relax the configurations associated with the higher temperature peak.

The two regions around 240 and 270 K may be caused by different types of amorphous relaxation mechanisms, such as from the loose ends of the polymer molecules or from the molecular segments with both ends confined in crystalline regions. However, the mechanisms responsible for the relaxational behavior observed here have not been determined.

The author wishes to thank R. G. Christensen for the molecular weight determinations and C. H. Pearson for the assistance in calorimetric measurements.

5. References

[1] Beatty, C. L., and Karasz, F. E., Bull. Am. Phys. Soc. Ser. II, **16,** 1391 (1971).
[2] Beatty, C. L., Ph. D. thesis, University of Massachusetts (1972).
[3] Dainton, F. S., Evans, D. M., Hoare, F. E., and Melia, T. P., Polymer **3,** 277 (1962).
[4] Sterrett, K. F., Blackburn, D. H., Bestul, A. B., Chang, S. S., and Horman, J. A., J. Res. Nat. Bur. Stand. (U.S.), **69C** (Engr. and Instr.) No. 1, 19–26 (Jan.–Mar. 1965).
[5] Chang, S. S., and Bestul, A. B., J. Res. Nat. Bur. Stand. (U.S.) **77A** (Phys. and Chem.), No. 4, 395–405 (July–Aug. 1973).
[6] Chang, S. S., J. Res. Nat. Bur. Stand. (U.S.), **78A** (Phys. and Chem), No. 3, 387–400 (May–June 1974)
[7] Stehling, F. C., and Mandelkern, L., Macromol. **3,** 242 (1969).
[8] Illers, K. H., Koll. Z **250,** 426 (1972); **252,** 1 (1974).
[9] Lee, S., and Simha, R., Macromol. **7,** 909 (1974).
[10] Chang, S. S., J. Polymer Sci. Sym. **43,** 43 (1973).
[11] Suga, H., and Seki, S., J. Non-cryst. Solids **16,** 171 (1974).
[12] Chang, S. S., Rev. Sci. Instr. **40,** 822 (1969).

(Paper 80A1–881)

JOURNAL OF RESEARCH of the National Bureau of Standards—A. Physics and Chemistry
Vol. 80A, No. 1, January–February 1976

Computer Simulation of Metastable Fluid States in the Lennard-Jones System

Harold J. Raveché

Institute for Basic Standards, National Bureau of Standards, Washington, D.C. 20234

and

William B. Streett

Science Research Laboratory, U.S. Military Academy, West Point, New York 10996

(November 11, 1975)

Using the Monte Carlo method in statistical mechanics, we have simulated high density metastable states. We find that nucleation from a three dimensional fluid array to a crystalline solid is possible, but that periodic boundary conditions and the small size of the system inhibit the formation of perfect crystals. Evidence for the existence of an amorphous solid state has also been observed, and the pair correlation function of this state exhibits some of the features associated with random close-packed arrays of hard spheres. The possible relation between these simulations and the formation of glassy states in real systems is briefly discussed.

Key words: Glassy state; Lennard-Jones system; Monte Carlo simulation; nucleation; overcompression; supercooling.

1. Introduction

Thermal and structural properties of metastable fluid states associated with subcooling are of interest in several problems, including glass formation, nucleation and crystal growth, and disordered alloys.

We report briefly on Monte Carlo [1][1] simulations of metastable states in systems of 108 and 256 particles interacting through the Lennard-Jones 6–12 potential function. The energy and length parameters are denoted by ϵ and σ, respectively. With N_A the Avogadro constant and k_B the Boltzmann constant, the following reduced units are used: volume, σ^3; pressure, ϵ/σ^3; energy, $N_A\epsilon$; and temperature, ϵ/k_B. We report simulations at temperatures of $T=0.80$, 1.17, and 2.74 for densities between 1.05 and 1.38. Pressures for these states are well into the kilobar range.

The computations proceed as follows. The coordinates of a disordered fluid array, obtained from an equilibrated simulation at a liquid-like density, are scaled to a high density at a temperature at which the lowest energy state is that of a crystalline (fcc) solid [2]. (The initial configuration thus has the character of a metastable fluid state, which can be realized in a real fluid by undercooling or overcompression.) We then determine whether the simulation converges to particular values of the pressure and internal energy, and whether, on the molecular level, it converges to a state which is not noticeably labile.

We find that the thermodynamic properties do in fact converge, after runs of the order of 10^7 configurations, but that the resulting pressures and energies are higher than those of the crystalline solid at the same density and temperature. Examination of the molecular structure indicates that some of these runs converged to distorted fcc crystals, while others converged to comparatively amorphous states, with structures similar to the random close-packed structures studied by Finney [3] and Bernal [4]. Such structures have been discussed by Turnbull [5] as a possible model for the ideal glass state.

Although the sequence of configurations generated in a Monte Carlo simulation is produced by a random process, each configuration differs from the preceding one by at most a small displacement of a single particle. Hence it is not unreasonable to consider that the progress of the simulation bears an approximate relation to the progress of real time. Examination of the molecular structures resulting from these simulations may therefore provide some insight into crystal nuclea-

[1] Figures in brackets indicate the literature references at the end of this paper.

tion and glass formation in metastable fluids composed of simple molecules. Nucleation phenomena similar to those reported here have recently been observed in molecular dynamics simulations of the same model [6]. Previous work on soft-sphere systems [7] also indicates similar results for repulsive potentials which vary as the inverse twelfth power of the internuclear separation.

2. Results and Discussion

The results for the pressure and energy at $\rho=1.375$ and $T=2.74$ are shown in figure 1a; this density is

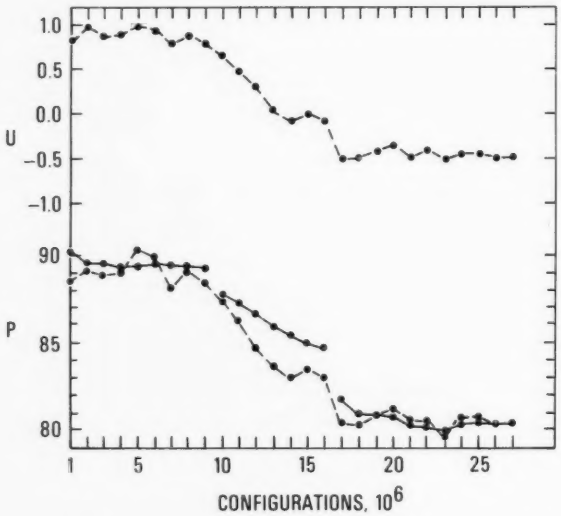

FIGURE 1a. *The pressure and energy (in Lennard-Jones units) as a function of the number of configurations at $\rho=1.375$ and $T=2.74$.*

The dashed curves are averages over the most recent 10^5 configurations and the solid curves is the cumulative average. The breaks in the solid curve indicate that the particle coordinates at these points were used to initiate a new simulation.

about 30 percent beyond the freezing density which was reported [2] for the $T=2.74$ isotherm. The solid curves are the cumulative averages and the dashed curves are the averages over the most recent 10^5 configurations. The breaks in the solid curve at 9×10^6 and 16×10^6 configurations indicate that the particle coordinates at these points were used to initiate a new simulation. The very close agreement between the solid and dashed curves beyond 17×10^6 clearly indicates convergence. (The corresponding results for the internal energy behave similarly.) The nearly horizontal curves at the left of figures 1a and 2a were characterized by extensive displacements of the particles from their initial positions—in other words "liquid-like" behavior. As the pressure and energy decreased, the net particle displacements over each 10^5 configurations likewise decreased. At the horizontal portion of the curves at the end of each run, the molecular structure was no longer labile; that is, the particles appeared to be locked into a fixed array undergoing only small displacements from their mean positions as the computation proceeded. The pressure and energy converged to values of 80 and -0.5, respectively. The pressure and energy obtained from a simulation of an fcc array at the same density and temperature are 72 and -1.9, respectively.

The pair correlation function, $g(r)$ at 5×10^6 and at 27×10^6 is shown by the solid curves in figure 1b and figure 1c, respectively. For comparison, the correlation function for a simulation of an fcc array at the same density and temperature is shown by the dashed curve in figure 1c. The local maxima in this curve occur approximately at the first, second, third, etc., nearest neighbor distances of the fcc solid. The results in figures 1b and 1c suggest that nucleation has occurred

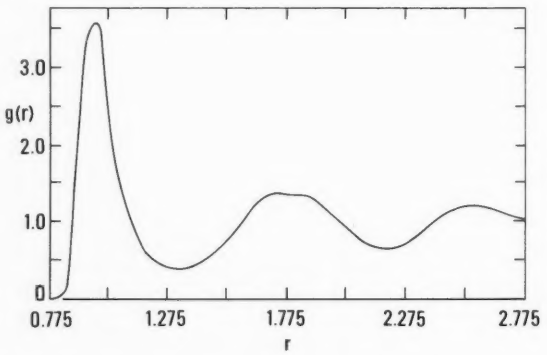

FIGURE 1b. *The pair correlation function, g(r), for the simulation in figure 1a at 5×10^6 configurations.*

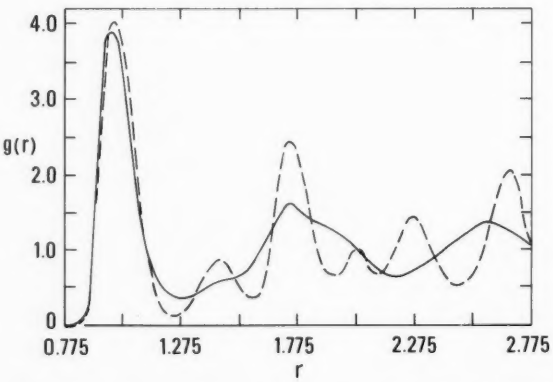

FIGURE 1c. *The same as figure 1b except solid curve is at 2.7×10^7 configurations and the dashed curve is from the simulation begun from fcc array.*

and that the initially metastable fluid has converged to an imperfect crystalline array. Visual inspection of three-dimensional structure at 27×10^6 configurations by means of stereoscopic pairs of 35 mm photographs confirms the existence of distorted crystalline planes.

More striking evidence for nucleation to a crystalline array was obtained at $\rho = 1.105$ and $T = 0.80$, which is less than one-half the freezing temperature [2] at this density. The results for the pressure and the average root mean square displacement of a particle (rms) from its initial position are shown in figure 2a.

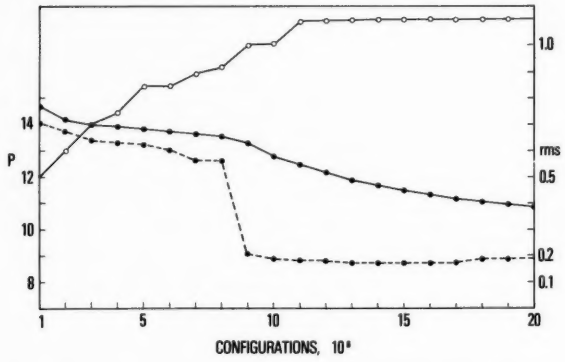

FIGURE 2a. *The pressure and average root mean square displacement (rms) for $\rho = 1.105$ and $T = 0.80$.*

The rms (open circles) is in units of the distance parameter, σ.

The pressure over the most recent 10^5 configuration converged to 8.93 and the result for a run begun from fcc positions was 9.03. The internal energy for both runs converged to the same value, -7.17. The behavior of the rms suggests that as the system equilibrates the positions of the atoms are not particularly labile. This can be qualitatively interpreted as restricted diffusion.

The pair correlation for the runs are shown in figure 2b, as before the dashed curve is for the run begun from fcc coordinates and the solid curve is for the run begun from a random array. Both curves are identical to radial distances comparable to the second nearest-neighbor distance and the close similarity for larger interatomic separation clearly indicates crystalline order. These results should be compared with figure 2c which shows the pair correlation function at

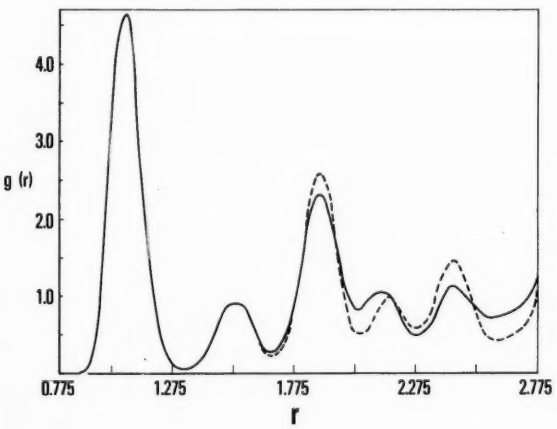

FIGURE 2b. *The pair correlation function,* g(r), *at 2.0×10^7 configurations for the simulation shown in figure 2a.*

The result for the simulation begun from fcc array is given by dashed curve.

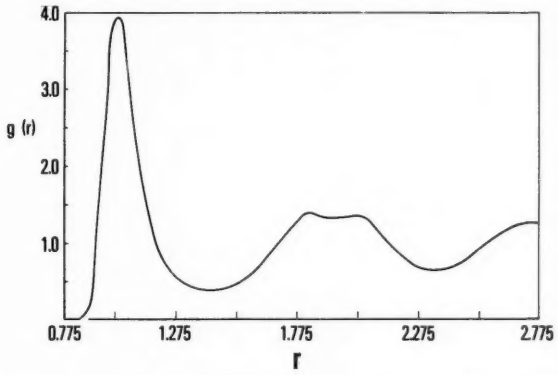

FIGURE 2c. *The pair correlation function at 2.0×10^6 configurations for the simulation in figure 2a.*

2.0×10^6 configurations in the course of the run begun from the random array. Evidently the local order in the random system underwent distinct changes between 2.0 and 20×10^6 configurations.

The formation of a perfect crystalline lattice in these simulations is greatly hindered by the periodic boundary conditions which are used to avoid surface effects. Unless the crystal nucleates with its principal axes parallel to the axes of the reference coordinate system, it will necessarily undergo a severe strain at the boundaries of the cube in which the particles are confined. It therefore seems likely that homogeneous nucleation has occurred in these runs but that the failure to reach a perfect crystalline structure is an artifact of the periodic boundary conditions and perhaps of the small size of the system.

Similar computations on the $T = 2.74$ isotherm were performed at $\rho = 1.30$ which is approximately 20 percent beyond the freezing density [2]. The results are given in figures 3a and 3b. The general behavior of the pressure and energy is similar to the previous simulation. (The pressure and energy after convergence are 59 and -2.4, respectively, compared to 53 and -3.3 for a simulation of an fcc array at the same temperature and density.) The molecular order, however, suggests different features. The pair correlation function in figure 3b shows no evidence of the fcc ordering indicated by the solid curve in figure 2b. Visual inspection of the atomic coordinates at 19×10^6 configurations by means of stereoscopic pairs of photographs indicated an amorphous structure, with little evidence of distorted crystalline planes. During the same sequence of configurations, the molecular structure gradually ceased to be labile and the particles

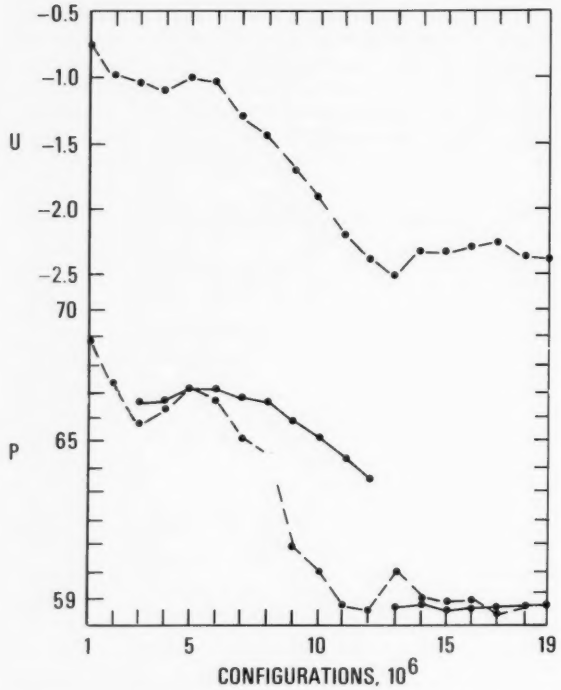

FIGURE 3a. *The same as figure 1a except $\rho = 1.30$.*

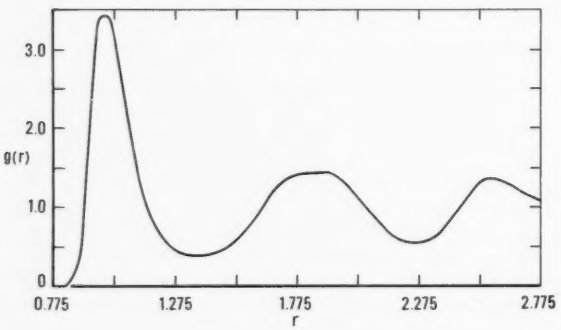

FIGURE 3b. *The pair correlation function, g(r), for the simulation shown in figure 2a at 1.9×10^7 configurations.*

became locked onto a disordered array. This was also manifested in the pair correlation function which did not change by more than ± 1 percent beyond 14×10^6 configurations.

We infer from this that the molecular order became locally more close-packed as the pressure and energy converged. The amorphous structure at convergence is suggestive of the formation of a glassy state. In figure 3b there is no evidence of the subdued second nearest neighbor peak at $r \simeq 1.45$, present in the solid curve of figure 2b. In previous studies [2] we have observed that the existence of fcc lattice structure results in a subdued peak or "step" in this region of the pair correlation function. The pair correlation shown in figure 3b exhibits some of the features found in studies of random close-packed arrays of hard spheres [3]. In particular, the broad second maximum can be interpreted as two separate peaks, centered at approximately $r = 1.75$ and $r = 1.95$. Bernal [4] attributes the first of these to the presence of tetrahedra which share a common base, and the second to the collineation of three particles.

The relation between the structure of a random close-packed system and that of an ideal glass has been discussed in detail by Turnbull [5]. It is sufficient to remark here that the structure of the glass state in macroscopic systems is still an important unresolved problem.

We have investigated the reproducibility of the simulations in the metastable region by repeating the calculations with initial coordinates obtained from a random number generator. The results for $\rho = 1.30$ and $T = 2.74$ are shown in figure 4a. These should be compared to the results shown in figure 3a which, as we have noted, are for a simulation begun with the coordinates of an equilibrated run at liquid-like densities [2]. The dashed curves indicate the simulations are reproducible to within 4 percent and we conjecture that the differences would be smaller if the simulation in figure 4a had been continued to the same number of configurations as that in figure 3a.

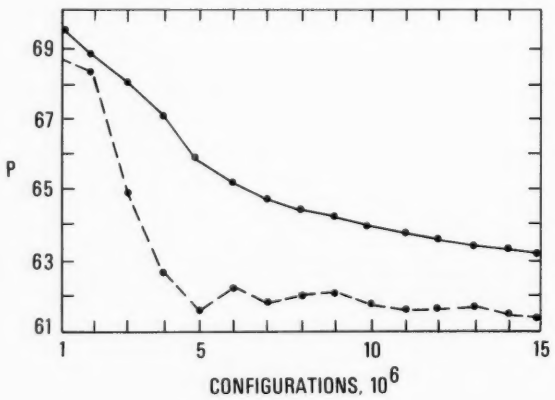

FIGURE 4a. *The pressure for simulation at $\rho = 1.30$ and $T = 2.74$ begun from coordinates obtained from a random number generator.*

The pair correlation function obtained from the simulation in figure 4a at 15×10^6 is quite similar to that shown in figure 3b. In particular the function shows no evidence of the crystallinity shown in figures 1b and 2b.

The constant pressure heat capacity for the Lennard-

Jones system can be computed in terms of pressure and energy fluctuations, ΔP and ΔU respectively, by

$$C_p = \frac{\langle (\Delta U)^2 \rangle}{k_B T} - \frac{1}{k_B^2 T^3} \times \left[\frac{\langle \Delta P \Delta U \rangle^2}{\langle (\Delta P)^2 \rangle / k_B T - 7PV + 8U/V^2} \right].$$

The first term on the right is the constant volume heat capacity and the second term represents the ratio of the square of the compressibility to the expansivity. For potentials of the Lennard-Jones type (integer power law function) the ratio can be written in terms of pressure and energy fluctuations [8].

The results for the configurational heat capacity for the simulation shown in figure 4a are given in figure 4b. Since the pressure and energy fluctuations

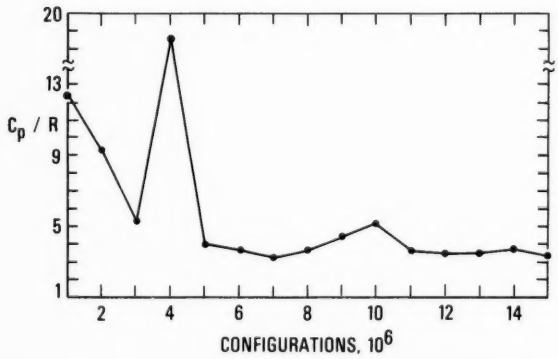

FIGURE 4b. *The constant pressure heat capacity in units of the gas constant for the simulation shown in figure 4a.*

are large, the heat capacity also has large fluctuations. For reference, we note that the heat capacity of the crystalline solid was estimated to be 3.4 which is close to the result for the glassy state shown in figure 4b.

Size effects have been studied by performing simulations on 108 particle systems. There is one noticeable difference between the 108 and 256 particle systems: the convergence is not as complete in the smaller system. That is, the converged values of the pressure and energy in the smaller system are higher than those in the larger system at the same density and temperature. This is shown in figure 5 where we have plotted results from both the 108 (denoted by triangles) and the 256 (denoted by solid circles) particle systems on the $T=1.17$ isotherm [2]. The circled crisscross denotes the density at which both size systems were initially prepared in a fluid array. After the systems had reached convergence in pressure and energy, the density in each system was successively decreased and the coordinates from each preceding simulation were used to begin a new run. From figure 5 we note that

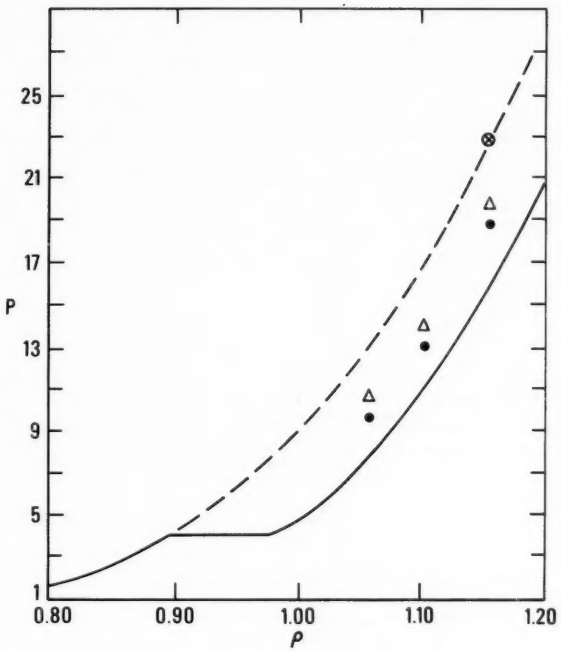

FIGURE 5. *Results on the* T = *1.17 isotherm with 108* (△) *and 256* (·) *particle systems.*

The circled crisscross denotes the density. The density was successively decreased and the coordinates of each preceding state were used to initiate a new simulation.

data points for both size systems form smooth curves which give higher pressures than those of the fcc crystalline phase. As with the results on the $T=2.74$ isotherm, the data in figure 5 show that nucleation is possible but that the periodic boundary conditions and small size prevent complete crystallization. Below densities of approximately $\rho=1.05$, the systems "melt" and, as expected, the pressures join to the fluid branch.

In summary, we have shown that nucleation from a fluid to a crystalline array is possible in a small three dimensional system with periodic boundary conditions. The results indicate that there is an amount of overcompression or supercooling which must be exceeded to observe the characteristic decrease in pressure and internal energy. That is, unless the overcompression is of a certain magnitude, the thermodynamic properties of the initially random arrays appear to fluctuate about values which are typical of a smooth extension of the equilibrium fluid phase. For the isotherms we have investigated the lower limit of overcompression appears to be 15–20 percent. For a given density, the investigations suggest that even a larger amount of supercooling may be required. We have examined the role of size in determining the completeness of the observed crystallization. In addition, we have found evidence for the existence of an amorphous close-packed array which has some of the characteristics of

a model proposed [5] for the glass state in macroscopic systems. If the existence of this state is confirmed in additional studies, it may prove useful in the study of the molecular structure of the glass state. Since we have seen that the small systems can undergo nucleation to a crystal, this suggests that the amorphous solid state may be a well defined metastable state between the fluid and crystalline phases.

The computations suggest further investigations at high densities and lower temperatures. We have preliminary results for several states which are consistent with those reported here.

We are grateful to the U.S. Military Academy Academic Computer Center and to the Peaceful Uses of Nuclear Explosives Branch of the Energy Research and Development Administration for generous grants of computing time. We are indebted to Mrs. Pamela Kingsbury and Dr. Leroy Schroder for their invaluable help with ORTEP. We also wish to acknowledge the very kind assistance of Lt. Foss Smith and Capt. John Robertson with the computer.

3. References

[1] For a review see, for example: Wood, W. W., in Physics of Simple Liquids edited by H. N. V. Temperley, J. S. Rowlinson and G. S. Rushbrooke (North-Holland, Amsterdam, 1968).
[2] Streett, W. B., Raveché, H. J., and Mountain, R. D., J. Chem. Phys. **61**, 1960 (1974).
[3] Finney, J. L., Proc. Roy. Soc. Lond. A **319**, 479 (1970).
[4] Bernal, J. D., Proc. Roy. Soc. Lond. A **280**, 299 (1964).
[5] Turnbull, D., Contemp. Phys. **10**, 473 (1969).
[6] Rahman, A., private communication.
[7] Hiwatari, Y., Matsuda, H., Ogawa, T., Ogita, N., and Ueda, A., Progr. Theor. Phys. **52**, 1104 (1974).
[8] Brown, W. Byers, Phil. Trans. **A250**, 221 (1957).

(Paper 80A1–882)

JOURNAL OF RESEARCH of the National Bureau of Standards—A. Physics and Chemistry Vol. 80A, No. 1, January–February 1976

Relative Enthalpy of Solid Beryllium Aluminate (Chrysoberyl), $BeO \cdot Al_2O_3$, from 1175 to 2025 K, and of Liquid Beryllium Aluminate from 2170 to 2350 K*

S. Ishihara** and E. D. West***

(October 30, 1975)

The relative enthalpy of solid beryllium aluminate $BeO \cdot Al_2O_3$ from 1180 to 2025 K and liquid beryllium aluminate from 2170 to 2350 K was measured by "drop" calorimetry using an adiabatic "receiving type" calorimeter. The thermodynamic functions from 1175 to 2025 K and the enthalpy of melting at 2146 K are reported.

Key words: Beryllium aluminate; chrysoberyl; drop calorimetry; enthalpy measurements; high temperature calorimetry; specific heat; thermodynamic properties.

1. Introduction

Naturally occurring $BeO \cdot Al_2O_3$ (chrysoberyl) has variable and appreciable amounts of impurities such as Cr, Fe, Si, Na, Li, K, and Ti [3, 4, 5].[1] Little or no accurate work has been done on the thermodynamic properties of this material in its natural state. The heat capacity of synthetic 1:1 beryllium aluminate from 16 to 380 K and the relative enthalpy from 273 to 1173 K have been previously measured at the National Bureau of Standards [1, 2]. The present work has been undertaken to extend the range of accurate thermodynamic data on this material to near its melting temperature. $BeO \cdot Al_2O_3$ is reported to melt at 2146 ± 10 K[2] [6]. We have made some enthalpy measurements beyond this temperature in a welded capsule so that the enthalpy of melting can be estimated.

2. Experimental Procedures

2.1. Sample

The $BeO \cdot Al_2O_3$ sample used in this work was prepared by Semi-Elements Inc. of Saxonburg, Pa.,[3] by arc-fusion of a stoichiometric mixture of high purity powdered BeO and Al_2O_3. The homogeneity of the lot has been adequately established and the sample is from the same lot as described in references [1, 2]. The fine material in the samples was removed by passing it thru a 16-mesh stainless steel screen. Occasional dark particles remaining on the screen were discarded.

After 2.5 years storage in a plastic bottle on a laboratory shelf the water content was determined to be 0.16 percent by the Microchemical Analysis Section of the National Bureau of Standards. The sample was heated to 1325 K in a carbon-hydrogen-nitrogen analyzer. The water in the sample was separated by a gas chromatographic column and then detected by thermoconductivity. This result is consistent with the 0.2 percent mass loss observed in our furnace under similar conditions.

A new spectrochemical analysis of the sample showed small differences from the earlier ones [1, 2]. The results of the analyses are tabulated in table 1. Six samples designated A, B, C, D, G, and H were used in this work of which C and D were not analyzed because they duplicate A and unexposed samples, respectively. The only significant difference between the exposed and unexposed samples is the small amount of container material found in the former. This could be due to abrasive action of the hard material on filling and emptying the container, chemical combination, or sublimation. After exposure to higher temperatures (1700 K and above) the surface of the crystals appeared slightly grayish and the fused sample showed patches of gray areas; however, no difference in chemical composition between the light and gray areas could be detected.

The samples are identified as in tables 1 and 2. A brief history of the samples is as follows:

A. Heated in an unsealed molybdenum container. Total mass loss in two experiments at 1700 K was 0.38 percent.

* This work was sponsored by the Advanced Research Projects Agency, Department of Defense, under ARPA Order No. 20, and by the U.S. Air Force Office of Scientific Research under Order No. OAR ISSA 65-8.

** Deceased.

*** Present address: Calorimetrics, Inc., Box 4146, Boulder, CO 80302.

[1] Figures in brackets indicate the literature references at the end of this paper.

[2] IPTS 1968.

[3] Certain commercial materials and products are identified in this paper to adequately specify the experimental procedure. Such identification does not imply recommendation or endorsement by the National Bureau of Standards.

597-633 O - 76 - 5

TABLE 1. *Impurities detected in the spectrochemical analyses of* $BeO \cdot Al_2O_3$

	Mass %					
	Ref. [1, 2]	Unexposed	A	B	G	H
Ag	< 0.0001	—	—	—	< 0.001	—
Ba	—	< 0.001	< 0.001	—	< .001	< 0.001
Ca	.001–.01	.001–.01	.001–.01	< 0.001	< .001	< .001
Cr	—	< .001	< .001	—	.001–.01	.001–.01
Cu	.01–.1	.001–.01	< .001	.001–.01	.001–.01	.01–.1
Fe	.001–.01	.01–.1	.01–.1	.01–.1	.001–.01	.01–.1
Mg	.001–.01	.01–.1	.01–.1	.01–.1	.01–.1	.01–.1
Mn	—	< .001	< .001	—	< .001	< .001
Mo	—	—	.01–.1	.01–.1	.001–.01	—
Na	—	—	—	—	.01–.1	.01–.1
Ni	.01–.1	—	—	—	—	—
Pb	< .001	—	—	—	—	—
Si	< .01	.01–.1	.01–.1	.001–.01	.001–.01	.001–.01
Sn	< .001	—	—	—	—	—
Sr	—	—	—	—	.001–.01	.001–.01
V	.001–.01	—	—	—	—	—
W	—	—	—	—	—	< .001

B. Heated in an unsealed molybdenum container. Mass loss on heating to 1700 K was 0.4 percent and additional loss on heating to 2000 K, 0.07 percent. There was no further significant change in mass.

C. Heated in an unsealed molybdenum container. Mass loss on heating to 1180 K was 0.25 percent with an additional loss of 0.1 percent on heating to 1700 K. There were no further significant changes.

D. Heated in an unsealed molybdenum container. Mass loss on heating to 1180 K was 0.24 percent.

G. Heated 6 hours in a platinum crucible in the flame of Meker burner at 1200 K before loading in a molybdenum inner container. During the sealing process by electron beam welding, the container lost 3.06 mg. Because of the extremely localized heating of the process, the mass loss was taken to be molybdenum. No further significant mass changes were observed.

H. Pretreated as in G but loaded in a tungsten inner container. During the welding process this container lost 2.70 mg. There were no further significant mass changes.

2.2. Containers

Tungsten and molybdenum, both 99.95 percent pure, were used as container materials. Two types of containers are used. The first type, which we call an outer container, is used at lower temperatures where sample mass losses are negligible. It is not sealed, so that the sample can be loaded into the container as small lumps and removed to determine a sample and container mass for each experiment. The second type, used at higher temperatures and throughout the liquid range, consists of the unsealed outer container and an inner container vacuum sealed by electron beam welding after adding a weighed amount of sample. This technique has the advantage that the mass of the inner container does not change and any significant changes in mass of the outer container can be accounted for experimentally. It has the disadvantage that the experiment gives the combined enthalpy of the sample plus the inner container, for which a correction must be made.

To determine this correction, the enthalpy of a molybdenum sample, machined from the same rod used for the inner container, was determined in the same series of measurements and in the same outer container, whenever the enthalpy of an inner container with sample was measured.

2.3. Enthalpy Measurements

The method of enthalpy measurements and the apparatus used in this work [15] will be described briefly. After the capsule (full or empty) has reached temperature equilibrium in the furnace it is lifted from the furnace into a "receiving" type adiabatic calorimeter operating near room temperature. If the position, flight time, shutter sequence, emissivity, and the furnace temperature are the same, the difference in heat energy received by the calorimeter from the full and empty capsule is the change in enthalpy of the contents. An automatic servo-regulated lifting device is used to keep the position and flight time of the capsule the same. The furnace is inductively heated and a Leeds and Northrup automatic optical pyrometer monitors and controls the temperature of the graphite core or the bottom of the capsule by sighting on it through a prism at the bottom end of the furnace. A number of changes have been made since the previous description of the apparatus [15] and are described as follows.

When the apparatus was moved from Washington, D.C. to Gaithersburg, Md. to a laboratory in which the temperature is regulated to ± 1 K, the new environment eliminated much of the problem associated with the effect of room temperature on the automatic optical pyrometer. This effect was further reduced

by replacing some temperature-sensitive germanium transistors with more stable silicon transistors.

A solid state reference voltage supply has replaced the mercury cell. The stability of the furnace temperature depends directly on the constancy of this supply. The variations in the furnace temperature are now so small that they have a negligible effect on the measured heat (< .02%).

For measurement of the temperature of the adiabatic calorimeter, a copper resistance thermometer wound noninductively and cemented with an epoxy resin in a groove in the copper block has replaced the platinum resistance thermometer. Comparisons made between the two thermometers over a period of 3 years indicated that the copper thermometer was stable within the imprecision of the measurement. Its resistance is about 80 Ω and the change in resistance per degree is about three times as large as the resistance change in the platinum thermometer. It also has the advantage of excellent thermal contact with the calorimeter so that its excess temperature due to heat generated by the thermometer current is estimated to be 6×10^{-5} K at 2 mA, compared to 2×10^{-3} K for the platinum thermometer. The change in excess temperature for ordinary variations in thermometer current is now negligible. Electrical calibrations of the adiabatic calorimeter conducted with the copper thermometer over a period of 2½ years in this laboratory now have an estimated standard deviation of 0.004 percent.

Recirculated chilled water at 10.5 °C is now used to cool the induction heater and the furnace ends, and has replaced the tap water and water economizer used in the old location. Since the power to maintain the furnace at a preset temperature does not change during the day, the temperature gradient in the furnace is more stable.

The experimental procedure is now designed to account for mass gains of the outer container. Three or four individual experiments are made in a day and are ordered so that the first and last experiments are duplicates. When the mass of the outer container changes between the first and last experiments, any difference in the total heat for these experiments, after appropriate corrections, is assumed to be proportional to the mass gain and intermediate experiments are corrected according to the mass gain in each. In practice, the correction factor in joules per milligram is determined by plotting determinations for all experiments and drawing a smooth curve through them. Above 2000 K the correction factor is virtually constant. The magnitude of this correction ranges from negligible at temperatures below 1600 K to 5 percent of the enthalpy of the liquid $BeO \cdot Al_2O_3$ at the higher temperatures. (The liquid sample is about one-half the mass of the solid sample.) Masses are now determined after each individual experiment, which considerably slows the work but permits the empirical correction for each experiment. The advantage of the empirical correction is that it does not assume any particular chemical process for the mass gain.

The chronological sequence of the furnace temperatures for the measurements on the solid work was selected randomly. The measurements in the premelting region and in the liquid phase were run on later dates after the machining, engineering, and welding problems were solved for the inner container.

The sequence for the empty and full experiments was staggered in order not to introduce a bias due to gradual change in the furnace insulation.

2.4. Results

Presented in table 2 are the results of the individual experiments. The quantity of heat delivered to the calorimeter includes the small corrections for the

TABLE 2. *Enthalpy measurements of solid, premelting and liquid* $BeO \cdot Al_2O_3$[a]

Furnace temp. (K), date, and container material	Heat to calorimeter at 298.15 K Joules	Millimoles $BeO \cdot Al_2O_3$ and sample designation	Enthalpy $H_T - H_{298.15}$ $KJ \cdot mol^{-1}$	% Deviation from smoothed curve
1182.2	4549.9	15.456 D	139.62	0.008
2-6-67	2391.9			
Molybdenum	2391.1			
	4677.8	16.370 B	139.69	.043
1182.2	4674.4	16.370 B	139.52	−.080
2-3-67	2390.5			
Mo	2390.5			
	4675.8	16.370 B	139.60	−.021
1308.4	2760.7			
2-21-67	5417.4	16.370 B	162.29	−.078
Mo	5418.7	16.370 B	162.38	−.024
	2760.6			
1411.3	6039.0	16.369 B	181.21	−.012
2-13-67	3072.7			
Mo	3072.5			
	6038.5	16.369 B	181.91	−.023

TABLE 2. *Enthalpy measurements of solid, premelting and liquid* $BeO \cdot Al_2O_3$[a]—Continued

Furnace temp. (K), date, and container material	Heat to calorimeter at 298.15 K Joules	Millimoles $BeO \cdot Al_2O_3$ and sample designation	Enthalpy $H_T - H_{298.15}$ $KJ \cdot mol^{-1}$	% Deviation from smoothed curve
1411.2	6154.3	17.025 C	181.07	-.076
1-30-67	3071.6			
Mo	3071.3			
	6155.7	17.022 C	181.20	−.005
1511.9	3376.7			
2-16-67	6650.6	16.369 B	200.01	.080
Mo	6651.5	16.369 B	199.93	.040
	3378.9			
1612.4	7272.5	16.368 B	218.18	−.229
2-27-67	3701.3			
Mo	3703.0			
	7276.5	16.368 B	218.31	−.168
1717.2	7935.1	16.477 B	239.33	.288
1-18-67	3991.6			
Mo				
1719.6	3973.0			
1-11-67	7945.0	16.603 A	239.23	.055
Mo	7945.4	16.603 A	239.21	.048
	3973.7			
1818.9	8601.2	16.369 B	258.28	−0.049
2-23-67	4373.4			
Mo	4374.8			
	8599.4	16.369 B	258.08	−.126
1923.0	4771.9			
3-1-67	9334.1	16.368 B	278.74	−.167
Mo	9336.0	16.367 B	278.95	−.090
	4770.4			
2026.7	10048.7	16.387 B	300.62	−.027
1-20-67	5122.4			
Mo	5120.2			
	10047.6	16.371 B	300.98	.094
2033.3	4330.3			
5-24-67	9419.7	10.830 G	303.72	.534
W, sample	[b](8258.5)	(76.1002)	(51.60)	
in sealed Mo	4332.6			
container				
2095.4	4620.5			
6-5-67	9983.4	10.830 G	321.37	
W, Mo	4626.8			
	[b](8744.6)	(76.1002)	(53.94)	
2125.2	4611.1			
5-29-67	10649.0	10.830 G	380.29	
W, Mo	[b](8804.1)	(76.1002)	(55.11)	
	4609.8			
2137.3	5600.0			
7-17-67	12210.6	7.5154 H	396.68	
W, W	12229.2	7.5154 H	397.75	
	5610.6			
2177.1	5737.5			
7-26-67	13243.0	7.5154 H	504.69	−.04
W, W	13244.6	7.5154 H	504.91	0.00
2200.1	12494.9	10.8297 G	510.30	.05
6-7-67	[b](9359.4)	(76.1002)	(57.94)	
W, Mo	4951.5			
	12497.3	10.8297 G		

TABLE 2. *Enthalpy measurements of solid, premelting and liquid* $BeO \cdot Al_2O_3$[a]—Continued

Furnace temp. (K), date, and container material	Heat to calorimeter at 298.15 K Joules	Millimoles $BeO \cdot Al_2O_3$ and sample designation	Enthalpy $H_T - H_{298.15}$ $KJ \cdot mol^{-1}$	% Deviation from smoothed curve
2253.6	5243.6			
6–9–67	[b](9802.6)	(76.1002)	(59.91)	
W, Mo	13002.8	10.8297 G	523.73	.20
2253.8	5365.6			
6–23–67	13174.9	7.5154 H	521.89	−.16
W, W	5357.6			
2307.49	13899.3	7.5154 H	535.96	−.07
7–7–67	5858.5			
W, W	13909.5	7.5154 H		
2355.0	6203.7			
7–11–67	14456.6	7.5154 H	549.23	.03
W, W	6190.6			

[a] Relative molecular mass is 126.9728; density of solid, 3.71 gm/cm³.
[b] Molybdenum experiment.

enthalpy of the container and its contents between the final calorimeter temperature and 298.15 K. These corrections were at most 2 percent of the measured heat so that the effect of the uncertainty in the data used in making them [1, 8, 9, 10] is negligible. Wherever the correction data were presented in calorie units, they were converted to joules by multiplying by the conversion factor 4.1840. In column 2 the larger figures for a given day are the measured heats for a full capsule and the smaller figures refer to the empty capsule. To account for the tungsten inner container in the premelting and liquid range the correction data were taken from reference [7]. The enthalpy for the molybdenum inner container was measured along with the $BeO \cdot Al_2O_3$ when this material was used, and is tabulated in the table along with the other experiments for the day. Weighing was done in air and the correction for buoyancy is based on a density of 3.71 gm/cm³ for chrysoberyl. The temperature scale is IPTS 1968 [11, 12].

Equation (1) (see below) represents the enthalpy of solid $BeO \cdot Al_2O_3$; it was computed by the method of least squares [13]. Since the uncertainty in the temperature is greater at higher temperatures, the results of individual experiments were weighted inversely to the magnitude of the molar enthalpy. The coefficients of eq (1) were calculated using the results reported herein with the results of Ditmars and Douglas [2] and Furukawa and Saba [1]. The joining of the data sets is shown in figure 2. Equation (1) and the coefficients of the equation are as follows:

$$H_T - H_{298.15} = (A/3)T^{-3} + (B/2)T^{-2} + CT^{-1} + D \ln (T) + ET + (F/2)T^2 + (G/3)T^3 + (H/4)T^4 + (I/5)T^5 + J \qquad 1180 < T < 2030 \quad (1)$$

[4] ln designates natural logarithm.

where $H_T - H_{298.15}$ = relative enthalpy in $kJ \cdot mol^{-1}$

T = temperature (K)

$A = -1.846_{00} \times 10^{7}$

$B = 8.189_{59} \times 10^{5}$

$C = -1.438_{99} \times 10^{4}$

$D = -1.248_{90} \times 10^{2}$

$E = 5.066_{04} \times 10^{-1}$

$F = -5.069_{47} \times 10^{-4}$

$G = 4.592_{67} \times 10^{-7}$

$H = -2.141_{71} \times 10^{-10}$

$I = 4.075_{17} \times 10^{-14}$

$J = 623.2_{97}$

The estimated standard deviation of the observed points from the smoothed curve is ±0.142 percent for the range 1180 to 2100 K.

Beyond 2125 K and up through 2137 K premelting of chrysoberyl is evidenced by the sharp departure of the observed enthalpies from the smoothed solid and liquid curves. (See fig. 1.) There is a gradual change of the dimensions of the inner container in this range as well as at the higher temperatures as the sample is cycled to room temperature. Presumably, this is caused by the rapid expansion and contraction of chrysoberyl. The tungsten container ultimately fractured thus limiting the number of experimental points.

For the liquid range the enthalpy of chrysoberyl can be represented by the equation:

$$H_T - H_{298.15} = 7683_{94.} - 462.4_{16}\,T + 0.1568_{10}\,T^2$$
$$\text{J} \cdot \text{mol}^{-1} \text{ for } 2175 < T < 2355 \qquad (2)$$

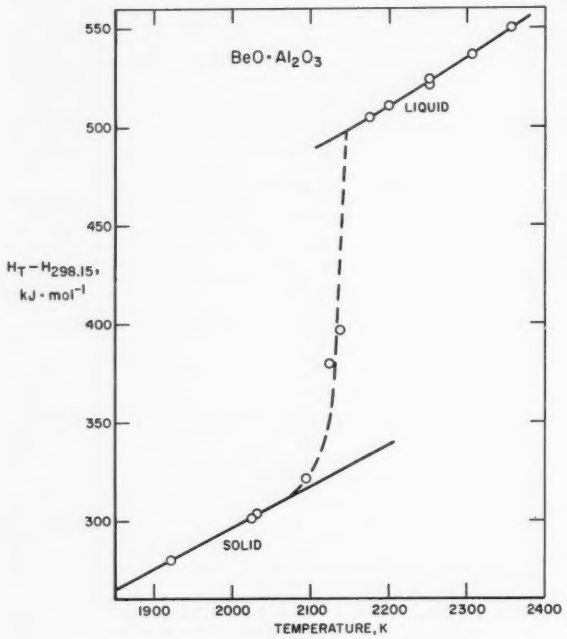

FIGURE 1. *Enthalpy relative to 298.15 K measured near the melting temperature.*

The root mean square deviation of a single determination (3 individual experiments) from the smoothed curve is ±0.16 percent.

Taking 2146 K on the International Practical Temperature Scale of 1968 to be the melting temperature [6], the enthalpy of fusion is calculated to be 171.5 kJ · mol^{-1} by extrapolating eqs (1) and (2) to this temperature. An uncertainty of ±10 K in the melting temperature will have an effect on the enthalpy of fusion no larger than ±0.10 percent. Extrapolation of the smoothed curves will introduce an uncertainty estimated to be ±0.3 kJ · mol^{-1} at 2146 K.

A few measurements on a sample of molybdenum from the same rod used for the inner container have been made at 2033, 2095, 2125, 2200, and 2254 K. The results are listed in table 2 along with those for chrysoberyl. These experiments were carried out simultaneously because the best data found in literature [14] claim a maximum error of ±1.2 percent. The results obtained are within 0.48 percent of the reported values.

3. Discussion

3.1. Polynomial Curve Fitting for the Solid Phase

The usual method of fitting the enthalpy measurements to an empirical equation by the method of least squares [13] was employed to establish how well we can expect the curve to represent the observed data from 1180 to 2030 K. The estimated standard deviation of the observed enthalpies of the solid phase from a curve fit (not shown) of this work alone is ±0.10 percent.

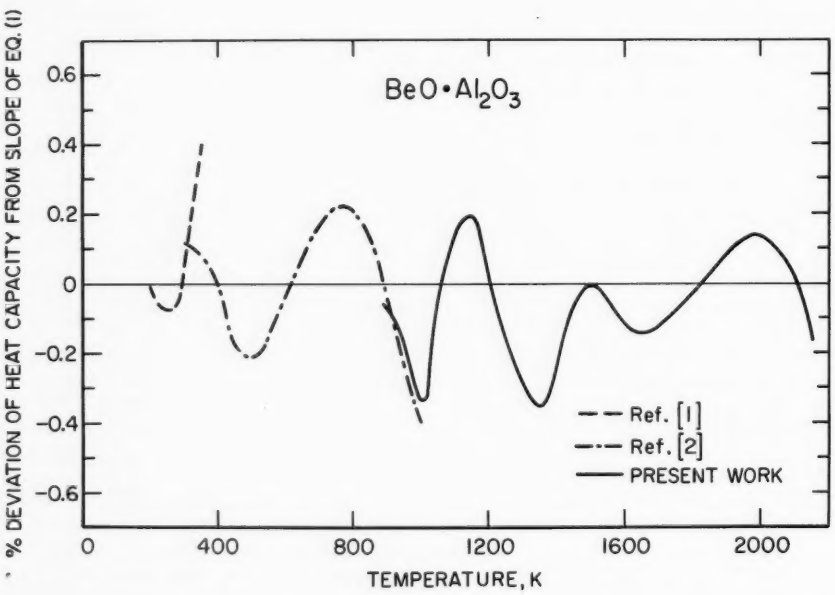

FIGURE 2. *The effect of "smooth joining" of the enthalpies of 1:1* $BeO \cdot Al_2O_3$ *on the heat capacities.*

Since accurate thermodynamic data on this material at lower temperatures are available from earlier works [1, 2], it was decided to make use of their results to extend the range down through 273 K. Certain conditions must be set to do this. First is that the heat capacity of the substance is well behaved and normal throughout the region of study. There is no evidence that this is not so. The amount of impurities is small. The BeO and $BeO \cdot 3Al_2O_3$ phases were not detected. Lang, Fillmore, and Maxwell [6] redetermined the equilibrium diagram of the beryllia-alumina system and their results indicate no phase transition in this temperature range. References [1, 2] report no unusual behavior in the heat capacities at lower temperatures.

Second is that the enthalpy and heat capacity curves are smooth functions throughout this range. This is reasonably assured if the first condition is satisfied and if all the energy, temperature and mass measurements are compared to the same standards during calibration and observations.

A third condition set on the curve fit is that the equation justifies the accuracy of measurements for the three studies at different temperature ranges.

Equation (1) can be used down to 273 K with little or no loss in accuracy. Figure 2 compares the values of the heat capacities from equation (1) with the present work and with those reported in references [1, 2].

3.2. Liquid Phase and the Heat of Fusion

Equation (2) represents the relative enthalpy of chrysoberyl in the liquid phase for the range 2175 to 2355 K. A polynomial of 2d degree was selected having least squares deviation and 95 percent confidence limits because a straight line representation (usually assigned to enthalpies for such a small temperature range and small number of observations) does not adequately represent the observed values.

The uncertainty limits on the heat of fusion of ± 3.5 kJ $\cdot$ mol^{-1} includes 1.5 kJ $\cdot$ mol^{-1} for the extrapolation error of the solid curve, 1.5 kJ $\cdot$ mol^{-1} for the extrapolation error of the liquid curve, and an error of 0.5 kJ $\cdot$ mol^{-1} due to the combined effect of the temperature uncertainty and of the compromise in merging our results with lower temperature work.

Not enough observations in the premelting stage, $2025 < T < 2150$, were made to give a definitive explanation to its cause except to state that molybdenum and tungsten, the inner container, were detected in the post-measurement spectral analyses of the samples.

3.3. Errors

There are three principle sources of error involved in the present calorimetric method—one, the temperature measurements; two, the energy measurements; and three, the sample purity and behavior.

The stability of both the solid state circuitry and standard reference lamp in the automatic optical pyrometer was examined by repeated calibrations (5) during the 4 years of usage. The uncertainty ranged from ± 4 K at 3000 K to ± 0.7 K at 1325 K (with the usual precautions in frequent checks on optical alignment, focus, and cleanliness). This compares closely with the ± 0.1 percent deviation that we obtained in the curve fitting.

The operational procedure was designed so that we could evaluate the imprecision of the energy measurements for the solid range. This turned out surprisingly simple because the furnace temperature can be controlled to ± 0.02 percent during a day's work. By making duplicate observations on the same day at one furnace temperature, the imprecision of the entire temperature range of the solid phase was expressed as:

$$S_p^2 = \frac{1}{2n} \sum_{i=1}^{n} d_i^2$$

where

S_p = estimated imprecision
n = number of observations made at different temperatures
d_i = percent difference of the two enthalpy measurements at a given temperature.

We calculate $S_p = \pm 0.046$ percent.

Spectrochemical analyses of exposed and unexposed chrysoberyl show very little difference in metallic impurities. Molybdenum found in the exposed sample (less than 0.1%) can only come from the container. If we assume that the atomic specific heat is the same for the elements involved, the error in the enthalpy would be less than 0.002 percent. Although this small amount introduces a bias to the overall measurement, corrections were not applied because the uncertainty is overshadowed by the greater uncertainty in the furnace temperature, because four samples were used making it difficult to estimate the amount of molybdenum impurity present in each experiment, and because the weight losses reported in section 2.1 might not be entirely due to evaporation of chrysoberyl as we have assumed.

Considering all the errors that were discussed we believe that other systematic errors encountered in this measurement are negligible compared to the estimated uncertainty of ± 0.32 percent in the relative enthalpy of the solid phase.

The thermodynamic functions (see table 3) were prepared by routine smoothing and numerical integration of the heat capacities from eq (1). The enthalpy and entropy values at 273.15 K are from references [1, 2].

The authors gratefully acknowledge the contributions from the following members of the NBS staff: P. Pfaff, J. W. Bradley, and R. R. Orwick developed the machining, milling and sealing techniques of the tungsten and molybdenum capsules; R. A. Paulson determined the moisture content by gas chromatog-

raphy; V. C. Stewart and E. K. Hubbard examined the samples for impurities; M. L. Reilly developed and later modified the automatic data analysis procedure to fit our needs; E. Lewis, Jr. calibrated the automatic pyrometer and investigated the sources of errors in this instrument.

TABLE 3. *Molar thermodynamic functions of chrysoberyl*

Solid phase

Mol = 0.1269728 KG 1 Cal = 4.1840 J

T	C_p	$(H_T^0-H_0^C)$	$(H_T^0-H_0^C)/T$	$(S_T^0-S_0^C)$	$-(G_T^0-H_0^C)$	$-(G_T^0-H_0^C)/T$
K	*J/K*	*J*	*J/K*	*J/K*	*J*	*J/K*
273.15	97.036	10558.	38.652	57.430	5129.1	18.778
275.00	97.688	10738.	39.047	58.087	5236.0	19.040
280.00	99.420	11230.	40.110	59.863	5530.8	19.753
285.00	101.11	11732.	41.165	61.638	5834.6	20.472
290.00	102.76	12241.	42.213	63.411	6147.2	21.197
295.00	104.37	12759.	43.253	65.181	6468.7	21.928
298.15	105.36	13090.	43.904	66.295	6675.8	22.391
300.00	105.94	13285.	44.285	66.948	6799.0	22.663
310.00	108.96	14360.	46.323	70.472	7486.1	24.149
320.00	111.83	15464.	48.325	73.977	8208.4	25.651
330.00	114.56	16596.	50.292	77.460	8965.6	27.168
340.00	117.16	17755.	52.221	80.919	9757.5	28.699
350.00	119.63	18939.	54.112	84.351	10583.	30.240
360.00	121.98	20147.	55.964	87.755	11444.	31.790
370.00	124.21	21378.	57.779	91.127	12338.	33.348
373.15	124.89	21770.	58.343	92.183	12627.	33.840
380.00	126.34	22631.	59.555	94.468	13266.	34.913
390.00	128.36	23904.	61.294	97.776	14228.	36.482
400.00	130.28	25197.	62.995	101.05	15222.	38.056
410.00	132.11	26510.	64.658	104.29	16249.	39.632
420.00	133.86	27839.	66.285	107.49	17308.	41.209
430.00	135.52	29186.	67.876	110.66	18398.	42.788
440.00	137.11	30550.	69.432	113.80	19521.	44.366
450.00	138.62	31928.	70.953	116.90	20674.	45.944
460.00	140.07	33322.	72.440	119.96	21859.	47.519
470.00	141.45	34730.	73.894	122.99	23073.	49.093
480.00	142.77	36151.	75.315	125.98	24318.	50.664
490.00	144.04	37585.	76.705	128.94	25593.	52.231
500.00	145.25	39031.	78.064	131.86	26897.	53.794
550.00	150.58	46432.	84.422	145.96	33846.	61.538
600.00	154.97	54074.	90.124	159.26	41479.	69.133
650.00	158.53	61916.	95.257	171.81	49759.	76.553
700.00	161.75	69928.	99.897	183.68	58649.	83.785
750.00	164.45	78084.	104.11	194.94	68117.	90.823
800.00	166.83	86368.	107.96	205.63	78133.	97.667
850.00	168.95	94763.	111.49	215.81	88671.	104.32
900.00	170.87	103260.	114.73	225.52	99706.	110.78
950.00	172.61	111840.	117.73	234.80	111210.	117.07
1000.00	174.20	120510.	120.52	243.70	123180.	123.18
1050.00	175.67	129260.	123.11	252.23	135580.	129.12
1100.00	177.03	138080.	125.53	260.44	148390.	134.91
1150.00	178.30	146960.	127.80	268.34	161610.	140.54
1173.15	178.85	151100.	128.80	271.89	167870.	143.10
1200.00	179.48	155910.	129.93	275.95	175220.	146.02
1250.00	180.60	164910.	131.93	283.30	189200.	151.37
1300.00	181.67	173970.	133.82	290.40	203550.	156.58
1350.00	182.71	183080.	135.62	297.28	218240.	161.66
1400.00	183.75	192240.	137.32	303.94	233270.	166.63
1450.00	184.80	201450.	138.94	310.41	248630.	171.47
1500.00	185.91	210720.	140.48	316.69	264310.	176.21

TABLE 3. *Molar thermodynamic functions of chrysoberyl*—Continued

Solid phase						
Mol = 0.1269728 KG 1 Cal = 4.1840 J						
T	C_p	$(H_T^0-H_0^C)$	$(H_T^0-H_0^C)/T$	$(S_T^0-S_0^C)$	$-(G_T^0-H_0^C)$	$-(G_T^0-H_0^C)/T$
1550.00	187.10	220040.	141.97	322.81	280300.	180.84
1600.00	188.41	229430.	143.40	328.77	296590.	185.37
1650.00	189.83	238890.	144.78	334.59	313170.	189.80
1700.00	191.56	248420.	146.13	340.28	330050.	194.15
1750.00	193.52	258050.	147.46	345.86	347200.	198.40
1800.00	195.79	267780.	148.77	351.34	364630.	202.57
1850.00	198.45	277630.	150.07	356.74	382330.	206.67
1900.00	201.57	287630.	151.39	362.08	400300.	210.69
1950.00	205.23	297800.	152.72	367.36	418540.	214.64
2000.00	209.49	308160.	154.08	372.61	437040.	218.52
2050.00	214.44	318760.	155.49	377.84	455800.	222.34
2100.00	220.19	329620.	156.97	383.07	474820.	226.11
2146.00	226.25	339890.	158.38	387.91	492550.	229.52

H_0^C and S_0^C apply to the reference state of the solid at zero deg K. temperature scale is IPTS 1968.

4. References

[1] Furukawa, G. T., and Saba, W. G., J. Res. Nat. Bur. Stand. (U.S.), **69A** (Phys. and Chem.), No. 1, 13–18 (Jan–Feb. 1965).
[2] Ditmars, D. A., and Douglas, T. B., J. Res. Nat. Bur. Stand. (U.S.), **71A** (Phys. and Chem.), 89–95 (Mar.–Apr. 1967).
[3] Palache, C., Berman, H., and Frondel, C., The System of Mineralogy **1**, 718 (J. Wiley and Sons, New York, 1944).
[4] Apollonov, V. N., Zap. Vses. Mineral. Obshchest. **96**, (3), 329 (1967). (Russ.)
[5] Pegmatites S. Rhodesia, Symp., Salisbury, S. Rhodesia 1962, 35–9 (Pub. 1963). (Eng.)
[6] Lang, A. M., Fillmore, C. L., and Maxwell, L. H., J. Res. Nat. Bur. Stand. (U.S.), 48, No. 4, 298–312 (1952) RP2316.
[7] West, E. D., and Ishihara, S. National Bureau of Standards Report No. 9803, National Bureau of Standards, U.S. Department of Commerce, January 1, 1968.
[8] Reilly, M. L., and Furukawa, G. T., "Critical analysis of the heat capacity data of the literature and evaluation of thermodynamic properties of Cr, Mo, and W from 0 to 300 K, to be published.
[9] Starrett, K. F., and Wallace, W. E., J. Am. Chem. Soc. **80**, 3176 (1958).
[10] Furukawa, G. T., private communication.
[11] The International Practical Temperature Scale 1968, Metrologia **5**, No. 2, 35 (1969).
[12] Douglas, T. B., J. Res. Nat. Bur. Stand. (U.S.), **73A** (Phys. and Chem.), No. 5, 451–470 (Sept.–Oct. 1969).
[13] Natrella, M. G., Experimental Statistics, NBS Handbook 91.
[14] Kirillin, V. A., Sheindlin, A. E., and Chekhovskoi, V. Ya., Int. J. Heat Mass Transfer **5**, 1 (1962).
[15] Precision Measurement and Calibration (Selected NBS Papers on Heat), Nat. Bur. Stand. (U.S.), Spec. Publ. 300, Vol. **6**, 220–225 (Feb. 1970).

(Paper 80A1–883)

JOURNAL OF RESEARCH of the National Bureau of Standards — A. Physics and Chemistry
Vol. 80A, No. 1, January-February 1976

Publications of the National Bureau of Standards*

Citations with Selected Abstracts

J. Res. Nat. Bur. Stand. (U.S.), **79A** *(Phys. and Chem.),* No. 6 (Sept.-Oct. 1975), SD Catalog No. C13.22/sec.A:79/6.

Corrections to paper entitled "Third Virial Coefficient for Air-Water Vapor Mixtures," R. W. Hyland and E. A. Mason.

The use of synchrotron radiation as an absolute source of vuv radiation, D. L. Ederer, E. B. Saloman, S. C. Ebner, and R. P. Madden.

Absolute determination of electrochemical equivalent and the atomic weight of zinc I. Method, apparatus, and preliminary experiments, G. Marinenko and R. T. Foley.

Absolute determination of the electrochemical equivalent and the atomic weight of zinc. II. Final determination, G. Marinenko and R. T. Foley.

Absolute isotopic abudance ratios and the atomic weight of a reference sample of potassium, E. L. Garner, T. J. Murphy, J. W. Gramlich, P. J. Paulsen, and I. L. Barnes.

Absolute isotopic abundance ratios and the atomic weight of a reference sample of silicon, I. L. Barnes, L. J. Moore, L. A. Machlan, T. J. Murphy, and W. R. Shields.

Homogeneous nucleation in polyethylene: molecular weight dependence, G. S. Ross and L. J. Frolen.

On the growth rate of spherulites and axialites from the melt in polyethylene fractions: regime I and regime II crystallization, J. D. Hoffman, L. J. Frolen, G. S. Foss, and J. I. Lauritzen.

Monogr. 139. **Interactions of high energy particles with nuclei,** W. Czyż, Nat. Bur. Stand. (U.S.), Monogr. 139, 73 pages (Sept. 1975) SD Catalog No. C13.44:139, $1.35.

Key words: diffractive production; diffractive scattering; Glauber model; hadronic components of photons; high energy scattering; multiple scattering; neutrino-nucleus interactions; shadowing effects.

Elastic scattering and diffractive production processes induced in nuclear targets by high energy projectiles are discussed in this article. Special attention is paid to the interaction of high energy hadrons and photons. Interactions of high energy electrons and neutrinos are briefly mentioned. The common features of all these processes are emphasized throughout the article: The multiple scattering and shadowing processes inside of the target nuclei. An effort is made to develop a unified way of treating nuclear interactions of particles which are either hadrons or exhibit some hadronic components in such interactions.

This article is divided into five sections: 1) Introduction, 2) Description of multiple scattering, 3) Elastic scattering of hadrons from nuclei, 4) Diffractive dissociation and diffractive excitation, 5) Diffractive production of hadrons in hadron-nucleon collisions.

Monogr. 144. **The rotary-vane attenuator as an interlaboratory standard,** W. Larson, Nat. Bur. Stand. (U.S.), Monogr. 144, 70 pages (Nov. 1975) SD Catalog No. C13.44:144, $5.05.

Key words: attenuation; interlaboratory standard; measurement; rotary-vane attenuator.

This paper presents a comprehensive report on the measurement and the use of the rotary-vane attenuator as an interlaboratory standard.

Methods of attenuation measurement developed at NBS are used to supply data for the evaluation of the deviations from theoretical $\cos^2$ law due to rotor misalignment, gear eccentricity, resettability, resolution, and insufficient maximum attenuation.

A precision rotary-vane attenuator with an optical readout capable of 1 second of arc angular resolution has an effective attenuation resolution of 0.00005 dB at a 3 dB dial setting, and 0.0005 dB at a 30 dB dial setting. This type of precision attenuator is an effective standard for use in the dual detection microwave bridge measurement system.

Monogr. 149. **Measurement assurance program — A case study: Length measurements. Part 1. Long gage blocks (5 in to 20 in),** P. E. Pontius, Nat. Bur. Stand. (U.S.), Monogr. 149, 75 pages (Nov. 1975) SD Catalog No. C13.44:149, $1.35.

Key words: measurement algorithm; measurement assurance; measurement process; measurement unit; process variability; uncertainty.

The differences between the methods of traditional metrology and the measurement assurance programs are briefly discussed. The historical data relative to long gage blocks (5 in to 20 in) are analyzed to provide a basis for comparison with results from new measurement processes formulated in accordance with the philosophies of the measurement assurance programs. The results from the new processes are in agreement with the work of the past. The current length values assigned and associated uncertainties are shown for selected long gage blocks used in the dissemination of length by the National Bureau of Standards. These long gage blocks are a part of a growing collection of similar well characterized artifact standards for use in comparative measurement processes. The methods and techniques used in developing the new measurement process are discussed in some detail. It is the author's intent that, in addition to the technical content, this paper be largely tutorial in the area of measurement process analysis. This paper is, in essence, a report on the extension of the techniques first suggested in NBS Monograph 103 "Realistic Uncertainties and the Mass Measurement Process" to the area of length measurement.

Monogr. 152. **A gage block measurement process using single wavelength interferometry,** J. S. Beers, Nat. Bur. Stand. (U.S.),

**Publications with prices and SD Catalog numbers may be purchased directly from the Superintendent of Documents, U.S. Government Printing Office, Washington, D.C. 20402 (foreign: one-fourth additional). Microfiche copies of the above, plus paper copy and microfiche versions of NBS Interagency Reports (NBSIR's), may be purchased from the National Technical Information Service (NTIS), Springfield, Va. 22161. Prices are subject to change. Reprints from the NBS Journal of Research and non-NBS publications may often be obtained directly from the authors.*

Monogr. 152, 34 pages (Dec. 1975) SD Catalog No. C13.44:152, 85 cents.

Key words: calibration; gage blocks; interferometery; laser; length; measurement process; uncertainty.

The interferometric transfer of the length unit from its defined wavelength to NBS reference standard gage blocks is basic to the gage block calibration program at NBS. The interferometric measurement process using a laser light source and a Kosters type gage block interferometer is described here. Continuous evaluation and refinement of the process is aided by statistical treatment and control chart techniques. All error sources, both random and systematic, are evaluated and the process is maintained in a state of statistical control.

H115. Supplement 1. **Energy conservation program guide for industry and commerce (EPIC),** R. G. Massey, Ed., Nat. Bur. Stand. (U.S.), Handb. 115, Suppl. 1, 89 pages (Dec. 1975) SD Catalog No. C13.11:115/Suppl. 1, $2.25.

Key words: energy conservation; energy conservation guide; energy conservation opportunities; energy conservation program; industrial energy conservation.

The Energy Conservation Program Guide for Industry and Commerce (EPIC) is a handbook to assist business firms to establish an on-going conservation program. Supplement contains simplified management program, additional conservation opportunities, case studies, and sources of information.

H117. **Examination of vapor-measuring devices for liquefied petroleum gas. A manual for weights and measures officials,** S. Hasko, Nat. Bur. Stand. (U.S.), Handb. 117, 25 pages (Dec. 1975) SD Catalog No. C13.11:117, 75 cents.

Key words: bell prover; calibration; inspection; liquefied petroleum gas; pressure; report form; temperature; temperature compensator; test; vapor meter; volume.

A manual for State and local weights and measures officials for the examination and test of liquefied petroleum gas vapor measuring devices. Definitions, test methods, and testing apparatus (including description and calibration procedures) are given. Inspection and test procedures are reviewed. A proposed test report form along with suggestions on reporting the results of a test are included. Provision is made for accommodating a changeover to metric units of registration in the definitions, correction tables, procedures, and in reporting a test. Supersedes NBS Handbook 45.

H118. **MUMPS Language Standard,** J. T. O'Neill, Ed., Nat. Bur. Stand. (U.S.), Handb. 118, 144 pages (Dec. 1975) SD Catalog No. C13.11: 118, $2.70.

Key words: data handling language; interactive computing; interpretive computer programming language and operating system; medical automation; minicomputer-based systems; MUMPS; MUMPS Development Committee; MUMPS Language Standard.

This NBS Handbook contains a three-part description of various aspects of the MUMPS computer programming language. Part I, the MUMPS Language Specification, consists of a stylized English narrative definition of the MUMPS language which was adopted and approved for publication as a Type A release of the MUMPS Development Committee on March 12, 1975. Part II, the MUMPS Transition Diagrams, represents a formal definition of the language described in Part I, employing a form of line drawings to illustrate syntactic and semantic rules governing each of the language elements; it was adopted and approved for publication as a Type A release of the MUMPS Development Committee on September 17, 1975. Part III, the MUMPS Portability Requirements, identifies constraints on the implementation and use of the language for the benefit of parties interested in achieving MUMPS application code portability; it was adopted and approved for publication as a Type A release of the MUMPS Development Committee on September 17, 1975.

A bibliography of other MUMPS Development Committee documents is included.

SP260-51. **Standard reference materials: Glass filters as a Standard Reference Material for spectrophotometry—selection, preparation, certification, use, SRM 930,** R. Mavrodineanu and J. R. Baldwin, Nat. Bur. Stand. (U.S.), Spec. Publ. 260-51, 118 pages (Nov. 1975) SD Catalog No. C13.10:260-51, $1.90.

Key words: accuracy in spectrophotometry; glass filters; spectral bandpass; spectrophotometry; standard reference materials; stray radiation; testing of spectrophotometers; transmittance (absorbance) accuracy; wavelength accuracy.

This publication describes various factors which can affect the proper functioning of a spectrophotometer and suggests means and procedures to assess and control these factors. Particular consideration is given to the long and short term stability of a spectrophotometer, to the wavelength accuracy, the spectral bandpass, the stray radiation, and the accuracy of the transmittance or absorbance scale. A description is given of the means and Standard Reference Materials (SRM's) which can be used to control these factors, together with the methods for the preparation, certification, and use of such materials (SRM 930). The results obtained in actual use of SRM 930 are examined in some detail. An appendix contains the reproduction of several publications relevant to the subject discussed in this work.

SP260-53. **Standard Reference Materials: Standardization of pH measurements,** R. A. Durst, Nat. Bur. Stand. (U.S.), Spec. Publ. 260-53, 48 pages (Dec. 1975) SD Catalog No. C13.10:260-53, $1.05.

Key words: buffers; buffer solutions; glass electrode; pH; pH buffers; pH electrode; pH measurement; pH standards.

One of the most widely performed analytical measurements in chemical laboratories is that of pH using the glass electrode. In order to insure the consistency of these measurements, the National Bureau of Standards has adopted an operational scale of pH defined in terms of the pH(S) of a series of standard buffer solutions. Certified samples of buffer materials, from which the standard reference solutions of reproducible pH can be prepared, are issued by the NBS. At present, the operational scale is defined by the pH of seven primary and three secondary standard solutions.

This report is concerned primarily with a discussion of the method used at the NBS for the assignment of pH values to the standard buffer solutions, a description of the NBS measurement facilities, and a summary of the characteristics of these standards. A brief discussion of the types of electrodes used and the calibration of pH instrumentation is also presented.

SP329. Supplement 2. **An index of U.S. voluntary engineering standards,** W. J. Slattery, Ed., Nat. Bur. Stand. (U.S.), Spec. Publ. 329, Suppl. 2, 472 pages (May 1975) SD Catalog No. C13.10:329, Suppl. 2, $9.35.

Key words: engineering standards, index of; index of standards, recommended practices, specifications, test methods; Key-Word-in-Context index of voluntary standards; KWIC index of standards; standards, voluntary, index of.

This supplement contains the permuted titles of more than 5,700 voluntary engineering standards, specifications, test methods, codes and recommended practices published by 164 U.S. technical societies, professional organizations and trade associations. Each title can be found under all the significant key words which it contains. These key words are arranged alphabetically down the center of each page together with their surrounding context. The date of publication or

last revision, the standard number and an acronym designating the standards-issuing organization appear as part of each entry.

SP366-2. **Bibliography on atomic line shapes and shifts (July 1973 through May 1975),** J. R. Fuhr, G. A. Martin, and B. J. Specht, Nat. Bur. Stand. (U.S.), Spec. Publ. 366 Suppl. 2, 75 pages (Nov. 1975) SD Catalog No. C13.10:366/Suppl. 2, $1.35.

Key words: atomic; instrumental broadening; line shapes; line shifts; pressure broadening; resonance broadening; Stark broadening; van der Waals broadening.

This is the second supplement to the NBS Special Publication 366, "Bibliography on Atomic Line Shapes and Shifts (1889 through March 1972)." It contains about 400 references and covers the literature from July 1973 through May 1975. As before, the bibliography contains five major parts: (1) All general interest papers are catalogued according to the broadening mechanisms (and, further, according to special topics under several of the mechanisms) and as to whether the work is a general theory, a general review, a table of profiles or parameters, a comment on existing work, a study of general experimental measurement techniques, or an experimental effort of general importance. Also included are selected papers on important applications of line broadening and on miscellaneous topics relating to atomic spectral line shapes and shifts. (2) In Part 2, all papers containing numerical data are ordered as to element, ionization stage, and broadening mechanism (in the case of foreign gas broadening the perturbing species are listed), and it is indicated whether the data are experimentally or theoretically derived. (3) While in the two preceding parts of the bibliography the references are listed for brevity by identification numbers only, in Part 3 all references are listed completely by journal, authors, and title and are generally arranged chronologically and alphabetically within each year according to the principal author. (4) This section contains a list of all authors and their papers. (5) A final section provides corrections or additions to the first bibliography and supplement.

SP396-2. **Critical surveys of data sources: Ceramics,** D. M. Johnson and J. F. Lynch, Nat. Bur. Stand. (U.S.), Spec. Publ. 396-2, 52 pages (Dec. 1975) SD Catalog No. C13.10:396-2, $1.10.

Key words: carbon (graphite); ceramics; composites; data sources; glasses; properties.

A directory was compiled for selected sources of property data of ceramics, glasses, carbon/graphite and composite materials containing a ceramic component. Included is an assessment of the scope, assets and deficiencies of the most prominent sources. These include handbooks, technical compilations, information/data centers, technical societies, and trade associations or institutes. The directory is indexed by materials and properties.

SP400-17. **Semiconductor measurement technology: Progress report, October 1 to December 31, 1974,** W. M. Bullis, Ed., Nat. Bur. Stand. (U.S.), Spec. Publ. 400-17, 79 pages (Nov. 1975) SD Catalog No. C13.10:400-17, $1.40.

Key words: boron nitride; boron redistribution; capacitance-voltage methods; Darlington pairs; deep depletion; dopant profiles; electrical properties; electron beam evaporator; electron beam induced damage; electronics; epitaxial layer thickness; filar eyepiece; flying-spot scanner; hermeticity; hydrogen chloride gas; image shearing eyepiece; laser interferometry; measurement methods; microelectronics; micrometrology; MOS devices; oxide films; photomask inspection; resistivity; scanning electron microscope; scanning low energy electron probe; semiconductor devices; semiconductor materials; semiconductor process control; silicon; test patterns; thermally stimulated current; thermal resistance; thermal response; ultrasonic bonding; wire bonds; x-ray photoelectron spectroscopy.

This progress report describes NBS activities directed toward the development of methods of measurement for semiconductor materials, process control, and devices. The emphasis is on silicon device technologies. Principal accomplishments during this reporting period include (1) initiation of development of measurement technology for characterizing boron nitride diffusion sources and hydrogen chloride purging gas, (2) application of dc electrical methods with a sensitivity of about 0.1 μm to the measurement of critical dimensions such as the width of diffusion windows, (3) completion of an initial comparison of line-width measurements made with an image shearing eyepiece and a filar eyepiece, and (4) development of procedures for measuring electrically the thermal resistance of the output transistor of integrated Darlington pairs. Also reported are the intermediate results of an interlaboratory evaluation of standard reference wafers for resistivity, evaluation of the deep-depletion method for measuring dopant density with an MOS capacitor, progress on development of mathematical models of dopant profiles, initial results of the reevaluation of Irvin's curve for n-type silicon, analysis of thermally stimulated current and capacitance measurements on MOS capacitors, study of surface carbon contamination which occurs during measurement of silicon by x-ray photoelectron spectroscopy, preliminary measurements of absorbed dose from electron-beam evaporation of aluminum films, initial evaluation of the CCD test structure operating as an MOS capacitor and an MOS transistor, analysis of a TV-microscope system for photomask inspection, initial study of calibration procedures and artifacts for photomask metrology, analysis of the range of applicability of MOS C-V methods for epitaxial layer thickness measurement, use of an optical flying-spot scanner, assessment of damage to selected integrated circuits caused by inspection with a scanning electron microscope, mathematical modeling of ultrasonic bonding, a dry gas method for gross leak testing, and measurements of transistor thermal response. Supplementary data concerning staff, publications, workshops and symposia, standards committee activities, and technical services are also included as appendices.

SP400-20. **Semiconductor measurement technology: Optical and dimensional-measurement problems with photomasking in microelectronics,** J. M. Jerke, Nat. Bur. Stand. (U.S.), Spec. Publ. 400-20, 42 pages (Oct. 1975) SD Catalog No. C13.10:400-20, $1.00.

Key words: integrated circuits; microelectronics; micrometrology; photolithography; photomask; semiconductor technology.

Photomasks are the basic artifacts for transferring design geometry to the semiconductor wafer in integrated circuit (IC) production. Currently, photolithographic techniques using optical equipment are the primary means for both fabricating masks and using masks to print patterns on wafers. The present study was to identify the major optical and dimensional-measurement problems related to the fabrication and use of masks.

The results show that the primary optical problems are those related directly to the use of optical instruments for dimensional measurements of IC pattern geometry. Furthermore, most suppliers and users of optical equipment for mask fabrication do not conduct sufficient optical testing to determine imaging performance. The basic limitations derived from light diffraction and coherence continue to limit the quality of masks and IC devices with sub-micrometre geometry, and acceptable units are produced generally on a best-effort basis. The primary dimensional-measurement problems are (1) accurate measurements below about 10 μm, (2) edge definition or location of a physical edge for a line, and (3) mask registration. Recommendations to improve the accuracy of dimensional measurements are given.

A bibliography of publications related to the optical and micrometrological aspects of photomasking is included.

SP406. **Computer performance evaluation: Report of the 1973 NBS/ACM Workshop,** T. E. Bell, B. W. Boehm, and S. Jeffery, Eds., Nat. Bur. Stand. (U.S.), Spec. Publ. 406, 180 pages (Aug. 1975) SD Catalog No. C13.10:406, $2.45.

Key words: computer architecture; computer performance evaluation; installation management; measurement; modeling; monitoring; operating systems; performance objectives.

An ACM/NBS Workshop on Computer Performance Evaluation (CPE) was held in San Diego, Calif., in March 1973. The papers, workshop discussions, conclusions, and recommendations presented in this volume address specific problems in making computer performance evaluation a commonplace and productive practice.

While several of the conclusions indicate that improvements are needed in performance analysis tools, another suggests that improved application of CPE could be achieved by better documentation of analysis field to develop its full potential. Participants noted that the common emphasis on data collection or modeling, to the exclusion of considering objectives, often seriously degrades the value of performance analysis.

SP417. **Directory of United States standardization activities,** S. J. Chumas, Ed., Nat. Bur. Stand. (U.S.), Spec. Publ. 417, 228 pages (Nov. 1975) SD Catalog No. C13.10:417, $6.75.

Key words: codes; consensus system; directory; Federal Government—standardization; industry standards activities; national standards activities; recommended practices; specifications; standardization activities; standards; states standardization activities; test methods.

This Directory serves as a guide to standardization activities in the United States. It supersedes a Directory of the same title, issued in 1967, as National Bureau of Standards Miscellaneous Publication 288. Included in the Directory are summaries of the standardization activities of trade associations, technical and other professional societies representing industry and commerce, and state and Federal governments. For the first time this Directory covers nonengineering and nonindustry organizations. SP417 contains current descriptive summaries of more than 580 organizations.

Criteria for inclusion are that the organizations have standardization activities such as standards-writing groups, that they assist in the development of standards, or that they issue standards or disseminate standards information.

The standardization activities summaries are grouped into three sections: associations, states, and agencies of the Federal Government. In each section, the summaries are arranged alphabetically by organization. Two types of indexes are included in SP417 to assist the reader in identifying an activity: (1) a subject of index key words taken from the summaries; and (2) a listing of organizations classified into 24 subject areas. Supersedes NBS Misc. Publ. 288.

SP427. **Secondary ion mass spectrometry.** Proceedings of a Workshop on Secondary Ion Mass Spectrometry and Ion Microprobe Mass Analysis, held at the National Bureau of Standards, Gaithersburg, Md., September 16-18, 1974, K. F. J. Heinrich and D. E. Newbury, Eds., Nat. Bur. Stand. (U.S.), Spec. Publ. 427, 230 pages (Oct. 1975) SD Catalog No. C13.10:427, $3.00.

Key words: Auger electron spectroscopy; elemental depth profiling; ion microprobe mass analysis; ion optics; local thermal equilibrium (LTE); mineral analysis; secondary ion mass spectrometry (SIMS); surface analysis.

This book is the formal report of the Workshop on Secondary Ion Mass Spectrometry (SIMS) and Ion Microprobe Mass Analysis held at the National Bureau of Standards in September 1974. Invited and contributed papers cover a range of topics in the SIMS field: design of SIMS instrumentation; factors affecting secondary ion collection; techniques of reducing secondary ion mass spectra to yield quantitative compositional information; comparisons of SIMS with Auger electron spectroscopy (AES); techniques of obtaining elemental depth profiles and the instrumental and physical factors affecting such profiles; and applications of SIMS to the study of geological samples. The papers include both tutorial reviews and detailed reports on current research in SIMS. The volume should be of interest to all workers in the SIMS and surface analysis fields.

SP425, Volumes I and II. **Nuclear cross sections and technology.** Proceedings of a Conference held in Washington, D.C., March 3-7, 1975, R. A. Schrack and C. D. Bowman, Eds., Nat. Bur. Stand. (U.S.), Spec. Publ. 425, Vol. I, 487 pages, Vol. II, 553 pages (Oct. 1975) SD Catalog No. C13.10:425, $19.45.

Key words: biomedical; conference; cross section; nuclear; standards; technology.

These proceedings are the compilation of 221 papers presented at the Conference on Nuclear Cross Sections and Technology held in Washington, D.C. on March 3-7, 1975. The Conference summarized the present status of nuclear cross sections and technology and discussed future cross section needs. Special emphasis is placed on reactor technology and biomedical applications of nuclear science and the measurement of standard cross sections.

SP430. **Household weights and measures,** Nat. Bur. Stand. (U.S.), Spec. Publ. 430, 2 pages (Sept. 1975) SD Catalog No. C13.10:430, 25 cents.

Key words: consumer metric information; International System of Units; kitchen measurement units; metric system; weights and measures.

This card presents weights and measures tables most useful for household (kitchen) purposes. It also introduces metric information for consumer use.

SP436. **Detection, diagnosis, and prognosis,** T. R. Shives and W. A. Willard, Eds., Nat. Bur. Stand. (U.S.), Spec. Publ. 436, 366 pages (Dec. 1975) SD Catalog No. C13.10:436, $4.25.

Key words: diagnostic case histories; diagnostic systems; failure detection; failure diagnosis; failure prevention; failure prognosis.

These Proceedings consist of a group of nineteen submitted papers and discussions from the 22nd meeting of the Mechanical Failures Prevention Group which was held at the Grand Hotel in Anaheim, California on April 23-25, 1975. Failure detection, diagnosis, and prognosis represent the central theme of the Proceedings. Technology and techniques, ongoing diagnostic programs, and coming requirements in the field of DD&P are discussed. In addition, several case histories are presented.

SP437. **National Bureau of Standards Annual Report FY 1975,** P. A. Powell and S. A. Washburn, Eds., Nat. Bur. Stand. (U.S.), Spec. Publ. 437, 32 pages (Dec. 1975) SD Catalog No. C13.10:437, $1.05.

Key words: annual report; computer; energy; environment; measurement; product safety; research; science; standards; technology.

This publication highlights the major achievements of the National Bureau of Standards during FY75 and describes how resources were utilized during this period. In addition, the report will contain sections featuring the Bureau's interaction with the public and private sectors and emphasizing the historical perspective in relation to the Bureau's 75th anniversary and the nation's bicentennial. This publication will serve as (1) an annual accounting of major NBS activities and (2) promotional information on NBS services and capabilities.

Sections of the report feature: increasing measurement competence, sharing measurement techniques, exploring our energy options, expanding computer utilization, preserving environmental quality, promoting better materials use, improving product safety, providing information as a resource, organization, funds and facilities, people.

NSRDS-NBS53. **Crystal structure transformations in inorganic nitrites, nitrates, and carbonates,** C. N. R. Rao, B. Prakash, and M. Natarajan, Nat. Stand. Ref. Data Ser., Nat. Bur. Stand. (U.S.), 53, 48 pages (May 1975) SD Catalog No. C13.48:53, $1.15.

Key words: carbonates; crystal structure transformation; nitrates; nitrites; phase transformation; x-ray diffraction data.

A critical survey of the data describing crystal structure transformations in inorganic nitrites, nitrates, and carbonates is compiled. Data on crystallographic, thermodynamic, spectroscopic, electrical, dielectric, and other properties are given for each solid. Experimental techniques used to obtain the data are given and comments on the data are included in the tables. The literature is surveyed up to June 1973. References have been selected on the basis of their pertinence to the data cited.

NSRDS-NBS56. **Crystal structure transformations in inorganic sulfates, phosphates, perchlorates, and chromates,** C. N. R. Rao and B. Prakash, Nat. Stand. Ref. Data Ser., Nat. Bur. Stand. (U.S.), 56, 38 pages (Nov. 1975) SD Catalog No. C13.48:56, 85 cents.

Key words: chromates: crystal structure; crystal structure transformations; perchlorates; phase transformations; phosphates; sulfates; thermodynamic data; x-ray diffraction data.

Literature dealing with crystal structure transformations of simple inorganic sulfates, phosphates, perchlorates and chromates has been critically reviewed. Data on thermodynamic, crystallographic, spectroscopic, dielectric and other properties are given. Experimental techniques employed to obtain the data are indicated and comments on the data are made wherever necessary. All pertinent references to the published literature (up to 1974) are listed.

BSS72. **Fire endurance of gypsum board walls and chases containing plastic and metallic drain, waste and vent plumbing systems,** W. J. Parker, M. Paabo, J. T. Scott, D. Gross and I. A. Benjamin, Nat. Bur. Stand. (U.S.), Bldg. Sci. Ser. 72, 114 pages (Sept. 1975) SD Catalog No. C13.29/2:72, $1.80.

Key words: ABS; DWV; fire endurance; fire spread; fire test; gases; plastic pipe plumbing; PVC; smoke.

The use of plastic pipe in plumbing systems of multiple-occupancy buildings has raised considerations regarding fire safety. To provide needed data, ten full-scale fire endurance tests were performed involving a total of 39 plumbing chase and wall assemblies containing plastic and metal drain, waste, and vent (DWV) systems typical of installations serving one or two story buildings. Two tests were conducted using plumbing chase configurations simulating kitchen sink drain systems. The PVC DWV piping in these installations did not contribute to spread of fire from one side of the construction to the other. Six fire endurance tests were conducted in which the performance of ABS, PVC, copper and iron was compared directly in kitchen sink drain systems as installed in wood-stud and gypsum-board walls. The stacks ranged from 2 inch to 4 inch in diameter and laterals from 2-1/2 inch to 4 inches. In these tests it was noted that the plumbing configuration and wall construction details, particularly the sealing of plumbing penetrations, seriously affected the fire endurance of the barrier. Satisfactory performance was achieved when certain conditions were met. In the two tests involving nominal 2 by 4 steel-stud-and-gypsum-board walls it was determined that the one-hour fire resistance rating of the wall was reduced considerably when ABS or PVC DWV was installed within it using the construction details described in this report. These details included back to back 1-1/2-in diameter laterals feeding directly into 2-in diameter stacks.

BSS74. **The buffeting of tall structures by strong winds,** E. Simiu and D. W. Lozier, Nat. Bur. Stand. (U.S.), Bldg. Sci. Ser. 74, 90 pages (Oct. 1975) SD Catalog No. C13.29:2/74, $1.55.

Key words: accelerations; buffeting; building codes; buildings; deflections; dynamic response; gust factors; structural engineering; wind engineering; wind loads.

Certain shortcomings of current procedures for computing alongwind structural response have been shown to result in unrealistic estimates of tall building behavior under the action of strong winds. Differences between predictions of fluctuating response based on various such procedures may be as high as 200 percent. In recent years, advances in the state of the art have been made which provide a basis for significantly improved alongwind response predictions. The purpose of the present work is to present a procedure for calculating alongwind response which incorporates and utilizes these advances. The basic structural, meteorological and aerodynamic models employed are described, and expressions for the alongwind deflections and accelerations, consistent with those models, are derived. A computer program is presented for calculating the alongwind response of structures with unusual modal shapes or for which the contribution of the higher modes to the response is significant. For more common situations, a simple procedure is presented which makes use of graphs and on the basis of which rapid manual calculations of the alongwind deflections and accelerations can be performed. Numerical examples are given to illustrate the use of the computer program and of the graphs. Results of numerical calculations are used to discuss some of the approximations and errors inherent in the models employed.

BSS77. **Acoustical and thermal performance of exterior residential walls, doors and windows,** H. J. Sabine, M. B. Lacher, D. R. Flynn, and T. L. Quindry, Nat. Bur. Stand. (U.S.), Bldg. Sci. Ser. 77, 170 pages (Nov. 1975) SD Catalog No. C13.29/2:77, $2.35.

Key words: acoustics; air infiltration; air leakage; architectural acoustics; building acoustics; doors; energy conservation; heat loss from buildings; heat transfer; sound transmission loss; thermal resistance; thermal transmittance; windows.

Laboratory tests of sound transmission loss, thermal transmittance, and rate of air leakage were conducted on full scale (9 feet high × 14 feet wide; 2.7 × 4.3 meters) specimens of typical residential exterior wall constructions, either unbroken or penetrated by a door or window. The walls were of wood frame construction with gypsum board drywall interior finish and exterior finishes of wood siding, stucco, or brick veneer. Additional acoustical tests were run on a number of individual doors and windows. A total of 109 acoustical tests and 48 thermal tests are reported. The resultant data are compared with literature data on similar constructions. Correlations developed among the several quantities measured will assist more rational design where both energy conservation and noise isolation must be considered.

BSS78. **Pre-design analysis of energy conservation options for a multi-story demonstration office building,** T. Kusuda, J. E. Hill, S. T. Liu, J. P. Barnett, and J. W. Bean, Nat. Bur. Stand. (U.S.), Bldg. Sci. Ser. 78, 64 pages (Nov. 1975) SD Catalog No. C13.29/2:78, $1.25.

Key words: building design; building energy analysis; energy conservation options; energy design optimization; heating and cooling load calculation.

The design phase of the GSA-Manchester Building included extensive analysis of the building design and operation to determine the potential for energy conservation. Described in this report are highlights and a summary of the calculations performed during the design phase. The analysis included a study of the exterior shell, ventilation rate, lighting and occupancy levels, room temperature controls, and nighttime flushing of the building using outdoor air, on the predicted yearly energy consumption of the building.

BSS79. **Energy conservation potential of modular gas-fired boiler systems,** G. E. Kelly and D. A. Didion, Nat. Bur. Stand.

(U.S.), Bldg. Sci. Ser. 79, 54 pages (Dec. 1975) SD Catalog No. C13.29:2/79, $1.15.

Key words: boiler oversizing; efficiency vs. heating load; modular boilers; modular concept; seasonal efficiency.

The modular concept of boiler operation was examined in a laboratory test of five gas-fired, cast iron, hydronic boilers. Four of the boilers, each having an input rating of 85,000 Btu per hour, were arranged so that they could either be operated like a single boiler (i.e., all of the boilers either on or off) or as a modular installation in which the boilers are sequentially fired to match the number in operation with the heating load. The fifth boiler had an input rating of 300,000 Btu per hour and was operated as a single boiler installation. Efficiency vs. heating load curves were obtained for the single boiler installation, the four small boilers run like a single boiler and the modular installation operated with and without water flowing through the "idle" modules. These efficiency curves were then used to theoretically predict the effect of the modular concept and boiler oversizing on the seasonal efficiency of gas-fired heating plants. It was found that under certain conditions the use of a gas-fired modular boiler installation instead of a single large boiler could result in considerable energy savings.

FIPS PUB 21-1. **COBOL,** M. V. Vickers, Standards Coordinator, Nat. Bur. Stand. (U.S.), Fed. Info. Process. Stand. Publ. (FIPS PUB) 21-1, 4 pages (Dec. 1, 1975) SD Catalog No. C13.52:21-1, 30 cents.

Key words: COBOL; data processing; Federal Information Processing Standard; information interchange; information processing; programming language; software; standards conformance.

This FIPS PUB announces the adoption of the American National Standard COBOL (X3.23-1974) as the Federal Standard COBOL. This revision supersedes FIPS PUB 21 and reflects major changes and improvements to the COBOL specifications. The American National Standard defines the elements of the COBOL Programming Language and the rules for their use. The standard is used by implementors as the reference authority in developing compilers and by users for writing programs in COBOL. The primary purpose of the standard is to promote a high degree of interchangeability of programs for use on a variety of automatic data processing systems.

The COBOL language is intended for use in computer applications that emphasize the manipulation of characters, records, and files.

FIPS PUB 42. **Guidelines for benchmarking ADP systems in the competitive procurement environment,** J. F. Wood, Standards Coordinator, Nat. Bur. Stand. (U.S.), Fed. Info. Process. Stand. Publ. (FIPS PUB) 42, 8 pages (Dec. 1975) SD Catalog No. C13.52:42, 45 cents.

Key words: benchmarking; benchmark mix demonstration; computer selection; Federal Information Processing Standard; workload representation.

This publication provides general guidelines to be used by Federal agencies as best practices of benchmark mix demonstrations for validating hardware and software performance in context with processing the users' expected actual workload. It treats selection of the benchmark mix, sanitation of the benchmark mix, planning for the benchmark mix demonstration, and conducting the benchmark mix demonstration.

FIPS PUB 43. **Aids for COBOL program conversion (FIPS PUB 21 to FIPS PUB 21-1),** M. V. Vickers, Standards Coordinator, Nat. Bur. Stand. (U.S.), Fed. Info. Process. Stand. Publ. (FIPS PUB) 43, 54 pages (1975) SD Catalog No. C13.52:43, $1.10.

Key words: COBOL; Federal Standard COBOL; program conversion; programming aids; programming languages.

Since COBOL is a "living" language, in the sense that it is under constant development and clarification, the Federal community which relies heavily on COBOL to satisfy their programming needs has a large degree of assurance that COBOL will continue to meet their data processing needs as future generation systems are introduced. However, along with the advantage of having more sophisticated and better COBOL tools to interact with new systems requirements, there is a short term disadvantage. As clarifications and new facilities are added, they must interact with the language specifications already standardized, and this interaction sometimes requires changes in source programs. An analysis, in the form of narrative descriptions and syntax comparisons, is provided to aid in the transitioning of COBOL programs for use with compilers developed in accordance with the 1968 COBOL Standard (FIPS PUB 21) to compilers developed in accordance with the 1974 COBOL Standard (FIPS PUB 21-1).

TN667. **Upper-bound errors in far-field antenna parameters determined from planar near-field measurements. Part I: Analysis,** A. D. Yaghjian, Nat. Bur. Stand. (U.S.), Tech. Note 667, 120 pages (Oct. 1975) SD Catalog No. C13.46:667, $1.85.

Key words: antennas; error analysis; far-field pattern; near-field measurements; planar scanning; plane-wave spectrum.

General expressions are derived for estimating the errors in the sum or difference far-field pattern of electrically large aperture antennas which are measured by the planar near-field scanning technique. Upper bounds are determined for the far-field errors produced by (1) the nonzero fields outside the finite scan area, (2) the inaccuracies in the positioning of the probe, (3) the distortion and nonlinearities of the instrumentation which measures the amplitude and phase of the probe output, and (4) the multiple reflections. Computational errors, uncertainties in the receiving characteristics of the probe, and errors involved with measuring the input power to the test antenna are briefly discussed.

TN672. **Time domain automatic network analyzer for measurement of RF and microwave components,** W. L. Gans and J. R. Andrews, Nat. Bur. Stand. (U.S.), Tech. Note 672, 176 pages (Sept. 1975) SD Catalog No. C13.46:672, $2.40.

Key words: attenuation; discrete Fourier transform; fast Fourier transform; insertion loss; jitter; microwave measurement; mismatch; network analyzer; noise; pulse generator; pulse measurement; sampling oscilloscope; scattering parameters; spectral analysis; time domain analysis.

This technical note describes in detail a new NBS instrument for the measurement of the scattering parameters (S_{ij}) of RF and microwave components. The instrument is the Time Domain Automatic Network Analyzer (TDANA). It utilizes time domain pulse measurements to obtain frequency domain parameters. The frequency range is dc to 18 GHz with a lower upper limit for large values of attenuation. The instrument consists of three major components: an ultra-fast pulse generator, a broadband sampling oscilloscope, and a digital minicomputer.

TN673. **Using six-port and eight-port junctions to measure active and passive circuit parameters,** C. A. Hoer, Nat. Bur. Stand. (U.S.), Tech. Note 673, 29 pages (Sept. 1975) SD Catalog No. C13.46:673, 80 cents.

Key words: admittance; automated precision measurements; correlator; current; impedance; microwave circuit parameters; microwave measurements; phase angle; power; ratio; reflection coefficient; reflectometer; self-calibration; six-ports; vector voltmeter; voltage.

This review paper brings together a number of old and new methods for measuring voltage, current, power, impedance, and phase angle using only amplitude type detectors. Vector voltmeters and reflectometers can be constructed to measure all of these quanti-

ties in terms of four amplitude measurements made on four arms of a six-port junction. Whereas previous uses of this type of instrument depended on precision components for accuracy, new equations switch this dependence primarily to detector linearity and only secondarily on the properties of the measuring device itself.

TN873. **Electro-optical deflection measuring device,** R. A. Crist, R. D. Marshall, and H. I. Laursen, Nat. Bur. Stand. (U.S.), Tech. Note 873, 24 pages (Dec. 1975) SD Catalog No. C13.46:873, 75 cents.

Key words: buildings; deflections; instrumentation; structural response; wind loads.

The development and testing of an electro-optical device for the direct measurement of lateral deflections of tall structures are described. The device utilizes a tracking telescope mounted on a fixed reference and a light source attached to the structure of the level for which lateral deflections are to be measured. Operating characteristics of the system are based on the results of tests carried out over a period of several months in one of the elevator shafts of a 12-story building.

TN883. **Waterproofing materials for masonry,** E. J. Clark, P. G. Campbell, and G. Frohnsdorff, Nat. Bur. Stand. (U.S.), Tech. Note 883, 86 pages (Oct. 1975) SD Catalog No. C13.46:883, $1.45.

Key words: accelerated weathering; durability of waterproofing materials; masonry; performance criteria; waterproofing materials; water repellent materials.

The initial effectiveness and durability characteristics of fifty-five clear masonry waterproofing materials were evaluated using laboratory tests. This report contains the results of initial performance tests including water absorption, water vapor transmission, resistance to efflorescence and change in appearance. Durability tests, including periodic measurement of water absorption after exposures to accelerated weathering and outdoor exposures, were also conducted. Based on test results, performance criteria for clear waterproofing materials were developed. In addition, recommendations for the application of waterproofing materials were formulated. Finally, the report contains a summary of a survey concerning field experiences with waterproofing and a brief theoretical discussion of water flow.

TN884. **Calibration of unrecorded low and medium density type magnetic disk pack surfaces,** N. P. Goumas, Nat. Bur. Stand. (U.S.), Tech. Note 884, 23 pages (Oct. 1975) SD Catalog No. C13.46:884, 45 cents.

Key words: calibration factor; computer amplitude reference; computer storage media; disk calibration; disk pack; magnetic disk; Standard Reference Surface; unrecorded disk surface.

This publication describes the design requirements and the operation of the NBS test bed that is used for calibrating unrecorded magnetic disk pack surfaces for low and medium density use. The signal level calibration is made with respect to a reference level that is derived from the NBS Standard Amplitude and Data Reference Surfaces that are held in repository at NBS. The techniques for calibrating the measurement system with the NBS repository Reference Surfaces and the calibration of candidate reference disks are described in detail.

TN885. **A technical review of the Nicaraguan building regulatory system,** R. N. Wright and I. A. Lamana, Nat. Bur. Stand. (U.S.), Tech. Note 885, 85 pages (Oct. 1975) SD Catalog No. C13.46:885, $1.45.

Key words: architecture; building; building codes; building design; disaster mitigation; earthquakes; engineering; environmental hazards; housing; inspection and testing; safety.

This report on the Nicaraguan Building Regulatory System has been prepared under the auspices of the Organization of American States and the United States Agency for International Development. It presents an overview of the building regulatory system in Nicaragua; its activities in review of designs, issuance of building permits, inspection of construction, control of quality of materials, and issuance of occupancy permits. The technical bases for these activities are the building code and standards, the laboratory facilities for control of the quality of building materials, and the processes for development and application of codes and standards. Recommendations address the status and development of this system and its technical bases.

The losses in the December 23, 1972, Managua Earthquake provided dramtic evidence of the need for effective implementation of good building standards. Repetitions of these tragic losses elsewhere in Nicaragua and in a reconstructed Managua are certain unless a good building code is developed and adopted, its use and design by architects and engineers enforced by careful review of designs, and the implementation of these designs by the builders assured by inspection of construction and testing of building materials. A summary and critical review of U.S. building regulatory practices for areas with severe natural hazards is presented in Appendix B for guidance in building regulatory system planning and development. A survey of housing performance in Managua is presented in Appendix C to illustrate that earthquake resistant construction is feasible and economical for Nicaragua and other nations with comparable resources.

TN886. **Modification of fluorescent luminaires for energy conservation,** R. W. Beausoliel, W. J. Meese, and G. Yonemura, Nat. Bur. Stand. (U.S.), Tech. Note 886, 15 pages (Oct. 1975) SD Catalog No. C13.46:886, 65 cents.

Key words: capacitors; energy conservation; fluorescent lamp; fluorescent luminaire; lighting efficiency; power factor.

Reducing energy consumption in existing buildings by reducing the number of lamps presents technical problems when more than one fluorescent lamp operates from a single ballast. A preliminary investigation was made whereby capacitors were substituted for one fluorescent lamp in a two-lamp luminaire which operated with a single ballast. Under optimum conditions, lighting efficiency (foot-candles per watt) was nearly as high at reduced power input as it was with two lamps operating normally. No failures in lighting equipment or capacitors occurred and no fire hazards, other safety hazards or other unsatisfactory occurrences were observed. A more thorough investigation involving a number of parameters is needed to ascertain the feasibility of this modification.

TN887. **Six data base management systems: Feature analysis and user experiences,** E. Fong, J. Collica, and B. Marron, Nat. Bur. Stand. (U.S.), Tech. Note 887, 84 pages (Nov. 1975) SD Catalog No. C13.46:887, $1.45.

Key words: data base applications; data base management systems; selection criteria; software features; system evaluation; system features; user experiences.

This report presents an objective overview of features of six selected data base management systems (DBMS) and Federal user experiences with these systems. Application criteria were developed in order to aid in the evaluation and selection of DBMS.

The advantages of generalized DBMS over traditional methods of software system development are discussed. The criteria for choice of the six systems' features are presented. The data reported were gathered from two sources: vendors and users. Vendor information consisted of side-by-side presentation of features of the six DBMS. User experiences reported are summarized under appropriate headings. This information is used to derive application criteria for assessing the usability and operational suitability of DBMS to a variety of data processing requirements.

The six systems reviewed are: ADABAS, IMS/VS, INQUIRE, MODEL 204, SYSTEM 2000, and TOTAL.

597-633 O - 76 - 6

TN888. **Nuclear Science Education Day,** F. J. Shorten, Ed., Nat. Bur. Stand. (U.S.), Tech. Note 888, 95 pages (Nov. 1975) SD Catalog No. C13.46:888, $1.65.

Key words: biology; career; ecological; electricity; energy; environment; fusion; medicine; nuclear; power; radiation; reactor; research; utilities.

These proceedings are a collection of invited papers given at the Nuclear Science Education Day Conference held on November 29, 1973 at the National Bureau of Standards, Gaithersburg, Md. The program was sponsored jointly by the ANS (Washington Chapter) and the NBS for secondary school science teachers and outstanding science students in the Washington area. Four main topics are covered: research and development in nuclear energy applications; man, environment, and nuclear energy; nuclear science frontiers; and career opportunities in nuclear science.

TN890. **Productivity measurement in R&D: Productivity measurement experiment (PROMEX) in selected research and development programs at the National Bureau of Standards,** J. T. Hall and R. A. Dixon, Nat. Bur. Stand. (U.S.), Tech. Note 890, 52 pages (Dec. 1975) SD Catalog No. C13.46:890, $1.10.

Key words: impact; objectives, output; performance measurement; production indices; production measurement.

This report describes an experiment in productivity measurement conducted at the National Bureau of Standards. The experiment concludes that no matter how sophisticated the analysis and synthesis processes become, statistical counts of output media (e.g., publications, citations, invited talks) will not serve as reliable measures of R&D productivity.

The conduct of the experiment included a work sampling study, a communications study, an output analysis, a value analysis approach to developing criteria for selection and evaluation of programs, construct of a rating system for evaluation of programs, and construction of a model of the R&D process.

TN892. **Retrofitting a residence for solar heating and cooling: The design and construction of the system,** J. E. Hill and T. E. Richtmyer, Nat. Bur. Stand. (U.S.), Tech. Note 892, 99 pages (Nov. 1975) SD Catalog No. C13.46:892, $1.70.

Key words: retrofitted solar residence; solar collector; solar heating and cooling system; solar-powered absorption refrigeration.

During 1972 and 1973, the National Bureau of Standards conducted controlled laboratory tests on a factory-built four-bedroom house having a floor area of 110 m^2 (1200 ft^2) equipped with a conventional gas furnace and central electric air conditioner incorporated into a forced air distribution system. During 1974, the house was moved onto the NBS grounds and a solar heating and cooling system was designed to be added to the house. Calculations have been made to show that more than 75 percent of the yearly energy needs for heating, cooling, and supplying domestic hot water could be obtained from the sun.

This report deals with the design and construction of the retrofitted system. It consists of 45 m^2 (485 ft^2) of double-glazed, flat-plate solar collector, 5.7 m^3 (1500 gallons) of water storage, and a 10,000 W (3 ton) lithium bromide absorption air cooling unit.

TN893. **Computer programs for structural chemistry: MATCH1 and MATCH2, FORTRAN programs to predict and evaluate mutual orientation of polycrystals,** B. Dickens and L. W. Schroeder, Nat. Bur. Stand. (U.S.), Tech. Note 893, 71 pages (Jan. 1976) SD Catalog No. C13.46:893, $1.30.

Key words: computer calculations; crystal structure; epitaxy; lattice misfit; pattern recognition; twinning.

Two computer programs to evaluate possible structural matches for use in epitaxy and twinning studies have been written in FORTRAN V for the UNIVAC 1108. They should be readily convertible to other comparable computers.

The first program MATCH1, requires knowledge of the unit cell parameters. It obtains all matching networks in two unit cell lattices and sorts the matches into an order of probable epitaxy (or twinning if the two unit cells are the same) based solely on criteria of dimensional mismatch and network area.

The second program, MATCH2, requires knowledge of positional parameters of the atoms in the crystal structures. It calculates the degree of structural fit for slices supplied from visual inspection of the crystal structures or as matching networks determined by MATCH1.

The slice comparison is carried out in terms of the vector set of the environment of each atom in each slice. The procedure is not valid when the twin operation is a rotation about the normal of the compositional plane or a reflection in a mirror parallel to this plane. The atomic patterns comprising the slices are matched piece by piece in MATCH2. A third program, MATCH3, will match whole patterns once three fiducial atoms in each pattern have been picked from the output of MATCH2 and will handle all the twinning cases. MATCH3 will be described in a future National Bureau of Standards Technical Note.

CIS6. **Color in our daily lives,** D. B. Judd, Nat. Bur. Stand. (U.S.), Consum. Inf. Ser. 6, 32 pages (Mar. 1975) SD Catalog No. C13.53:6, $1.75.

Key words: color; environment; experimenting with; harmony; hues; illumination; light; personal uses; relationships; uses.

If you are like most consumers, color is at once a delight, a challenge, and a problem. Color is a delight because it can convert an otherwise drab costume, scene, or room into a thing of beauty. It is a challenge because it brings out our creative ability and enables us to brighten and enliven our surroundings at a comparatively cheap cost. It is a problem because, improperly used, it can fail in its purpose, and if we are unsure of the ways in which colors go together, the choice of a tie, a lipstick, a drapery fabric, or a wall paint to match furniture and carpet can become an unpleasant chore.

Because of the importance of color in our daily lives, and the widespread lack of knowledge about the relationship of colors, we are pleased to bring you this extraordinary booklet as a part of our Consumer Information Series. It has been written in simple language, but in its scientific accuracy, and in the precise selection and printing of illustrative colors, it meets the exacting standards of a scientific treatise. Although it was designed to be of practical value to you in solving everyday color problems, we believe Color in Our Daily Lives will also become a treasured possession.

CIS8. **Making the most of your energy dollars in home heating and cooling,** M. Jacobs and S. Petersen, Nat. Bur. Stand. (U.S.), Consum. Inf. Ser. 8, 20 pages (June 1975) SD Catalog No. C13.53:8, 70 cents.

Key words: building economics; consumer information; energy conservation; home economics; home improvements; insulation.

This booklet is a consumer-oriented adoption of BSS64 (Retrofitting Existing Housing for Energy Conservation: An Economic Analysis) which provides basic energy conservation information of an economic nature to homeowners. It is concerned primarily with energy conservation improvements which will decrease heating and cooling costs in houses. Investment in insulation, storm windows and doors, and weatherstripping/caulking is examined with regards to different climates and different energy prices in order to determine the combination of these improvements which will provide the greatest long-run economies in space heating and cooling to the homeowner. Information of a general nature on the proper use of such improvements is outlined and further references are listed.

NBSIR 73-256. **Development of reference materials for atmospheric analysis of the occupational environment: Filter samples containing toxic metals,** R. Mavrodineanu, J. R. Baldwin, and J. K. Taylor, 16 pages (Oct. 1973). Order from NTIS as COM 75-11443, $3.25.

Key words: analysis of toxic materials; atmospheric analysis; industrial hygiene; reference materials.

Techniques are described that may be used to prepare filters on which are deposited prescribed amounts of heavy metals, for use as reference materials in industrial atmospheric analysis. Working solutions, prepared from pure metals and highly purified acids and water, are pipetted onto the filters held in jigs to facilitate their application. The techniques were used to prepare three sets of reference materials containing the following metals: Set 1—Pb, Cd, Zn, Sn; Set 2—Pb, Zn, Mn; Set 3—Be. The amounts of each metal deposited on the filters correspond to those expected when collecting personal samples, in atmospheres when the concentrations are both below and above the TLV levels.

NBSIR 73-257. **A system for producing test atmospheres containing hydrogen cyanide,** E. P. Scheide, E. E. Hughes, and J. K. Taylor, 12 pages (Oct. 1973). Order from NTIS as COM 75-11444, $3.25.

Key words: gas blending system; hydrogen cyanide; ion selective electrode; occupational safety.

A system capable of producing well-defined test atmospheres of HCN in air (or any other desired diluent) and an analytical system for the analysis of these gas mixtures is described. This system provides a means of calibration of the various analytical systems for HCN now in use. The analytical unit of the system can also be used for the determination of hydrogen cyanide in industrial atmospheres. By collecting the HCN in a sodium hydroxide solution, and measuring the cyanide content by the use of a cyanide-ion selective electrode, concentrations of HCN in air between 5 and 500 ppm were measured. This method is rapid and convenient and can easily be performed by a technician or adapted to automation.

NBSIR 73-258. **A gas dilution system for acrolein,** E. P. Scheide, E. E. Hughes, and J. K. Taylor, 11 pages (Oct. 1973). Order from NTIS as COM 75-11445, $3.25.

Key words: acrolein; gas chromatography analysis; gas dilution system; occupational safety.

A system capable of producing well-defined test atmospheres of acrolein in air (or any other desired diluent) and an analytical system for the analysis of these gas mixtures is described. Using a bulk mixture of 9.0 ppm acrolein in nitrogen, and accurately blending this with a stream of clean, dry air, concentrations between 0.05 and 0.50 ppm can be produced. This system provides a means of calibration of the various analytical systems for acrolein now in use.

NBSIR 73-259. **A gas dilution system for methyl bromide,** E. P. Scheide, E. E. Hughes, and J. K. Taylor, 11 pages (Oct. 1973). Order from NTIS as COM 75-11446, $3.25.

Key words: gas chromatography analysis; gas dilution system, methyl bromide; occupational safety.

A system capable of producing well-defined test atmospheres of methyl bromide in air (or any other desired diluent) and an analytical system for the analysis of these gas mixtures is described. Using a bulk mixture of 1000 ppm methyl bromide in nitrogen, and accurately blending this with a stream of clean, dry air, concentrations between 5 and 100 ppm can be produced. This system provides a means of calibration of the various analytical systems for methyl bromide now in use.

NBSIR 73-260. **A gas dilution system for arsine-air mixtures,** P. A. Pella, E. E. Hughes, and J. K. Taylor, 14 pages (Oct. 1973). Order from NTIS as COM 75-11440, $3.25.

Key words: arsine; gas-blending; Gutzeit method; spectrophotometry.

A gas-blending system originally designed for chlorine-air mixtures was modified for producing arsine-air mixtures in the concentration range from 0.02 to 0.25 ppm. This system has been tested in order to provide accurately known concentrations of arsine-in-air for calibration of analytical monitoring devices. An analytical method has been developed for checking the concentration of arsine in the working standard and consists of the spectrophotometric measurement of an arsine-diethyldithiocarbamate complex in solution.

NBSIR 73-261. **A gas dilution system for hydrogen fluoride-air-mixtures,** P. A. Pella, E. E. Hughes, and J. K. Taylor, 23 pages (Oct. 1973). Order from NTIS as COM 75-11441, $3.25.

Key words: fluoride analysis; gas-blending; HF-air mixtures; ion-specific electrode.

A gas-blending system was constructed for producing hydrogen fluoride-air mixtures in the concentration range from 1 to 20 ppm for the purpose of calibrating analytical monitoring devices. The system has been tested by measuring these HF concentrations using a fluoride ion-specific electrode.

NBSIR 74-381. **Electromagnetic attenuation properties of clay and gravel soils,** D. A. Ellerbruch, 24 pages (Aug. 1974). Order from NTIS as COM 75-10522, $3.25.

Key words: attenuation; clay; gravel; measurements; microwave; skin depth.

The objective of this work was to establish the feasibility of using active microwave techniques to differentiate between the different subsurface layers in a pavement system. The electromagnetic attenuation properties of clay and gravel soils were measured as a function of moisture content and frequency. Measurements were done at frequencies in the 0.5-4.5 GHz range. Soil samples were compounded in the laboratory at approximately 10, 50 and 90 percent saturation. Sample thickness was in the range 2.5-20.3 cm. Each homogeneous sample was sealed in a polyethylene container to retain the total moisture and to maintain a constant moisture content with depth.

NBSIR 73-415. **Noble metal constitution diagrams: Part II,** R. M. Waterstrat and R. C. Manuszewski, 170 pages (Aug. 1975). Order from NTIS as COM 75-11448, $6.25.

Key words: alloy phases; constitution diagrams; noble metals; phase diagrams; phase equilibria; platinum group metals.

Six binary constitution diagrams involving the noble metals are presented. These diagrams include the V-Ru, V-Rh, Nb-Os, Nb-Pd, Nb-Pt and Ta-Pd alloy systems.

Experimental alloys were prepared from starting materials having a nominal purity of at least 99.9 percent and precautions were taken to insure that no significant contamination was introduced during alloy preparation and heat-treatment. Temperatures were measured to an accuracy within ± 20 °C.

NBSIR 74-461. **The calibration of small volumetric laboratory glassware,** J. Lembeck, 34 pages (Dec. 1974). Order from NTIS as PB246623, $4.00.

Key words: burets; capacity; flasks; meniscus; pipets; volumetric calibration.

This report describes a procedure for testing small volumetric apparatus. The procedure is based upon a determination of the volume of water either contained or delivered by the vessel. There are techniques described for cleaning, reading the meniscus, filling, draining and weighing the contained or delivered volume.

NBSIR 74-557. **Non-metallic antenna-support materials,** N. Halsey, D. E. Marlowe, and L. Mordfin, 45 pages (June 1974). Order from NTIS as COM 75-11439, $3.75.

Key words: composite materials; fiber-reinforced-plastic rod; glass-reinforced-polyester rod; guys, antenna; processing parameters, pultrusion; pultrusion; reinforced plastic rod; stress rupture of FRP rod; test methods, FRP rod; weatherability, FRP rod.

Thirteen samples of pultruded, glass fiber-reinforced-polyester rod material were manufactured using a different combination of the manufacturing process parameters for each. These samples were tested to evaluate the effects of nine different process parameters on the properties and characteristics of the rods. Elevated-temperature stress-rupture tests under saturated humidity were used as an accelerated measure of long-term weatherability. The test results were somewhat inconsistent, but it appears that certain process parameters, such as collimation and ultrasonic agitation of the rovings during pultrusion, were beneficial to both tensile strength and weatherability. Other parameters, such as pretensioning of the rovings, were beneficial to weatherability but detrimental to tensile strength. Additives to the resin system were generally detrimental.

A high speed tension test method was developed and it was found that the strength of the rod is substantially greater under high loading rates.

An approximate relationship was observed between transverse tensile strength and electrical breakdown voltage. However, neither of these characteristics, nor surface hardness, correlated with axial tensile strength or weatherability.

NBSIR 74-590. **A study of the feasibility of establishing generic environmental test parameters for all consumer products,** S. D. Toner, 9 pages (Mar. 1975). Order from NTIS as COM 75-11434, $3.25.

Key words: environmental tests; product safety.

A study was conducted to determine the feasibility of establishing a set of generic environmental test parameters that would be applicable to all types of consumer products, with a potential for developing injury producing hazards as a result of environmentally induced failure. It was concluded that this approach is not a practical one. It is apparent that the safeness of a product or type of product should be determined on the basis of simulated environmental tests appropriate to its specific end use.

NBSIR 74-620. **An in-line density and viscosity sensor,** L. O. Olsen and F. W. Ruegg, 20 pages (Nov. 1974). Order from NTIS as PB246622, $3.50.

Key words: capillary tubes; density sensor; flow nozzle; laminar flow; liquid properties; viscosity sensor.

In-line density and viscosity sensors for liquids are developed to utilize measurements of differential pressure across a nozzle and a coiled capillary tube respectively, with known flowrates through each provided by a flow generator. Theory and principles of operation and instructions for calibration and use of the sensors are discussed, along with design consideration for the sensors and associated equipment. A calibration of the sensors demonstrated that viscosity and density each could be measured with a computed standard deviation of one percent. Viscosity was varied over the range of about 1 to 11 centistokes whereas density of the fluids used was near 0.8 g cm^{-3}. Application of well known similarity considerations is used to make the results applicable to other liquid densities, provided influence of other liquid properties (high vapor pressure, for instance) does not interfere.

NBSIR 74-629. **Thermal properties of selected plastic piping used in housing,** M. Tryon, 28 pages (Apr. 1975). Order from NTIS as COM 75-11281, $3.75.

Key words: ABS; coefficient of expansion; CPVC; glass transition temperature; hardness; PB; polybutene; polyvinyl chloride; PVC; residual stress; thermoplastic piping.

In a study of four thermoplastic piping materials, the following performance-related properties were measured: coefficient of thermal expansion, glass transition temperature, residual stress, hardness, and hardness-temperature coefficient. The purpose of the study was to determine typical values of these properties for each of the piping materials. Results are given with recommendations for performance tests and changes in previously-proposed interim performance criteria.

NBSIR 74-632. **Comparison of accelerated aging of book papers in 1937 with 36 years natural aging,** W. K. Wilson and E. J. Parks, 96 pages (Dec. 19, 1974). Order from NTIS as PB246554, $5.00.

Key words: accelerated aging; aging; natural aging; paper, permanent; paper, stability; permanent papers; record papers; stability of paper.

A group of 36 book papers made in the NBS paper mill in 1937 were tested in 1937 before and after accelerated aging for 72 hours at 100 °C, and in 1973 after 36 years of natural aging. The data show that fairly good correlations exist between accelerated aging and natural aging when changes in alpha cellulose, copper number and, to a lesser extent, tearing strength, were used as criteria of change. pH is a reasonably good criterion of stability. It appears that zero span tensile strength, wet strength as a percentage of dry strength, and brightness are useful criteria for evaluating the aging of paper. When data in this report are compared with data from earlier reports, it appears that dry accelerated aging at 100 °C more nearly corresponds to natural aging than accelerated aging at 90 °C and 50 percent relative humidity.

NBSIR 75-649. **Computer applications at the Ecuadorian Institute of Standardization (INEN): Observations and recommendations,** J. Hilsenrath, 16 pages (Apr. 1975). Order from NTIS as PB241237, $3.25.

Key words: computer applications; OMNITAB II: Minitab; statistical computing; text editing.

This report contains specific suggestions for computer applications at the Ecuadorian Bureau of Standards (INEN). The suggestions, based on observations and discussion during a 10-day visit by the author in Quito, Ecuador, cover editing and typesetting of Ecuadorian standards, data storage and retrieval, and statistical analysis of experimental data.

NBSIR 75-652. **Procedures for estimating sound power from measurements of sound pressure,** C. I. Holmer, 78 pages (July 1975). Order from NTIS as COM 75-11399, $4.75.

Key words: air compressors; error of sound power measurement; noise; noise measurement; sound power level; standard test procedures for sound power measurement.

This report describes investigations of the accuracy and precision of various measurement methodologies for determining the estimated sound power output of "large" machines in the free field over a reflecting plane. One purpose of this investigation is to place empirical error bounds on many of the free field measurement procedures currently proposed or in use; and in particular, compare the results of "near-field" and "far-field" measurements. The sources used for the investigation included 17 portable air compressors of various types (powered by internal combustion engines), a "reference" sound source, and a loudspeaker driven by a pure tone source. The data recorded include sound pressure level (A-weighted, linear, and 1/3-octave band) on an 84 point hemispherical array of seven metre radius, and "near-field" measurements, sampled every square metre, on a rectangular surface one metre from the machine surface. These data were reduced to provide information on the deviation of "near field" sound power determinations from "far-field" power level (using subsets of the data as appropriate to various methodologies). The measured data for seventeen sources suggests that the value of a

sound power estimate based on "near-field" sound pressure level measurements may be an upper bound to the sound power level estimated from far field measurements, subject to the limitations of sampling error. Estimates of total achievable measurement error of A-weighted sound power level of near field determinations relative to far field determinations are made for several measurement methodologies, based on the experimental data.

NBSIR 75-666. **Post optimality and parametric analysis with the National Bureau of Standards' linear programming subroutine RVSMPX,** T. B. Ayers, 47 pages (Feb. 1975). Order from NTIS as COM 75-11381, $3.75.

Key words: algorithms; linear programming; parametric programming; post-optimality analysis.

This report is a sequel to NBS Report 10695 (February 1972), "The National Bureau of Standards' Linear and Quadratic Programming Subroutines," which documented one phase of an effort to provide users, of the facility operated by the National Bureau of Standards' Computer Services Division, with reliable, clearly-described solution algorithms for selected frequently-arising classes of special mathematical problems. The present report presents subroutines which perform post-optimality analysis and parametric programming studies on linear programming problems solved by the National Bureau of Standards' RVSMPX subroutine. (The present versions of these codes use internal storage only).

NBSIR 75-688. **Performance of mobile homes—A field inspection study,** L. F. Skoda, J. H. Pielert, W. E. Greene, and W. G. Street, 119 pages (June 1975). Order from NTIS as COM 75-11222, $5.25.

Key words: enforcement process; field inspection; house trailers; housing; Hurricane Agnes; mobile homes; performance data; standards.

A field inspection study of mobile homes was conducted for the Department of Housing and Urban Development. The objective of the study was to evaluate the causes of mobile home problems by physically inspecting available units at various locations in the United States. A total of 257 units were inspected consisting mostly of mobile homes purchased by HUD and used as temporary housing for victims of the 1972 Hurricane Agnes disaster. The total number of problems found was 3,528 for the 257 units inspected. Of these problems, 2120 were directly related to inadequacies in the ANSI A119.1 Standard for Mobile Homes or the mobile home enforcement process (plan review, certification of designs, plant inspection), 934 were routine maintenance problems, and 374 were attributed to mechanical electrical appliances and equipment. This report presents a computer listing of all problems plus photographic examples of observed problems.

The number of mobile homes included in this study is small when compared to the total number of mobile homes now in use in the United States. Additionally, this was a problem oriented study and did not attempt to document the many areas of satisfactory mobile home performance.

NBSIR 75-693. **Measurement methodology for determining the sound output of model airplanes and noise producing bicycle attachments,** M. A. Cadoff and W. A. Leasure, Jr., 24 pages (Apr. 1975). Order from NTIS as COM 75-11194, $3.25.

Key words: bicycle attachments; children; consumer safety; model airplanes; noise; toys.

In recent years, a great concern has been expressed for consumer protection and safety, especially for children. As an outgrowth of this concern, acoustical testing of potentially-hazardous noise producing toys has been carried out at the National Bureau of Standards for the Consumer Product Safety Commission under the authority of the Toy Safety Act of 1969. This report outlines a methodology which was developed to measure the noise levels of model airplanes and noise producing bicycle attachments. The technical back-up and rationale for the development of the methodology are discussed. In addition, data taken using the proposed methodology are presented.

NBSIR 75-700. **Results of full-scale fire tests with photoelectric smoke detectors,** R. W. Bukowski and R. G. Bright, 55 pages (Sept. 1975). Order from NTIS as COM 75-11280, $4.25.

Key words: fire detectors; ionization chamber smoke detectors; photoelectric smoke detectors; smoke detectors; Taguchi gas sensors.

In February 1974, a series of full-scale fire tests were conducted to determine whether photoelectric-type smoke detectors could respond to the same types of fires used to assess the performance of ionization-type smoke detectors. The types of fires employed in the tests are the same as those outlined in Underwriters' Laboratories, Inc., Standard No. 167. In addition to the UL-167 standard fires, fires involving polyurethane (flaming mode) and cotton (smoldering mode) were added to the test series. One detector, utilizing a Taguchi gas sensor (TGS), was included in the test series for evaluation purposes. The test results indicated that the better photoelectric smoke detectors, i.e., those having little obstruction to slow-moving smoke can, in general, detect the same test fires as the ionization chamber smoke detectors in approximately the same time scale. For the smoldering cotton fire, the photoelectric detectors were significantly faster than the ionization chamber detectors. The TGS fire detector was unable to detect most of the test fires.

NBSIR 75-701. **Evaluation of smokeproof stair towers and smoke detector performance,** F. C. W. Fung and R. H. Zile, 23 pages (Sept. 1975). Order from NTIS as COM 75-11282, $3.25.

Key words: high-rise buildings; photoelectric smoke detector; smoke control; smoke movement simulation; smokeproof tower.

A study was made by the National Bureau of Standards to evaluate the effectiveness of a smokeproof stairwell tower installed in a high-rise apartment building. Tests were also made of photoelectric-type corridor smoke detectors. A quantitative experimental technique of smoke simulation and smoke movement measurement was used. Factors diminishing the effectiveness of the stair towers, preventing smoke infiltration and limiting the response of the detectors, are noted.

NBSIR 75-702. **Design criteria for firefighters' turnout coats,** J. W. Eisele, 37 pages (Oct. 1975). Order from NTIS as COM 75-11433, $3.75.

Key words: firefighters; firefighter's turnout coats; protective clothing.

These design criteria cover requirements for the sizing, construction, outer shell, inner linings, weight, and thickness for firefighters' turnout coats as well as test methods, labeling requirements, and design considerations. Included also is a list of options and other items of concern to potential users of the criteria and a sample purchase specification to be used in conjunction with the criteria.

NBSIR 75-703. **A failure hypothesis for masonry shearwalls,** F. Y. Yokel and S. G. Fattal, 38 pages (May 1975). Order from NTIS as COM 75-11278, $3.75.

Key words: brick; failure; failure theories; masonry; shear strength; shear test; shear walls; stress distribution; stresses; structural engineering.

Various failure hypotheses for wall panels subjected simultaneously to diagonal compressive load and to vertical compressive edgeload are compared with the results of thirty-two tests on four types of brick masonry walls which were published elsewhere. It is concluded that failure can occur by joint separation or by splitting. A

failure hypothesis is advanced which is shown to be in good agreement with the test results examined.

NBSIR 75-705. **Thermal and flow characteristics of the ASTM E 84 tunnel test method,** J. G. Quintiere and J. W. Raines, 38 pages (Sept. 1975). Order from NTIS as COM 75-11217, $3.75.

Key words: ASTM E 84; carpets; energy balance; flame spread; mass balance; test method.

Five experiments were conducted using an ASTM E 84 tunnel test facility. These included a calibration test, three standard tests involving carpet materials, and one test in which a carpet material was tested on the floor of the duct. In addition to the measurements recorded during a standard test, instrumentation was added to measure inlet air velocity, temperature within the test section of the duct, and heat flux. From these measurements mass and energy balances were determined for each experiment. The results indicate that inlet air mass flow rate dropped during a test and appears to depend on the extent of burning in the duct. The energy balance results indicate that for the calibration run about half of the energy of the gas burner is lost by radiation and convection to the walls in the test section of the tunnel. During combustion of a test specimen, significant energy losses occur in the last 9 feet of the test section even after the flame tip has reached the exit of the tunnel.

NBSIR 75-721. **Economic objectives of utility companies and developers in evaluating a MIUS,** B. J. Bartter, 39 pages (Nov. 1975). Order from NTIS as PB246864., $4.00.

Key words: economic incentives; housing development; integrated utilities; utilities.

This report provides information to the Department of Housing and Urban Development-Modular Integrated Utility System (HUD-MIUS) program about the *economic* decision-making process for implementation of a MIUS by utility companies, developers, and a combination of these two groups.

Information was obtained through informal telephone interviews from these participant groups about their economic analysis of utility investment alternatives. The content of these conversations was synthesized into economic criteria which are perceived by each participant to be most important in evaluating alternative utility investments. From the analysis of these economic criteria, the possible combinations of participants and roles in the implementation of a MIUS are specified. These combinations are ranked, according to the degree of likelihood that each method will actually be employed.

The conclusion of this report is that a MIUS is most likely to be implemented by a governmental body, such as a municipal utility or governmental developer.

NBSIR 75-729. **Nondestructive tests to determine concrete strength—A status report,** J. R. Clifton, 39 pages (July 1975). Order from NTIS as PB246858, $4.00.

Key words: compressive strength; concrete; flexural strength; formwork removal; nondestructive testing; surface hardness.

Individual and combined nondestructive test methods have been critically reviewed as potential methods to determine safe formwork removal times. The techniques reviewed are the Windsor probe, the Schmidt Rebound Hammer, pull-out measurements, push-out cylinders, ultrasonic pulse velocity measurements, and the maturity and equivalent age concepts. The individual methods themselves do not give good estimates of the in situ strengths of concretes and it is recommended that future research emphasize combined methods.

A proposed research program which emphasizes combined nondestructive test methods has been developed.

NBSIR 75-730. **Equilibrium penny-like crack in indentation fracture,** B. R. Lawn and E. R. Fuller, Jr., 28 pages (Sept. 1975). Order from NTIS as COM 75-11461, $3.75.

Key words: contact fracture; degradation; Hertzian cracks; indentation fracture; median vents; penny crack.

A study is made of the mechanics of two basic types of indentation fracture, *cone cracks* ("blunt" indenters) and *median cracks* ("sharp" indenters). The common feature which forms the central theme in this work is that both crack types, in their well-developed stages of growth, may be regarded as essentially "penny-like." On this basis a universal similarity relation is derived for equilibrium crack dimension as a function of indentation load. Experimental measurements confirm the general form of this relation. A more detailed fracture mechanics analysis is then given, to account for additional, contact variables evident in the data. Notwithstanding certain analytical limitations, the study serves as a useful basis for investigating a wide range of contact-related problems, both fundamental and applied, in brittle solids.

NBSIR 75-733. **An evaluation of proposed safety requirements for infants' pacifiers,** S. D. Toner and H. A. Baker, 20 pages (Aug. 1975). Order from NTIS as COM 75-11139, $3.25.

Key words: consumer products, CPSC proposed regulation; pacifiers; product safety; safety requirements; safety testing.

This report is concerned with a review of a regulation proposed by the Consumer Product Safety Commission on the safety of infants' pacifiers. In addition, the results of a laboratory evaluation of the efficacy of various requirements and testing procedures are given.

NBSIR 75-737. **Mathematical methods of site selection for electronic message systems (EMS),** C. Witzgall, 44 pages (June 1975). Order from NTIS as COM 75-11472, $3.75.

Key words: communication; cost-benefit; deployment; electronic transmission; facility location; mail; mathematical programming; message network synthesis; network optimization; satellite; service improvement.

The concept of electronic message (mail) transmission has been the subject of several feasibility studies during the past decade. It requires the installation of electronic message handling facilities at selected locations. If transmission is to be via communications satellite, then any such facility can transmit to and receive from any other one. In this report, the mathematical aspects of choosing the number and locations of these facilities are examined. An inventory of solution methods is presented, along with recommendations as to which among them should be employed or developed further.

NBSIR 75-738. **A method and means of calibrating an air-bearing force plate for use with a towed pavement friction test trailer,** R. W. Kearns and J. F. Ward, 40 pages (Dec. 1974). Order from NTIS as COM 75-11279, $3.75.

Key words: calibration procedures; force plate; pavement skid resistance; skid accident reduction; tire-pavement interface forces.

The equations for the variation of the external forces acting at the tire-pavement interface of a symmetrical two-wheeled towed trailer are given. Estimates, derived from experimental results, have been made for the displacement of the tire-plate interface with respect to the ground of an unrestrained locked test tire on the trailer. A description of the force plate calibration test frame, instrumentation and test method is given. The means of applying simultaneous vertical (normal) and horizontal (longitudinal) forces at the contact surface of the air-bearing plate in accordance with the equations are discussed. The change in force plate output with changes in the dimensions of the trailer calibrated in-turn with the force plate are given. A method of locating the coordinate axes of the internal force sensors with respect to level is given. Consistent application of these methods to both the force plate and trailer transducer calibrations results in reduced vertical-to-horizontal cross-axis differences.

NBSIR 75-746. **Preparation of reference data sets for**

character recognition research, M. L. Greenough and R. M. McCabe, 52 pages (June 30, 1975). Order from NTIS as COM 75-11432, $4.25.

Key words: character recognition; context research; data bases; optical character recognition; pattern recognition; reading machines.

A reference data set contained on magnetic tape has been generated for research in optical character recognition and related fields. The data set contains video data in 16 levels for each point in a 24 × 24 scanning grid, applied to approximately 30 000 characters. The input material, on some 2200 simulated address mailpieces, includes a range of character quality from excellent to poor.

The data set was prepared by first microfilming the address fields and printing positive transparencies. Then preselected characters were scanned in the NBS FOSDIC. Through the use of calibrated gray scales which were filmed and scanned along with the addresses, corrections were applied to assure linearity of overall response.

A second reference data set was also prepared from the same input material of simulated mailpieces. Through analysis of the recognition results printed out during runs on one address reader, details of identification on both alphabetic and numeric recognition modes were noted. These were encoded into six-character groups on the data tapes, formatted to provide one such group for each input character in the original addresses. Recognition results are shown for approximately 110 000 input characters.

NBSIR 75-760. **Proceedings of piezoelectric and pyroelectric symposium-workshop,** M. G. Broadhurst, 222 pages (Sept. 1975). Order from NTIS as COM 75-11436, $7.25.

Key words: electrets; hydrophone; piezoelectric; polymers; polyvinylidene fluoride; pyroelectric; radiometer; transducers.

The purpose of this Symposium-Workshop was to bring together scientists and program managers from federal (primarily DoD), industrial, university, and foreign laboratories who are involved in the research on and manufacture of piezoelectric and pyroelectric polymer materials and devices, in order to exchange information about and stimulate further work on the new and rapidly developing measurement technology involving polymer transducers. This meeting is particularly important at this time because highly active polymer films are not yet available to device manufacturers in the U.S. or to potential users such as DoD.

NBSIR 75-761. **The demonstration of experimental lead paint hazard abatement methods in Washington, D.C.,** T. H. Boone, H. W. Berger, A. P. Cramp, and H. A. Jackson, 105 pages (June 1975). Order from NTIS as COM 75-11377, $5.25.

Key words: abatement; barrier materials; building materials; housing; lead-based paint; lead poisoning; paint removal.

This report describes the first stage of an experimental lead paint hazard abatement program carried out in 30 dwelling units in Washington, D.C. The entire program will ultimately involve the abatement of lead paint hazards in a total of approximately 250 dwelling units located in three or more cities.

The procedures, demonstrated in Washington, included: paint removal methods using chemical solvents and a heat producing device; the replacement of components such as windows, doors and wood trim; and the installation of flexible sheet and rigid board barrier materials over existing lead paint on wall.

The report presents procedures and the forms used in inspecting and selecting dwellings for lead paint hazard abatement, evaluations of the suitability and implementation characteristics of the abatement methods and recommendations for their use.

Subsequent reports will present the results of comparable programs in additional cities and a final report will compare the cost-effectiveness of the alternative abatement methods.

NBSIR 75-763. **Thermodynamic and transport properties of ethylene and propylene,** I. A. Neduzhii (Principal Author), 210 pages (June 1972). Order from NTIS as COM 75-11276, $7.25.

Key words: critically evaluated data; ethylene; propylene; thermodynamic properties data; transport properties data.

A comprehensive review of the data on the thermodynamic and transport properties of ethylene and propylene is given. Subjects covered include equation of state for liquid and vapor, second virial coefficient, enthalpy, etc., heat capacity, speed of sound, viscosity, and thermal conductivity. New experimental measurements are given for several properties, especially speed of sound, densities of the liquid and transport properties. Tables of properties covering the temperature range from 160 K to 500 K are given. The book has been translated into English from the original Russian.

NBSIR 75-766. **Properties and interactions of oral structures and restorative materials,** J. M. Cassel, 51 pages (July 1975). Order from NTIS as COM 75-11376, $4.25.

Key words: adhesive materials; composites; dental materials; polymer grafting; resins; restorative materials; sealants; wear resistance.

A diversity of experimental approaches is being investigated to develop techniques which can be applied in formulation of adhesive restorative and caries-preventive dental materials. A newly developed testing procedure, still in the evaluation stage, has demonstrated expected ranking of adhesive bond strengths within a group of selected coating agents, both coupling and release types. Deterioration on exposure to water of cohesive bond strength in the Bis-GMA matrix has been indicated without concurrent deterioration of the coupling agent. A monomer system with potential as a composite or pit and fissure sealant resin and giving a polymerizable liquid of desired viscosity at room temperature was derived from three low-melting, crystalline isomers of ether-ester linked aromatic dimethacrylates. A series of monomers of varying chemical structure was evaluated for possible application in photopolymerization experiments designed to investigate modification of hard tissue by grafting. Modifications to extend the running time of a dental restorative wear-generating experiment three-fold and which allow the computerized recording of ten, instead of two, depth of wear measurements around the circular wear track have significantly reduced the standard error of measurement. Surface coating techniques being developed to strengthen interfacial bonding in dental cements and other dental materials show more promise with titanate than with carbon reinforcing fibers.

NBSIR 75-767. **A methodology for establishing conditioning requirements for building materials and composites,** L. W. Masters and M. Tryon, 35 pages (Oct. 1975). Order from NTIS as PB246879, $4.00.

Key words: building composite; building material; conditioning; equilibration; gypsum wallboard; mettodology; relative humidity; structural sandwich panel; temperature; testing.

The measured properties of building materials and their composites sometimes reflect the conditions to which they have been exposed while being prepared for test. Conditioning these materials to some standard reference state is sometimes used to minimize this effect.

A methodology for establishing conditioning requirements for building composites and materials is presented and its use illustrated by applying it to two building composites.

NBSIR 75-770. **The equation of state for ammonia,** L. Haar and J. Gallagher, 27 pages (Sept. 1975). Order from NTIS as COM 75-11370, $3.75.

Key words: ammonia; correlation; gas; liquid; thermodynamic properties; thermodynamic surface.

An outline is presented of the basic results of the extensive correlation for the thermodynamic properties of ammonia recently completed at this laboratory. Computer programs are presented for the calculation of thermodynamic properties in the range including the triple point temperature to 5/3 the critical temperature and pressures from the dilute gas to 8000 bar.

NBSIR 75-772. **The dynamic response of helicoid anemometers,** J. M. McMichael and P. S. Klebanoff, 54 pages (Nov. 1975). Order from NTIS as PB246861, $4.50.

Key words: air; analytical; anemometer; dynamic response; experimental; lag; unsteady flow.

The results of an analytical and experimental investigation of the dynamic response of a helicoid anemometer are presented. The experimental investigation was conducted using the NBS Unsteady Flow Facility and data are presented which illustrate the dynamic behavior in a spatially uniform, fluctuating flow with varying amplitudes, frequencies, and mean velocities. An analytical model governing the dynamic response is also presented and compared with the experimental results.

NBSIR 75-774. **Calibration of Kerr systems used to measure high voltage pulses,** R. E. Hebner, Jr., 51 pages (Aug. 7, 1975). Order from NTIS as COM 75-11364, $4.25.

Key words: automated measurements; dielectrics; dividers; electrical measurement; electric fields; electro-optics; high voltage measurements; insulating fluids; Kerr effect; nitrobenzene; pulse measurements; space charge.

The purpose of this work is to define, develop and refine techniques for calibrating pulse voltage measurement systems, particularly those based on the electro-optic Kerr effect. The approach used exploits the assumed frequency independence of the Kerr coefficient of nitrobenzene. Theoretically, the Kerr coefficient should exhibit the same frequency dependence as the relative permittivity. Measurements have shown the relative permittivity to be approximately frequency independent over the frequency range from direct voltage to 10^9 Hz. The realization of this calibration approach has been hampered by the fact that the electric field distribution, in the liquid exhibiting the electro-optic Kerr effect, is itself frequency dependent.

This report describes the present best comparison of cell calibration under direct voltage with calibration under low frequency alternating voltage and calibration under pulsed high voltage. The results under all three types of waveforms agree to within ± 0.5 percent. From these results it can be inferred that it is feasible to use an electro-optic Kerr system as an independent, and possibly more accurate, device against which to calibrate other pulse voltage measurement systems.

In addition to this discussion of Kerr system calibration, the report contains two appendices. One presents an improved technique for analysis of data obtained from a Kerr system and the other discusses space charge in a nitrobenzene-filled Kerr cell.

NBSIR 75-778. **ETIP: THE FIRST 18 MONTHS. A progress report of the experimental technology incentives program, National Bureau of Standards,** J. D. Lewis, 74 pages (Aug. 1975). Order from NTIS as PB246435, $4.50.

Key words: civilian R&D policy; ETIP; incentives; innovation; procurement policy; regulatory policy; small business policy; technology.

This internally prepared report describes the overall accomplishments of the experimental Technology Incentives Program in carrying out its mission. Progress is compared with the plans that were established in a program plan approved by the Secretary of Commerce in February of 1974. An appendix to the report describes the purpose and shows progress of each of the individual projects that ETIP has launched.

NBSIR 75-781. **Optical materials characterization,** A. Feldman, D. Horowitz, R. M. Waxler, I. H. Malitson, and M. J. Dodge, 24 pages (Aug. 1975). Order from NTIS as COM 75-11375, $3.25.

Key words: birefringence; elastic constants; infrared-laser window materials; interferometry; KCl; photoelasticity; polycrystalline ZnSe; refractive index; stress-optical constants; thermal coefficient of refractive index; ZnSe.

The refractive index of each of two prismatic samples of chemical vapor deposited (CVD) ZnSe was measured from 0.5086 μm to 18.2 μm by means of the minimum-deviation method on a precision spectrometer. Data were obtained at temperatures near 20 and 34 °C and each set of data was fitted to a three-term Sellmeier-type dispersion equation, which permits refractive index interpolation within several parts in 10^{-5}. From the data obtained at the two temperatures, dn/dT was calculated for both samples. A comparison of refractive index and dn/dT is made with other types of ZnSe. Preliminary photoelastic data are presented for single crystal specimens of Ge, reactive atmosphere processed (RAP) KCl, and KCl doped with KI. The Ge data, which were obtained at 10.6 μm differ from previously reported data. Data on the two types of KCl were obtained at 10.6 μm, 0.633 μm and 0.644 μm. These data are compared with values from the literature. Also presented are revised photoelasticity data for CVD ZnSe. The design of an improved stressing apparatus that was developed for the measurement of photoelastic constants is discussed.

NBSIR 75-783. **Validation of the DELCAP airport simulation model,** J. F. Gilsinn, 169 pages (July 1975). Available from the author, NBS, Washington, D.C. 20234.

Key words: airport; airport capacity; airport simulation; models; model validation; runway capacity; simulation; validation.

This report documents exercises of the DELCAP airport simulation model performed to validate the outputs of that model. Airport throughput levels were calculated by DELCAP for five runway configurations, with three or four appropriate operating policies chosen for each, and for three different mixes of aircraft types. These estimates from DELCAP agreed well, generally within 6 to 8 percent, with current values provided by the FAA. An attempt at validating DELCAP's delay-figure output, using existing data on scheduled and actual times of aircraft departures and arrivals, is also reported. It proved unsuccessful, because available data are not sufficient to isolate that portion of total delay which DELCAP is designed to measure, i.e., terminal area ATC delay. A collection effort to accumulate the necessary data is formulated. Appendices to the report contain program listing, flowcharts, descriptions of program changes from earlier versions, and user instructions for the model's operation.

NBSIR 75-784. **Fire incidents involving flammable liquids, gas, and dry explosives,** E. A. Tyrrell, 58 pages (Oct. 1975). Order from NTIS as PB246862, $4.50.

Key words: accidents; burn injuries; burn severity; explosives; fabric fires; FFACTS; flammable liquids; gas; gasoline; ignition-causing activities; ignition sources; injury disposition.

From the NBS Flammable Fabrics Accident Case and Testing System as of December 1973, flammable liquids, gas, and dry explosives were found to be involved in 832 incidents, injuring 863 victims. Volatile flammable liquids represented 77 percent of the incidents; 72 percent of these liquids were gasoline. Male victims outnumbered females more than 3 to 1. Young adults, ages 21-45, and youth, ages 13-20, were injured most frequently. Children and youth were injured primarily through what was considered as play activities. Adults generally were injured while engaged in activities traditionally considered as being oriented to the particular sex involved. Streetwear, particularly shirts/blouses, was reported most frequently as igniting

first. Thirty-six percent of the fabrics represented in these incidents were contaminated with a flammable liquid. Most of the victims sustained burn injuries covering 1-10 percent of their bodies; only 6 percent sustained burn injuries covering 61 percent or more of their bodies. Most of the victims were hospitalized for treatment of their injuries. Although the very young and the elderly were involved in these incidents less frequently than other age groups, they generally were burned more severely and represented 46 percent of the victims who died in the hospital or were dead on arrival.

NBSIR 75-785. **The review of standardization and measurement services at the Ecuadorian Institute for Standardization,** R. Estrada and H. S. Peiser, 17 pages (June 27-29, 1974). Order from NTIS as PB246345, $3.50.

Key words: AID; development assistance; economics; Ecuador; less developed countries; measurement services; review; standardization; survey.

An international team of standards and measurement specialists visited the Ecuadorian Institute for Standardization on June 27-29, 1974, to review the operations of that organization in light of the recommendations made two years earlier by a Survey of Standardization and Measurement Services in Ecuador conducted by a team which was organized and sponsored by the U.S. National Bureau of Standards and the U.S. Agency for International Development. The review consists of the historical background of the Institute, results of the 1972 Survey, and recommendations for future planning.

NBSIR 75-787. **Piezo- and pyroelectric properties of electrets,** M. G. Broadhurst and G. T. Davis, 55 pages (Oct. 1975). Order from NTIS as COM 75-11471, $4.25.

Key words: electrets; piezoelectricity; polarization; polymers; polyvinylchloride; polyvinylfluoride; polyvinylidenefluoride.

A model for piezo- and pyroelectricity in polymers is presented. These effects are true piezo- and pyroelectricity rather than electrostriction, conduction, electromechanical effects or the motion of conductors in the field of space charges. Two distinct types of polymers can be piezoelectric. Amorphous polymers are piezo- and pyroelectric by virtue of a nonequilibrium but kinetically stable net dipole orientation. The semicrystalline polymers are piezoelectric due to alignment of polar, ferroelectric crystals dispersed in the amorphous phase. In both types the magnitudes of the piezo- and pyroelectric effects are in accord with the expected temperature and pressure dependence of the dipolar polarization. Space charges embedded in the polymer normally will not produce a piezo- or pyroelectric current. Those embedded near the crystal-liquid interfaces tend to reduce the piezo- and pyroelectricity. Improved orientation of dipoles and reduction of ionic impurities should increase p and d for PVF_2 by a factor of three above typical values presently reported. The sensitivity of amorphous polymers is limited mainly by dipole moment per unit volume and breakdown strength.

NBSIR 75-794. **Heat transfer in furnaces for CIB cooperative program and heat balance analysis of wall furnace,** J. B. Fang and J. T. Scott, 48 pages (Nov. 1975). Order from NTIS as PB247203, $4.00.

Key words: fire resistance ratings; fire test furnace; heat balance; heat transfer; temperature-time curve.

Tests were conducted in the NBS wall panel furnace as part of a CIB international cooperative program to measure and compare heat transfer in fire endurance furnaces. Additionally, a heat balance analysis showed that a cellular concrete block wall specimen absorbed more heat by convection than by radiation. The rate of radiant heat transfer was found to decrease slowly, while the furnace exhaust heat loss increased during the test from 42 to 58 percent of the heat output. The calculated radiant heat fluxes incident at furnace walls was found to be somewhat lower than the experimental values measured at the test wall.

NBSIR 75-795. **Recommended criteria for retrofit materials and products eligible for tax credit,** W. J. Rossiter, Jr. and R. G. Mathey, Eds., 44 pages (Nov. 1975). Order from NTIS as PB246866, $4.00.

Key words: caulks and sealants; clock thermostats; energy conservation; insulation; retrofitting; storm doors; storm windows; tax credit; vapor barriers; weatherstripping.

The Federal Energy Administration requested the National Bureau of Standards to develop criteria for retrofitting for possible use by the Internal Revenue Service in implementing the Presidential initiative authorizing tax credit to homeowners. Criteria are recommended for materials and products considered eligible for proposed tax credit for retrofitting one and two family residences to conserve energy. The materials considered include insulation and vapor barriers, storm windows and doors, caulking and weatherstripping, and clock thermostats. A list of these retrofit materials was compiled by generic type and recommendations made on their installation.

In addition to recommended criteria for materials and products eligible for tax credit, desired levels of performance for the retrofit materials are presented as a guide to homeowners to achieve maximum benefits in energy conservation through retrofitting.

NBSIR 75-797. **An evaluation of a range-top warning light system,** M. E. Stefl and J. J. Persensky, 22 pages (July 1975). Order from NTIS as COM 75-11465, $3.25.

Key words: consumer products; human factors; kitchen; ranges; reaction time; safety; warning lights.

A descriptive analysis of In-Depth Injury Investigations of range-related accidents revealed a series of incidents where range-users were unaware that surface elements were energized. One proposed solution to this problem involved a system of four warning lights to indicate individual surface unit activation. A laboratory study using human subjects evaluated the effectiveness of such a system. The backgrounds against which the warning lights were fitted and the intensity of the lights were not shown to influence subjects' responses in a reaction time task; however, the position of the lights and the type of ancilliary task being performed by the subject did. These results are discussed in terms of product design and safety, and implications of the study for methodological development are considered.

NBSIR 75-804. **Generation of standard EM fields for calibration of power density meters 20 kHz to 1000 MHz,** M. L. Crawford, 44 pages (Jan. 1975). Order from NTIS as COM 75-10395, $3.75.

Key words: hazard level fields; power density meter calibration; TEM transmission cells.

This report describes techniques for calibrating power density meters used by the Department of Defense in measuring high intensity (hazard level) RF fields in the frequency range 20 kHz to 1000 MHz. It reports on part of the work sponsored by the Calibration Coordination Group (CCG), of the Department of Defense covering the frequency range 20 kHz to 20 GHz.

Several techniques were considered for producing a standard field including parallel plate and parallel wire transmission lines, transverse electromagnetic mode (TEM) transmission cells, various directive antennas and open ended waveguide (OEG). The major emphasis in this report is on the TEM cells, which are recommended for the frequency range 20 kHz to 500 MHz. Design and evaluation details and an error analysis associated with the TEM cell measurement system are given. Power density levels can be established in the cells from a few $\mu W/cm^2$ to 100 mW/cm^2 with uncertainties less than $\pm$ dB.

Limited information is also given describing the use of OEG, the recommended technique for the frequency range 500 MHz to 2.6

GHz, and giving the results of intercomparisons among parallel plate lines, TEM cells, OEG, and standard gain horns.

NBSIR 75-807. **Turbulent natural convection of liquid deuterium, hydrogen, and nitrogen within enclosed vessels,** D. E. Daney, 82 pages (Feb. 1975). Order from NTIS as COM 75-10396, $4.75.

Key words: cryogenic; heat transfer; hemisphere; horizontal cylinder; liquid deuterium, liquid hydrogen, liquid nitrogen; natural convection; sphere; vertical cylinder.

Quasi-steady natural convection of liquid deuterium, hydrogen, and nitrogen within a sphere, hemisphere, horizontal cylinder, and vertical cylinder has been studied experimentally for the case of a nearly isothermal wall. A single expression relating the Nusselt and Rayleigh numbers,

$$Nu = 0.104\,Ra^{0.332},$$

fits the deuterium and nitrogen data over the range $7 \times 10^8 < Ra < 6 \times 10^{11}$, while the hydrogen Nusselt numbers are 8 percent lower. The temperature field within the vessels is virtually free of horizontal temperature gradients. A single dimensionless temperature profile characterizes the vertical temperature distribution for each vessel shape, with the profiles for the sphere, hemisphere, and horizontal cylinder being nearly identical.

NBSIR 75-809. **Non-planar near-field measurements: Spherical scanning,** P. F. Wacker, 67 pages (June 1975). Order from NTIS as COM 75-10989, $4.25.

Key words: antennas; arrays; coordinate transformations; data processing; group representations; measurements; near field; non-planar; patterns; scanning; spherical; symmetry.

The advantages and limitations of near-field antenna measurements are compared with those of conventional far-field measurements. Further, the advantages and limitations of planar, circular cylindrical, and spherical scanning are compared.

Spherical scanning is advantageous for arrays steered well off-axis and for antennas with wide angle side lobes, but the data processing has been quite impractical except for very simple antennas and probes. A new highly efficient data processing scheme is given for spherical scanning with and without probe pattern correction. The translation-of-centers transformation of the probe pattern coefficients (required only with the probe pattern correction) is carried out once and for all for a given probe, scanning radius, and frequency. The routine computations involve Fast Fourier "Transforms" and multiplication by matrices with constant elements, matrices which are independent of the detailed nature of the probe, the radius of the scanning sphere, the points at which measurements are made, and the nature of the test antenna. The FFT's and matrix multiplications supplant matrix inversion, ordinary solution of simultaneous equations in more than two unknowns, ordinary numerical integration, and (in routine processing) ordinary evaluation of functions, even for computation of the far field. Except for the truncation of the infinite series of spherical modes, no analytical or data processing approximations are made, even in the use of the FFT.

So that readers may draw from their understanding of planar and cylindrical scanning, a unified theory of near-field data processing is given, treating planar, cylindrical, and spherical scanning as mere special cases.

NBSIR 75-810. **Semi-annual report on materials research in support of superconducting machinery,** R. P. Reed, J. G. Hust, M. B. Kasen, H. M. Ledbetter, R. P. Mikesell, R. E. Schramm, L. L. Sparks, R. L. Tobler, and W. F. Weston, 201 pages (Apr. 1975). Order from NTIS as COM 75-10919, $5.25.

Key words: composites; elastic properties; fracture; liquid helium; mechanical properties; structural materials; superconducting machinery; thermal conductivity.

Results of six months of study on materials in support of superconducting machinery (October 1974 through March 1975) are reported to the sponsor, the Advanced Research Projects Agency of the U.S. Department of Defense. The report is divided into five sections: thermal conductivity, magnetothermal conductivity, fatigue and fracture-toughness properties, properties of advanced composites, and elastic properties. The temperature range 4 to 300 K is covered by the study. Materials studied are either being used or are candidates for use in superconducting machinery and include: aluminum alloys, composites, copper, age-hardened, nickel-base superalloys, stainless steels, and titanium alloys.

Special results of the study include: thermal conductivity data for comparison of the effects of heat treatment on age-hardenable alloys, the first determination of a complete set of elastic constants for a composite at liquid helium temperature, boron-aluminum composite tensile data at 4 K, and a summary of fatigue crack-growth rate behavior at 4 K for a number of different structural alloys. These data provide considerable insight into material characteristics at extremely low temperatures, assisting in material selection and efficient design.

NBSIR 75-812. **The Kapitza conductance of the (100) surface of copper and polycrystalline indium and niobium,** N. S. Snyder, 51 pages (June 1975). Order from NTIS as COM AD-A012889, $3.75.

Key words: heat transfer to helium II; interfacial thermal resistance; Kapitza conductance of copper; Kapitza conductance of indium; Kapitza conductance of niobium; x-ray diffraction examination of single crystal lattice damage; (100) surface of copper.

Measurements of the Kapitza conductance to liquid helium II across the (100) surface of single crystals of copper are presented. The temperature range of these measurements was 1.6 to 2.1 K.

The sample surfaces were subjected to several different treatments. Some surfaces were cleaned by low energy argon ion bombardment, annealed in an ultrahigh vacuum system, and preserved under vacuum until purified liquid helium was admitted. Other surfaces were intentionally damaged by machining and/or exposure to the atmosphere. The conductance after these latter treatments was found to be about a factor of three higher than that of the more ideally cleaned and annealed surfaces, and a significant increase in the temperature dependence of the conductance was also observed. Indications are that these effects on the conductance are produced primarily by the last few atomic layers of the solid, so extensive cold-working, which impairs the thermal conductivity of the bulk, need not be undertaken to improve surface heat transfer. This finding has important implications for the design of practical heat transfer surfaces. Good reproducibility was found for the conductances of similarly treated surfaces and good correlation with studies of damage carried out by x-ray diffraction. The relationship of these results to the numerous current theories of the Kapitza conductance is discussed. Conductance measurements of polycrystalline niobium and indium are presented in the appendices.

NBSIR 75-814. **A modified Benedict-Webb-Rubin equation of state for parahydrogen-II,** H. M. Roder and R. D. McCarty, 54 pages (June 1975). Order from NTIS as COM 75-11132, $4.25.

Key words: critical point; density; enthalpy; equation of state; hydrogen; index of refraction PVT; saturation properties; scaling laws; specific heat.

A 32 term modified Benedict-Webb-Rubin equation of state has been applied to data for parahydrogen. The adjustable parameters in the equation of state were determined using 2665 points including very recent measurements at low temperatures and high pressures. The new values extend the range of the PVT data sufficiently to war-

rant a refitting of the equation of state. Temperatures for the data range from the triple point to about 700 K with pressures reaching 3000 atmospheres near ambient temperatures. The PVT data were adjusted to the T_{68} scale. In addition, extensive modifications have been made to the previously accepted PVT surface in the region near the critical point. These adjustments have been made on the basis of more recent refractive index data and the application of scaling law equations. Detailed comparisons between experimental and calculated values are given for density. Corresponding comparisons are made for enthalpy and the specific heat at constant pressure.

NBSIR 75-816. **Performance characteristics of a liquid helium pump,** P. R. Ludtke, 55 pages (July 1975). Order from NTIS as COM 75-11133, $4.25.

Key words: cavitation; cryogenic motors; induction motors; liquid helium pumps; motor efficiency; net positive suction head; pump efficiency; pump performance.

Part A of this report presents performance data for a simple, preinduced, single stage, centrifugal liquid helium pump powered by a close-coupled submersible cryogenic induction motor. Data on pump efficiency and the motor efficiency are given, and the effects of decreasing the pump leakage loss and removing the pre-inducer were also investigated.

Part B describes a study of the cavitation characteristics of the pump in liquid helium I. The net positive suction head at cavitation of the pump was extensively investigated, and found to be near zero; the effects of removing the inducer, changing the pump inlet geometry, and varying the helium temperature were determined.

NBSIR 75-901. **Smoke and carbon monoxide formation from materials tested in the smoke density chamber,** T. Y. King, 40 pages (Oct. 1975). Order from NTIS as PB246860, $4.00.

Key words: carbon monoxide; electrostatic precipitation; heat flux; oxygen depletion; particulate mass; scanning electron microscope; smoke.

The effects of physical and chemical factors on the smoke and carbon monoxide generated by burning polymers and red oak in the NBS Smoke Density Chamber are reported.

Smoke and carbon monoxide formation was found to depend on irradiance level and oxygen concentration in the chamber. Smoke optical density correlations with particulate mass density showed that the ratio of these two varied with material composition and burning conditions.

NBSIR 75-903. **San Antonio Veterans Administration Hospital smoke movement study,** F. C. W. Fung and R. H. Zile, 37 pages (Nov. 1975). Order from NTIS as PB246859, $4.00.

Key words: experiments; full-scale; gas tracer; interstitial space; penetration through ceiling; smoke movement; smoke simulation; sulfur hexa-fluoride (SF_6); Veterans Administration Hospital.

A series of full-scale smoke movement experiments was conducted using a sulfur hexa-fluoride (SF_6) gas tracer, smoke simulation system. The experiments were designed to study smoke movement in a hospital building with an interstitial space between floors. The penetration of smoke through ceiling and interstitial space and the vertical smoke movement in such a building were investigated.

NBSIR 75-908. **Characterization of sharp points and edges by electrical breakdown,** J. Cohen, 21 pages (Aug. 1975). Order from NTIS as PB247270, $3.50.

Key words: consumer products; electrical breakdown; gases; hazard; high voltage; sharp edges; sharp points; threshold.

Experiments were made to determine the feasibility of using the phenomenon of electrical breakdown in air to characterize sharp metallic edges and points. A fixed voltage was applied between a sample edge or point and a parallel plane, and the threshold gap length for breakdown observed. Results were quite favorable for edges, but not for points, and the polarity on the sample was required to be negative.

NBSIR 75-909. **Index of automated system design requirements as derived from the OMB Privacy Act implementation guidelines,** D. K. Branstad and R. A. Krell, Standards Coordinators, 14 pages (Oct. 1975). Order from NTIS as PB246863, $3.50.

Key words: computer; data processing; index; information processing; privacy; requirements definition; security; systems design.

This index is a list of certain requirements which must be considered by Federal technical and administrative personnel in order to comply with those provisions of the Privacy Act of 1974 relating to automated systems design and development. This index has been derived from the Office of Management and Budget (OMB) guidelines for implementing those provisions. Each requirement listed contains a reference to an applicable part of the Privacy Act and to a page and column number of the OMB guidelines as they appear in the *Federal Register.* Therefore, these documents must be used in conjunction with this index. Furthermore, a familiarity with these documents will increase the utility of this index.

This column lists all outside publications by the NBS staff, as soon as possible after issuance as practical. For completeness, earlier references not previously reported may be included from time to time.

Albus, J. S., **A new approach to manipulator control: The cerebellar model articulation controller (CMAC),** *Trans. ASME –J. Dyn. Syst. Meas. Control* **97,** No. 3, 220-227 (Sept. 1975).

Key words: adaptive control; cerebellum model; control theory; manipulator control; Perceptron.

CMAC is an adaptive system by which control functions for many degrees of freedom operating simultaneously by referring to a table rather than by mathematical solution of simultaneous equations. CMAC combines input commands and feedback variables into an input vector which is used to address a memory where the appropriate output variables are stored. Each address consists of a set of physical memory locations, the arithmetic sum of whose contents is the value of the stored variable. The CMAC memory addressing algorithm takes advantage of the continuous nature of the control function in a way which promises to make it possible to store the necessary data in a physical memory of practical size.

Albus, J. S., **Data storage in the cerebellar model articulation controller (CMAC),** *Trans. ASME Series G, J. Dyn. Syst. Meas. Control* **97,** No. 3, 228-233 (Sept. 1975).

Key words: cerebellar model; control theory; data storage; distribution memory; hierarchical control; manipulator control.

The storage of manipulator control functions in the CMAC memory is accomplished by an iterative process which, if the control function is sufficiently smooth, will converge. There are several different techniques for loading the CMAC memory depending on the amount of data which has already been stored and the degree of accuracy which is desired. The CMAC system lends itself to a "natural" partitioning of the control problem into manageable subproblems. At each level the CMAC controller translates commands from the next higher level into sequences of instructions to the next lower level. Data storage, or training, is accomplished first at the lowest level and must be completed, or nearly so, at each level before it can be initiated at the next higher level.

Andrews, J. R., Lawton, R. A., **Picosecond pulse research at NBS,** *Proc.* 1974 *Joint Measurement Conference, Gaithersburg, Md., Nov.* 12-14, 1974, 123-140 (Instrument Society of America, Pittsburgh, Pa., 1975).

Key words: oscilloscopes; pulse; pulse generators; pulse measurement; transmission lines.

A general review of pulse measurement research at the National Bureau of Standards is described which includes work with electrical pulse generators using mechanical switches, avalanche transistors, snap off diodes, tunnel diodes, and laser pulses. Pulse transmission studies which include skin effect, nonuniform dielectric, lossy liquid dielectric and superconductivity are also mentioned together with pulse measurement techniques which include oscillographic techniques and pulse autocorrelation. The interfacing of picosecond pulse measurement instruments with a minicomputer is also described. This has resulted in an Automatic Pulse Measurement System (APMS) which has already been used to measure transmission coefficient, S_{21}, of some microwave networks.

Armstrong, G. T., Johnson, W. H., **Standard reference materials for combustion calorimetry,** *Proc. Third Int. Conf. on Chemical Thermodynamics, Baden near Vienna, Austria, Sept.* 3-7, 1973, **VIII,** 55-72 (International Union of Pure and Applied Chemistry, Oxford, England, 1974).

Key words: acetanilide; bomb calorimetry; calorimetry; chlorobenzoic acid; combustion; creatinine; fluorobenzoic acid; nicotinic acid; reference materials; thermochemical; thermochemical standards; thianthrene; urea.

Combustion measurements using a rotating bomb adiabatic aneroid calorimeter have been used to make a preliminary evaluation of ten substances as potential thermochemical reference materials for combustion of organic compounds containing N, S, Cl and F. p-chlorobenzoic acid, p-fluorobenzoic acid, and urea are recommended for acquisition, certification, and distribution. Thianthrene may also be suitable. For the ten substances including in addition to the above: o- and m-chlorobenzoic acids, o-fluorobenzoic acid, nicotinic acid, acetanilide, and creatinine, typical combustion data are given, showing corrections applied; and mean thermodynamic functions at 25 °C are given together with error estimates. The results are compared with other work. Recommendations and a discussion of the role of standard reference materials for thermochemistry are given.

Armstrong, G. T., **The infrastructure of the thermochemical measurement system,** (Proc. Quatrieme Conf. Int. de Thermodynamique Chimique, Montpellier, France, Aug. 26-30, 1975), Chapter in *Thermochimie* **I,** 11-18 (Centre de Recherches de Microcalorimétrie et de Thermochimie du C.N.R.S., Marseille, France, 1975).

Key words: calorimetry; chemical energy; chemical thermodynamic data; energy scale (chemical); equilibrium measurements; mass spectrometry; measurement system; spectroscopy; state measurements; thermochemistry.

The thermochemical measurement system outlined here is an extension of the concept of a measurement system in that it deals with a class of physicochemical information, rather than with a metrology. Thermochemical quantities are defined, classified as archival thermochemical data, and thermochemical laboratory test data, and their source methodologies are categorized as calorimetry, equilibrium and state measurements, optical and mass spectrometry and theory. The relationship of thermochemical to nonthermochemical calorimetry is outlined. The propagation of measurements from standards laboratory to ultimate user is described for archival and for test laboratory thermochemical data.

Arora, V. K., Peterson, R. L., **Quantum theory of Ohmic galvano- and thermomagnetic effects in semiconductors,** *Phys. Rev. B* **12,** No. 6, 2285-2296 (Sept. 15, 1975).

Key words: galvanomagnetism; quantum transport theory; semiconductors; thermomagnetism.

A density-matrix formalism developed earlier for the evaluation of Ohmic magnetoconductivity is further elaborated and applied to other magnetotransport effects in nonpolar semiconductors in the presence of a magnetic field of arbitrary strength. The difference from earlier transport theories lies in a natural extension of the scattering dynamics beyond the strict Born approximation. The well-known divergence difficulties of older theories, usually removed by any of a number of *ad hoc* cutoff procedures, do not appear here. The transverse-conductivity expression turns out to be equivalent to that of some earlier theories of cyclotron resonance extrapolated to zero frequency, but derived in a different way. When applied to elastic scattering of electrons in a simple model of a semiconductor, the theory gives galvanomagnetic and thermomagnetic coefficients within the range of values usually seen experimentally, showing the basic correctness of the theory. It is then applied to the magnetophonon effect, where the resonance peaks are shown to be finite. An interesting inversion of one of the peaks in the Ettingshausen-Nernst coefficient is found. Landau-level broadening and phonon drag are not included in the present paper, although they can be incorporated when deemed important.

Ausloos, P., Lias, S. G., Eyler, J. R., **Reactions of halomethyl ions with carbonyl-containing compounds,** *Int. J. Mass Spectrom. Ion Phys.* **18,** No. 3, 261-271 (1975).

Key words: carbonyl compound; four-center reactions; halocarbon ions; ion cyclotron resonance; ion-molecule reaction; rate constants.

The mechanisms of the reactions of CF_3^+, CF_2Cl^+, CCl_2F^+, and CCl_3^+ with aldehydes, ketones, esters, acids, and acetic anhydride have been examined, and rate constant determinations have been made. Both four-center reactions and displacement reactions are observed. For aldehyde and ketone reactants, a four-center reaction resulting in the formation of a monohalogenated carbonium ion predominates; the importance of this reaction vis-a-vis more exothermic displacement processes is explained in terms of a preference for attack by the ion at the carbonyl oxygen atom. In the case of reactions of CX_3^+ (X = F, Cl) ions with esters or acids, the most commonly observed reactions are displacements and four-center reactions resulting from attack by the ion at the acyl oxygen. The displacements result in the formation of acylium ions, and the four-center reactions, in the formation of CX_2OR^+ ions (R = alkyl group). The competition between these two reactions is examined in terms of the relative exothermicities of the two channels and the time required for reaction to occur in the ion–molecule complex. The results indicate that, for ion–molecule reactant pairs which react through only one channel, the probability that an ion–molecule collision will lead to reaction is influenced by the exothermicity of reaction.

Ayres, T. R., Linsky, J. L., **Stellar model chromospheres. III. Arcturus (K2 III),** *Astrophys. J.* **200,** No. 3, 660-674 (Sept. 15, 1975).

Key words: Ca II emission; chromospheres, stellar; photospheres, stellar.

We construct models for the upper photosphere and chromosphere of Arcturus based on the H, K, and IR triplet lines of Ca II and the *h* and *k* lines of Mg II. The chromosphere model is derived from complete redistribution solutions for a five-level Ca II ion and a two-level Mg II ion. A photospheric model is derived from the Ca II wings using first the "traditional" complete redistribution limit and then the more realistic partial redistribution approximation. In particular, the temperature and mass column densities for the temperature minimum region and the chromosphere-transition region boundary are computed and the pressure P_0 in the transition region and corona estimated. We find $T_{min}/T_{eff} \approx 0.77$ for Arcturus, Procyon, and the Sun and a trend of increasing mass at the temperature minimum with

decreasing gravity. We find P_0 to be about 1 percent of the solar value, and on this basis estimate the surface brightness of the Arcturus transition region and coronal spectrum to be much less than for the Sun. Finally, the partial redistribution calculation for the Ca II K line indicates that the emission width is at least partially determined by damping rather than Doppler broadening, suggesting a reexamination of previous explanations for the Wilson-Bappu effect.

Ayres, T. R., Linsky, J. L., **Stellar model chromospheres. IV. The formation of the Hε feature in the sun (G2 V) and Arcturus (K2 III),** *Astrophys. J.* **201,** No. 1, 212-221 (Oct. 1, 1975).

Key words: chromospheres, stellar; Hε emission; photospheres, stellar.

The formation of the Balmer series member Hε in the near red wing of the Ca II H line is discussed for two cases: the Sun (Hε absorption profile) and Arcturus (Hε emission profile). It is shown that although the Hε source functions in both stars are dominated by the Balmer continuum radiation field through photoionizations, the line formation problems in the two stars are quantitatively different, owing to a substantial difference in the relative importance of the stellar chromosphere temperature inversion compared with the stellar photosphere.

Becker, D. A. **Accuracy and precision in activation analysis—counting,** (Proc. Second Int. Conf. on Nuclear Methods in Environmental Research, Univ. of Missouri, Columbia, Mo., July 29-31, 1974), Paper in *Nuclear Methods in Environmental Research*, J. R. Vogt and W. Meyer, Eds., CONF 740701, pp. 69-80 (Available from the National Technical Information Service, Springfield, Va., 1974).

Key words: accuracy; errors in activation analysis; precision; radiation detection.

Accuracy and precision in activation analysis was investigated with regard to counting of induced radioactivity. The various parameters discussed include configuration, positioning, density, homogeneity, intensity, radioisotopic purity, peak integration, and nuclear constants. Experimental results are presented for many of these parameters. The results obtained indicate that counting errors often contribute significantly to the inaccuracy and imprecision of analyses. The magnitude of these errors ranges from less than 1 percent to 10 percent or more in many cases.

Beers, Y., **A simplified discussion of energy storage associated with an electrostatic field,** *Am. J. Phys.* **43,** No. 8, 739-740 (Aug. 1975).

Key words: electrostatic; energy.

This note gives a simplified derivation for the energy associated with an electrostatic field by extended use of the expression for the energy of a parallel plate capacitor.

Behringer, K., Ott, W. R., **Measurement of the Ly-α Stark profile in a pure hydrogen arc,** *Proc. XIth Int. Conf. on Phenomena in Ionized Gases, Prague, Czechoslovakia, Sept.* 10-14, 1973, *Paper* 4.5.1.1, pp. 396 (Czechoslovak Academy of Sciences, Prague, Czechoslovakia, 1973).

Key words: high temperature; hydrogen arc; line broadening; Lyman alpha; optically thin; Stark profile.

The Stark profile of the hydrogen line Ly-α requires the least elaborate theoretical treatment of all hydrogen lines, reflected in the fact that all calculations reported so far show very similar results. Yet one of the two different type published experiments [1,2], even after reexamination [3], shows significant deviations from the theoretical profile. From the available data, it is not clear whether a physical effect went undetected in the experiments or whether the calculations should be revised. An investigation on the Ly-α profile under very different experimental conditions is reported here. While self-absorption in the previous experiments has been lowered by greatly diluting the hydrogen plasma with inert gases like Ar or He, in this investigation thin line wings are achieved in a pure plasma by operating at very high temperatures. Above 17,000 K the emission coefficient of Ly-α in a constant pressure, almost completely ionized plasma decreases rapidly with increasing temperature. The absorption coefficient does even more so because the blackbody radiation at the wavelength of Ly-α increases drastically. The properties of a pure hydrogen plasma are very well known and allow very accurate diagnostic measurements. The electron density at these high temperatures is close to 1.8×10^{17} cm^{-3} and almost independent of the temperature, certainly an advantage in a line broadening experiment. The high temperature arc plasma has been shown to be very close to local thermodynamic equilibrium [4].

Bender, P. L., **Laser measurements of the lunar distance,** *Rev. Geophys. Space Phys.* **13,** No. 3, 271-272, 291 (July 1975).

Key words: crustal movements; earth rotation; geophysics; lasers; lunar cartography; lunar gravity; moon; plate tectonics.

Progress since 1971 on laser measurements of the lunar distance is reported. The current status of analysis work based on lunar distance data is described. New lunar and geophysical results which have been obtained by the joint efforts of a number of different institutions are discussed briefly.

Berger, H., **An evaluation of radiographic paper for thermal-neutron radiography,** *Proc. American Nuclear Society Meeting, New Orleans, La., June* 8, 1975, pp. 148-149 (1975).

Key words: image quality; neutron converters; neutron radiography; neutron scintillator; thermal neutron detection; x-radiographic paper.

X-ray sensitive paper is evaluated for use as an image detector for thermal neutron radiography. With a gadolinium oxysulfide scintillator the paper requires an exposure of 6×10^7 n/cm^2 and yields a radiograph displaying 25 to 50 μm spatial resolution and 4 to 6 percent contrast. The paper is convenient (10 second processing) and inexpensive, and provides good quality images.

Berger, H., **Radiographic nondestructive testing,** *Stand. News* **3,** No. 3, 21-29 (Mar. 1975).

Key words: dimensional measurement; gamma radiography, image enhancement; neutron radiography; nondestructive testing; proton radiography; real-time techniques; three-dimensional radiography; x-radiography.

This article is a review of radiographic nondestructive testing for a planned nondestructive testing issue of Standardization News (ASTM). Several new ideas in radiographic methods are described following a brief review of conventional gamma and x-radiography. New ideas discussed include high definition radiography, xeroradiography, electron radiography, image enhancement, real-time systems, three-dimensional methods, neutron radiography, and proton radiography.

Berger, H., **Summary/Conference on Emerging Techniques for Nondestructive Field Testing,** *Mater. Eval.* **XXXIII,** No. 7, 189-191 (July 1975).

Key words: airport pavements; bridge inspection; neutron testing; pipeline inspection; railroad inspection; transportation; vehicle inspection.

The Conference on Emerging Techniques for Nondestructive Field Testing held August 13-14, 1974, at the Transportation Systems Center in Cambridge, Mass., was jointly organized by the American Society for Nondestructive Testing (ASNT) and the U.S. Department of Transportation (DOT). More than 100 persons attended to learn more about the conference theme, "Opportunities for NDT in Transportation."

A primary purpose of the meeting was to make the NDT community aware of some of the nondestructive testing objectives and problems of DOT, in the expectation that organizations or individuals who had solutions, or potential solutions to such problems would make them available. The meeting itself provided the initial opportunity for this interaction.

The meeting proceedings, as contained in this issue of *Materials Evaluation*, provide a larger audience for this interaction possibility. My suggestion—read the papers and offer ideas or comments for possible solutions to NDT problems to the authors, or to the Conference Chairman, Dr. Michael Lauriente, Office of the Secretary of Transportation, U.S. Department of Transportation, Washington, D.C. 20590. We hope many readers of *Materials Evaluation* will respond and make the conference theme a reality!

Berger, R. E., **Effect of contact lens motion on the oxygen tension distribution under the lens,** *Am. J. Optom. Physiol. Opt.* **51,** No. 7, 441-456 (July 1974).

Key words: contact lens; contact lens motion; diffusion; hydrodynamics; mathematical model; oxygen; oxygen tension; oxygen tension distribution.

A method of predicting the oxygen tension distribution under a contact lens is illustrated for some simple, but practical, lens motions. A hydrodynamic theory is used to find those regions which receive fresh tear fluid during a blink. Then a diffusion model is solved to find the oxygen tension distribution at all times between blinks. The results are compared with earlier models in which details of the fluid flow were neglected, as were variations of oxygen tension with position under the lens. Depending on the motion of the lens, the tear fluid exchange factor can be quite large without eliminating regions in which the oxygen tension is below critical levels. The results suggest that the situation can be improved if the lens is designed for large displacements, with the blink, in the direction parallel to the cornea.

Bernstein, L. S., Kim, J. J., Pitzer, K. S., Abramowitz, S., Levin, I. W., **Potential function for the ν_7 vibration of phosphorus pentafluoride,** *J. Chem. Phys.* **62,** No. 9, 3671-3675 (May 1, 1975).

Key words: high amplitude; internal rotation; PF_5; pseudorotation; Raman; vibration.

The gas phase Raman spectrum of the ν_7 fundamental of PF_5 has been observed under spectral resolutions approaching 1 cm^{-1}. With the use of a two dimensional harmonic oscillator basis set and a potential function of the form $V(\rho,\phi)=(1/2)a\rho^2 - b\cos(3\phi)\rho^3+c\rho^4$, an adequate fit to the ν_7 region was obtained. The barrier to axial-equatorial fluorine atom interchange was estimated to be 1371 cm^{-1} (3.92 kcal/mole).

Bishop, M., Dimarzio, E. A., **Models of diffusion in lyotropic liquid crystals,** *Mol. Cryst. Liq. Cryst.* **28,** 311-333 (1975).

Key words: asymmetric diffusion coefficients; diffusion in liquid crystals; lyotropic liquid crystal.

The asymmetric diffusion of small molecules in a liquid crystal host is examined via three models. The small molecules are represented by spheres and the liquid crystal host by aligned cylinders. DASH is a continuum model which allows one to use the results of electrical conductivity problems to calculate the diffusion coefficient. LASH is an extension of polymer lattice counting models. CASH is a molecular dynamics computer simulation which provides experimental data to check the analytical models. It is found that DASH is a better representation of the diffusion asymmetry than LASH for the low liquid crystal densities examined on the computer. The cylinder sphere pair correlation function is also calculated in CASH and this gives evidence for liquid order around the liquid crystals.

Blackburn, D. L., **An electrical technique for the measurement of the peak junction temperature of power transistors,** *Proc. 13th Annual Reliability Physics Conf., Las Vegas, Nev., Apr.* 1-3, 1975, pp. 142-150 (Electron Devices and Reliability Groups, IEEE, New York, N.Y., July 1975).

Key words: method of measurement, electrical; semiconductor devices; temperature, peak; thermal properties; transistors, power, safe-operating area.

A technique is described which uses straightforward electrical measurement procedures to determine the peak junction temperature of power transistors. To determine the peak temperature, standard electrical measurement techniques are altered to account for the difference between the distributions of the calibration and measurement currents in the active area of the device. For relatively uniform temperature distributions, the electrically determined peak junction temperature is only about 6 percent or less below the infrared measured peak temperature whereas the standard electrically measured temperature is about 10 to 25 percent below the infrared measured peak temperature. For severely nonuniform temperature distributions, when only about 20 percent of the total active area of the device is dissipating power at steady state, the electrically determined peak temperature is within 11 percent of the infrared measured peak temperature while the standard electrically measured temperature is more than 40 percent below the infrared measured peak temperature. Device operating conditions for which the junction temperature as determined by standard electrical methods, infrared techniques, and the electrical peak temperature technique equals the manufacturer's specified maximum safe operating temperature are compared with one another and with the manufacturer's specified safe operating limits. It is suggested that the electrical peak temperature technique can be used to generate more realistic safe operating area limits and to determine the validity of specified safe operating limits of power transistors. Devices used in this study include TO-66 and TO-3 encased devices, of both mesa and planar structure, with clip and wire leads, manufactured by a variety of techniques (epibase, single-diffused, and multiple-diffused).

Bowen, R. L., **Adhesive bonding of various materials to hard tooth tissues. IX. The concept of polyfunctional surface-active comonomers,** *J. Biomed. Mater. Res.* **9,** No. 5, 501-510 (Sept. 1975).

Key words: adhesion; bonding; composites; coupling agents; monomers; polymers; primers; sealants.

The concept of surface-active comonomers of higher functionality is proposed as a means of increasing reliability of the bonding between preventive and restorative dental materials and tooth structures.

Bowman, C. D., **A shelf in the "subthreshold" photofission cross section,** *Phys. Rev. C* **12,** No. 3, 856-862 (Sept. 1975).

Key words: photofission; cross section; fission barrier shape; fission isomer; bremsstrahlung beams.

The influence of a double-humped fission barrier on the photofission cross section far below the top of the barrier is considered. In the region about 2 MeV below the top of the outer barrier and at a cross section in the region of $10^{-9} - 10^{-6}$ b the photofission is expected to become almost entirely isomeric or delayed fission. When this occurs a "shelf" should appear in the photofission cross section where the cross section changes with energy far more slowly than at higher γ-ray energy. The cross section on the shelf can therefore be orders of magnitude higher than otherwise expected. While the angular distribution near the top of the barrier is expected to have a well-defined and nonisotropic angular dependence, the angular distribution on the shelf is expected to be isotropic. The cross sections, although small, appear to be measurable with bremsstrahlung beams in the 3- to 5-MeV range using a several hundred μA electron beam. Successful ex-

periments of this type should provide information on the shape of the inner and outer barriers at much lower excitation energies than possible by other techniques.

Bowman, C. D., Schröder, I. G., Dick, C. E., Jackson, H. E., **Very low energy photofission of ^{238}U,** *Phys. Rev. C* **12,** No. 3, 863-870 (Sept. 1975).

Key words: bremsstrahlung beam; cross section; fission barrier shapes; γ-ray strength; isomeric fission; level density; photofission.

The photofission cross section of ^{238}U was measured in the 2.75- to 5.75-MeV range. Cross sections as small as 2×10^{-11} b were detected. A shelf was observed which had been predicted to occur in the cross section owing to the dominance of radiative decay of levels in the second well. Barrier penetrabilities for both inner and outer barriers were determined from these measurements and together with penetrabilities from other measurements were used to infer a potential shape for ^{238}U. The total γ-ray strength function in the second well at 4.25 MeV was found to be 1.3×10^{-5}. From comparison of expected and measured cross sections at the lowest energies, the density of levels effective in photofission at 3 MeV was found to be greater than 4 per MeV.

Bowman, H. A., Schoonover, R. M., Carroll, C. L., **The utilization of solid objects as reference standards in density measurements,** *Metrologia* **10,** 117-121 (1974).

Key words: density; density calibration; density measurement; density standard; volume standard.

NBS has measured the densities of four single crystal silicon objects to a standard deviation of 0.26 ppm with a systematic error of 0.7 ppm. These objects will be used as working standards to which density work in the United States will be referred. A redundant hydrostatic comparison test involving two standards at a time has been devised, the use of which facilitates the efficient propagation of the density information contained in these crystals into other objects which may be used as standards by other laboratories. This article describes a method of employing this redundant comparison procedure.

Brauer, G. M., Termini, D. J., **Modification of collagenous surfaces by grafting polymeric side chains to collagen and soft and hard tissues,** Chapter 8 in *Advances in Chemistry Series*, No. 145, pp. 175-195 (American Chemical Society, New York, N.Y., 1975).

Key words: bone; collagen; grafting modification of collagenous surfaces; hard tissue; rat skin; soft tissue.

Collagen, soft tissue, and bone can be modified at 37 °C by allowing them to react with acrylic, methacrylic, or vinyl monomers using ceric ions, persulfate-bisulfite or comonomers forming donor-acceptor complexes as initiators. The polymeric methacrylate side chain is chemically attached to collagen; similar bonding may occur on reaction with other monomers. With rat skin, the reaction takes place mainly at the surface whereas a higher yield of more homogeneous product is formed on grafting onto collagen. Grafting onto bone is best accomplished with persulfate-bisulfite initiator. Modification of the collagenous surface is indicated by changes in wettability, decreased water sorption, and improved resistance to mold growth; e.g, hydrophobic, oleophobic surfaces are obtained with fluorinated monomers. The modified surfaces could be useful as adhesion-promoting liners for restorative materials.

Braun, W., Kurylo, M. J., Kaldor, A., **Infrared laser enhanced reactions: V→V and V→T energy transfer in the O_3-SiF_4-O_2 system,** *Chem. Phys. Lett.* **28,** No. 3, 440-444 (Oct. 1, 1974).

Key words: apparatus and methods; deactivation; energy transfer; infrared laser; luminescence; ozone.

Rapid V→V energy transfer between SiF_4 and O_3 has been observed following laser excitation of either O_3 or SiF_4. A CO_2 laser tuned to either the 9.6 μ P(30) or P(32) transitions was used to promote vibrational excitation in O_3 and SiF_4, respectively. In experiments employing the P(32) transition, the V→V transfer to O_3 and subsequent reaction of $O_3^\dagger$ with NO were used to obtain the rate constant of V→T deactivation of $SiF_4^\dagger$ by O_2.

$$SiF_4^\dagger + O_2 \xrightarrow{k_2} SiF_4 + O_2,$$

$$k_2 = (6.3 \pm 1.4)\times 10^{-13}\ \text{cm}^3\ \text{molecule}^{-1}\ \text{s}^{-1}.$$

Fractional modulation measurements of the chemiluminescence generated by the O_3 + NO reaction were used in experiments employing the P(30) transition to obtain a rate constant for the V→V energy transfer between $O_3^\dagger$ and SiF_4.

$$O_3^\dagger + SiF_4 \xrightarrow{k_{-3}} SiF_4^\dagger + O_3,$$

$$k_{-3} = (3.8 \pm 0.5)\times 10^{-11}\ \text{cm}^3\ \text{molecule}^{-1}\ \text{s}^{-1}.$$

Bridges, J. M., **Arc measurements of Fe II oscillator strengths,** *Proc. XIth Int. Conf. on Phenomena in Ionized Gases, Prague, Czechoslovakia, Sept.* 10-14, 1973, *Paper* 4.5.3.5, pp. 418 (Czechoslovak Academy of Sciences, Prague, Czechoslovakia, 1973).

Key words: arc plasma; iron; lifetimes; oscillator strength; transition probabilities; wall-stabilized arc.

Fe I and Fe II lines were measured in emission from a wall-stabilized arc, which was operated in argon with an admixture of $FeCl_3$. Lines were selected for measurement which would permit a check on the consistency of several previously reported data. These include oscillator strength measurements of Fe II lines as well as lifetime values for several atomic levels of Fe I and Fe II. Overall, good consistency was found among most of the data.

Bright, R. G., **Recent advances in residential smoke detection,** *Fire J.* **68,** No. 6, 69-77 (Nov. 1974).

Key words: detection; detectors; fire fatalities; gas detectors; ionization chamber detectors; performance standards; photoelectric detector.

The loss of life by fire in the home is a significant problem in the U.S. Had the homes been equipped with an early-warning, fire detection device between 40 and 50 percent of the people killed in these fires might have been saved. One early warning fire detection device which shows great promise is the single-station, smoke detector. This fact is being recognized by more and more code authorities in the U.S. As a consequence, an increasing number of the U.S. building codes are requiring the installation of single-station smoke detectors in all new housing.

There are problems, however, with several of the single-station, smoke detectors on the market. In addition, there is a lack of good published performance standards for these detectors, standards that would improve the quality of smoke detectors offered for sale in the marketplace and would eliminate many of the problems.

The National Bureau of Standards, in conjunction with the approvals testing laboratories and the detector manufacturers, is developing performance standards for the single-station, smoke detector. Development and publication of these standards will have a material effect on improving the quality of smoke detectors sold in the U.S.

Brown, C. P., Yeates, E. J., Van Hoesen, M. J., **Use and cost of on-line systems at the National Bureau of Standards Library,** *Proc. Am. Soc. Inf. Sci. Annual Meeting, Boston, Mass., Oct.* 26-30, 1975, **12,** 132-133 (Oct. 1975).

Key words: evaluation; National Bureau of Standards; on-line information retrieval systems; use statistics.

The National Bureau of Standards Library has had a year of ex-

perience in offering on-line information retrieval systems to users. Users were encouraged and assisted to access systems directly if they wished. Cost and use statistics for selected data bases are given.

Brown, D. W., Lowry, R. E., **Radiation-induced polymerization of tetrafluorethylene and 1,2,3,4,5-pentafluorostyrene at high pressure,** *J. Polym. Sci. Polym. Chem. Ed.* **13,** No. 7, 1677-1689 (July 1975).

Key words: copolymerization; pentafluorostyrene; polymerization; pressure radiation; reactivity ratios; tetrafluoroethylene.

Tetrafluoroethylene (A) and 1,2,3,4,5-pentafluorostyrene (B) were irradiated at 15 °C at autogenous pressure by use of 30-92 mole-percent A and at 5000 atm by use of 42-99.9 mole-percent A. The high-pressure results indicate that the reactivity ratio r_A for monomer addition to A-ended radicals is 0.005; the other reactivity ratio r_B appears to vary from 15 to 60 generally increasing with the A content of the charge. At autogenous pressure r_A is small, but a precise determination is not possible because of the very low polymerization rate when the A content of the charge is high. However, if r_A is less than 0.01, then values of r_B vary from 15 to 50, again generally increasing with the A content of the charge. Mixtures of A and B exhibit positive deviations from Raoult's Law. Activity coefficients were measured at autogeneous pressure and used in an attempt to correct r_B for the non-ideality of solution. The range of r_B was reduced only slightly to 8-27, and charges with high A contents now generally gave low values of r_B; consequently, this approach was not regarded as a success. Another attempt was made to account for the apparent variation in r_B by ascribing influence to the penultimate units of the radicals. Improved agreement between theoretical and observed compositions resulted, but significant discrepancies remained unexplained. Rate data agreed well with those calculated from a theoretical copolymer rate equation using values of r_A and r_B of 0.0045 and 40, respectively. The equation predicts an almost proportional decrease in rate with increasing proportions of A in the charge from 0 to 99 mole-percent A.

Buchbinder, L. B., **Human activity patterns and injury severity in fire incidents involving apparel,** *J. Fire Flammability Consumer Product Flammability* **1,** 4-18 (Mar. 1974).

Key words: accident patterns; apparel; apparel fires; burn injury; FFACTS; fire; flammable fabrics; flammable liquids; garment fires; garment parameters; injury severity; victim's activity; victim's reactions.

Activities preceding an apparel fire accident are identified and related to age, sex, and the severity of burn injury. After age six, activity patterns were strongly related to the victim's sex, with men the primary victims of accidents involving flammable liquids, gases, or high voltage electricity, and women more susceptible to direct flame ignition. The majority of cases studied had burns over less than 20 percent of the total area of their body. When flammable liquids were involved, there tended to be fewer minor injuries and more moderately serious injuries than in accidents not involving intermediary materials. Age and defensive capability were major factors determining extent of injury, with persons over 65 and those with limited ability suffering more serious injuries than other groups. Included are recommendations for remedial action.

Buchbinder, L. B., **Human behavioral patterns vs. injury severity for apparel fire victims,** *Proc. Seventh Annual Meeting, Information Council on Fabric Flammability, New York, N.Y., Dec.* 5, 1973, pp. 236-253 (Information Council on Fabric Flammability, New York, N.Y., July 1, 1974).

Key words: apparel; apparel fires; burn injury; defensive capability; FFACTS; fire; flammable fabrics; garment fires; garment parameters; injury severity; reaction patterns; victims.

This study is based on information from 1,126 fire accident cases in the NBS computerized data base, FFACTS. The defensive actions taken by persons involved in apparel fires are described and the effect of these reactions on the severity of the resultant burn injuries is discussed. In general, "running" was the most frequent first reaction with "beating flames with hands" and "trying to remove clothing" ranking second and third in frequency. However, the relative frequency of reactions varied with age, sex and type of accident. The effectiveness of various reactions was analyzed considering both the extent of injury incurred, measured by the percent total area of body burned, and the number of additional reactions required to extinguish the fire. The victim's defensive capability (i.e., his ability to recognize danger and take appropriate action) was also found to have an effect on the level of injury severity.

Buhl, D., Snyder, L. E., Lovas, F. J., Johnson, D. R., **Silicon monoxide: Detection of maser emission from the second vibrationally excited state,** *Astrophys. J.* **192,** L97-L100 (Sept. 1, 1974).

Key words: maser; M-type stars; molecular emission, Orion Nebulae; silicon monoxide; rotational transitions.

The $J = 1 - 0$ rotational transition of the second vibrational state ($v = 2$) of SiO has been detected in late M-type variable stars and in the center of the Orion Nebula. This transition of SiO requires 3520 K of excitation for pumping the observed maser line. The ground ($v = 0$), and third ($v = 3$) vibrational states were not detected.

Burley, N. A., Burns, G. W., Powell, R. L., **Nicrosil and Nisil: Their development and standardization,** (Proc. Symp. European Conf. on Temperature Measurement, Teddington, England, Apr. 9-11, 1975), Chapter 4 in *Temperature Measurement*, B. F. Billing and T. J. Quinn, Eds., Inst. Phys. Conf. Ser. No. 26, pp. 162-171 (1975).

Key words: calibration; nickel-base alloys; nickel-chromium alloys; nickel-silicon alloys; reference tables; temperature measurements; thermal emf; thermocouples; thermoelectric reference data; thermometry.

This paper reviews the development of the new nickel-base thermocouple alloys Nicrosil and Nisil by the Australian Defense Standards Laboratories (now the Materials Research Laboratories of the Australian Government Department of Defence), and their standardization by the U.S. National Bureau of Standards.

The relevant properties of the new alloys are described, and they are shown to have much higher environmental, structural and thermoelectrical stabilities, and to be more suitable for use at the higher operating temperatures, than existing Type K nickel-base thermocouple materials.

The standardization procedures are summarized, including the derivation of reference tables. Calibration data were obtained, over the range 5 K to 1575 K, from prototype alloys specially fabricated by five major manufacturers of base-metal thermocouple alloys in the UK, the USA and Sweden.

Burns, G. W., Hurst, W. S., **Thermocouple thermometry,** (Proc. Symp. European Conf. on Temperature Measurement, Teddington, England, Apr. 9-11, 1975), Chapter 4 in *Temperature Measurement*, B. F. Billing and T. J. Quinn, Eds., Inst. Phys. Conf. Ser. No. 26, pp. 144-161 (1975).

Key words: base-metal thermocouples; cryogenic thermocouples; noble-metal thermocouples; nonstandardized thermocouples; refractory metal thermocouples; standardization; temperature measurement; thermocouples; thermometry.

A broad overall view of the current status of thermocouple thermometry is given. The salient features and limitations of standard thermocouple types are reviewed, and some of the recent changes in standardization are noted. Some of the nonstandardized thermocouple types are discussed, giving particular attention to those employed at cryogenic temperatures and to those intended for use above the

temperature limits or under conditions where the standard types are inadequate. Commonly used materials for insulation and protection are described, and some examples are noted of applications where stringent requirements are placed on thermocouple performance.

Cali, J. P., **Meaningful measurement in clinical chemistry,** *Proc. San Diego Biomedical Symp., San Diego, Calif., Feb.* 6-8, 1974, **13,** 499-505 (1974).

Key words: accuracy; clinical chemistry; measurement; reference methods; standard reference materials.

Compatibility of measurement in clinical chemistry is of utmost importance if results are to be comparable between laboratories and across time and distance. It is shown that compatibility may most easily be brought about on a measurement system based on accuracy. Five components are required to bring about meaningful measurement in clinical chemistry: (1) A rational, self-consistent system of units of measurement; (2) The materials to realize in practice the defined units and their derivatives; (3) The availability of accurate methods of measurement, analysis, or test based on the well-characterized materials (SRM) of 2; (4) The transfer method; (5) The assurance of the long-term integrity of the measurement process.

The National Bureau of Standards (NBS) is now providing a comprehensive supply of SRM's for the clinical chemistry laboratory. In addition, it is cooperating with professional societies and other government agencies to help develop reference methods.

Cali, J. P., Stanley, C. L., **Measurement compatibility and Standard Reference Materials,** Chapter in *Annual Review of Materials Science* **5,** 329-343 (Annual Reviews Inc., Palo Alto, Calif., 1975).

Key words: measurement; measurement compatibility; reference methods; Standard Reference Materials.

The role of Standard Reference Materials (SRM's) in helping to provide measurement compatibility is explored. Measurement compatibility is simply the ability of elements within a measurement infrastructure to achieve the same measurement values. It is shown that measurement compatibility results when measurements are made on the basis of accuracy. SRM's are well-characterized materials whose properties are certified on the basis of accuracy. Therefore, laboratories within a measurement infrastructure become compatible when SRM's are used.

Sections cover these topics: (a) sources of information concerning the current availability and types of SRM's produced; (b) two examples of the impact of SRM's are given; and, (c) a discussion of future directions and needs is expounded.

Cali, J. P., **Tying methodology to standards,** *Lab World* **25,** No. 7, 22-24 (July 1974).

Key words: clinical chemistry; standard reference materials.

This is an interview of Mr. Cali by one of the editors of *Lab World* concerning the status of our NBS Clinical Standard Reference Materials Program. Topics discussed were the financing of the program, the technical output of the program, the goals of the program, the problems of accuracy in clinical chemistry, and how reference methods and SRM's are used to bring and to improve the accuracy in this field. Future possibilities and directions are also discussed as well as interactions between NBS and other government agencies and professional societies.

Carpenter, B. S., Gilliam, D. M., Reimer, G. M., **Induced fission tracks in glass from monoenergetic and thermal neutrons,** *ANS Trans.* **18,** 90 (1974).

Carpenter, B. S., Reimer, G. M., **Fission track technique for uranium determination in coal and fly ash standard reference materials,** (Proc. Second Int. Conf. on Nuclear Methods in Environmental Research, Univ. of Missouri, Columbia, Mo., July 29-31, 1974), Paper in *Nuclear Methods in Environmental Research,* J. R. Vogt and W. Meyer, Eds., CONF 740701, pp. 141-143 (Available from the National Technical Information Service, Springfield, Va., 1974).

Key words: coal; fission track technique; fly ash; mica detector; polycarbonate detector; rapid analysis; uranium.

The analysis of coal and combustion waste products for uranium will become increasingly important with the greater use of coal for supplying energy needs. A fission track technique, as demonstrated with NBS Standard Reference Material Trace Elements in Coal (SRM 1632) and Trace Elements in Fly Ash (SRM 1633), provides a rapid and inexpensive method for U analysis.

Carpenter, B. S., Samuel, D., Wassermann, I., **The location of lithium in the brain,** *ANS Trans.* **18,** 85-86 (1974).

Casella, R. C., **Algorithm for computing the number of independent real parameters in the phonon dynamical matrix,** *Phys. Rev. B* **11,** No. 12, 4795-4800 (June 15, 1975).

Key words: counting independent parameters; phonon dynamical matrix; time reversal symmetry.

The effects of time-reversal symmetry in reducing the maximum number $\mathfrak{N}$ of real parameters in the phonon dynamical matrix at fixed $\vec{k}$ are taken into account to yield the following result: either (I) $-\vec{k}$ is *not* in the star of $\vec{k}$ in which case $\mathfrak{N}^{I}=\Sigma_r n_r^2$, or (II) it *is*, in which case $\mathfrak{N}^{II}=\Sigma_{r\epsilon(a)}n_r(n_r+1)/2 \quad +\Sigma_{r\epsilon(b)}n_r^2/2+\Sigma_{r\epsilon(c)}n_r(n_r-1)/2$. Here, n_r denotes the number of times the rth irreducible representation of the little group G^k occurs in the reducible representation $\Delta^{\vec{R}}$ at wave vector $\vec{k}$. $\Delta^{\vec{R}}$ is of dimension $3n$, where n is the number of atoms per unit cell. In the expression for $\mathfrak{N}^{II}$, one sums over all r in cases (a), (b) and (c), respectively, where (a), (b), and (c) refer to the three cases of Wigner in the Herring criterion. The analysis is also applied to compute a lower upper bound $\mathfrak{N}'$ within the rigid-molecule model as discussed group theoretically in the context of inelastic-neutron-scattering experiments by Casella and Trevino.

Casella, R. C., Robertson, B., **Direct tests for violation of *CP* invariance,** *Phys. Rev. D* **8,** No. 3, 968-970 (Aug. 1, 1973).

Key words: *CP*-violation; decays; direct tests; kaon; lepton-asymmetry; momentum-dependence; Weisskopf-Wigner.

Two tests are proposed for directly establishing violation of *CP* invariance in neutral-kaon decay. Provided that there exist only two neutral kaons, these tests rely only on the principles of quantum theory and relativistic kinematics and, in particular, are independent of the Weisskopf-Wigner approximation made in the theory of Lee, Oehme, and Yang. One of these tests can be made using data that will soon be available and the other can be made with existing techniques.

Caswell, R. S., Coyne, J. J., Randolph, M. L., **Studies of energy deposition by neutrons,** (Proc. 2d Symp. on Neutron Dosimetry in Biology and Medicine, Neuherberg/Munich, Germany, Sept. 30-Oct. 4, 1974), Paper in *Proc. 2d Symp. on Neutron Dosimetry in Biology and Medicine,* B. G. Berger and H. G. Ebert, Eds., 1, 29-47 EUR 5273 d-e-f (Mar. 1975).

Key words: fluence; kerma; kerma factors; microdosimetry; neutron dosimetry; neutron energy deposition.

Neutrons generate secondary particles (p, α, C, N, O, etc.) when they interact with tissue. It is through these secondary particles that nearly all of the energy deposition and biological effects occur. It is therefore of interest to determine the total energy transferred to the charged particles (kerma), the initial spectrum of the secondary particles, the slowing-down spectrum, and the details of the energy deposition by these secondary charged particles. We are continuing to study all of these quantities. Further along in the energy deposition

597-633 O - 76 - 7

process, one is interested in the delta-ray production cross sections and absorbed dose distributions due to the delta rays. We have not yet focused on this problem. In this report we shall discuss kerma calculations and some studies of the energy deposition in spherical volumes.

Chang, C. C., Dodge, W. R., Murphy, J. J. II, **^{3}He(γ,d)^{1}H cross section from 10 to 21 MeV,** *Phys. Rev. C* **9,** No. 4, 1300-1308 (Apr. 1974).

Key words: cross section structure; excitation energy distribution function; ^{3}He electrodisintegration; ^{3}He excited states; ^{3}He photodisintegration.

A measurement of the ^{3}He(*e*,*d*)^{1}H 90° differential cross section between 10 and 21 MeV was made. The ^{3}He(*e*,*d*)^{1}H cross section was converted into a ^{3}He(γ,*d*)^{1}H cross section. The shape of the ^{3}He(γ,*d*)^{1}H cross section agrees with recent theoretical calculations. We find no evidence for the anomalies (structure) in the ^{3}He(γ,*d*)^{1}H 90° differential cross section at excitation energies of 14.5 and 19.5 MeV reported in two recent experiments.

Chew, W. M., Xenoulis, A. C., Fink, R. W., Schima, F. J., Mann, W. B., **The L/K electron capture ratio in first-forbidden ^{81g}Kr decay,** *Nucl. Phys.* **A229,** 79-92 (1974).

Key words: deduced Q_{EC}, log *ft*, *J* π; enriched ^{80}Kr target; isotope separated sources; measured L/K EC ratio; multiwire proportional counter; radioactivity ^{81g}Kr [from (n,γ)].

The L/K electron capture (EC) ratio of ^{81g}Kr was measured to be 0.146 ± 0.005 utilizing the wall-less, anticoincidence, multiwire proportional counter technique and a reactor-produced, mass separated ^{81g}Kr source. From this value, the Q_{EC} and log *ft* values were determined to be 305_{-29}^{+38} keV and 11.6 respectively, assuming EC decay only to the ground state. If there is 4 percent EC branching to a reported 276 keV level, Q_{EC} becomes 322_{-14}^{+31} keV from which $(L/K)_{g.s.} = 0.144 \pm 0.005$, log $ft = 11.6$ for EC to the ground state, $(L/K)_{276} = 0.213 \pm 0.005$, and log $ft = 11.4$ for 4 percent feeding to the 276 keV level. In order to be confident of these results, an extensive systematic comparison of experimental and theoretical L/K ratios was made for both first-forbidden non-unique and unique transitions. From this comparison, a $7/2^+$ ground state assignment for ^{81}Kr is confirmed.

Choi, C. S., Abel, J. E., Dickens, B., Stewart, J. M., **The crystal structure of 1,3,5,7-tetraceto-1,3,5,7-tetrazacyclo-octane,** *Acta Crystallogr.* **B29,** Part 4, 651-656 (Apr. 1973).

Key words: crystal structure; organic crystal; x-ray diffraction.

The crystal of 1,3,5,7-tetraceto-1,3,5,7-tetrazacyclo-octane, $C_{12}N_4O_4H_{20}$, is tetragonal, $a = b = 10.540(2)$ and $c = 12.137(3)$ Å, with 4 molecules per unit cell. Systematic absences are consistent with space group $P4_12_12$ (enantiomorphous to $P4_32_12$). The structure was solved by direct methods and refined to a final *R* index $R_w = 0.037$ and $R = 0.039$ for 1244 observed reflections. The molecule consists of alternate CH_2 and $N-CO-CH_3$ groups in a puckered C–N ring, having a boat shape conformation with a twofold rotation axis through the center of the C–N ring and perpendicular to the mean plane of the puckered ring. The heavy atoms of each acetyl group are essentially coplanar with its neighbouring nitrogen atom. The molecular thermal motion may be represented chiefly by three motions: a libration about the twofold rotation axis and two intramolecular bending motions about the C–C diagonal of the C–N ring.

Choi, C. S., Prask, H. J., Prince, E., **Crystal structure of NH_4ClO_4 at 298, 78, and 10 K by neutron diffraction,** *J. Chem. Phys.* **61,** No. 9, 3523-3529 (Nov. 1, 1974).

Key words: crystal structure; low temperature; meta-stable compound; neutron diffraction; NH_4ClO_4; thermal motion.

The crystal structure of ammonium perchlorate has been studied at 298, 78, and 10 K by means of neutron diffraction. The NH_4ClO_4 crystal has an orthorhombic unit cell, space group *Pnma*, with four formula units per cell at all three temperatures. The unit cell dimensions at 298 K are $a = 9.20$, $b = 5.82$, $c = 7.45$ Å, as determined previously; at 78 K, $a = 9.02$, $b = 5.85$, $c = 7.39$ Å; and $a = 8.94$, $b = 5.89$, $c = 7.30$ for 10 K. Initial positions of H atoms were determined from a difference Fourier map of the room temperature data. However, a least-square refinement of these data did not converge. The thermal motions and orientations of the ammonium groups at low temperature (10 and 78 K) were determined by means of a constrained refinement which treated the ammonium group as a rigid body; these results are compared with the results obtained by the conventional least-squares method. Both refinements show that the librational motions about one of the three principal axes have particularly large rms amplitudes: 21° for the 10 K structure and 30° for the 78 K structure. Each ammonium group is surrounded by 10 oxygen atoms with short N... O distances ranging from 2.9 to 3.25 Å. The ClO_4^- group and NH_4^+ group each have essentially ideal tetrahedral structure. They are linked together by N-H... O type hydrogen bonds, one for each hydrogen, to form a three-dimensional network. Examination of the rms amplitudes for libration and the hydrogen bonding of the NH_4^+ ions indicates that two of the four hydrogens are bound identically, one hydrogen is bound more rigidly, and the fourth more weakly. These results suggest that the rotational motions of the ammoniums are quite complex even at 10 K.

Chuong, R., **Experimental study of surface and lattice effects on the solubility of hydroxyapatite,** *J. Dent. Res.* **52,** Supplement to No. 5, 911-914 (Sept.-Oct. 1973).

Key words: hydroxyapatite; nonstoichiometry; solid-to-solution ratio; solubility; surface chemistry.

Brown et al. have formulated a thermodynamic treatment for the solubility of hydroxyapatite in which recognition of a distinction between surface and lattice contributions is explicitly made. Verification of the applicability of this approach to the $Ca(OH)_2$-H_3PO_4-H_2O system has been carried out by Avnimelech et al. The purpose of the present study is to apply the theory of Brown et al. to the quaternary system $Ca(OH)_2$-H_3PO_4-H_2O-HCl. Three solution series, each involving a given HCl concentration, were prepared with solid-to-solution ratios of 0.2, 0.4, 0.5, 0.8, 1.0, and 2.0 g/100 ml. Solutions were agitated for 5 days at 25 °C, after which they were filtered. pH, Ca and P were determined and ion activity products and electroneutrality unbalances were calculated. The findings indicate that the Ca/P ratios in the final solutions varied with both the solid-to-solution ratio and the initial HCl concentration. However, the ion activity products for hydroxyapatite were essentially constant. These results indicate that the contribution of the surface to the overall dissolution reaction relative to that of the lattice must be taken into account, but in conformity with theory standard solubility product principles are applicable to the final equilibrium reaction.

Clark, A. F., Moulder, J. C., Runyan, C. C., **Combustion of bulk titanium in oxygen,** (Proc. 15th Int. Symp. on Combustion, Tokyo, Japan, Aug. 25-31, 1974), Paper in *Fifteenth Symposium (International) on Combustion*, pp. 489-499 (The Combustion Institute, Pittsburgh, Pa., 1974).

Key words: combustion; Hilbert transform; laser ignition; oxygen; titanium.

The combustion of bulk titanium in one atmosphere oxygen is studied using laser ignition and several analytical techniques. These were high-speed color cinematography, time and space resolved spectra in the visible region, metallography (including SEM) of specimens quenched in argon gas, x-ray and chemical product analyses, and a new optical technique, the Hilbert transform method. The cinematographic application of this technique for visualizing phase objects in the combustion zone is described. The results in-

dicate an initial vapor phase reaction immediately adjacent to the molten surface but as the oxygen uptake progresses the evaporation approaches the point of congruency and a much reduced evaporation rate. This and the accumulation of the various soluble oxides soon drive the reaction zone below the surface where gas formation causes boiling and ejection of particles. The buildup of rutile cuts off the oxygen supply and the reaction ceases.

Collard, J. J., **U.S. law enforcement receives scientific support,** *Int. Crim. Police Rev. No.* 262, 261 (Nov. 1972).

Key words: building systems; communications equipment; concealed objects detectors; emergency equipment; Law Enforcement Standards Laboratory; procurement guidelines; protective equipment; security systems vehicles; voluntary standards; weapons.

In January 1971, at the request of the U.S. Department of Justice, the National Bureau of Standards established a new organization, the "Law Enforcement Standards Laboratory." This Laboratory, which is presently funded entirely by the National Institute of Law Enforcement and Criminal Justice, the research arm of the Law Enforcement Assistance Administration, has been given the task of developing voluntary performance standards, specifications, and guidelines for equipment used by U.S. law enforcement and criminal justice agencies. The objective of this program is to assist Federal, state and local law enforcement organizations in the selection and procurement of equipment used by these agencies. In addition to standards development, the Laboratory is developing the methods for measuring the actual performance levels of the equipment.

Compton, P. R., **National Measurement System study,** *Natl. Conf. Stand. Lab. (NCSL) Newsletter* **13,** No. 3, 10-14 (Nov. 1973).

Key words: flow measurement study; fluid flow measurement system; measurement system identity; technology assessment.

A technological assessment of gas and liquid flow measurements, excluding cryogenics, is being conducted. A description is being prepared of the interrelationships that exist within and between the identifiable parts of the fluid flow measurement system which is identified as an important component of the overall National Measurement System. The approach of this study is to gather pertinent information from contacts throughout the system. The technology assessment has identified many attributes that can be used to quantify this system. A data base is being developed which will be helpful in recognizing major trends of future applications of fluid flow measurement.

Copley, J. R. D., Rowe, J. M., **Short-wavelength collective excitations in liquid rubidium observed by coherent neutron scattering,** *Phys. Rev. Lett.* **32,** No. 2, 49-52 (Jan. 14, 1974).

Key words: collective excitations; liquid rubidium; neutron scattering; propagating modes; scattering function; short wavelength.

The short-wavelength collective excitations in liquid rubidium at 320 K have been studied by coherent neutron scattering. For values of $\kappa = 2\pi/\lambda$ up to 1.0 $Å^{-1}$, clear evidence of propagating modes was found from the shape of the scattering function $S(\kappa, \omega)$ at constant values of κ. This result shows that the existence of such modes does not depend upon either quantum effects or low thermal population of the modes.

Cosby, P. C., Bennett, R. A., Peterson, J. R., Moseley, J. T., **Photodissociation and photodetachment of molecular negative ions. II. Ions formed in oxygen,** *J. Chem. Phys.* **63,** No. 4, 1612-1620 (Aug. 15, 1975).

Key words: cross section; drift tube; experimental; molecule; negative ion; O_2^-; O_3^-; O_4^-; photodetachment; photodissociation.

Total photodestruction cross sections for O_2^-, O_3^-, and O_4^- ions have been measured over a photon energy range of 1.93-2.71 eV using a drift tube mass spectrometer coupled with an argon ion laser and a tunable dye laser. The O_2^- ion is found to photodetach at these photon energies with a cross section which varies from 1.2 to 2.2×10^{-18} cm^2. The O_3^- ion photodissociates to form O^- over this energy range with a cross section which varies from 0.1 to 7.3×10^{-18} cm^2 and exhibits structure indicative of the vibrational levels of a predissociating excited state. Structure is also observed in the O_4^- photodestruction cross section which varies from 1.0 to 2.2×10^{-18} cm^2, and in the O_2^- photodetachment cross section.

Cotton, I. W., **Computer networks: Capabilities and limitations,** (Proc. Int. Symp. on Structural Mechanics Software, Univ. of Maryland, College Park, Md., June 12-14, 1974), Paper in *Structural Mechanics Computer Programs*, W. Pilkey, K. Sczalski, H. Schaeffer, Eds., pp. 1043-1055 (University Press of Virginia, Charlottesville, Va., 1974).

Key words: computer networks; networks.

This paper is intended to provide an introduction to the capabilities and limitations involved with the use of today's computer networks. While the treatment is at times brisk, this is intentional, in order to emphasize the applicability of networks for a wide range of applications – and the equally wide range of problems.

Cotton, I. W., **Network management survey,** *Proc. Hawaii Int. Conf. on Systems Sciences, Univ. of Hawaii, Honolulu, Hawaii, Jan.* 8-10, 1974, 4 pages (1974).

Key words: computer network; management; network.

This report presents a condensation of the results of a study of management practices in different computer networks. Five networks were chosen as typical of different approaches to network implementation and management: Advanced Research Projects Agency (ARPA) Network, MERIT Network, Triangle Universities Computation Center (TUCC), Oregon State Regional Network, and Tymnet, a commercial network. A common format is employed to survey each network.

Cotton, I. W., **Some trade-offs in the design of minicomputer-based graphic systems,** *Proc. Compcon 74, Washington, D.C., Sept.* 1974, pp. 47-52 (1974).

Key words: computer graphics; cost-benefit analysis; economic analysis; graphics; minicomputers.

This report surveys the evolution of satellite graphics systems from closely coupled display channels to free-standing, minicomputer-based systems. Particular attention is paid to the assignment of functions to the host and satellite systems. Some intuitive types of analysis in support of this assignment are presented, followed by the description of an economic analysis which may be universally applied.

Cox, J. E., Bostock, J., Waterstrat, R. M., **Superconducting properties of A15 phase V-Ir alloys,** (Proc. 13th Int. Conf. on Low Temperature Physics-LT 13, Boulder, Colo., Aug. 21-25, 1972), Paper in *Low Temperature Physics-LT* 13, K. D. Timmerhaus, W. J. O'Sullivan, and E. F. Hammel, Eds., **3,** 480-484 (Plenum Publishing Corp., New York, N.Y., 1974).

Key words: A15 phases; iridium alloys; superconductivity; vanadium alloys.

Superconducting transition temperatures, T_0, and initial slopes of the critical magnetic field curves have been determined for A15 phase V-Ir alloys. Samples investigated range from $V_{61}Ir_{39}$ to $V_{75}Ir_{25}$ in 2 at.% steps. T_0 increases with increasing Ir content, from < 15 mK for $V_{75}Ir_{25}$ to 1.85K for $V_{61}Ir_{39}$. Low temperature ordering anneals

do not markedly affect the superconducting properties of these alloys. Metallurgical aspects of these materials are discussed.

Cox, J. E., Waterstrat, R. M., **Anticorrelation of atomic ordering with superconductivity in vanadium-based transition metal A15 alloys,** *Phys. Lett.* **46A,** No. 1, 21-22 (Nov. 19, 1973).

Key words: annealing temperature; atoms; stoichiometry; superconducting; transition temperature.

Measurements of the superconducting transition temperature (T_o) of V-Rh A15 alloys reveal that long range order induced by low temperature annealing may cause T_o to decrease rather than increase. The behavior of T_o with ordering is discussed for the systems V-Au, V-Pt, V-Ir, V-Os and V-Rh.

Coxon, B., **Preliminary communication: Nitrogen-15 n.m.r. spectroscopy of amino sugars,** *Carbohydr. Res.* **35,** C1-C3 (1974).

Key words: amino sugars; chemical shifts; magnitude spectra; nitrogen-15 nuclear magnetic resonance spectroscopy; nuclear Overhauser effects.

Derivatives of 6-amino-6-deoxy-D-galactose-6-^{15}N and -D-glucose-6^{15}N and the corresponding unlabeled compounds have been synthesized via reactions of appropriate 6-*O*-tolyl-*p*-sulfonyl or 6-deoxy-6-iodo derivatives with potassium phthalimide-^{15}N (or ^{14}N), followed by hydrazinolysis of the phthaloyl group. ^{15}N n.m.r. spectra of the amino sugar derivatives have been measured directly at 9 MHz by pulse-Fourier transform techniques. The recording of spectra of ^{15}N in natural abundance in the amino sugar derivatives was aided by proton irradiation which caused a substantial negative, nuclear Overhauser effect (NOE), even for derivatives in which the ^{15}N nucleus is not directly bonded to a proton. For example, irradiation of the protons of 6-deoxy-1,2:3,4-di-*O*-isopropylidene-6-phthalimido-α-D-galactopyranose (**1**) -6-^{15}N at 90 MHz inverted the ^{15}N signal and enhanced its intensity by a factor of 3.4, which indicates a NOE of −4.4. One half gram of this derivative (^{15}N enrichment, 99%) yielded a ^{15}N spectrum with a signal:noise ratio of 36:1 when excited by a single pulse. With ^{15}N at natural abundance in 0.75 g of **1**, 8,192 pulses (112 min) were required to give a ^{15}N signal:noise ratio of 13:1. The negative NOE on the ^{15}N signal of **1**-6-^{15}N was removed (with reinversion of the signal, but no shift) by addition of the relaxation reagent, chromium (III) acetylacetonate to a concentration of 0.02M.

Coxon, B., Tipson, R. S., Alexander, M., Deferrari, J. O., **Conformational analysis of acylated 1,1-bis(acylamido)-1-deoxypentitols by Fourier-transform, p.m.r. spectroscopy,** *Carbohydr. Res.* **35,** 15-31 (1974).

Key words: acylated 1,1-bis(acylamido)-1-deoxypentitols; conformational analysis; conformational nomenclature; exponential filtering; Fourier transform; p.m.r. spectroscopy.

The conformations of eight acylated 1,1-bis(acylamido)-1-deoxypentitols in solution have been studied by pulse, Fourier-transform, p.m.r. spectroscopy at 90 MHz. The *arabino* and *lyxo* derivatives adopt the zigzag conformation, whereas the *ribo* and *xylo* derivatives favor different sickle conformations. The validity of the conformational assignments of these derivatives by the p.m.r. method is discussed. The relative merits and accuracy of the continuous-wave and pulse-Fourier p.m.r. spectroscopic methods in the conformational analysis of carbohydrates are appraised, and the applicability of the exponential filtering technique to enhancement of either the sensitivity or the resolution of their spectra is demonstrated.

Cunitz, R. J., Galloway, W. D., Berman, C. M., **Behavioral suppression by 383-MHz radiation,** *IEEE Trans. Microwave Theory Tech.* **MTT-23,** No. 3, 313-316 (Mar. 1975).

Key words: behavior; behavioral suppression; exposure; microwave radiation; microwaves; product safety; radiation; radiation effects; resonant cavity; rhesus; suppression.

The heads of two rhesus monkeys were irradiated in a 383-MHz resonant cavity immediately before and during performance of a four-choice forced-choice serial reaction task. CW radiation at integral dose rates of 0.001-17.5 W were delivered to the head. No effects were observed below a critical dose level (≃ 23 W/kg) derived from integral dose rate and body mass. Above this level, behavioral suppression occurred, i.e., correct response rate was profoundly altered. The effect was completely reversible and repeatable in one of the subjects—the other subject did not recover completely and was sacrificed for histological examination which revealed no gross or microscopic damage. The nature of the effect suggests a neurochemical rather than an electrical or mechanical basis for the results.

Davis, G. T., Eby, R. K., **Low-temperature x-ray attachment,** *Rev. Sci. Instrum.* **46,** No. 9, 1285-1286 (Sept. 1975).

Key words: attachment, low-temperature; radiation shield; temperature gradient; x-ray.

A commercial high-temperature, high-vacuum diffractometer attachment, which was originally designed for heating samples from ambient temperatures to 2600 K using metal ribbon heaters, has been modified for low-temperature use. This has been accomplished simply by the construction of a new sample holder and a change of the port used for evacuation. With these modifications, controlled temperatures down to 100 K can be achieved easily.

Davis, R., **Impermanent balance between man and computer,** *Science* **186,** 99 (Oct. 11, 1974).

Key words: artifacts; balance; computer; impermanence; intelligence; power; science; technology.

This requested editorial discussed the relative but changing balance between man and computer in the accomplishment of so-called intellectual tasks. It highlights the impermanence of the balance and emphasizes the need for people to better understand their need to define the man-computer interrelationship.

Davis, R. M., **National Bureau of Standards: Its role in computer security,** *Proc. IBM Data Security Symp., Cambridge, Mass., Apr.* 10-11, 1973, Paper G-520-2838, 11 pages (1973).

Key words: Brooks Bill; computer security; congressional concern; controlled accessibility; data sensitivity; measures of risk; standards; user identification.

Problems of computer security are a major impediment to effective computer utilization today. These problems have technological, legal, moral and ethical aspects. The National Bureau of Standards is concentrating its efforts on the technological aspects of computer security. This NBS project is entitled "Controlled Accessibility to Computer Systems." There is considerable national concern over computer security expressed by Congress, Federal, state and local governments, private groups and citizen committees. The NBS efforts are aimed at meeting these concerns through the development and issuance of guidelines, quantitative measures of risk and effectiveness and standards. These mechanisms for resolving the problem are intended principally for government use although they should be of nearly equivalent utility in the private sector.

Davis, R. M., **Quality software can change the computer industry,** (Proc. Symp. on Computer Program Test Methods, Chapel Hill, N.C., June 21-23, 1972), Paper in *Program Test Methods*, W. C. Hetzel, Ed., pp. 303-311 (Prentice-Hall, Inc., Englewood Cliffs, N.J., 1973).

Key words: buyer; computer software; marketplace; performance measurement; quality; seller; specifications; validation.

There is probably no more elusive commodity bought and sold today than computer software. We have the almost ludicrous situation of a marketplace where the buyer does not know how to describe

his product. The soft market practices now existing in software transactions can be displaced by imposing quality control procedures during software production, by demanding specifications or documentation at the time of software transaction and by utilizing validation services and performance measurement services to support the buyer of software.

Davis, R. M., **Technology as a deterrent to dehumanization,** *Science* **185,** 737 (Aug. 30, 1974).

Key words: dehumanization; deterrent; technologies.

This requested editorial discusses the role of technology as one of the better deterrents to dehumanization. It cites the confusion surrounding the use of the newer technologies of computers, automation and communication in terms of their benefits or disadvantages to the public. It highlights the need for better scientific advice in these areas to senior policy makers.

DeGraaf, L. A., Rush, J. J., Livingston, R. C., **Neutron scattering study of the rotational motions and phase transitions in sodium- and caesium-hydrosulfides,** (Proc. IAEA 5th Symp. on Neutron Inelastic Scattering, Grenoble, France, March 1972), Paper IAEA-SM-155/B-6 in *Neutron Inelastic Scattering*, pp. 247-258 (International Atomic Energy Agency, Vienna, Austria, 1972).

Key words: hydrosulfides; libration; neutron scattering; phase transition; quasi-elastic scattering.

The atomic motions in sodium- and caesium-hydrosulfide have been studied with inelastic neutron scattering using a hybrid time-of-flight spectrometer at the NBS reactor. The incident neutron wavelength was 2.43 Å, the time-of-flight resolution 3.7 percent, and the momentum transfer range for elastic scattering covered in this experiment was 0.4-3.5 $Å^{-1}$. NaSH and CsSH are members of a broad group of compounds $M^+(XY)^-$ which have cubic symmetry in the crystalline phase just below the melting point, and a lower symmetry at temperatures below a crystal phase transition point. The measured inelastic neutron scattering spectra above and below the phase transition showed that librational motions about equilibrium orientations persist in passing through the transition. A temperature- and momentum-transfer(Q)-dependent broadening of the quasi-elastic scattering peaks, however, indicates a rapid reorientation of the SH^- ions in the high-temperature cubic phases. The experimentally obtained quasi-elastic scattering peaks have been compared with predictions for the shape of the quasi-elastic scattering as derived from different models, in which the SH^- ions were assumed to reorient with rapid jumps between a limited number of quasi-equilibrium orientations. Plots of the experimental full width at half maximum of the quasi-elastic peaks versus Q show oscillations as predicted by the theoretical calculations. The differences in the rotational disorder in the two compounds studied are discussed and relaxation times τ and activation energies for the SH^- motions are given. The τ values derived for fcc NaSH vary from 0.4 to 0.2 ps between T = 103 °C and T = 212 °C, while the values for bcc CsSH vary from 2 ps (T = 23 °C) to 0.90 ps (T = 140 °C).

Deslattes, R. D., Henins, A., Bowman, H. A., Schoonover, R. M., Carroll, C. L., Barnes, I. L., Machlan, L. A., Moore, L. J., Shields, W. R., **Determination of the Avogadro constant,** *Phys. Rev. Lett.* **33,** No. 8, 463-466 (Aug. 19, 1974).

Key words: Avogadro number; crystal repeat distance; density; isotopic abundance; silicon.

Measurements are reported on the densities and isotopic-abundance ratios of nearly perfect Si single crystals. These, when combined with optical interferometry of the crystal repeat distance, yield a new value for the Avogadro constant. This result, $N_A = 6.022\,0943 \times 10^{23}$ mol^{-1} (1.05 ppm), represents a more than thirty-fold reduction in the uncertainty of previous direct measurements.

Dibeler, V. H., McCulloh, K. E., **Enthalpy of formation of methyl and methylene radicals by photoionization studies of methane and ketene,** (Proc. IV Int. Conf. on Vacuum-UV Radiation Physics, Hamburg, Germany, July 22-26, 1974), Paper in *Vacuum-UV Radiation Physics*, E. E. Koch, R. Haensel, and C. Kunz, Eds., pp. 191-194 (Pergamon-Vieweg, Braunschweig, Germany, 1974).

Key words: enthalpy of formation; ions; mass spectrometry; methyl; methylene; photoionization; radicals; vacuum ultraviolet.

Photoion yield curves for CH_3^+ and CH_2^+ from methane have been remeasured near threshold at 298 and 115 K and the curve for CH_2^+ from ketene has been measured at 298, 215, and 130 K. For methane there is no evidence for the ion-pair process yielding $CH_3^+ + H^-$. The temperature shift of the CH_3^+ curve is $k\Delta T$, indicating only two available rotational degrees of freedom in the dissociation process. Including a negligible kinetic energy release at threshold, the estimated threshold at T = 0 results in $\Delta Hf_0°$ $(CH_3) = 35.6 \pm 0.2$ kcal mol^{-1}. No temperature shift is observed for the CH_2^+ curve from methane. Assuming zero kinetic energy release, the result $\Delta Hf_0°$ $(CH_2) = 93.7 \pm 0.5$ kcal mol^{-1} is obtained. The CH_2^+ curve from ketene exhibits a shift of $k\Delta T$ with temperature. Neglecting kinetic energy release, the estimated threshold at T = 0 results in $\Delta Hf_0°$ $(CH_2) = 93.5 \pm 0.4$ kcal mol^{-1}.

Dresser, M. J., Madey, T. E., Yates, J. T., Jr., **The adsorption of xenon by W(111), and its interaction with preadsorbed oxygen,** *Surface Sci.* **42,** 533-551 (1974).

Key words: desorption energy; desorption kinetics; physical adsorption; tungsten (111); work function; xenon.

The physisorption of Xe on W(111) and of Xe on partial layers of oxygen chemisorbed on W(111) has been studied using flash desorption and work function methods. It has been found that xenon adsorbs up to monolayer coverages at 104 K. Xenon desorbs from W(111) as a single binding state following first order kinetics. At low coverages ($\theta_{Xe} < 0.07$) the binding energy decreases with increasing coverage possibly because of the presence of high energy adsorption sites due to crystal imperfections and edge effects. For $\theta_{Xe} > 0.07$ the desorption data fit a first order rate expression with a desorption energy of 9.3 kcal/mol and preexponential $\nu = 10^{15}$ s^{-1}. The observed work function change of -1.1 ± 0.1 eV is consistent with monolayer estimates reported in field emission studies of physisorbed xenon on tungsten. The effect of preadsorbed oxygen layers on the physisorption of xenon on this surface is very striking. The energy of desorption shifts as much as 50 percent higher for a moderate exposure of oxygen. Several physisorption models are explored along with estimates of dispersion and electrostatic interaction contributions.

Dzubay, T. G., Rook, H. L., Stevens, R. K., **A chemiluminescent approach to measurement of strong acid aerosols,** Chapter 4 in *Analytical Methods Applied to Air Pollution Measurements*, R. K. Stevens and W. F. Herget, Eds., pp. 71-83 (Ann Arbor Science Publishers, Inc., Ann Arbor, Mich., 1974).

Key words: ambient concentration; chemiluminescent measurement; continuous monitor; strong acid aerosols.

The deleterious effect of sulfuric acid aerosol on human health has been demonstrated. Currently, no real time monitors for strong acid aerosols are available. This work represents an effort to develop an instrument for monitoring strong acid aerosols in real time without going through collection and extractions procedures.

Ehrlich, M., **The use of pressed LiF for thermoluminescence dosimetry without furnace annealing,** *Phys. Med. Biol. Tech. Note* **19,** No. 5, 725-731 (1974).

Key words: dosimetry; fading; furnace annealing; glow curve; maximum heating temperature; peak height; reproducibility; sensitivity loss; supralinearity.

A method of LiF thermoluminescence dosimetry (TLD) requiring no furnace annealing is described which can be used with many general-purpose commercial TLD readers. With this method, one produces LiF TLD characteristics similar to those obtained after conventional annealing. Glow-curve areas following successive identical exposures of a sample reproduce to within a relative standard deviation of 1 percent, but peak heights are less reproducible. Supralinearity characteristics are similar to those of conventionally annealed samples. While fading is somewhat more pronounced, it is not prohibitive for many medical applications. Maximum nominal planchet temperatures of 300 °C during readout produce essentially complete annealing in the medical exposure range, without appreciable loss in sensitivity due to successive irradiations and readouts, while sensitivity losses sometimes amount to as much as 8-10 percent for maximum nominal readout temperatures of 400 °C.

Eisenhart, C., Samuel, S., **Wilks and the army experiment design conference series,** *Proc. Twentieth Conf. on the Design of Experiments in Army Research Development and Testing, Ft. Belvoir, Va., Oct.* 23-25, 1974, ARO Report 75-2, Pt. 1, 1-47 (Army Dept., Chief of Research, Development and Acquisition, 1974).

Key words: Annals of Mathematical Statistics; Army Experiment Design Conferences; Dodd, E. L.; educational testing; history of mathematical statistics in the U.S.A.; Hotelling, Harold; likelihood-ratio tests; multivariate analysis; order statistics; Princeton University; Rietz, H. L.; Shewhart, W. A.; statistical tolerance limits; Wilks, S. S.; Wishart, John.

A biography of Professor Samuel Stanley Wilks (1906-1964) of Princeton University, with particular attention to his early life, notes on the persons who shaped his professional development, review of his many facetted professional career and his role in initiating and launching the U.S. Army's annual series of Conferences on the Design of Experiments in Army Research, Development and Testing.

Ekin, J. W., Clem, J. R., **Magnetic coupling force of the superconducting dc transformer,** *Phys. Rev. B* **12,** No. 5, 1753-1765 (Sept. 1, 1975).

Key words: dc transformer; granular aluminum films; magnetic coupling; superconducting dc transformer; type II superconducting films; vortex coupling.

The temperature dependence and magnetic field dependence of the coupling force have been measured in two transformer systems, one with primary and secondary film thicknesses d_p and d_s comparable with the superconducting penetration depth λ ($d_p/\lambda_p \sim d_s/\lambda_s \sim 1$) and one with film thicknesses small compared with the penetration depth ($d_p/\lambda_p \sim d_s/\lambda_s \sim 10^{-1}$). The results show that (i) the coupling force is nearly two orders of magnitude greater in the thick-film transformer than in the thin-film transformer; (ii) there exists a transition field above which the coupling force decreases very rapidly, typical values for the transition field being quite low (~ 0.5 G); and (iii) the temperature dependence of the coupling force over much of the range investigated is simply proportional to the temperature dependence of $\lambda_p^{-2}\lambda_s^{-2}$. A Gibbs free-energy theory describing the coupling force has been numerically evaluated and compared with these data. The results show that the theory can be used to predict accurately both the absolute magnitude and the field and temperature dependences of the coupling force for wide-ranging values of the operating parameters.

Ekin, J. W., **Critical currents in granular superconductors,** *Phys. Rev. B* **12,** No. 7, 2676-2681 (Oct. 1, 1975).

Key words: critical current densities; critical currents; granular aluminum films; granular films; Type II superconducting films; vortex pinning.

A relatively simple principle is experimentally demonstrated for producing extremely low critical-current density materials for application in quantum flux-flow devices. Essentially the technique consists of making the scale of structural disorder in the material small compared with the vortex core size. The smaller this ratio, the smaller the effects of bulk pinning, and the smaller the resulting critical-current density. Data for this study were obtained using superconducting granular aluminum films evaporated in a cylindrical geometry designed to eliminate edge-pinning effects. The data show J_c to exhibit a sharp minimum as a function of grain size, with the lowest values of J_c occurring in those films having the smallest ratio $\langle D\rangle/(\zeta_0 l)^{1/2}$. Here $\langle D\rangle$ is the average grain size, ζ_0 is the BCS coherence length, and l is the electronic mean free path. The normal-state resistivity ρ_n can be used as an index of $\langle D\rangle/(\zeta_0 l)^{1/2}$ for the granular aluminum system, with the lowest critical-current densities occurring in films prepared to have a ρ_n of about 10 $\mu\Omega$ cm. In addition to discussing the dependence of the critical current on microstructure, data on the temperature dependence and electric field dependence of J_c are presented.

Ely, J. F., Hanley, H. J. M., **The statistical mechanics of nonspherical polyatomic molecules. Application to the properties of carbon dioxide,** *Mol. Phys.* **30,** No. 2, 565-578 (1975).

Key words: carbon dioxide; Clausius-Mossotti function; intermolecular forces; *m*-6-8 potential quadrupolar gas; second virial coefficient; viscosity coefficient.

Collision integrals and equilibrium pressure and dielectric second virial coefficients are calculated for a nonspherical *m*-6-8 model potential energy function. The results are applied in a correlation of the physical properties of carbon dioxide. It is shown that the inclusion of nonspherical contributions in the calculation of the collision integrals has a small but significant effect with respect to the accurate representation of data. The Mason-Monchick approximation that nonspherical molecules collide with fixed relative orientations is briefly discussed. Agreement between calculated and experimental values for the viscosity coefficient, the thermal conductivity coefficient, the second virial coefficients and the isotopic thermal diffusion factor is generally satisfactory.

Evans, A. G., **High-temperature slow crack growth in ceramic materials,** (Proc. Second Army Materials Technology Conf., Hyannis, Mass., Nov. 13-16, 1973), Chapter 17 in *Ceramics for High-Performance Applications,* pp. 373-396 (Army Materials and Mechanics Research Center, Watertown, Mass., 1974).

Key words: ceramics; crack healing; crack propagation; cyclic fatigue; failure prediction; high temperature; static fatigue.

High temperature slow crack growth processes in several ceramic materials are examined under static and cyclic loading conditions. Data obtained at temperatures up to 1400 °C are used for purposes of failure prediction and for analysis of the slow crack growth phenomena. It is shown that purity plays a major role in slow crack growth resistance particularly in the hot-pressed materials, and that cycling in the low frequency regime does not significantly enhance the rate of slow crack growth. The slow crack growth mechanisms appear to be primarily plasticity related, and some discussion of these is presented.

Evans, A. G., **The role of inclusions in the fracture of ceramic materials,** *J. Mater. Sci.* **9,** 1145-1152 (1974).

Key words: ceramics; failure prediction; fracture; inclusions; nondestructive inspection.

The stress concentrations that occur at inclusions due to thermal expansion and elastic modulus mismatch are discussed and the stress intensity factors at interface cracks that result from these stresses are calculated. It is shown that conservative failure prediction based on an equivalence between inclusion size and crack size is usually acceptable if the shear modulus μ or thermal expansion coefficient α for the inclusion is larger than the matrix values. If, however, μ and α are smaller for the inclusion than the matrix, extensive cracking can develop at the inclusions which may lead to premature

failure. For this case the only effective methods for failure prediction are techniques which give directly the maximum stress intensity factor, i.e., proof testing and/or acoustic emission.

Farmer, B. L., Eby, R. K., **Methyl branches in hydrocarbon crystals: Calculation of relaxation parameters,** *J. Appl. Phys.* **46,** No. 10, 4209-4217 (Oct. 1975).

Key words: mechanical relaxation; methyl branches; paraffins; polyethylene; potential energy calculations; relaxation mechanism; relaxation strength; site model.

A site model has been used in conjunction with potential-energy calculations to examine the role of isolated molecules with methyl branches in the mechanical relaxations of a linear hydrocarbon host crystal. The results indicate that there are two possible relaxation modes and that the one involving molecular rotation is energetically favorable over the one involving rotation and translation. For some modes of deformation, the calculated relaxation strengths are comparable to the experimentally measured ones. Furthermore, the barriers determined in this work yield calculated curves of the logarithmic decrement as a function of temperature which are comparable to the experimental ones. The relaxation is much weaker for unbranched chains in the planar zigzag conformation.

Fatiadi, A. J., **Symmetrical phenylosotriazoles from inositols,** *Carbohydr. Res. Note* **35,** 280-287 (1974).

Key words: conformation; half-chair; inositol; mercuric acetate, phenylosotriazole; p.m.r.; symmetrical.

The application of mercuric acetate reagent to conversion of inosose phenylosazones into phenylosotriazoles in 40–47 percent yield is described. Analysis of p.m.r. spectra of inositol phenylosotriazole esters (e.g., acetates, propionates, benzoates) and of their parent compounds on "decoupling" of their hydroxyl groups (by protonation, or deuterium exchange) showed a symmetrical pattern (presence of a simple, two-fold axis of symmetry in an AA′BB′ system); a half-chair conformation of these phenylosotriazole esters in solution was deduced from the p.m.r. spectra. Free inositol phenylosotriazoles in solution exist exclusively in a half-chair conformation.

Fife, D. W., **Network management for expanded resource sharing,** (Proc. EDUCOM Fall Conf., Princeton, N.J., Oct. 9-11, 1973), Chapter 7 in *Facts and Futures*, pp. 55-61 (The Interuniversity Communications Council, Princeton, N.J., 1974).

Key words: computer network management; computer networking research; management evaluation; resource sharing.

Computer networking technology is adequately developed now to support research and experimentation to expand computing resource sharing. Whether progress will be made depends upon organizational initiative among multiple institutions, to pool personnel and capital so as to effectively address the major issues in management approach, support and software design that limit the feasible interdependence of computing operations. The organizational requirements are partially revealed by examining progressive stages of resource sharing in organizational and operational terms rather than such technical aspects as load sharing or program sharing that have been introduced in the past. Five stages are identified, ranging from simply establishing multiple service access to the advanced stage where multiple institutions organize for joint development of new resources. A preliminary evaluation framework for new management arrangements results when these stages are mapped against the four functional levels inherent in computer network management.

Fife, D. W., **Primary issues in user needs,** (Proc. EDUCOM Working Seminar on the National Science Computer Network, Warrenton, Va., Nov. 1972), Chapter 10 in *Networks for Research and Education*, pp. 89-95 (The Massachusetts Institute of Technology, Cambridge, Mass., 1974).

Key words: computer networks; National Science Computer Network; network management.

The Institute for Computer Sciences and Technology of the National Bureau of Standards is assisting the National Science Foundation in technical planning to delineate major approaches and to derive guidelines for the trial experiments that may lead to a National Science Computer Network. The primary efforts of NBS are in network management requirements and application criteria for communications technology. User characteristics are being briefly studied for perspective on the objectives for the network and on the types of service it may provide. The goal of the NBS project is to describe by mid-1973 the basic types of experiments which address the central issues, together with appropriate evaluation criteria, so that NSF may use this technical framework in selecting an approach to the trial network.

Finkel, P. W., Miller, T. R., Weikel, M. K., **NBS replies to Dr. Barnett's critique,** *Lab World* **25,** No. 4, 6 and 16 (Apr. 1974).

Key words: chemistry; clinical laboratory capability; critique; hematology; microbiology; sampling.

The December 1973 issue of LAB WORLD published a critique of two NBS Interagency Reports. The Bureau has prepared a reply, written by the senior author of both NBS reports, and coordinated through the Institutes for Applied Technology and Materials Research.

Finkel, P. W., Miller, T. R., Weikel, M. K., **Reply to clinical chemistry article,** *Clin. Chem.* **20,** No. 4, 521, 523-524 (1974).

Key words: chemistry; clinical laboratory capability; critique; hematology; microbiology; sampling.

The February 1974 issue of CLINICAL CHEMISTRY published a critique of two NBS Interagency Reports. The Bureau has prepared a reply, written by the senior author of both NBS reports, and coordinated through the Institutes for Applied Technology and Materials Research.

Flynn, D. R., Blomquist, D. S., **Environmental noise measurement,** (Proc. Northeast Electronics Research and Engineering Meeting, Boston, Mass., Nov. 6-8, 1973), Paper in *NEREM (of the IEEE) 1973 Record*, pp. 40-43 (1973).

Key words: acoustics; noise; sound.

This paper is a digest of a paper to be given orally at the Northeast Electronics Research and Engineering Meeting (NEREM) of the IEEE in November 1973. Since its length was severely limited, the paper can only describe the subject matter to be covered in the oral presentation. A discussion will be given of current instrumentation for measurement of environmental noise and noise emission from machinery and equipment—in both occupational and community situations. Emphasis will be placed on available measurement standards, problem areas, and trends in sound measurement instrumentation.

Franklin, A. D., Dragoo, A. L., **Calculation of defect-formation energies in alkaline-earth oxides: Interionic forces,** Paper in *Defects and Transport in Oxides*, M. S. Seltzer and R. I. Jaffee, Eds., pp. 141-158 (Plenum Press, New York, N.Y., 1974).

Key words: alkaline earth oxides; Born-Mayer potential; first-neighbor interactions; ionicity; Lundquist three-body potential; second-neighbor interactions; shell model.

A model potential for the alkaline-earth oxides was developed and tested. The interionic potential contains the usual Coulombic and two-body short-range terms, such as those which have been used in previous alkali halide calculations, plus many-body terms which are incorporated by means of the Lundquist three-body approximation in which only the spherically symmetric term in the overlap-charge-den-

sity expansion is retained. The three-body interactions contribute to both the long-range and the short-range forces. Additional short-range central-force interactions between nearest-neighbor ions and next-nearest-neighbor ions are included; these are modeled by means of a Born-Mayer plus van der Waals potential. The electronic polarizabilities of the ions are described by a shell model. Parameters in the model potential and in the shell model are evaluated using the elastic constants and their pressure derivatives, the low- and high-frequency dielectric constants, the infrared dispersion frequency, and the equilibrium interionic separation. Three constraints on the shell model are required. The model does not give satisfactory results in that (1) the trend in an effective charge parameter, χ_o, through this family of oxides runs counter to that for the Phillips ionicities and (2) the Born-Mayer potential parameters appear to be highly anomalous compared with those for other ionic crystals. The principal weakness of the model apparently resides in its neglect of bond-bending (non-central force) terms, which results in an overestimate of the overlap contribution to the bond-stretching terms, in excessive deviations in the effective charges from the classical valences, and in departures of the Born-Mayer potential parameters from the values found in alkali halide and alkaline-earth fluorides.

Frederikse, H. P. R., Hosler, W. R., **High temperature electrical conductivity of aluminum oxide,** Chapter in *Mass Transport Phenomena in Ceramics*, A. R. Cooper and A. H. Heuer, Eds., **9,** 233-251 (Plenum Press, New York, N.Y., March 1975).

Key words: aluminum oxide: electrical conductivity; high temperature; ionic charge transport.

The electrical conductivity of polycrystalline and single crystal Al_2O_3 has been determined between 1000 and 1650 °C. Measuring the conductivity between the outside and inside surface of a thin-walled, hollow tube eliminates the adverse effects of gas or surface conduction. An analysis of possible electronic and ionic charge transport mechanisms shows that none of these processes fully accounts for the magnitude of the observed conductivity. Migration of Al^{3+} ions (or Al^{3+} vacancies) yields the largest values and offers at present the best explanation for electrical conduction in Al_2O_3.

Freund, S. M., Ritter, J. J., **CO_2 TEA laser-induced photochemical enrichment of boron isotopes,** *Chem. Phys. Lett.* **32,** No. 2, 255-260 (Apr. 15, 1975).

Key words: BCl_3 (boron trichloride); boron; CO_2 (carbon dioxide); enrichment; infrared; isotopes; TEA laser.

Mixtures of BCl_3 and H_2S are irradiated with 10.55 μm radiation (P(16)line of the 001-100 band of CO_2) from a TEA laser. After several hours of irradiation it is found that the maximum ^{10}B to ^{11}B ratio of recovered gaseous boron containing material (primarily unreacted BCl_3) is 0.413 ± 0.004. The corresponding ratio of the BCl_3 starting material is 0.242 ± 0.002. The ^{10}B concentration has therefore been increased from 19.5 to 29.2 percent. Further, by irradiating similar mixtures with 10.18 μm radiation (R(30) line of the same CO_2 vibrational band) this ratio changes to 0.169 ± 0.002, the ^{10}B concentration being lowered to 14.4 percent. All experiments are performed in a small static system and chemical procedures for recovering milligram quantities of BCl_3 selectively enriched in either isotope are described.

Fung, F. C. W., Suchomel, M. R., Oglesby, P. L., **The NBS program on corridor fires,** *Fire J.* **67,** No. 3, 41-48 (May 1973).

Key words: carpets with and without underlayment; corridor fires; energy models; finished interior; full scale experiments; interaction; measurements; smoke; smoke and flame spread; temperature; with and without forced air; velocity.

This report outlines the NBS full scale experimental program to investigate the growth and spread of fire and smoke into and through a corridor when a fire is initiated in an adjoining room. The program proposes energy models to investigate both the contribution of the corridor interior finish surfaces and their interactions under the full scale fire situation. As a status report it describes in detail the experimental facilities and approaches for the program.

A summary of the tests conducted to date is presented. It is shown that flames can propagate the length of a 30 foot corridor, with a combustible floor covering as the only source of fuel in the corridor, when initiated by 2.7 psf of wood cribs in an adjacent room. Typical quantitative measurements of temperature, velocity, smoke and energy are also presented. In addition, comparative discussions are presented for tests with and without forced air draft and carpet tests with and without underlayment.

Furukawa, G. T., Bigge, W. R., Riddle, J. L., Reilly, M. L., **The freezing point of aluminium as a temperature standard,** *Inst. Phys. Conf. Ser. No.* **26,** Chapter 7, 389-397 (1975).

Key words: aluminium point; calibration; freezing point; freezing-point cell; platinum resistance thermometer; tin point; zinc point.

Six platinum resistance thermometers were "calibrated" at the triple point of water and at the freezing points of tin, zinc and aluminium. By extrapolating the "quadratic relation" the freezing point of pure aluminium was found to be 660.407 ± 0.005 "degrees C." The advantages of having a platinum resistance thermometer calibrated at a fixed point (e.g., aluminium point) near the upper temperature limit are demonstrated.

Gallagher, A., **The spectra of colliding atoms,** (Proc. 4th Int. Conf. on Atomic Physics, Heidelberg, Germany, July 1974), Paper in *Atomic Physics* **4,** G. zu Putlitz, E. W. Weber, and A. Winnacker, Eds., pp. 559-574 (Plenum Publ. Corp. New York, N.Y., 1975).

Key words: line broadening; rubidium; sodium.

We discuss what can be learned from line shapes and the basic ideas of how they are interpreted with theoretical approximations. Only "pressure" or neutral-gas broadening will be considered, not "Stark" or plasma broadening. We will give examples of recent theoretical and experimental work, but this is not intended as a review and we will concentrate on our measurements in the far wings of the lines.

Geller, S. B., **Archival data storage,** *Datamation* **20,** No. 10, 72, 75-76, 80 (Oct. 1974).

Key words: archival language; archival quality; content decay; content density; content lifetimes; storage media.

This paper develops some archival language and discusses factors which must be considered when an archival data storage system is designed. These include types of contents, content decay rates, content and medium lieftimes, content density and system costs. Other archival storage quality factors such as information security and recovery are considered.

Geltman, S., **Coulomb correction for strong-field multiphoton free-free absorption,** *J. Phys. B Letter to Editor* **8,** No. 15, L374-L376 (1975).

Key words: absorption; bremsstrahlung; electrons; ions; laser; plasma.

A correction factor, which arises from the logarithmic phase factor in Coulomb waves, is shown to be necessary in the treatment of multiphoton free-free absorption in ultrastrong laser fields.

Giguere, P. T., Clark, F. O., **Radio search for HC_3N, HCN, OH, and detection of U8.19 in comet Kohoutek (1973f),** *Astrophys. J.* **198,** 761-764 (June 15, 1975).

Key words: comet; HCN; HC_3N; Kohoutek; OH; radio; search.

Comet Kohoutek (1973f) was observed with the NRAO 140-foot (43 m) radio telescope in the period 1974 January 4-7 in an attempt to detect the following molecular transitions: HC_3N, $J = 1\text{-}0$, $v = 0$; HC_3N, $J = 1\text{-}0$,$2\nu_7$, $l = 0$; HCN, $J = 6,1\nu_2$; and OH, $^2\Pi_{1/2}$, $J = 5/2$, $F = 3\text{-}3$. All results for these lines were negative. An unidentified line was possibly detected at 8189 MHz.

Gillispie, G. D., Khan, A. U., Wahl, A. C., Hosteny, R. P., Krauss, M., **The electronic structure of nitrogen dioxide. I. Multiconfiguration self-consistent-field calculation of the low-lying electronic states,** *J. Chem. Phys.* **63,** No. 8, 3425-3444 (Oct. 15, 1975).

Key words: dipole moment; excited states; MC-SCF; molecular geometry; NO_2; spectra.

Traditional spectroscopic analysis of the complex and irregular absorption spectrum of NO_2 has provided a relatively small amount of information concerning the nature of the excited states. An extensive *ab initio* investigation has been undertaken, therefore, to provide a basis for interpretation of the experimental results. Multiconfiguration self-consistent-field (MC-SCF) wavefunctions have been computed for the low-lying

$$\tilde{X}^2A_1, \tilde{A}^2B_2, \tilde{B}^2B_1, \tilde{C}^2A_2, {}^4B_2, {}^4A_2, \text{and } {}^2\Sigma_g^+$$

electronic states of NO_2. The minima of the $\tilde{A}^2B_2$, $\tilde{B}^2B_1$, and $\tilde{C}^2A_2$ states have all been found to be within 2 eV of the minimum of the $\tilde{X}^2A_1$ ground state; for these states, C_{2v} potential surfaces have been constructed for purposes of a spectral interpretation. The $^4B_2$, $^4A_2$, and $^2\Sigma_g^+$ states are all more than 4 eV above the minimum of the ground state and have been examined in less detail. The study described here significantly improves on previous NO_2 *ab initio* calculations in three important areas: (1) The double-zeta-plus-polarization quality basis set is larger and more flexible; (2) the treatment of molecular correlation is more extensive; and (3) the electronic energies have been calculated for several different bond lengths and bond angles in each state. For the four lowest doublet states the following spectral data have been obtained:

	T_e(eV)	R_e(Å)	θ_e(deg)
$\tilde{C}^2A_2$	1.84	1.27	110
$\tilde{B}^2B_1$	1.66	1.20	180
$\tilde{A}^2B_2$	1.18	1.26	102
$\tilde{X}^2A_1$	0.00	1.20	134
	(0.00)	(1.1934)	(134.1)
	$\omega_1(cm^{-1})$	$\omega_2(cm^{-1})$	μ(D)
$\tilde{C}^2A_2$	1360	798	0.05
$\tilde{B}^2B_1$	1192	960	0.00
$\tilde{A}^2B_2$	1461	739	0.46
$\tilde{X}^2A_1$	1351	758	0.37
	(1358)	(757)	(0.32)

The ground state experimental constants are included in parentheses. The estimated accuracy of the various parameters is ± 0.02 Å for bond length, ± 2° for bond angle, ± 10 percent for the vibrational frequencies, ± 0.10 D for dipole moments, and ± 0.3 eV for the adiabatic excitation energies. An unusual feature has been found for the $^2\Sigma_g^+$ state. The equilibrium geometry of this linear state has two unequal bond lengths of 1.20 and 1.42 Å and the inversion barrier is approximately 800 cm^{-1}.

Gills, T. E., LaFleur, P. D., **The determination of hafnium in standard reference materials using bis(2-ethylhexyl) phosphate (HDEHP) with neutron activation analysis,** (Proc. Int. Meeting on Activation Analysis, Saclay, France, Oct. 1-6, 1972), *J. Radioanal. Chem.* **19,** 235-237 (1974).

Key words: activation analysis; Ge(Li) detector; solvent extraction.

The method for the determination of hafnium in standard reference steels is described. The method combines neutron activation analysis with a solvent extraction procedure using bis(2-ethylhexyl) phosphate as the extractant. A subsequent back extraction into 2N hydrofluoric acid is done finally before counting. The samples were counted on a 60cc Ge(Li) in configuration with a 2048 channel analyzer. Using this method of analysis as described fast determination of hafnium can be made with routine 3-4 percent precision and accuracy.

Gills, T. E., McClendon, L. T., Maienthal, E. J., Becker, D. A., Durst, R. A., LaFleur, P. D., **Determination of toxic trace elements in body fluid reference samples,** (Proc. Eighth Annual Conf. on Trace Substances in Environmental Health, Univ. of Missouri-Columbia, Columbia, Mo., June 11-13, 1974), Paper in *Trace Substances in Environmental Health*, D. D. Hemphill, Ed., **VIII,** 273-280 (1974).

Key words: body fluids; fluorine; lead; mercury; reference samples; trace elements.

The measurement of elemental concentration in body fluids has been widely used to give indication of exposure to certain toxic materials and/or a measure of body burden. To understand fully the toxicological effect of these trace elements on our physiological system, meaningful analytical data are required along with accurate standards or reference samples. The National Bureau of Standards has prepared for the National Institute for Occupational Safety and Health (NIOSH) a number of reference samples containing selected toxic trace elements in body fluids. The reference samples produced include mercury in urine at three concentration levels, five elements (Se, Cu, As, Ni and Cr) in freeze-dried urine at two levels, fluorine in freeze-dried urine at two levels and lead in blood at two concentration levels. These reference samples have been found to be extremely useful for the evaluation of field and laboratory analytical methods for the analysis of toxic trace elements. In particular the use of at least two calibration points (i.e. "normal" and "elevated" levels) for a given matrix provides a more positive calibration for most analytical techniques over the range of interest for occupational toxicological levels of exposure.

Gladney, E. S., Rook, H. L., **Simultaneous determination of tellurium and uranium by neutron activation analysis,** *Anal. Chem.* **47,** No. 9, 1554-1557 (Aug. 1975).

Key words: environmental samples; neutron activation analysis; tellurium; uranium.

A procedure for the simultaneous determination of tellurium and uranium is described. The procedure utilizes thermal neutron activation followed by sample combustion and a gas phase separation of the volatile radionuclides of interest. This method is sensitive enough to permit the measurement of tellurium and uranium at their naturally occurring levels in materials of biological and environmental origin. The procedure has been successfully employed to determine the tellurium and uranium concentrations in three Standard Reference Materials (SRM's) currently being offered by the National Bureau of Standards, and in atmospheric particulate material collected in rural Maryland.

Goldberg, R. N., Prosen, E. J., Staples, B. R., Boyd, R. N., Armstrong, G. T., Berger, R. L., Young, D. S., **Heat measurements applied to biochemical analysis: Glucose in human serum,** *Anal. Biochem.* **64,** No. 1, 68-73 (Mar. 1975).

Key words: analysis; clinical chemistry; glucose; microcalorimetric; thermochemistry.

Microcalorimetric measurement of enthalpy change for the hexokinase catalyzed reaction of ATP with glucose (in TRIS/HCl buffer containing $MgCl_2$) was carried out with glucose concentrations from zero to 1350 mg · $liter^{-1}$. A linear relationship between measured heat and glucose concentration was found, from which the reaction enthalpy was calculated to be − 61.4 kJ · $mole^{-1}$. This linear relation, combined with calorimetric measurements of the same process carried

out with 0.15 ml samples of human serum, was used to calculate glucose concentrations in the serum. For 45 samples containing glucose levels ranging from 420 to about 4000 mg · liter^{-1} the results show only slight systematic differences from measurements made by the glucose oxidase procedure of Gochman and Schmitz.

Goldstein, J. I., Yakowitz, H., Newbury, D. E., **Introduction to practical scanning electron microscopy,** Chapter I in *Practical Scanning Electron Microscopy*, J. I. Goldstein and H. Yakowitz, Eds., pp. 1-19 (Plenum Press, New York, N.Y., 1975).

Key words: contrast; electron beam instrumentation; electron probe microanalyzer; instrumental development; scanning electron microscope; signal processing.

This chapter traces the evolution of the scanning electron microscope and the electron probe microanalyzer from birth to the present. A number of major developments both instrumental and methodological are outlined. The purpose is to familiarize the novice with these developments; for the experienced SEM user, the chapter aim is to remind one of the significant stages of instrumental development. Points touched upon include the discovery and exploitation of various SEM contrast mechanisms such as topographic, voltage and magnetic contrast as well as stages in the development of signal and image processing.

Goodman, L. J., Colvett, R. D., Caswell, R. S., **An international neutron dosimetry intercomparison,** *Proc. Second Symp. on Neutron Dosimetry in Biology and Medicine, Neuherberg/Munchen, Germany, Sept. 30-Oct. 4, 1974*, EUR 5273d-e-f, pp. 627-662 (1974).

Key words: absorbed dose; intercomparison; kerma; neutron dosimetry; neutron radiobiology; neutron therapy.

An International Neutron Dosimetry Intercomparison, sponsored by the International Commission on Radiation Units and Measurements, has been completed at the Radiological Research Accelerator Facility at Brookhaven National Laboratory. Fourteen groups of scientists, from six countries, performed measurements to determine the separate neutron and photon (x- and gamma-ray) tissue kermas in free air for four energies of monoenergetic neutrons, 15.5, 5.5, 2.1, and 0.67 MeV, and for a source of fission neutrons, ^{252}Cf. For the two highest energies, measurements were also made to determine the separate absorbed doses in tissue of neutrons and of photons at three depths in a large water phantom.

Green, R. E., Jr., Farabaugh, E. N., Crissman, J. M., **X-ray topographic examination of large paraffin single crystals,** *J. Appl. Phys.* **46,** No. 10, 4173-4180 (Oct. 1975).

Key words: microstructure; paraffin crystals; plastic deformation; polymer crystals; radiation damage; x-ray topography.

The internal microstructure of large melt-grown paraffin (*n*-eicosane, $C_{20}H_{42}$) single crystals was examined by the Lang x-ray diffraction projection topographic technique. Crystal selection was facilitated by use of an electro-optical system which permitted instantaneous display of Laue transmission x-ray diffraction patterns on a television monitor. The crystals were oriented and topographic diffraction planes were selected by the use of a standard (001) stereographic projection plotted from computed angles between crystallographic planes. A second electro-optical system which permitted direct viewing of the topographic images was used for rapid alignment of the Lang camera and ensured uniformly exposed topographs. X-ray topographs were obtained from crystals in the as-grown, plastically deformed, and γ-irradiated states. The results indicate that both plastic deformation and γ irradiation caused marked changes in the microstructure of the crystals, and that x-ray topography can be successfully exploited to determine such changes in hydrocarbon crystals.

Grum, F., Cameron, J., **Detector intercomparison results,** *Electro-Opt. Systems Design*, pp. 82-84 (Nov. 1974).

Key words: interlaboratory test; photodiode detectors; photometry.

The results of an intercomparison of measurement of spectral sensitivity of two silicon photodiodes are presented. The comparison was part of the activities of CORM (Council for Optical Radiation Measurement). The manufacturer, nine industrial laboratories, and NBS measured the two cells. The results were statistically analyzed and are presented here in tabular and graphical form.

Grundl, J. A., Dudey, N. D., Popek, R. J., **Measurement of absolute fission rates,** *Trans. Amer. Nucl. Soc.* **17,** 516-517 (1973).

Key words: absolute fission rates; neutron dosimetry; reactor fuels; reactor materials.

Recently, the accuracy requirements for fast reactor fuels and materials dosimetry surpassed the existing capabilities of fission foil activation measurements. In order to improve this capability by direct calibration of activation detectors, absolute fission rates per nucleus have been measured in fast neutron fluxes suitable for both fission activation foils and for fission fragment detectors. This paper presents results for absolute fission fragment emission rates from ^{239}Pu, ^{235}U, ^{238}U, and ^{237}Np exposed to the first of these fast neutron fluxes, the spectrum of the CFRMF Reactor at ANC.

Haas, S. S., Dickson, G., Brauer, G. M., **A proposed specification for acrylic bone cement,** *J. Biomed. Mater. Res. Symp.* **9,** No. 6, 105-117 (1975).

Key words: biomaterial; bone cement; orthopaedic material; poly(methyl methacrylate); specification; surgical bone cement.

A proposed specification covering handling characteristics and physical and chemical properties of bone cement composed primarily of methyl methacrylate has been prepared on the basis of data from the authors' studies and from various other sources. Under handling characteristics, requirements included relate to dough, handling and setting time, proper plasticity for insertion and temperature rise on setting. Mechanical properties specified include compressive strength and indentation and recovery characteristics. Maximum limits are proposed for water sorption and solubility. Suggested packaging requirements are also included.

Hagan, L., **Reports of observatories for 1973/74, National Bureau of Standards, Washington, D.C.,** *Bull. Am. Astron. Soc.* **7,** No. 1, 165-169 (1975).

Key words: atomic energy levels; atomic line shapes; atomic spectra; atomic transition probabilities; bands, molecular; energy levels, atomic; line shapes, atomic; molecular bands; molecular spectra; rotational constants.

Research at the National Bureau of Standards in spectroscopy pertinent to astronomy is summarized. Publications on atomic spectra, atomic transition probabilities and line broadening, and molecular spectra are referenced and work in progress is discussed.

Haight, W. C., **Establishment of OS AIDS as an RTOS task,** *Interchange* **5,** No. 3, 5-6 (June 1974).

Key words: debugging; Interdata 70; OS AIDS; RTOS; software.

A technique is detailed that allows OS AIDS, a debugging utility program, to be established as an RTOS system task. This expands the RTOS environment to comprehensively support all phases of program preparation at the user level. Modifications that must be made to AIDS and to the Task Establisher Task, TET, prior to task creation are defined. Conceptual problems that can occur when AIDS runs in a multi-programming environment are discussed.

Haight, W. C., Hawes, H. W., **An automated tuneup—Calibration of jet engine fuel controls,** *Proc. 1974 ASSC Conf. Record on Automated Support Systems for Advanced Maintainability, San*

Diego, Calif., Oct. 30—Nov. 1, 1974, 12 pages (IEEE Aerospace and Electronics Systems Society, San Diego, Calif., 1974).

Key words: automation; calibration; fuel control; jet engine; minicomputer; multi-task; performance testing; process control; real-time; RTOS.

The National Bureau of Standards (NBS) has designed an automated process control system for the calibration of jet engine fuel controls. The principal aim of this system is to relieve the test operator of the necessity of setting up test conditions and to provide a means of fast and accurate data acquisition. When operated under a vendor-supplied real-time operating system, the NBS software affords ease of modification to suit changing test requirements, ease of maintenance, and a degree of transferability between similar applications. Attributes contributing to these design goals include a modular program structure, use of a high-level programming language (FORTRAN) for applications routines, a well-structured file system and utility package, and a mnemonic test-oriented language developed for coding test procedures.

Hanley, H. J. M., Watts, R. O., **Molecular dynamic calculation of the thermodynamic properties of methane,** *Aust. J. Phys.* **28,** 315-324 (1975).

Key words: methane; molecular dynamics; potential function; specific heat; statistical mechanical ensembles; thermodynamic properties; three body forces.

Thermodynamic properties of methane in the dense gas and liquid states have been calculated by the method of molecular dynamics. The methane pair interactions were modelled using a spherically symmetric *m*-6-8 potential, and the most significant three-body and quantum effects were included. Agreement between calculated and experimental values for the energy and pressure is generally good except at low temperatures and high densities. The specific heat at constant volume is also briefly discussed.

Harman, G. G., **A metallurgical basis for the nondestructive wire-bond pull-test,** *12th Annual Proc. IEEE Reliability Physics, Las Vegas, Nev., April 2-4, 1974*, pp. 205-210 (Nov. 15, 1974).

Key words: bond pull test (nondestructive); metallurgical; reliability (microelectronic); transistors; wire bond.

Nondestructive wire-bond pull tests are often specified by high-reliability electronic device users in order to eliminate weak, poorly made wire bonds. The main problem with the test has been in establishing a pull-force level which will assure that the bonds are adequately strong but will not damage them during the test. In the present work, factors affecting the nondestructive wire-bond pull-test are examined. The variables, such as wire and bond-loop elongation, bond geometry, bond deformation, and the mean and standard deviation of the destructive bond pull test are studied to determine their influence on the nondestructive test. Different pull-force criteria are derived for wire with high elongation, such as is used in power devices, and for wire with low elongation, typically used for bonding integrated circuits.

Harman, G. G., **Metallurgical failure modes of wire bonds,** *12th Annual Proc. IEEE Reliability Physics, Las Vegas, Nev., April 2-4, 1974*, pp. 131-141 (Nov. 15, 1974).

Key words: bonds (wire); failure modes; metallurgical failure modes; microelectronic; thermocompression bonds; ultrasonic bonds.

Various metallurgical failure modes of gold and aluminum wire bonds are described. Examples are taken from both low and high power devices. Whenever possible, known methods of avoiding these failure modes are given.

Wire bond failure modes can be divided into two categories. The first is comprised of those failure modes that are caused by poorly controlled or poorly designed manufacturing processes that result in lower product yield or higher per unit bonding cost, as well as those processes that predispose the device to early field failure. The second category is comprised of the failure modes of adequately made bonds that are caused to fail by environmental stresses during the operating life of the device.

The most frequent causes of failures are discussed in detail. These include nonoptimized bonding schedules, cracks in the heels of ultrasonic bonds, intermetallic formation, poor metallization, and inadequate glassivation removal. Assuming that the package is hermetic, or for plastic devices that humidity and other corrosion producers are not present, then the primary wire bond failure modes in the second category result from environmental temperature exposure and the number of power or thermal cycles experienced by the device during operation. Both of these can induce intermetallic formation. The latter can cause metallurgical flexure-fatigue at the bond heel or in the wire.

Harrison, J. O., Jr., **Computer program characteristics,** (Proc. Seminar on Metric Conversion Engineering and Manufacturing, Gaithersburg, Md., Dec. 12-13, 1974), Appendix B in *ANMC-74-1, Metric Conversion in Engineering and Manufacturing*, L. Perica, Ed., pp. 133-136 (American National Metric Council, Washington, D.C., May 1974).

Key words: computer program; metric conversion; round off.

At least six computer programs to assist manufacturing companies in metric conversion are now available. The principal characteristics of these programs and the requirements for programs for metric conversion are discussed. NBS' plans to issue a metric conversion package are described.

Harrison, J. O., Jr., **Metric conversion and the COMMON computers,** *Proc. COMMON Users Group, Hollywood, Fla., Oct. 14-16, 1974*, 22 pages (1974).

Key words: conversion; FORTRAN; Metric System.

The NBS Computer Program Package for Metric Conversion is written in American National Standard FORTRAN and is designed to compile and run on a wide variety of large scale computers with little or no modification. This paper consists largely of a description of the package and a discussion of its applicability to the COMMON Computers consisting of the IBM System 370, System 360, the 1130, 1800, System 3, and System 7.

The package has been satisfactorily tested on a System 370 Model 165. It may be expected to compile and run satisfactorily on any 370 or on any 360 Model 22.195 of adequate configuration when one of the available AMERICAN NATIONAL STANDARD FORTRAN Compilers is used.

It will probably not run on the 1130, the 1800, the System 3, or System 7 with any IBM supplied FORTRAN compiler due to the extensive use made of features contained in ANS FORTRAN but not in ANS BASIC FORTRAN.

The package should compile and run on a 1130 of adequate configuration with a DNA 1130 ANS FORTRAN Computer with little or no modification.

Harrison, S. H., LaFleur, P. D., Zoller, W. H., **Evaluation of lyophilization for the preconcentration of natural water samples prior to neutron activation analysis,** *Anal. Chem.* **47,** No. 9, 1685-1688 (Aug. 1975).

Key words: freeze drying; instrumental neutron activation analysis; lyophilization; neutron activation analysis; preconcentration; radioactive tracers; river water; trace elements; tracers; water.

A method for the concentration of trace elements in water by lyo-

philization is described. This method has important applications in the multielement analysis of natural water samples by neutron activation. The results of the evaluation of trace element retention yields, using radioactive tracers, indicate that at least Na, Sc, V, Cr, Fe, Co, Zn, As, Se, Br, Rb, Sr, Ag, Cd, Sb, Cs, Ba, Tb and Ce are retained quantitatively (greater than 95%) in the freeze dried residue of a river water sample. Hg and I were found to be lost substantially and Au was retained at almost the 95 percent level. A bag made from linear polyethylene film is used as the sample container for freeze drying and neutron irradiation and is the only measurable blank in the preconcentration process. The results of a typical analysis of a freeze dried estuarine sample with the determined sample/blank ratios for each element are presented.

Harvey, W. W., Kruger, J., **The passivity of gallium arsenide,** (Proc. 3d Int. Conf. on Passivity of Metals, Cambridge, England, July 1970), Paper in *Electrochim. Acta* **16,** 2017-2037 (1971).

Key words: electrochemistry; ellipsometry; gallium arsenide; passivity.

Both p- and n-type gallium arsenide in aqueous electrolytes display the phenomenon of passivity once sufficiently high prepassive cds are attained. This can be achieved for the n-type by illumination, whereby a transition is observed from hole-limited anodic dissolution to passive film formation as the light intensity is increased. Ellipsometric studies reveal that the passive film on either n- or p-GaAs dissolves at a comparatively high rate, and so reaches a steady-state thickness in a rather short time.

Coulometric measurements indicate that the passive film contains gallium and arsenic in their +3 oxidation states. The ionization of Ga and As at the GaAs/film interface is shown to require holes, in like manner to anodic dissolution in the absence of a passive film. The electrical and optical properties of the passive film suggest uniformity of composition for thickness greater than about 50 Å, whereas thinner films show higher conductivity and refractive index.

The passive film on GaAs supports typically large electric fields and exhibits negligible electronic conductivity and porosity. Under proper conditions a nonpassive anodic film can be formed at potentials in the active region. It is much less soluble than the passive film, continues to thicken indefinitely and therefore appears to be porous.

Hasegawa, S., Stokesberry, D. P., **Automatic digital microwave hygrometer,** *Rev. Sci. Instrum.* **46,** No. 7, 867-873 (July 1975).

Key words: humidity; hygrometer; microwave refractometer.

This hygrometer is designed to measure the humidity of atmospheric air over the vapor pressure range 3-7400 Pa (0.03-74 mbar). The instrument is an adaption of a microwave refractometer using two cavities operating at 12 GHz. One cavity is exposed to the moist test air and the other is exposed to the same air sample with all the water vapor removed. Both cavities are maintained at the same fixed temperature in a thermostated oven and at the same total pressure. The difference in frequency between the cavities is automatically nulled by a tuning probe in the sampling cavity. The instrument was calibrated by two independent methods. One involved the measurement of the resonance frequency of the sampling cavity as a function probe penetration and using this in a theoretically derived equation for vapor pressure. The second involved the measurement of the probe penetration as an empirical function of known vapor pressure of a test gas. These two methods yielded results which agreed on the average to better than 0.5 percent for vapor pressures up to 3050 Pa (30.5 mbar).

Hastie, J. W., **Sampling reactive species from flames by mass spectrometry,** *Int. J. Mass Spectrom. Ion Phys.* **16,** No. 1/2, 89-100 (Jan. 1975).

Key words: flames; laser excitation; mass spectrometry; radicals.

Recent studies on sampling reactive species from flames and related laser-excited systems are described. Consideration is given to the possible effect of probe-related perturbations on the experimental data. It is concluded that such perturbations are not significant under the present experimental conditions.

Heimbach, C. R., O'Connell, J. S., **Influence on the neutron's charge distribution on nuclear Coulomb energies,** (Proc. Conf. Int. Few Body Problems in Nuclear and Particle Physics, Laval Univ., Quebec City, Canada, Aug. 27-31, 1974), Paper in *Few Body Problems in Nuclear and Particle Physics,* R. J. Slobodrian, B. Cujec, and K. Ramavataram, Eds., pp. 94-95 (Les Presses de L'Université Laval, Quebec, Canada, 1974).

Key words: charge distribution; Coulomb energy; deuteron; electrostatic; interaction potential; neutron.

The electrostatic interaction energy of a deuteron was computed for a model in which the neutron charge distribution was taken as a superposition of two exponentials of total charge +e and −e. Because the interaction potential is of short range the result is sensitive to the interior deuteron wave function. For a Reid hard-core wave function the computed energy is 1 keV.

Herron, J. T., Huie, R. E., **Rate constants for the reactions of ozone with ethene and propene, from 235.0 to 362.0 K,** *J. Phys. Chem.* **78,** No. 21, 2085-2088 (1974).

Key words: air pollution; ethene; kinetics; mass spectrometry; ozone; propene; rate constant.

The rate constants for the reactions of ozone with ethene and propene have been measured over the temperature range 235.0-362.0 K, using a stopped-flow system coupled to a beam-sampling mass spectrometer. The rate constants found, at a total pressure of about 500 N m^{-2}, in the presence of molecular oxygen, were $k(C_2H_4) = (5.42 \pm 3.19) \times 10^9 \exp(-2557 \pm 167/T)$ cm^3 mol^{-1} sec^{-1} and $k(C_3H_6) = (3.70 \pm 1.42) \times 10^9 \exp(-1897 \pm 109/T)$ cm^3 mol^{-1} sec^{-1}.

Heydemann, P. L. M., **Pressure measurement and calibration,** *Proc. ASME Pressure Vessels and Piping Materials Nuclear Conf., Miami, Fla., June 24-28, 1974,* Paper 74-PVP-43, pp. 1-8 (American Society of Mechanical Engineers, New York, N.Y., 1974).

Key words: calibration; pressure measurement; primary pressure standards.

The National Bureau of Standards maintains a group of primary pressure standards in its laboratories in Gaithersburg, Md. These standards are dead weight piston gages with controlled clearance. Special experimental and computational methods have been developed for the calibration of these primary standards. From this group of standards calibrations are disseminated to industry by means of transfer standards, which are calibrated against the primary standards with the cross float method. Specialized computer programs are used for the evaluation of the cross float in order to obtain best sets of characteristic gage coefficients. Pressure calibration services available from NBS presently cover the range from 2 kPa (0.3 psi) to 400 MPa (60,000 psi) and an expansion to 2.5 GPa (375,000 psi) is in preparation. In addition NBS provides training courses, data evaluation service and extensive, free consultations. Facilities exist for long term performance testing of transducers and for research and development work under contract. This report is written to make petroleum engineers aware of the availability of these services.

Hill, J. E., Kusuda, T., **Dynamic characteristics of air infiltration,** *ASHRAE Trans.* **81,** Part 1, 168-185 (1975).

Key words: air infiltration; dynamic pressure differential; wind velocity.

Currently available methodology for estimating air leakage into and out of buildings does not directly take into account the fluctuating nature of the outdoor wind conditions. The air leakage into and out of

commercial building offices was studied with particular attention to the time history of outdoor wind velocity and pressure differential across the window. It was found that the air leakage measured was generally quite different from that which could be calculated. The reason for this discrepancy was postulated to be due to a complex process caused by the dynamically varying pressure differential across the window, flow occurring through the window in both directions simultaneously, and finally to the particular experimental configuration used.

Hilsenrath, J., **The utility and economics of an on-line reference data network,** (Proc. Conf. on Mechanism of Explosions and Blast Waves, Naval Weapons Station, Yorktown, Va., Nov. 13-15, 1973), Paper in *Proceedings of the Conference on Mechanism of Explosions and Blast Waves,* Section XVII, 1-21 (Picatinny Arsenal, Dover, N.J., 1973).

Key words: data files; data network; data on-line; international data service; on-line data; reference data service; standard reference data.

This paper describes a prototype on-line data retrieval and data computation system and discusses the scientific, technical and organizational characteristics required to make such a system an economically viable reality.

The general characteristics of the envisioned system are: 1. Authoritative data collections and well documented sources stored on a reliable time-shared computer system; 2. Extended precision representation and computing where required; 3. Efficient programs to generate data not explicitly stored; 4. Easy to use conversational on-line access from inexpensive terminals; 5. A reliable and extensive communication network to eliminate or reduce toll charges; 6. Low user charges.

As envisioned, the charges for connect time should cover the communications costs, the computer costs, and the monthly cost of keeping the data and programs stored on the disc. The economics of the situation argue for building up the data files from small self-contained segments so as to expedite the collection, validation and maintenance of the data base; and to minimize the search time for the user. Of equal importance is the fact that the more compact a particular file is, the fewer uses of it will be required to cover its monthly storage cost.

Examples are given of the use of the system for solving a number of problems in thermodynamics and thermochemistry and in chemical kinetics.

Hockey, B. J., Lawn, B. R., **Electron microscopy of microcracking about indentations in aluminium oxide and silicon carbide,** *J. Mater. Sci.* **10,** 1275-1284 (1975).

Key words: brittle solids; dislocation networks; electron microscopy; healing; indentations; microcracking; moiré patterns.

Transmission electron microscopy is used to examine the nature of microcracking about small-scale indentations in two highly brittle solids, sapphire and carborundum. The observed crack geometry is discussed in terms of an earlier model of indentation fracture beneath a point force, in which both loading and unloading half-cycles contribute to the crack growth. The residual interfaces are generally found to exhibit moiré fringe contrast, and occasionally to contain dislocation networks. These observations are discussed in relation to spontaneous closure and healing mechanisms, and the associated "lattice mismatch" is estimated at about one part in a thousand. It is suggested that cleavage steps comprise the main source of obstruction to lattice restoration across the interfaces. Mechanical and thermal treatments of the indented specimens are found to influence the extent of the residual cracking. Some practical implications concerning the strength degradation of brittle solids are discussed.

Holmer, C. I., **Estimation of sound power in the free field over a reflecting plane. Errors associated with far field and near field measurements,** *Proc. Noise-Con 75, Gaithersburg, Md., Sept. 15-17, 1975,* pp. 429-438 (Noise Control Foundation, Poughkeepsie, N.Y., 1975).

Key words: error of sound power; far-field power; near-field power; sound power estimation.

A review is presented of several sound power estimation procedures for free field above a reflecting plane condition. Particular emphasis is placed on potential sources of measurement error. Both near field and far field procedures are included in the discussion. Estimates of magnitudes of individual sources of error are discussed.

Hosler, W. R., Capps, W., Plante, E. R., **Some physical and chemical properties of coal slags,** *Proc. 14th Symp. on Engineering Aspects of Magnetohydrodynamics, The Univ. of Tennessee Space Institute, Tullahoma, Tenn., April 8-10, 1974,* pp. IV.7.1-IV.7.5 (1974).

Key words: coal slags; MHD; thermionic emission; vaporization; viscosity.

Thermionic emission, viscosity and vaporization studies of molten synthetic coal slags are described. Thermionic emission of a combustor type slag was determined in 1 atm air, 1 atm O_2, and 0.01 atm O_2 in N_2. Sizeable flows of electrons and positive ions were detected at temperatures as low as 1200-1300 °C. Viscosities of one real and several synthetic slags are shown between 1585 °C and their liquidus temperature (1250-1350 °C). These melts are quite fluid in this temperature range. From the modulated-beam mass spectrometer studies it appears that initial stages of evaporation of some synthetic melts are characterized by a nonequilibrium process involving a slower than expected decomposition of Fe_3O_4. SiO evaporation from the slag solution proceeds at a rate consistent with the SiO_2 in solution having an activity near unity.

Howell, B. F., Simmons, J. H., Haller, W., **Loss of chemical resistance to aqueous attack in a borosilicate glass due to phase separation,** *Am. Ceram. Soc. Bull.* **54,** No. 8, 707-709 (Aug. 1975).

Key words: borosilicate glass; chemical durability; phase separation.

The chemical durability of a borosilicate glass was measured by a powder extraction test (ASTM C 225-68). It was found that a progressive decrease in chemical durability occurred during prolonged heat treatments at temperatures ranging from 29 to 84° below the immiscibility temperature. Following these extreme thermal histories, which are not normally encountered in standard forming and annealing conditions, the amount of extractable alkali increased by as much as 20 fold.

Hruska, G. R., Koidan, W., **Free-field method for sound-attenuation measurement,** *J. Acoust. Soc. Am.* **58,** No. 2, 507-509 (Aug. 1975).

Key words: acoustic centers; attenuation of sound; sound absorption.

A free-field method is described for measuring the attenuation of sound at ultrasonic frequencies. It makes use of the systematic deviation from the inverse square law caused by attenuation when a sound receiver is drawn away from a sound source. Measurements of attenuation from 20 to 100 kHz, made in air in a small anechoic chamber under ambient environmental conditions, were in good agreement with theoretical calculations. The sum of the distances between the acoustic centers of the transducers and the vibrating elements is obtained as a by-product of the procedure.

Huebner, R. H., Celotta, R. J., Mielczarek, S. R., Kuyatt, C. E., **Apparent oscillator strengths for molecular oxygen,** *ANL-*

75-3, Part 1, *Biology and Medicine UC-48*, pp. 49-52 (Argonne National Laboratory, Radiological and Environmental Research Division, Argonne, Ill., July 1973-July 1974).

Key words: electron; energy loss; molecular oxygen; oscillator strengths; spectra.

The oscillator strengths for molecular oxygen are determined from electron energy loss measurements and are compared to the available optical data.

Huebner, R. H., Celotta, R. J., Mielczarek, S. R., Kuyatt, C. E., **Apparent oscillator strengths for nitrous oxide,** (Proc. IX Int. Conf. on Physics of Electronic and Atomic Collisions, Seattle, Wash., July 24-30, 1975), Abstract in *Electronic and Atomic Collisions*, J. S. Risley and R. Geballe, Eds., **2,** 1043-1044 (University of Washington Press, Seattle, Wash., 1974).

Key words: electron energy loss; low energy electron impact; N_2O; oscillator strengths.

The apparent oscillator strengths for N_2O in the energy loss range of 4.5 to 14 eV are presented at 0.01 eV intervals. Measurements were made with an incident energy of 100 eV and at a scattering angle of within 20 milliradians of the incident direction.

Huebner, R. H., Celotta, R. J., Mielczarek, S. R., Kuyatt, C. E., **Dipole oscillator-strength distributions derived for several hydrocarbons from electron energy-loss spectra,** *ANL-75-3*, Part 1, *Biology and Medicine UC-48*, pp. 45-48 (Argonne National Laboratory, Radiological and Environmental Research Division, Argonne, Ill., July 1973-July 1974).

Key words: electron; energy loss; oscillator strengths; spectra.

A summary is presented of the technique used to determine dipole oscillator strength values from electron energy loss spectra. Data on benzene is presented as an example.

Huebner, R. H., Fergurson, C. H., Celotta, R. J., Mielczarek, S. R., **Apparent oscillator-strength distributions derived from electron energy-loss measurement: Methane and *n*-hexane,** *ANL-75-3*, Part 1, *Biology and Medicine UC-48*, pp. 41-44 (Argonne National Laboratory, Radiological and Environmental Research Division, Argonne, Ill., July 1973-July 1974).

Key words: electron; energy loss; methane; *n*-hexane; oscillator strengths; spectra.

The derivation of oscillator strengths from electron energy loss spectra are discussed and results obtained for methane and *n*-hexane are compared to optical data.

Huebner, R. H., Fergurson, C. H., Celotta, R. J., Mielczarek, S. R., **Apparent oscillator strength distributions derived from electron energy-loss measurements: Methane and *n*-hexane,** *Proc. IVth Int. Conf. on Vacuum-Ultraviolet Radiation Physics, Hamburg, Germany, July 22-26, 1974*, Article 111, 4 pages (1974).

Key words: electron; electron scattering; energy loss; methane; *n*-hexane; oscillator strength.

Electron energy loss spectra were obtained for methane from 8.0 to 14.0 eV and for *n*-hexane from 0–20 eV with the NBS Model AN-1 electron impact spectrometer. These data were obtained for 100 eV incident electrons scattered within about 20 milliradians of the forward direction. Relative oscillator strengths were derived from the data by correcting for the finite angular acceptance of the apparatus with the assumption that the generalized oscillator strength can be approximated by its optical oscillator strength limit. The apparent oscillator strength distributions are placed on an absolute scale by normalization at one energy to a df/dE value determined optically. Comparisons of these results with available photoabsorption and other electron impact measurements will be presented.

Hughes, E. E., **Development of standard reference materials for air quality measurement,** (Proc. Int. Instrumentation-Automation Conf. & Exhibit, New York, N.Y., Oct. 28-31), *ISA Reprint 74-704*, 13 pages (Instrument Society of America, Pittsburgh, Pa., 1974).

Key words: air pollution; carbon monoxide; gas analysis; gas standards; nitric oxide; nitrogen dioxide; sulfur dioxide.

The National Bureau of Standards is engaged in a continuing program involving gaseous Standard Reference Materials for air pollution measurements. Preparation of such materials requires definition of the stability, homogeneity and accuracy of the samples. This information is obtained by long-term studies of the gas systems, by development of absolute methods of analysis and by analysis of large numbers of samples prepared in bulk. The results of studies, extending over several years, of low concentration of carbon monoxide in nitrogen and nitric oxide in nitrogen are reported. Over one thousand samples of these materials have been analyzed and the stability with time and the within-batch homogeneity have been characterized. Accuracy is achieved by use of gravimetric standards and with dynamic dilution systems. Accuracy attainable by either method is described.

The use of permeation tubes of sulfur dioxide and nitrogen dioxide is necessary in some situations because of the reactivity of the gases. Data covering the stability and accuracy of these devices has been collected over a period of several years.

Huie, R. E., Herron, J. T., **Reactions of atomic oxygen (O^3P) with organic compounds,** Paper in *Progress in Reaction Kinetics*, K. R. Jennings and R. B. Cundall, Eds., **8,** No. 1, Part 1, 1-80 (Pergamon Press, Great Britain, 1975).

Key words: atomic oxygen; gas phase; kinetics; mechanism; organic compounds; rate constants.

The reactions of atomic oxygen (O^3P), in the gas phase, with organic compounds are reviewed. The various techniques used in these studies are discussed critically. The kinetics and mechanisms of the reactions of atomic oxygen with organic compounds are discussed in detail.

Huie, R. E., Herron, J. T., **Temperature dependence of the rate constants for reactions of ozone with some olefins,** (Proc. Symp. on Chemical Kinetics Data for the Upper and Lower Atmosphere, Warrenton, Va., Sept. 15-18, 1974), *Int. J. Chem. Kinet. Symp.*, No. 1, 165-181 (John Wiley & Sons, Inc., New York, N.Y., 1975).

Key words: air pollution; kinetics; mass spectrometry; olefin; ozone; photochemical smog; rate constant.

The temperature dependence of the rate constants for the reactions of ozone with some olefins has been studied using a stopped-flow reactor in conjunction with a beam sampling mass spectrometer. The effect of molecular oxygen on the measured rate constants was studied, and it was concluded that molecular oxygen scavenges free radical species which could further react with ozone. Rate constants, measured in the presence of molecular oxygen, are as follows (in units of $cm^3\ mol^{-1}\ s^{-1}$): $\log k$ (1-butene) $= (9.247 \pm 0.033) - (1686 \pm 20)/2.303T$; $\log k$ (2-methylpropene) $= (9.281 \pm 0.026) - (1671 \pm 23)/2.303T$; $\log k$ (cis-2-butene) $= (9.272 \pm 0.087) - (956 \pm 54)/2.303T$; $\log k$ (*trans*-2-butene) $= (9.555 \pm 0.069) - (1051 \pm 43)/2.303T$; $\log k$ (2-methyl-2-butene) $= (9.582 \pm 0.119) - (826 \pm 78)/2.303T$; and $\log k$ (2, 3-dimethyl-2-butene) $= (9.230 \pm 0.237) - (294 \pm 196)/2.303T$.

A good linear correlation is found between the activation energy for the reaction and the ionization potential of the olefin.

Ito, J., **Synthetic indium silicate and indium hydrogarnet,** *Am. Mineral.* **53,** 1663-1673 (Sept.-Oct. 1968).

Key words: crystal chemistry; flux growth; garnet; hydrogarnet;

indium silicates; inorganic synthesis; solid solubility silicates; x-ray powder analysis.

The following indium silicates were synthesized hydrothermally and in air: indium grossular, $Ca_3In_2Si_3O_{12}$; indium aegirine, $NaInSi_2O_6$; indium beryl, $Be_3In_2Si_6O_{18}$; indium thortveitite, $In_2Si_2O_7$; indium melanotekite, $Pb_2In_2Si_2O_9$; and strontium indium hydrogarnet, $Sr_3In_2(OH)_{12}$.

Complete solid solubility was found between ferric iron and indium silicates and hydrogarnet end members. Single crystals of indium aegirine up to 2 cm in length were grown in a Na_2WO_4 flux by slow cooling.

The crystal chemical and geochemical behavior of trivalent indium is similar to that of scandium. The ionic radius of trivalent indium of 0.81 Å given by Pauling is confirmed.

Iverson, W. P., **Anaerobic corrosion: Metals and microbes in two worlds,** *Dev. Ind. Microbiol.* **16,** 1-10 (1975).

Key words: anaerobic corrosion; cathodic depolarization theory; Charles Thom Award; *Desulfovibrio desulfuricans*; hollow whiskers; mechanism; microbial corrosion; mild steel; oxidizing agent; Schreibersite; sulfate-reducing bacteria; Vivianite.

Charles Thom Award address presented by the author at the General Meeting of the Society for Industrial Microbiology held at Memphis State University, 11-16 August 1974. (The Thom Award honors the first president of the Society for Industrial Microbiology. The later Charles Thom was a noted microbiologist who worked for the U.S. Department of Agriculture and his research on molds helped to produce many of today's antibiotics).

The author's investigations of the mechanism of anaerobic corrosion by sulfate-reducing bacteria, which led to the observation that a marine strain produced extracellularly, a strong oxidizing agent which caused extensive corrosion of mild steel under anaerobic conditions, are detailed. The formation of hollow whiskers, structures which resemble fungal mycelium, by the reaction of ferrocyanide or ferricyanide on metals are described.

Jacox, M. E., Milligan, D. E., **Matrix isolation study of the infrared spectrum of thioformaldehyde,** *J. Mol. Spectrosc.* **58,** No. 1, 142-157 (1975).

Key words: CH_3S; CH_3SH; dimethyldisulfide; infrared spectrum; matrix isolation; pyrolysis; *s*-trithiane; thioformaldehyde; ultraviolet photolysis; vacuum ultraviolet photolysis.

H_2CS has been trapped in argon and nitrogen matrices at 14 K as a product of the pyrolysis of *s*-trithiane or $(CH_3S)_2$ and of the ultraviolet or vacuum ultraviolet photolysis of CH_3SH. A small concentration of H_2CS has also been observed upon vacuum ultraviolet photolysis of a mixture of CH_4 and H_2S in an argon matrix. The isotopic data support the assignment of absorptions at 993 and at 1063 cm^{-1} to the out-of-plane deformation and the C=S stretching fundamentals of H_2CS. Absorptions in the CH stretching region which were assigned to H_2CS in an earlier gas-phase study were confirmed in the matrix experiments. Studies of the vacuum ultraviolet photolysis of CD_3SH have provided information on the mechanism of the photolysis process.

Jennings, D. A., Evenson, K. M., Jimenez, J. J., **New CO_2 pumped CW far-infrared laser lines,** *IEEE J. Quantum Electron.* **QE-11,** No. 8, 637 (Aug. 1975).

Key words: IR; laser, optically pumped; waveguide cavity.

A single-frequency CW CO_2 laser has been used to pump ethyl alcohol, methyl chloride, ethyl chloride, and methylene chloride, generating 8 new CW far-infrared (FIR) laser lines from 254 to 1700 μm.

Johnson, C. R., ***D*-stability and real and complex quadratic forms,** *Linear Algebra and Appl.* **9,** 89-94 (1974).

Key words: *D*-stable matrix; positive diagonal matrix; quadratic forms; spectrum.

The problem of characterizing the class of *D*-stable matrices has remained unsolved since its suggestion in a paper by Arrow and McManus [1] in 1958. In this note we present a necessary condition involving real quadratic forms which is not sufficient and a sufficient condition involving complex quadratic forms which is not necessary.

Johnson, C. R., **Inequalities for a complex matrix whose real part is positive definite,** *Trans. Amer. Math. Soc.* **212,** 149-154 (1975).

Key words: eigenvalues; Hadamard inequality; positive definite; real part.

Denote the real part $A \in M_n(C)$ by $H(A) = 1/2(A + A^*)$. We provide dual inequalities relating $H(A^{-1})$ and $H(A)^{-1}$ and an identity between two functions of A when A satisfies $H(A) > 0$. As an application we give an inequality (for matrices A satisfying $H(A) > 0$) which generalizes Hadamard's determinantal inequality for positive definite matrices.

Johnson, C. R., **The Hadamard product of A and A^*,** *Pacific J. Math.* **51,** No. 2, 477-481 (1974).

Key words: angular field of values; diagonal; diagonally dominant; field of values; Gersgorin; Hadamard product; Hermitian; positive definite; spectrum.

Coefficient-wise multiplication was introduced by Hadamard and has been studied for certain square matrices by I. Schur and later authors. For $A \epsilon M_n(C)$, the n by n complex matrices, this paper examines the Hadamard product of A and A^*. Upper estimates are given for the largest characteristic root of this necessarily Hermitian product, and three conditions on A sufficient for the product to be positive definite are presented.

Jones, F. E., **Magnetic retention of evaporation or sputtering masks (Abstract only),** *Rev. Sci. Instrum. Letter to Editor* **46,** No. 6, 793 (June 1975).

Key words: evaporation; magnetic retention; masks; sputtering; substrates; thin films.

The "use of a magnet to clamp a magnetic metal mask to the substrate during sputtering" of thin film patterns has been described by Ingle. A similar technique was described previously by Jones and Castle in this journal and in a patent.

Kahles, J. F., Field, M., Young, R. D., Whitehouse, D. J., **Survey on surface roughness and surface integrity requirements for machined components,** *CIRP Annals* **23,** No. 1, 185-186 (1974).

Key words: CIRP; surface; surface finish; surface integrity; surface questionnaire; surface survey.

CIRP Committee "S" has developed a survey to determine surface roughness and surface integrity requirements for machined components. Specifically, the survey is designed to develop a comprehensive international response concerning the status of surface technology as related to all types of material removal processes, and the surface conditions produced which affect parts performance. The design of the survey is discussed, the status is outlined, and a partial list of survey questions is presented.

Karo, A., Krauss, M., Wahl, A. C., **Recent applications of the multiconfiguration self-consistent field method to polarizabilities, excited states, Van der Waals forces, and triatomic surfaces,** (Proc. Int. Symp. on Atomic, Molecular and Solid-State Theory and Quantum Biology, Sanibel Island, Fla., Jan.

21-27, 1973), *Int. J. Quantum Chem. Symp.* No. 7, 143-159 (John Wiley & Sons, New York, N.Y., 1973).

Key words: CO; energy surface; F_2; hydrides; LiH_2; MC-SCF; O_2^-; O_3; polarizability; Van der Waals.

In this brief presentation recent and new applications of the multiconfiguration self-consistent field (MCSCF) method to the direct calculation of atomic polarizabilities [1,2], excited states of the same symmetry [3-5], Van der Waals forces [6-10], and triatomic energy surfaces [11-12] are presented.

These calculations utilizing the BISON [14] system, have been carried out over the past several years as part of collaborative research between Argonne National Laboratory, the National Bureau of Standards, and the Lawrence Livermore Laboratory.

Kashiwagi, T., **A radiative ignition model of a solid fuel,** *Combust. Sci. Technol.* **8,** 225-236 (1974).

Key words: ignition; ignition boundary; solid fuel.

A theoretical model describing radiative ignition of a solid fuel is constructed and is numerically analyzed. The model includes the effects of gas phase reaction and a finite value of the absorption coefficient of the solid (in-depth absorption of incident radiation). It is found that the gas phase reaction must be included in the model in order to understand radiative ignition of a solid fuel and to find its ignition boundary. The in-depth absorption of the incident radiation by a solid fuel significantly affects the ignition delay time. The results indicate that there is a finite range of values for pyrolysis or gas phase reaction activation energy for which ignition will occur. This finding has a direct bearing on efforts to reduce material ignitability.

Kashiwagi, T., **A study of flame spread over a porous material under external radiation fluxes,** *Proc. Fifteenth Symp. (International) on Combustion, Tokyo, Japan, Aug. 25-31, 1974,* pp. 255-265 (The Combustion Institute, Pittsburgh, Pa., 1974).

Key words: flame spread; floor covering materials; ignition.

Characteristics of horizontal flame spread over the surface of a porous material, a carpet in this study, are studied experimentally and theoretically under various external radiant fluxes ($0.1-0.27$ cal/cm^{2}sec). It is observed that the size of flame is increased significantly by increasing the external radiant flux. This increases the radiative heat feedback from the flame so that it becomes comparable to or greater than the convective heat feedback. The external radiation can also cause an unstable motion of the flame front. This effect is probably due to the production of volatile pyrolysis products ahead of the flame front instead of under it. The theoretical calculation indicates that the thermal emission loss from the heated sample is significant and the internal radiation in the porous material must be included in the model.

Kashiwagi, T., **Experimental observation of flame spread characteristics over selected carpets,** *J. Fire Flammability Consumer Product Flammability* **1,** 367-389 (Dec. 1974).

Key words: flame spread; floor covering material; heat release rate; ignition.

A small laboratory size experiment was used to observe the characteristics of flame spread over various carpets under various constant external radiant fluxes ($0.10 \sim 0.27$ cal/cm^2 sec or $0.4 \sim 1.15$ w/cm^2). The results indicate that a minimum radiant flux is necessary to sustain flame spread over a carpet surface for the carpets tested. By increasing radiant flux, the flame spread velocity increases sharply and can reach several sm/sec. At a high external radiant flux, preheating time is the controlling factor for flame spread velocity. Ignitability, weight loss, and net heat release rate were also measured under various radiant fluxes. The effect of an underlayment on ignitability, flame spread speed, weight loss, and net heat release rate, was also observed for various carpets.

Kaufman, V., Sugar, J., **Spectrum of six-times ionized rhenium (Re VII),** *Phys. Rev. A* **12,** No. 4, 1402-1403 (Oct. 1975).

Key words: energy levels; rhenium; spectrum.

Six terms of the $4f^{14}5s^25p^6(^1S_0)nl$ doublet system of Re VII have been found, including $nl = 5d$, $5f$, $6s$, $6p$, $6d$, and $7s$. Thirteen spectral lines were classified in this system of levels. The partially resolved hfs of the $6s$-$6p$ multiplet was used to derive a value for the hyperfine splitting of the $6s$ level in agreement with a predicted value. The ionization energy of Re VII derived from the ns series is 82.74 ± 0.06 eV.

Kidnay, A. J., Miller, R. C., Parrish, W. R., Hiza, M. J., **Liquid-vapour phase equilibria in the N_2-CH_4 system from 130 to 180 K,** *Cryogenics* **15,** No. 6, 531-540 (Sept. 1975).

Key words: Henry's constants; liquid-vapor phase equilibria; methane; nitrogen.

Isothermal composition measurements for both the equilibrium liquid and vapour phases have been determined for the nitrogen + methane system at eight temperatures between 112.00 and 180.00 K, and at pressures from 1 to 49 atm (1 to 50 bar). The internal consistency of these data is checked by comparing experimental and calculated thermodynamically consistent vapour phase compositions. Derived Henry's constants are used to provide a comparison between these data and those of other investigators.

Klein, W., **Behavior of distribution functions in the thermodynamic limit,** *J. Math. Phys.* **15,** No. 8, 1181-1185 (Aug. 1974).

Key words: distribution functions; finite volumes; Kirkwood Salsburg equation; perturbation expansion; strip operator; thermodynamic limit.

Ruelle has proven that the solutions of the Kirkwood-Salsburg equation for a finite volume Λ become, in the limit as $\Lambda \to \infty$, the solutions to the Kirkwood-Salsburg equation for an infinite volume, i.e.,

$$\lim_{\Lambda-\infty}\rho_\Lambda \to \rho + \lim_{\Lambda-\infty}\epsilon(\Lambda), \lim_{\Lambda-\infty}\epsilon(\Lambda) \to 0.$$

The form of ϵ is not obtained. We show that for the first order contribution to the solution of the Kirkwood-Salsburg equations obtained via a perturbation scheme developed in an earlier paper that

$$\epsilon(\Lambda) \leq \lim_{R-\infty}\epsilon^{-k'aR},$$

where k'_a is a positive real constant which can be specified and R is the minimum distance from the container walls to the particles of the system.

Krasny, J. F., Winger, J. H., **Current status of flammability test development at the National Bureau of Standards,** *Proc. 8th Annual Meeting Information Council on Fabric Flammability, New York, N.Y., Dec. 5, 1974,* 5 pages (1974).

Key words: apparel; carpets; curtains; draperies; fabrics; flammability; garments; test methods; textiles; upholstered furniture.

Tests for the flammability of textile items, that are presently under development at NBS, are described.

Kusch, P., Hessel, M. M., **Perturbations in the $A\ ^1\Sigma_u^+$ state of Na_2,** *J. Chem. Phys.* **63,** No. 9, 4087-4088 (Nov. 1, 1975).

Key words: alkali dimer; magnetic rotation; molecular constants; perturbations; sodium molecule; spectroscopy.

Perturbations have been observed in the $A\ ^1\Sigma_u^+$ state of the diatomic sodium molecule. For each rotational perturbation three discontinuities have been observed. This indicates the $^1\Sigma$ state is perturbed by a $^3\Pi$ state.

Kuyatt, C. E., **Electron energy analyzer design,** *Proc. 31st An-*

nual Meeting Electron Microscope Society of America, New Orleans, La., Aug. 13-17, 1973, C. J. Arceneaux, Ed., pp. 280-281 (Claitor's Publ. Div., Baton Rouge, La., 1973).

Key words: angular aperture; computer optimization of electron optics; electron beam transport; electron energy analyzers; field aperture.

The design of electron energy analyzers is discussed, with special emphasis on the electron optical system used to transport electrons from the source to the energy dispersing element.

Lang, W. W., Flynn, D. R., **Noise power emission level for product designation,** *Noise Control Eng.* **4, No. 3, 108-113 (May-June 1975).**

Key words: acoustics; machinery noise; noise; sound; sound power.

A brief discussion is given of some of the advantages of using sound-power rather than sound pressure at a particular location to describe the noise emission from a particular source. To avoid confusion between sound pressure levels and sound power levels, both of which are usually expressed in decibels, it is proposed that in communications with users, the sound power levels of stationary sources be expressed in terms of Noise Emission Number, which is numerically equal to the A-weighted sound power level expressed in bels rather than decibels.

Lashof, T. W., **A calibration check service for paper and board test instruments,** *TAPPI* **57,** No. 1, 5 (Jan. 1974).

Key words: collaborative reference program; interlaboratory testing; laboratory performance; paper test methods.

Brief editorial description of NBS-TAPPI Collaborative Reference Program, including participants, advantages, methods included, procedure, and related programs.

Laufer, A. H., Bass, A. M., **Mechanism and rate constant of the reaction between methylene and methyl radicals,** *J. Phys. Chem.* **79,** No. 16, 1635-1638 (1975).

Key words: combination; flash photolysis-gas chromatography; methyl; methylene; radicals; rate constant.

The chemistry of the reaction between methyl and triplet methylene radicals has been examined by means of flash photolysis of azomethane and ketene followed by gas chromatographic analysis of the hydrocarbon products. Using the combination rate constant of triplet $CH_2 = 5.3 \times 10^{-11}$ cm^3 molecule^{-1} sec^{-1} and the combination of $CH_3 = 9.5 \times 10^{-11}$ cm^3 molecule^{-1} sec^{-1}, a value of $1.0 \pm 0.1 \times 10^{-10}$ cm^3 molecule^{-1} sec^{-1} for the reaction $^3CH_2 + CH_3 \rightarrow C_2H_5^* \rightarrow C_3H_4 + H$ has been determined.

Laufer, A. H., Bass, A. M., **Rate constants of the combination of methyl radicals with nitric oxide and oxygen,** *Int. J. Chem. Kinet.* **VII,** No. 5, 639-648 (1975).

Key words: combination; kinetics; methyl; nitric oxide; oxygen; rate constants.

Rate constants for the combination of methyl radicals with NO and O_2 have been measured by flash photolysis of azomethane coupled with product analysis by gas chromatography. Values of the rate constants have been obtained over the pressure region from 50 to 700 torr with He, N_2, and Ar as quenching molecules.

The high-pressure limits were obtained through an RRKM model calculation and were found to be

$$CH_3 + NO + M \rightarrow CH_3NO + M$$

$$k_\infty = 3.2 \times 10^{-11} \text{ cm}^3/\text{molec} \cdot \text{sec}$$

$$CH_3 + O_2 + M \rightarrow CH_3O_2 + M$$

$$k_\infty = 1.7 \times 10^{-12} \text{cm}^3/\text{molec} \cdot \text{sec}$$

The rate constants were measured relative to the methyl combination reaction k_1 with $k_1 = 9.5 \times 10^{-11}$ cm^3/molec · sec. The RRKM model suggests $D_0(CH_3 - O_2) = 32 \pm 3$ kcal/mole.

LaVilla, R. E., **The O $K\alpha$ and C $K\alpha$ emission and O K absorption spectra from O_2 and CO_2. IV,** *J. Chem. Phys.* **63,** No. 6, 2733-2737 (Sept. 15, 1975).

Key words: molecular CO_2; molecular oxygen; O and C $K\alpha$ x-ray emission spectra; O K absorption spectra.

The oxygen and carbon $K\alpha$ emission and oxygen K absorption spectra of the molecular gases O_2 and CO_2 are reported. The spectra were obtained on two different spectrometers, both with single flat crystal configurations. All the emission spectra were excited by direct electron bombardment and are in fair agreement with an interpretation based on allowed electric dipole transitions between single vacancy states and molecular orbital theory for the molecules. The oxygen K absorption of O_2 and CO_2 is dominated by a strong resonance peak before the K-shell threshold which is interpreted as being due to the transition of oxygen K electrons to the first unoccupied valence orbital of the respective molecules.

Leasure, W. A., Jr., Bender, E. K., **Tire-road interaction noise,** *J. Acoust. Soc. Am.* **58,** No. 1, 39-50 (July 1975).

Key words: acoustics; noise (sound); tire noise; transportation noise.

The relative importance of tire noise to overall vehicle noise is established. A general description is then given of the tire engineering process and of tire structures. The important parameters influencing tire noise are discussed, based on presently available data, followed by an identification of unknown and contradictory areas. The basic mechanisms of tire-noise generation, although not well understood, are investigated largely from a theoretical viewpoint. Areas for future research and development are identified based on gaps in the existing physical data base and a rather primitive level of understanding of noise-generating mechanisms.

Leasure, W. A., Jr., Mathews, D. E., Cadoff, M. A., **Automobile tire noise: Results of a pilot study and review of the open literature,** *Report DOT/TST-76-4,* 75 pages (Office of Noise Abatement, Department of Transportation, Washington, D.C., Aug. 1975). (Available from the National Technical Information Service, Springfield, Va. 22161.)

Key words: acoustics; automombile; noise (sound); tire noise; transportation noise.

Automobiles, the primary mode of transportation in the United States, contribute significantly to the noise environment due to the large number in operation. In this report, one aspect of automobile noise is discussed; namely, the contribution to overall vehicle noise resulting from the interaction of the tires with the road surface. The results of this pilot study, which investigated the influence of selected parameters on automobile tire noise levels, in conjunction with a review of the open literature, serve as the basis for comparison of parametric trends between truck (for which an extensive noise data base exists) and automobile tires. As was the case with trucks, vehicle speed, road surface characteristics and tread design are major factors affecting automobile tire noise. The effect of pavement surface is more significant for automobile tires than for trucks since the texture within the tire-road interaction zone is on the same scale as the tread element spacing typical of passenger car tires. Load and wear, significant factors for truck tires, do not affect automobile tires as much due to the fact that the majority of automobile tires utilize rib tread designs. On the basis of the limited data available in the literature, factors such as inflation pressure, number of plies, tire dimensions, tire cord material, etc., do not appear to be significant factors affecting automobile tire noise.

Lechner, J. A., **Applying statistics in criminalistics,** (Proc. 8th

597-633 O - 76 - 8

Annual Crime Countermeasures Conf., Lexington, Ky., April 16-19, 1974). Paper in *Proc. 1974 Carnahan and Int. Crime Countermeasures Conf., UKY BU* **105,** 113-123 (Aug. 1974).

Key words: acceptance tests; confidence intervals; criminalistics; errors; goodness of fit; normal distribution; significance tests; standards; statistics.

This paper is intended to tell "why-we-do-it-this-way." After preliminary remarks on randomness, errors, and distribution functions, various techniques of statistical analysis are discussed. These include significance tests, confidence intervals, and goodness of fit test. Finally, several examples will be discussed: 1) Performance requirements for breath alcohol testers; 2) Bivariate discrimination for gunshot residue detection; and 3) Matching "profiles," e.g., trace element analyses or the output of a speech frequency analyzer.

Ledbetter, H. M., Weston, W. F., Naimon, E. R., **Low temperature elastic properties of four austenitic stainless steels,** *J. Appl. Phys.* **46,** No. 9, 3855-3860 (Sept. 1975).

Key words: bulk modulus; chromium alloys; compressibility; Debye temperature; Doring effect; elastic constants; iron alloys; magnetic transition; nickel alloys; Poisson's ratio; pulse-echo method; sound velocity; Young's modulus.

The elastic properties of four austenitic stainless steels—AISI 304, AISI 310, AISI 316, and A286—are reported over the temperature range 300-4 K. These properties include longitudinal modulus, shear modulus, Young's modulus, bulk modulus (reciprocal compressibility), Poisson's ratio, and elastic Debye temperature. Elastic constants were determined from measurements of longitudinal and transverse soundwave velocities using an ultrasonic (10 MHz) pulse-superposition method. Measurements were made in the absence of a magnetic field; these alloys undergo paramagnetic-to-antiferromagnetic transitions at low temperatures. For all four alloys, the shear modulus behaves regularly with respect to temperature. The other elastic constants, all of which have a dilatational component, decrease anomalously at temperatures below 80 K. The largest anomaly, about 3 percent, is in the bulk modulus of the 304 alloy; this modulus is lower at 0 than at 300 K. Results are interpreted on the basis of the Döring effect, which results from a large volume magnetostriction in the magnetic phase. This may be the first report of a Döring effect in antiferromagnetic materials.

Lee, T. G., Huggett, C., **Interlaboratory evaluation of ASTM E 84-70 tunnel test applied to floor coverings,** *J. Test. Eval.* **3,** No. 1, 3-14 (1975).

Key words: ASTM E84; building materials; carpets; fire tests; flame spread tests; floor coverings; interlaboratory evaluation; smoke measurement; tunnel test.

Results of an interlaboratory evaluation of the American Society for Testing and Materials (ASTM) Test for Surface Burning Characteristics of Building Materials (E 84-70), involving eleven laboratories and nine materials including four carpets, are reported. Data on flame spread, smoke, and fuel contribution were analyzed statistically to determine the reproducibility and repeatability of the test method. Selected physical characteristics of each tunnel are tabulated and compared relative to specifications in the test method. The between-laboratory coefficient of variation (reproducibility) in flame spread classification (FSC) was found to range from 7 to 29 percent for the four carpets and from 18 to 43 percent for the other materials tested. The between-laboratory coefficients of variation for smoke developed and fuel contribution ranged from 34 to 85 percent and from 22 to 117 percent, respectively, for all materials tested. The causes of higher variability in smoke and fuel contribution measurement between laboratories are not definitely known but may reasonably be attributed to variations in tunnel construction, instrumentation, and operation in different laboratories.

Lewis, D. C., **On the determination of the minority carrier lifetime from the reverse recovery transient of *pn*R diodes,** *Solid-State Electron.* **18,** 87-91 (1975).

Key words: carrier lifetime; reverse recovery; semiconductor diodes.

The determination of the minority carrier lifetime of *pn* diodes with abrupt junctions and recombination (R) contacts is discussed. It is confirmed that the base transit time of diodes with sufficiently small base widths (less than approximately three minority carrier diffusion lengths) affects the reverse recovery transient and that large error can be introduced if the minority carrier lifetime of a diode with a small base width is computed using an expression which was derived for diodes with an infinite base width. Approximations to the general expression for the minority carrier lifetime as a function of the storage time and base width are developed, and the errors associated with their use are analyzed. In addition the effect of measurement errors on the determination of lifetime in short base diodes is discussed.

A procedure is described which can be used to compute the minority carrier lifetime of *pn*R diodes in which the ratio of the base width to the minority carrier diffusion length is larger than some small number. The applicability of the procedure and the approximations which are developed are a function of the ratio of the diode base width to the minority carrier diffusion length (W/L), and the forward to reverse current ratio (I_f/I_r) at which the experimental measurements are made. An example is given which shows that less than 1 percent error is introduced in the computed lifetime by the approximations if the lifetime is computed from measurements made at $I_f/I_r = 4$ and 8 for diodes such that $W/L > 2 \times 10^{-2}$.

Lide, D. R., Jr., **Preface,** *Proc. Conf. Critical Evaluation of Chemical and Physical Structural Information, Dartmouth College, Hanover, N.H., June 24-29, 1973,* D. R. Lide, Jr. and M. A. Paul, Eds., pp. iii-vii (National Academy of Sciences, Washington, D.C., 1974).

Key words: critical evaluation; crystal structure; data analysis; molecular structure.

The motivations for holding a conference on structural information are discussed. The use of structural data in chemistry, physics and related disciplines is reviewed. The major points brought out during the conference are summarized.

Lide, D. R., Jr., **The NSRDS experience,** (Proc. 4th Int. CODATA Conf. on Generation, Compilation, Evaluation and Dissemination of Data for Science and Technology, Tsakhcadzor, U.S.S.R., June 24-27, 1974), *CODATA Bull.* **14,** 6-9 (CODATA Secretariat, Paris, France, 1974).

Key words: data; Standard Reference Data Program; well-defined, measurable properties.

The Standard Reference Data Program deals primarily with physical and chemical property data. The properties covered are well-defined, measurable properties and the systems include pure substances and mixtures that can be adequately characterized. There is a strong emphasis on critical evaluation of the data by experienced scientists. The program is managed by the National Bureau of Standards under a mandate from the Congress of the United States to make critically evaluated reference data readily available to scientists, engineers and the general public.

Lide, D. R., Jr., **The Standard Reference Data System,** *Chem. Eng. Prog.* **67,** No. 11, 77-78 (Nov. 1971).

Key words: critically evaluated numerical data; National Standard Reference Data System; physical sciences.

The National Standard Reference Data System (NSRDS)

represents an effort to provide critically evaluated numerical data in the physical sciences. It is a decentralized program coordinated from the National Bureau of Standards, but enlisting the help of experts throughout the country. Activities of interest to chemical engineers are discussed.

Loevinger, R., **Dosimetry standards for fast electrons,** (Proc. XIII Int. Congress of Radiology, Madrid, Spain, Oct. 15-20, 1973), *International Congress Series No. 339*, **2**, 467-471 (Excerpta Medica, Amsterdam, The Netherlands, 1973).

Key words: absorbed dose; calorimeter; dosimetry; electrons; ionization chamber; radiation standard.

Graphite calorimeters are being developed at several national standards laboratories to serve as absorbed-dose standards for fast electron beams for radiation therapy. Two such calorimeters have been constructed at the National Bureau of Standards, and compared to ionization chambers of the same size and shape by determining the quotient of the calorimeter response by the ionization chamber response. That quotient will be the factor used to convert the response of an ionization chamber calibrated in absorbed-dose units in a cobalt-60 beam to absorbed-dose units in high-energy electron beams.

Lovas, F. J., **Application of microwave spectroscopy to chemical analysis,** *Anal. Instrum.* **12**, 103-109 (1974).

Key words: applications; chemical analysis; microwave; qualitative analysis; quantitative analysis; rotational spectra.

Traditional analytical techniques have been successfully employed on a great variety of systems for identifying stable reaction products as well as for purity analysis and reaction efficiency. However, most analytical techniques generally can only be applied to "well behaved" chemical systems. Since gas phase reaction products do not always follow the "well behaved" guideline, an alternate analytical tool, such as microwave spectroscopy, could prove beneficial for analyzing such systems and may well provide some new routes to synthetic chemistry. A general review of the present state-of-the-art for applications of microwave techniques to analytical studies will be presented. An attempt will be made to describe the limitations and advantages of microwave spectroscopy for probing chemical systems for product identification and for optimization of the efficiency of gas phase chemical reactions. As an illustration, some recent results obtained in our laboratory on the complex pyrolytic decomposition reactions of ethylamine will be described. Further examples of possible applications will be taken from typical industrial processes which employ vapor phase chemical synthesis techniques.

Lovas, F. J., Clark, F. O., Tiemann, E., **Pyrolysis of ethylamine. I. Microwave spectrum and molecular constants of vinylamine,** *J. Chem. Phys.* **62**, No. 5, 1925-1931 (Mar. 1, 1975).

Key words: dipole moment; ethylamine; pyrolysis reactions; rotational spectrum; structure; vinylamine.

Microwave rotational spectra assignable to gas phase vinylamine ($CH_2=CHNH_2$) have been detected in the pyrolysis decomposition products of ethylamine. Stark effect and hyperfine structure measurements have aided the assignment of the spectrum and allow the determination of the ^{14}N nuclear electric quadrupole coupling constants and the electric dipole moment for vinylamine. The spectrum of the first excited inversion vibrational state has been assigned. Relative intensity measurements indicate that the inversion state lies about 65 ± 25 cm^{-1} above the ground state. The spectral evidence suggests that vinylamine has a nonplanar equilibrium structure with $r_0(C-N)=1.40$ Å and $\angle CCN=125°$.

Ludtke, P. R., **Register of hydrogen technology experts,** *NASA CR-2624*, 80 pages (National Aeronautics and Space Administration, Washington, D.C., Oct. 1975). (Available from National Technical Information Service, Springfield, Va. 22161.)

Key words: accident investigation; hydrogen energy systems; hydrogen experts; hydrogen fuel; hydrogen production; hydrogen properties experts; hydrogen safety; hydrogen systems; hydrogen technology; hydrogen transportation.

This register presents the names of approximately 235 individuals who are considered experts, or very knowledgeable, in various fields of technology related to hydrogen. Approximately 90 organizations are represented. Each person is listed by organizational affiliation, address, and principal area of expertise. The criteria for selection of names for the register are extensive experience in a given field of work, participation in or supervision of relevant research programs, contributions to the literature, or being recognized as an expert in a particular field. The purpose of the register is to present, in easy form, sources of dependable information regarding highly technical areas of hydrogen technology, with particular emphasis on safety. The register includes two indexes: an alphabetical listing of the experts and an alphabetical listing of the organizations with which they are affiliated.

Lyon, G., Stillman, R. B., **Simple transforms for instrumenting FORTRAN decks,** *Software—Pract. Exper.* **5**, No. 4, 347-358 (Oct.-Dec. 1975).

Key words: computation and flow analysis; FORTRAN use; programming aids; syntax analysis.

A recent revival of interest in measuring program execution behaviour has led to a number of distinct approaches. Arguments are given for a fairly simple method of modifying FORTRAN source code to collect frequency counts. No symbol table is necessary and only a single reserved name is introduced into the source.

Machado, M. E., Linsky, J. L., **Flare model chromospheres and photospheres,** *Sol. Phys.* **42**, No. 2, 395-420 (June 1975).

Key words: chromosphere, sun; photosphere, sun; radiative transfer; solar flares.

Homogeneous plane-parallel model atmospheres for solar flares have been constructed to approximately simulate observations of flares. The wings of the Ca II lines have been used to derive flare upper photosphere models, which indicate temperature increases of ~ 100 K over the temperature distribution in the pre-existing facula at a height of 300 km above $\tau_{5000}=1$. In the case of flares covering sunspots the temperature rise seems to occur much higher in the atmosphere. We solve the transfer and statistical equilibrium equations for a three-level hydrogen atom and a five-level calcium atom in order to obtain the chromospheric flare models. The general properties of flares, including n_e, N_2, linear thickness, and Lyman continuum intensity are approximately reproduced. We find that with increasing flare importance the height of the upper chromosphere and transition region occur lower in the solar atmosphere, accounting for the factor of 60-600 increase in pressure in these regions relative to the quiet Sun. The Ca II line profiles agree with observations only by assuming a macrovelocity distribution that increases with height. Also the chromospheric parts of flares appear to be highly inhomogeneous. We show that shock and particle heated flare models do not agree with the observations and propose a thermal response model for flares. In particular, it appears that heating in the photosphere is an essential aspect of flares.

Magrab, E. B., Leasure, W. A., Jr., **Research in acoustics and noise measurements at the National Bureau of Standards,** *Proc. Noise-Conf., Gaithersburg, Md., Sept. 15-17, 1975*, W. W. Lang, Ed., pp. 191-200 (Noise Control Foundation, Poughkeepsie, N.Y., 1975).

Key words: audiometric standards; building acoustics; community noise; earphones; environmental noise; instrumentation; measurement methodologies; microphones; psychoacoustics; reverberation room; sound level meters.

A brief description of the National Bureau of Standards' recent research activities in acoustics and noise measurements is presented.

Maienthal, E. J., **Analysis of botanical standard reference materials by cathode ray polarography,** *J. Assoc. Off. Anal. Chem.* **55,** No. 5, 1109-1113 (1972).

Key words: aluminum; analysis; business; differential cathode ray polarography; iron; lead; nickel; orchard leaves.

The need for certified botanical and biological standards both in research and in industrial and field applications is leading to the development and production of a number of new Standard Reference Materials by the National Bureau of Standards. The first of these to be produced and certified is an orchard leaf standard. The determination of a number of important trace elements by cathode ray polarography was investigated and found to offer considerable advantages in sensitivity and accuracy over many other techniques. In addition, several elements may be determined simultaneously in the same solution. The methods were developed and applied to the analysis and certification of nickel, lead, bismuth, and iron in the orchard leaves. Results were also obtained for aluminum which has not yet been certified. Nickel was determined on 1 g samples after extraction with dimethylglyoxime and $CHCl_3$. Lead and bismuth were determined concurrently on 1 g samples after a sodium diethyldithiocarbamate separation. Iron and aluminum were determined on 0.25 g samples after cupferron separations. Details of the methods are given and the results are compared with those obtained by other techniques.

Maienthal, E. J., **The application of linear sweep voltammetry to the determination of trace elements in biological and environmental materials,** (Proc. Eighth Annual Conf. on Trace Substances in Environmental Health, Univ. of Missouri-Columbia, Columbia, Mo., June 11-13, 1974), Paper in *Trace Substances in Environmental Health,* D. D. Hemphill, Ed., **VIII,** 243-246 (1974).

Key words: analysis; biological and botanical samples; differential linear sweep voltammetry; environmental samples; fossil fuels; lunar samples.

The application of differential linear sweep voltammetry to the analysis of many types of environmental samples is described. The methods are applicable to the determination of many trace elements in almost any matrix. Results will be given and compared with those obtained by other techniques.

Maki, A. G., **High-resolution infrared spectrum of the $\nu_1+\nu_3$ band of ozone,** *J. Mol. Spectrosc.* **57,** No. 3, 416-427 (1975).

Key words: absorption spectra; infrared; molecular energy levels; ozone; pollution; spectra.

The $\nu_1+\nu_3$ band of ozone (O_3) near 2110 cm^{-1} has been measured and analyzed using a Watson-type Hamiltonian including all seven sextic centrifugal distortion terms. Two weak perturbations have been found between $K=n$ of $\nu_1+\nu_3$ and $K=n+3$ of $2\nu_3$. Those perturbations locate the band center for $2\nu_3$ at about 2058 cm^{-1}. Aside from those perturbations the interactions of $\nu_1+\nu_3$ with $2\nu_1$ and $2\nu_3$ have not been taken into account in the analysis. Effective band constants and an atlas listing line wavenumbers and assignments are given.

Maki, A. G., **High-temperature infrared spectrum of HCN near 3300 cm^{-1},** *J. Mol. Spectrosc.* **58,** 308-315 (1975).

Key words: high temperature; hydrogen cyanide; infrared; molecular term values; spectra; spectroscopy.

The infrared absorption of HCN near the fundamental band at 3311 cm^{-1} has been measured at temperatures up to 1200 K. Transitions involving high rotational states (up to $J=62$) have been measured. These give an improved value for the sextic centrifugal distortion term H_0. Many hot-band transitions have been observed and assigned to transitions originating in vibrationally excited states up to 4000 cm^{-1} above the ground state. These measurements give new data on vibrational states involving moderately high bending quantum numbers and indicate that new terms are needed to fit the ro-vibrational energy levels.

Manning, J. R., **Diffusion kinetics and mechanisms in simple crystals,** (Proc. Conf. Geochemical Transport and Kinetics, Warrenton, Va., June 4-6, 1973), Chapter in *Geochemical Transport and Kinetics,* pp. 3-13 (Academic Press Inc., New York, N.Y., 1974).

Key words: atom transport; diffusion in crystals; kinetic diffusion equations; mechanism for diffusion; random walk; vacancies.

The kinetic-atomic theory of diffusion is discussed and reviewed. Any such theory must involve a model providing a detailed picture of the paths as the atoms move through the material. Diffusion paths and diffusion mechanisms therefore are important in this theory and are discussed first. Both short-circuit diffusion mechanisms along easy diffusion paths and possible volume-diffusion mechanisms through regions of regular crystal structure are described. Simple random-walk diffusion equations are derived which yield expressions for the tracer diffusion coefficient D^* and the atom drift velocity v_F in terms of atom jump frequencies. It is noted that diffusion frequently occurs by a vacancy mechanism. When this is the case, the random-walk equations must be modified to include both correlation-factor effects and vacancy-wind effects. The origin and influence of these effects are discussed. A comparison is made between the kinetic-atomic diffusion equations and the thermodynamic-continuum diffusion equations. It is noted that cross terms which yield a dependence of the atom flux of species i on the concentration gradients or chemical potential gradients of other species k appear in these equations.

Manning, J. R., **Non-random diffusion in ionic crystals,** (Proc. Conf. on Mass Transport Phenomena in Ceramics, Cleveland, Ohio, June 3-5, 1974), Chapter in *Mass Transport Phenomena in Ceramics,* A. R. Cooper and A. H. Heuer, Eds., pp. 1-15 (Plenum Press, New York, N.Y., 1975).

Key words: correlation factor; diffusion; divacancy; driving force for diffusion; impurity diffusion; ion drift velocity; nonrandom diffusion; vacancy wind effect.

Nonrandom diffusion can result both from the presence of atomic driving forces and from the motion of defects in a crystal. Defect-related nonrandom effects appear in two different ways in the kinetic diffusion equations, as correlation effects and as defect-wind effects. The origins of these effects during diffusion in a driving force are discussed. Kinetic expressions for the drift velocity $\langle v_F \rangle$ are derived from expressions for the effective frequencies of independent atom jumps and are related to the tracer diffusion coefficient D^*. For impurity diffusion in an electric field, deviations from the Nernst-Einstein relation result from defect-wind effects. Recently developed equations for the ionic-impurity drift-mobility when diffusion occurs via divacancies moving on one of the sub-lattices in the NaCl structure are summarized. Possible extensions of the simple equations used here to more complex situations are discussed.

Manning, J. R., **Theory of diffusion,** (Proc. American Society for Metals Seminar on Diffusion, Cleveland, Ohio, Oct. 13-14, 1972), Chapter 1 in *Diffusion,* pp. 1-24 (American Society for Metals, Metals Park, Ohio, 1973).

Key words: atomic diffusion mechanisms; diffusion; random walk; review article; thermodynamic diffusion equations; vacancy diffusion mechanisms.

A survey of the theory of diffusion with emphasis on the role of atomic diffusion mechanisms. Random walk diffusion equations, modifications of these equations by atomic driving forces, correlation effects, vacancy wind effects, temperature and pressure dependences, the general thermodynamic diffusion equations, and the rela-

tion of planar diffusion to three-dimensional diffusion and the diffusion tensor are discussed.

Manson, S. T., Cooper, J. W., **Angular distribution of photoelectrons: Outer shells of noble gases,** *Phys. Rev. A* **2,** No. 5, 2170-2171 (Nov. 1970).

Key words: angular distribution; asymmetry; photoionization; rare gases.

Results of calculations of angular distributions of photoelectrons from the outer p subshells of Ne, Ar, Kr, and Xe are presented for electron energies between 0 and 2 Ry (27.2 eV).

Marcus, M., Merris, R., **A relation between the permanental and determinantal adjoints,** *J. Aust. Math. Soc.* **15,** Part 3, 270-271 (May 1973).

Key words: permanental adjoint; positive semidefinite hermitian matrix; symmetry class of tensors.

In this note an inequality is proved for generalized matrix functions. When specialized to the permanent, the inequality suggests a conjecture concerning a relation between the permanental and determinantal adjoints. The general inequality extends a conjectured inequality of Doković to another class of matrices.

Marcus, M., Newman, M., **Some results on unitary matrix groups,** *Linear Algebra and Appl.* **3,** 173-178 (1970).

Key words: bounded representations; Burnside; irreducibility; unitary groups; Weyl.

It is shown that an irreducible matrix group with uniformly bounded trace is itself uniformly bounded, and so equivalent to a unitary group. This result is used to prove that certain matrix groups preserving certain scalar valued functions are unitary.

Marshall, H. E., **Cost sharing and efficiency in salinity control,** (Proc. 15th Annual Western Resources Conf. on Salinity in Water Resources, Boulder, Colo., July 9-10, 1974), Chapter 8 in *Salinity in Water Resources,* J. E. Flack and C. W. Howe, Eds., pp. 139-152 (Merriman Publ. Co., Boulder, Colo., 1974).

Key words: Colorado River; cost sharing; efficiency; equity; salinity control.

The increase in salinity concentrations in the southwestern United States and Mexico imposes economic costs on water users. Cost-sharing rules influence the selection of techniques and of scales for salinity control projects, yet there is no established Federal policy for sharing the costs of salinity control. Based on efficiency and equity criteria, a package of rules is suggested. Charging salt polluters and salinity control beneficiaries are potential policies, the final choice being constrained by legal and political institutions. Two specific rules are for the Federal government to share in the same proportion costs of all techniques (structural and nonstructural) used to provide salinity control, and to share costs in proportion to benefits received at the margin. Implications are that nonfederal interests, especially irrigators, would bear most of the costs of salinity control.

Marshall, H. E., **"Cost sharing for recreation: Efficiency and equity:" Comment,** *Land Economics* **LI,** No. 3, 300-303 (Aug. 1975).

Key words: cost sharing; efficiency; equity; recreation; redistribution of income; water resources.

This comment critiques an article in *Land Economics* entitled "Cost Sharing for Recreation: Efficiency and Equity," by William Miller and Bruce Scherr. These authors presented in their article a general set of policy conclusions regarding cost sharing for recreation that were based on a case study they made of a Soil Conservation Service project and on theoretical work by Harold Marshall. This comment questions the validity of the conclusions and policy implications for the general case, clarifies the relationship of Marshall's work to that of Miller and Scherr, and suggests an alternative approach to measuring the redistribution of income effects of a recreation project.

Martin, W. C., **Atomic spectroscopy—Some data centers and compilations,** (Proc. 4th Int. CODATA Conf. on Generation, Compilation, Evaluation and Dissemination of Data for Science and Technology, Tsakhcadzor, U.S.S.R., June 24-27, 1974), *CODATA Bull.* **14,** 112-115 (CODATA Secretariat, Paris, France, 1974).

Key words: atomic data; atomic energy levels; atomic line shapes; atomic spectra; data compilations; gas lasers; transition probabilities.

The operation and current work of the NBS Atomic Energy Levels Data Center is reviewed briefly, and some of the other activities of this type, at NBS and elsewhere, are noted. The data include atomic wavelengths, energy levels, transition probabilities and line shapes and shifts, and gas laser transition data. References to some recent and forthcoming compilations of atomic spectral data are included.

Marvin, R. S., Hogenboom, D. L., **Viscosity of liquids,** Paper 2m in the *American Institute of Physics Handbook Third Edition,* pp. 2-187—2-202 (McGraw-Hill Book Co., New York, N.Y., 1972).

Key words: handbook article; liquids; viscosity.

Existing tabulations of the viscosity of liquids are described with selected examples from some of the more recent tabulations.

Marzetta, L. A., **A thermesthesiometer—An instrument for burn hazard measurement,** *IEEE Trans. Biomed. Eng.* **BME-21,** No. 5, 425-427 (Sept. 1974).

Key words: burn hazard; consumer products; contact temperature; thermesthesiometer; thermometry.

Surface temperature measurement alone is insufficent to establish the hazard to the human of contact with a hot or cold object. A metal surface is more likely to cause thermal injury than a plastic surface at the same temperature. An instrument equipped with a measuring probe has been developed for indicating the temperature that would be experienced if human contact were made with the hot surface in question. The correct value of interface contact temperature can be read for a selected contact time without knowing the composition or temperature of the heated material under test.

Marzetta, L. A., **Some measurement engineering innovations in consumer products,** *Proc. 1974 Joint Measurement Conference, Gaithersburg, Md., Nov. 12-14, 1974,* pp. 41-44 (Instrument Society of America, Pittsburgh, Pa., 1975).

Key words: consumer products; contact temperature; thermesthesiometer; thermometry.

Exploration of the problem concerning hazards in consumer products has shown that laboratory engineers can usefully apply basic measurement practices towards improving safety and developing new measuring tools. Some novel and relatively simple redesign features will be presented concerning a common household appliance that can significantly reduce its electrical and thermal hazards. Included in the paper are details of an instrument which tests for burn hazard by simulating the human response to contact with a hot surface. The advantage of the new instrumentation is that a thermal safety standard can be written around one specified contact temperature for nearly any material regardless of its composition or surface temperature.

Maximon, L. C., O'Connell, J. S., **Sum rules for forward elastic pion-nucleon scattering,** *Phys. Lett.* **51B,** No. 1, 31-34 (July 8, 1974).

Key words: dispersion relations; pion-nucleon amplitudes; pion-nucleon cross section; pion-nucleon scattering; pion-nucleus scattering; sum rules.

A number of energy weighted sum rules relating amplitudes and differential cross sections for forward elastic and charge exchange scattering to the total pion-nucleon cross section are derived from dispersion relations.

Mazur, J., McIntyre, D., **The determination of chain statistical parameters by light scattering measurements,** *Macromolecules* **8,** No. 4, 464-476 (July-Aug. 1975).

Key words: chain correlation; chain statistical parameters; light scattering; Monte-Carlo computations, chase transition; scattering function.

The effects of volume exclusion on polymer chain conformations can be determined from the study of the angular dependence of radiation scattered by chain molecules. It is found that useful information can be obtained only when the variable x is large, where x is the product of the square of the magnitude of the scattering vector and of the mean square radius of gyration. Hence, solutions of macromolecules of very high molecular weight are needed for these investigations. The theoretical treatment of the scattering function is based on several assumptions. The validity of these assumptions is examined by computing, using a Monte-Carlo technique, various moments of intramolecular separations and comparing the results so obtained, in the limit of a chain of infinite length, with the analytical results. The computations seem to verify the validity of the theoretical model. The scattering behavior of solutions of recently synthesized polystyrene of $M_W = 4.4 \times 10^7$ in cyclohexane at various temperatures and in benzene at 40° was investigated. From the log–log plots of the scattering function vs. x, a statistical parameter was calculated, whose value depends on the magnitude of long-range correlations between any pair of chain elements. It is found that above the Θ temperature this parameter is practically independent of temperature and that its numerical value was found to agree well with the value obtained from Monte-Carlo calculations. In the neighborhood of the Θ temperature, this parameter decreases rapidly with decreasing temperature, indicating a first-order transition in chain conformation.

McCamy, C. S., Derr, A. J., **Microdensitometry,** Article 15.6 in *SPSE Handbook of Photographic Science and Engineering,* W. Thomas, Jr., Ed., pp. 871-877 (John Wiley & Sons, New York, N.Y., 1973).

Key words: microdensitometry; microphotometry; optical density.

Microdensitometry is the science of measuring the optical densities of very small areas. Microdensitometers are usually equipped to scan along a line and continuously record the varying density with respect to distance. The principal application of microdensitometry is in the field of image structure analysis. The maximum resolving power of a transmission instrument is the quotient of the sum of the numerical apertures of the illuminating and sensing objectives to the wavelength of the light. With high numerical apertures, 1800 cycles/mm has been recorded.

Since microdensitometers measure optical density as a function of position, the principal calibrations are the photometric calibration and the length calibration. The photometric scales of microdensitometers are most often calibrated by placing a step tablet of known densities in the sample position. The length scale of a microdensitometer may be calibrated by scanning a glass scale or stage micrometer.

McCarter, R. J., **A new technique for thermal analysis of vapor-producing reactions,** *J. Appl. Polym. Sci.* **17,** No. 6, 1833-1846 (1973).

Key words: differential thermal analysis; DTA; kinetics; pyrolysis; TGA; thermal analysis; thermal degradation; thermogravimetric analysis.

An apparatus was developed for measuring the rate at which vapors are evolved during the thermal degradation of materials and thereby deriving the kinetics of such reactions. Requisite to the operating scheme of the apparatus is the provision of a high-temperature zone to convert condensable or tarry vapors into noncondensable form. The apparatus yields a direct measure of reaction velocity, rather than the integrated indication obtained with thermogravimetric analysis. This simplifies the identification and calculation of kinetic parameters. Increases in sensitivity and operating range are also achieved. Flexibility in operation is obtained that permits the separate recording of reactions that tend to overlap. Although the apparatus principally has been operated using a combustible gas indicator to meter the evolved vapors, a number of options are available for the latter function, including flowmeters and various continuous gas analyzers. The applicability of the method appears promising.

McCarty, R. D., **Hydrogen technological survey-thermophysical properties,** *NASA Spec. Publ.* **3089,** 530 pages (National Aeronautics and Space Administration, Washington, D.C., 1975).

Key words: computer programs; gaseous hydrogen; graphs; handbook thermophysical properties; hydrogen; liquid hydrogen; ortho-para modifications; property value uncertainties; solid; solid hydrogen; tables.

This handbook is the result of an extensive survey of the thermophysical properties of hydrogen, including densities and the thermodynamic, transport, electrical, optical, and molecular properties for the gaseous and fluid states. A thorough bibliography of published work on each property is given. Recommended references are cited for those properties which have been critically surveyed. Other references are listed which were reviewed but not considered as basic source material. Each property is described and defined; selected values are presented for the more common properties; and where appropriate, graphical presentations are also made. The major tables cover the range 25-5000 K with pressures to 15,000 psia (14-3000 K to 100 MPu). In addition, for property values beyond this range, recommended references are given, where available.

McClendon, L. T., **Selective determination of chromium in biological and environmental matrices,** (Proc. Eighth Annual Conf. on Trace Substances in Environmental Health, Univ. of Missouri-Columbia, Columbia, Mo., June 11-13, 1974), Paper in *Trace Substances in Environmental Health,* D. D. Hemphill, Ed., **VIII,** 255-257 (1974).

Key words: analysis; biological materials; chloroform; chromium; environmental materials; neutron activation; radiochemical separation; solvent extraction; tribenzylamine.

Chromium occurs in many biological and environmental materials but only in trace amounts (ppm level), which makes the determination by usual chemical methods very difficult and sometimes impossible. Destructive neutron activation analysis, utilizing the reaction $^{50}Cr(n, \gamma)\ ^{51}Cr$, can eliminate many of the difficulties encountered with other techniques. A detailed description of chromium determination in various biological (e.g. liver and urine) and environmental (e.g. coal and fly ash) samples using the NBS Reactor, coupled with a very selective radiochemical separation procedure, will be discussed.

McCormick, P. G., Burke, R. W., Doumas, B. T., **Precautions in use of soft-glass disposable pipets in clinical analyses,** *Clin. Chem. Scientific Note* **18,** No. 8,854-856 (1972).

Key words: clinical; contamination; errors; soft glass pipets; unwashed soft glass pipets.

Soft-glass, Pasteur-type pipets are widely used as disposable transfer pipets, especially in clinical and biochemical laboratories. These pipets possess an alkaline surface contamination that can affect the accuracy of chemical analyses if proper precautions are not taken. Microtitrations of aqueous rinsings from these pipets have consistently yielded values of 0.1 to 0.2 μmol of hydroxide equivalent per pipet. A possible detrimental effect of this residue was demonstrated, using chloroform solutions of bilirubin. Absorbance was diminished by as much as 5 percent when unwashed, soft-glass pipets were used to transfer these solutions to spectrophotometric cells. Absorption and fluorescence characteristics of other unidentified surface contaminants are also described. The effect of multiple rinsings is discussed and several ways are suggested for cleaning these pipets. Oven drying must be avoided, however, since it enhances alkali release.

McCrackin, F. L., Chang, S. S., **Simple calibration procedures for platinum resistance thermometers from 2.5 to 14 K,** *Rev. Sci. Instrum.* **46,** No. 5,550-553 (May 1975).

Key words: calibration of thermometers; low-temperature calibration of thermometers; platinum resistance thermometers; resistance thermometers; two-way structural analysis.

Calibration procedures are developed for platinum resistance thermometers in the temperature range 2.5-14 K. Two recommended methods require calibration points at the boiling point of liquid helium (4.215 K) and the triple point of hydrogen (13.81 K); in addition, the first method requires a point at 7.201 K while the second method requires the slope of the calibration curve at 13.81 K. For temperatures from 3.5 to 14 K, the calibrations are accurate to within 0.01 K for the first method and 0.025 K for the second method. For temperatures from 2.5 to 3.5 K, the calibrations are somewhat less accurate. Therefore, if a thermometer has been calibrated for temperatures of 13.81 K and above, its calibration may be easily extended to lower temperatures with sufficient accuracy for many applications. These calibration procedures were developed from two-way structural analysis of the accurate calibrations of 12 platinum resistance thermometers.

McCulloh, K. E., **Threshold energies for formation of OH^+ and NH_2^+ by dissociative photoionization of water and ammonia,** (Proc. IV Int. Conf. on Vacuum-UV Radiation Physics, Hamburg, Germany, July 22-26, 1974), Paper in *Vacuum-UV Radiation Physics,* E. E. Koch, R. Haensel, and C. Kunz, Eds., pp. 195-197 (Pergamon-Vieweg, Braunschweig, Germany, 1974).

Key words: ammonia; dissociative photoionization; NH_2^+, OH^+; photoionization; threshold energies; water.

A photoionization mass spectrometer incorporating a monochromator of 0.5 Å resolution has been employed to remeasure photoion yield curves near threshold for OH^+ from water vapor at temperatures of 215 and 298 and for NH_2^+ from ammonia at 160 and 298 K. From the observed temperature shifts of these curves it is inferred for both molecules that essentially the entire rotational energy is available for dissociative ionization. On this basis the threshold energies for formation of the fragment ions are corrected for the effect of rotationally excited molecules. The enthalpies of formation of OH^+ and NH_2^+ are discussed in relation to thermochemical quantities for the neutral OH and NH_2 radicals. Similar results are reported for OD^+, ND_2^+, and NHD^+ fragment ions.

McDaniel, C. L., Plante, E. R., **Phase relations involving seed-electrode-insulator materials in MHD,** *Proc. 14th Symp. on Engineering Aspects of Magnetohydrodynamics, Tullahoma, Tenn., Apr. 8-10, 1974,* pp. IV.6.1-IV.6.4 (University of Tennessee, Tullahoma, Tenn., 1974).

Key words: K_2SO_4-$LaCrO_3$ system; K_2SO_4-MgO system; phase relations; vapor pressure; vaporization equilibria.

The phase relations for the K_2SO_4-MgO and K_2SO_4-$LaCrO_3$ systems were determined using quenching techniques along with x-ray diffraction and DTA data. The systems were studied in open and closed Pt containers. The K_2SO_4-MgO system is a simple eutectic-type with the eutectic located at 1067 °C and ~ 2 mol percent MgO. A vaporization equilibria diagram was determined from calculations based on data from the condensed state phase diagram and thermodynamic data for pure K_2SO_4 assuming ideal behavior. Temperatures at which vapor-liquid equilibria occur were calculated for total pressures of 0.01, 0.1, and 1 atm. Similar principles were applied to predict condensation temperatures when combustion gases are present. Condensed state phase relations for the system K_2SO_4-$LaCrO_3$ were determined utilizing sealed Pt tubes for specimen containers. The K_2SO_4-$LaCrO_3$ system is a simple eutectic-type with the eutectic located at 1063 °C and ~ 2 mol percent $LaCrO_3$. The K_2SO_4-$LaCrO_3$ system in air (open system) is more complex and can not be represented by a binary-type system.

McLaughlin, W. L., **Radiation dosimetry with thin films,** (Proc. Third Conf. on Application of Small Accelerators, North Texas State Univ., Denton, Tex., Oct. 21-23, 1974), Paper in *Application of Small Accelerators. Vol.* **II. Industrial Applications of Small Accelerators,** I. L., Morgan and J. L. Duggan, Eds., pp. 65-85 (U.S. Energy Research and Development Admin. Office of Public Affairs and Technical Information Center, Springfield, Va., 1975).

Key words: cavity theory; depth dose; dose distributions; dosimetry; dyes; electron beams; radiochromic dyes; thin films.

A thin self-supported or laminated layer of radiation-sensing material is useful for measuring or monitoring the energy deposited by a radiation beam passing through that layer. If (1) the film is thin enough in relation to the range of the incident radiation particles in the absorbing material and (2) the incident radiation spectrum can be approximated sufficiently, the absorbed dose or dose rate in materials surrounding the thin layer can be determined by applying fairly simple cavity-theory considerations (i.e. factoring by stopping power ratios in the case of charged-particle beams). Some sensing materials that may be used as dosimeters in accelerator beams are thin calorimetric bodies, solid-state detectors, and ceramic, plastic, or dyed plastic layers. Major sources of error that must be accounted for are instabilities, nonlinearities, variations of response with dose-rate and spectral changes, environmental factors, inconsistencies in the quality of the sensing material, and imprecisions in the analysis of the radiation effect. A primary advantage afforded by thin-film dosimetry is its capability of supplying dose distribution data near interfaces of different materials.

McLaughlin, W. L., **Radiation sources and dosimetry,** *Food Irradiation Information* **4,** 44-45, 58 (Mar. 1975).

Key words: accelerators; dose distributions; dosimetry; electron beams; food irradiation; food preservation; gamma rays.

The program at the NBS Center for Radiation Research contributing to food preservation by irradiation includes measurement studies with several high-energy electron accelerators and radionuclide sources such as cobalt-60. Investigations are made on large-dose measurement systems, chemical dosimeters, and thin-film imaging systems used for high-resolution dose-distribution studies.

McLaughlin, W. L., Rosenstein, M., Levine, H., **Bone-and-muscle-equivalent solid chemical dose meters for photon and electron doses above one kilorad,** (Proc. Symp. on Biomedical Dosimetry, IAEA, Vienna, Austria, 1975), Chapter in *Biomedical Dosimetry,* pp. 267-281 (Int. Atomic Energy Agency, Vienna, Austria, 1975).

Key words: bone; dosimetry; dyes; electron dosimetry; energy dependence; gamma rays; muscle; radiochromic dosimeters; x-ray spectra.

Conventional solid dose meters, such as plastic films, powders, emulsions, glasses, ceramics and gels, have a response to ionizing photons and electrons that varies markedly over a broad spectrum when compared with the absorption characteristics of biological tissues. New radiochromic dyed plastic dose meters have been developed with x- and gamma-ray and electron energy absorption cross-sections (calculated) and radiatior energy responses (experimental) corresponding approximately to those for human muscle and bone, for a spectrum from a few keV to at least 10 MeV. Three-dimensional solid dose meters useful over the absorbed dose range of 10^3 to 10^6 rad are formed by thermosetting a selected combination of monomers containing the radiochromic dye in solution. Thin-film dose meters for the dose range 10^5 to 10^7 rad are formed by casting on optically flat surfaces strippable layers of special combinations of polymers and dyes in solution. The response of these systems to x and gamma rays and electrons has been studied over various radiation spectra, dose-rates and temperatures during irradiation.

Meijer, P. H. E., Niemeijer, T., **Quantum-mechanical approximation to the ground state of cerous magnesium nitrate,** *Phys. Rev. B* **11,** No. 7, 2612-2623 (Apr. 1, 1975).

Key words: antiferromagnetism; cerous magnesium nitrate; dipole-dipole coupling; ferromagnetism; ground state; permutation group; quantum mechanics; spin cluster; spin-Hamiltonian.

In this paper we perform a complete quantum-mechanical calculation of the ground-state energy of a system of spins 1/2 that are coupled by dipole-dipole forces. The only hypothesis used is the assumption that the ground state has two times the periodicity of the underlying magnetic lattice. This paper is the application to a specific crystal of results derived in a preceding paper. The Hamiltonian is decomposed in eight invariant pieces each with its own coupling constant. The basis wave functions are decomposed according to the eight one-dimensional representations of the permutation group that leaves the cluster invariant. The results are given in the form of tables applicable to any compound that has the spins situated on a Bravais lattice. The calculation is applied to cerous magnesium nitrate and we show that the results for the lowest state of each representation are leading to a spectrum that is different from the results obtained with the classical or Hartree method. Although the lowest state is still the same antiferromagnetic configuration, it turns out now that this state lies barely below the ferromagnetic state; the order in which the ferromagnetic and antiferromagnetic levels appear is different from the order obtained in a classical calculation.

Menis, O., Garn, P. D., Diamondstone, B. I., **The application of thermoanalytical methods to the environmental health problems,** (Proc. Fourth ICTA Conf., Budapest, Hungary, July 8-13, 1974), Chapter in *Thermal Analysis,* I. Buzas, Ed., **3,** 127-139 (Akademiai, Kiado, Budapest, Hungary, 1975).

Key words: calibration filters; chrysotile; environmental health; improved methodologies; particulates; quartz; self-generated atmosphere.

Differential thermoanalysis methods provided an independent measurement of quartz and chrysotile asbestos in the preparation of calibration standards needed by environmental control agencies. In this study it was found that 30-500 μg of chrysotile asbestos could be measured with a relative standard deviation of 15 percent. Sealed silver containers were used to provide a self-generating atmosphere which reduced the spread of the dehydroxylation peak and improved both selectivity and sensitivity. A repeat-measurement of the thermal curve, after the dehydroxylation, provided a correction for the matrix baseline. Under similar experimental conditions, microgram quantities of quartz were determined with a relative standard deviation of ~ 2 percent. However, there was a 50 percent difference between the NBS-ICTA SRM 759 and commercially prepared material. It was shown that this difference could be eliminated by thermally treating the commercial product.

Merris, R., Pierce, S., **Elementary divisors of higher degree associated tranformations,** *Linear and Multilinear Algebra* **1,** No. 3, 241-250 (1973).

Key words: elementary divisors; irreducible character; symmetry class of tensors.

Let V be a complex inner product space of dimension n and let $\overset{m}{\otimes}V$ be the space of m contravariant tensors over V. Given a subgroup G of S_m and an irreducible character χ on G, we define a subspace $V_\chi{}^m(G)$ in $\overset{m}{\otimes}V$. If $T: V \to V$ is linear, let $\Pi \cdot T: \overset{m}{\otimes}V \to V$ be the mth Kronecker product of T. Then $V_\chi{}^m(G)$ is invariant under $\Pi \cdot T$ and we let $K(T)$ be the restriction of $\Pi \cdot T$ to $V_\chi{}^m(G)$. In this paper we prove that if the rank of T is large enough, then the elementary divisors of $K(T)$ are linear if and only if the elementary divisors of T are linear. This result has previously been proved only for the case that χ is linear.

Meyerson, M. R., **The proposed Department of Commerce "Voluntary" Labeling Program,** (Proc. 1973 Technical Seminar for College Educators of Home Equipment, Dallas, Tex., Nov. 1-3, 1973), Paper in *Proceedings 1973 Technical Seminar for College Educators of Home Equipment,* pp. 9-10 (Association of Home Appliance Manufacturers, Chicago, Ill., 1973).

Key words: education; efficiency comparison; household appliances; household equipment; label developments; labeling; label specification; monitoring priorities; product classes; test methods; voluntary.

The features of the Department of Commerce Program for the Voluntary Labeling of Major Household Appliances and Equipment to Effect Energy Conservation are presented. These procedures were published in the Federal Register on October 26. The steps involved in carrying out the program are (1) setting of priorities among products, (2) establishment of product classes where appropriate, (3) setting of test methods to be used, (4) developing a system for comparing the efficiency of similar products, (5) development of a label that is meaningful to consumers, (6) publication of a Proposed Label Specification in the Federal Register with time for comment, (7) evaluation of comments, (8) publication of the Final Label Specification, (9) education of the public as to the meaning of the program, and (10) monitoring of the program to insure compliance.

Meyerson, M. R., **The role of the National Bureau of Standards in consumer product safety,** *Proc. Product Liability Prevention Conf., Newark College of Engineering, Newark, N.J., Aug. 22, 1974, IEEE Catalog 74CHO911-8R,* pp. 149-152 (1974).

Key words: consumer; product safety; regulation; standards.

A short history of NBS contributions to consumer product safety is presented. The role of NBS in providing technical support to Federal regulatory agencies, including the Consumer Product Safety Commission, is discussed; several safety-related research projects are described.

Meyerson, M., **The Department of Commerce voluntary labeling program for household appliances and equipment to effect energy conservation,** *Proc. Conf. on Improving Efficiency in HVAC Equipment and Components for Residential and Small Commercial Buildings, Purdue Univ., West Lafayette, Ind., Oct. 7-8, 1974,* pp. 222-225 (1974).

Key words: consumer information; efficiency; energy; label; refrigerator/freezers; room air conditioning.

The purpose and legal/administrative authority for the Department of Commerce Voluntary Labeling Program for Household Appliances and Equipment to Effect Energy Conservation are described. The procedures for executing this program are outlined, with examples of experience in developing labels for room air conditioners and refrigerator/freezers.

Miller, A., Bjergbakke, E., McLaughlin, W. L., **Some limitations in the use of plastic and dyed plastic dosimeters,** *Int. J. Appl. Radiat. Isotop.* **26,** No. 10, 611-620 (Oct. 1975).

Key words: absorbed dose rate; cellulose triacetate; dosimetry; dyed cellophane; dyed plastics; electron beams; gamma radiation; plastic films; polymethyl methacrylate; polyvinyl chloride; radiation processing; radiochromic dyes.

Several practical plastic and dyed plastic dosimeters were examined under irradiation conditions similar to those used for radiation processing of materials. Cellulose triacetate, polymethyl methacrylate, polyvinyl chloride, dyed polymethyl methacrylate, dyed cellophane and dyed nylon were given fractionated and uninterrupted absorbed doses in the megarad range with ^{60}Co γ-rays and 10 MeV electron beams. It was found that with some systems, differences in radiation response due to dose-rate and temperature dependence can cause large systematic errors in dose interpretation. Poor reproducibility of response may result from batch-to-batch differences or intra-batch variations in thickness, distribution of sensitizers and background optical density. When using these routine dosimeters, careful calibration of the response and monitoring of factors contributing to poor reproducibility are essential.

Miller, A., McLaughlin, W. L., **Absorbed dose distribution in a pulse radiolysis optical cell,** *Int. J. Radiat. Phys. Chem.* **7,** No. 5, 661-666 (1975).

Key words: absorbed dose rate; depth dose; dose distribution; dye films; electron beams; optical cell; pulse radiolysis; radiation dosimetry; radiochromic dyes.

When a liquid solution in an optical cell is irradiated by an intense pulsed electron beam, it may be important in the chemical analysis of the solution to know the distribution of energy deposited throughout the cell. For the present work, absorbed dose distributions were measured by thin radiochromic dye film dosimeters placed at various depths in a quartz glass pulse radiolysis cell. The cell was irradiated with 30 ns pulses from a field-emission electron accelerator having a broad spectrum with a maximum energy of ≈ 2 MeV. The measured three-dimensional dose distributions showed sharp gradients in dose at the largest penetration depths in the cell and at the extreme lateral edges of the cell interior near the optical windows. This method of measurement was convenient because of the high spatial resolution capability of the detector and the linearity and absence of dose-rate dependence of its response.

Miller, A., McLaughlin, W. L., **Imaging and measuring electron beam dose distributions using holographic interferometry,** *Nucl. Instrum. Methods* **128,** 337-346 (1975).

Key words: calorimetry; depth dose; dose distributions; dosimetry; electron beams; holographic interferometry; holography; isodose; radiation

Holographic interferometry was used to image and measure ionizing radiation depth-dose and isodose distributions in transparent liquids. Both broad and narrowly collimated electron beams from accelerators (2-10 MeV) provided short irradiation times of 30 ns to 0.6 s. Holographic images and measurements of absorbed dose distributions were achieved in liquids of various densities and thermal properties and in water layers thinner than the electron range and with backings of materials of various densities and atomic numbers. The lowest detectable dose in some liquids was of the order of a few kRad. The precision limits of the measurement of dose were found to be ± 4 percent. The procedure was simple and the holographic equipment stable and compact, thus allowing experimentation under routine laboratory conditions and limited space.

Miller, G. K., **Shirley Highway Bus-On-Freeway Project evaluation study,** (Proc. Social Experiments & Social Program Evaluation Symp., Gaithersburg, Md., May 22, 1972), Paper in *Social Experiments and Social Program Evaluation,* pp. 40-53 (Ballinger Publ. Co., 1974).

Key words: bus-on-freeway demonstration project; bus rider surveys; bus system evaluation; bus transit; traffic monitoring.

The Shirley Highway Bus-on-Freeway Demonstration Project seeks to ease traffic congestion and shorten travel times for bus and auto travelers commuting during rush hour periods via the Shirley Highway Corridor from Northern Virginia suburbs to employment centers in Washington, D.C. This and other project goals, which include reducing vehicle-caused air pollution and improving bus service, can be attained by effecting an auto-to-bus modal shift by persons commuting via the Corridor area. Three project elements—(1) an exclusive bus lane on the Shirley Highway and bus priority lanes within the District of Columbia; (2) improved bus service including new-look/new-feature buses; and (3) park-and-ride facilities will, according to the premise under which the project was conceived, effect this modal shift and achieve a substantially increased bus market share. The demonstration project is sponsored by the Department of Transportation.

The Technical Analysis Division, National Bureau of Standards, is evaluating project performance with emphasis on the effectiveness of the three project elements. This paper describes evaluation procedures used during the first year and identifies difficulties encountered with various monitoring procedures, as well as presenting preliminary conclusions and plans for future activities.

Mills, R. M., **A performance standard for walk-through metal detectors,** (Proc. 8th Annual Crime Countermeasures Conf., Lexington, Ky., Apr. 16-19, 1974), Paper in *Proc. 1974 Carnahan and Int. Crime Countermeasures Conf., UKY BU* **105,** 78-82 (Aug. 1974).

Key words: handgun detection; metal detector; performance standard; security; weapon detection.

The Law Enforcement Standards Laboratory at the National Bureau of Standards (NBS) is developing performance standards for equipment used in the criminal justice system. They will be promulgated primarily by the National Institute of Law Enforcement and Criminal Justice, Department of Justice. This paper discussed the development of a standard for walk-through metal weapon detectors. The standard contains requirements and test methods for such things as detection performance, effects of walking speed and throughput rate, alarm indicator, controls, stability, ambient and generated magnetic field, and interference with other detectors.

Mitchell, R. A., Woolley, R. M., Chwirut, D. J., **Analysis of composite-reinforced cutouts and cracks,** *AIAA J.* **13,** No. 6, 744-749 (June 1975).

Key words: adhesively bonded joints; composite materials; composite-overlay reinforcement; contour plotting; cracks, reinforcement of; cutouts, reinforcement of; finite element analysis; joints, adhesively bonded; reinforcement, composite overlay; reinforcement, cutouts and cracks.

Finite element computer analyses of the reinforcement of cutouts and cracks in metal sheet, by bonded overlays of composite material, are described. The analyses articulate the separate responses of the sheet, the overlays, and the adhesive. Contour plots of computed stress and strain fields are automatically generated by the computer programs. Strains measured on the surfaces of several reinforced sheet tensile specimens were, for the most part, in good agreement with strains predicted by the analyses. Qualitative correlations between certain failure modes observed in the test specimens and the stress distributions given by finite element analysis are apparent. The same analytical approach is currently being used to study weld/bond and fastener/bond joints, and it could be used to study other problems such as hole repair in metal or composite sheet and embedded defects in laminar material.

Mitchell, R. A., Woolley, R. M., Halsey, N., **High-strength end fittings for FRP rod and rope,** *J. Eng. Mech. Div. ASCE* **100,** No. EM4, 687-706 (Aug. 1974).

Key words: axisymmetric analysis; cables (ropes); composite materials; contour plotting; end fittings for FRP rod and rope; finite element analysis; FRP rod; FRP rope; materials testing; nonlinear analysis (shear); potted end fittings; structural engineering; tensile strength; transversely isotropic materials.

Improved structural end fittings of two basic types were developed for use with fiber-reinforced-plastic (FRP) rod and rope materials. Each type of end fitting is essentially a metal sleeve that is attached to the FRP material by a thick layer of potting material. Tensile tests demonstrated that the new end fittings can equal or approach the full tensile strength of E-glass-reinforced-plastic rod and rope. In tensile strength, the new fittings are superior to commercially available end fittings. An axisymmetric finite element analysis was developed to study the transfer of load from a rod or rope, through the potting material, to the metal fitting. In the analysis the FRP material and the potting material are assumed to be transversely isotropic. The results of both the analytical study and the laboratory tests indicate the importance of using a relatively thick layer of low-stiffness potting material with these fittings.

Molino, J. A., **A proposed method for measuring the annoyance due to speech interference by noise,** (Proc. NASA Minisymposium, Hampton, Va., Jan. 21-22, 1975), Paper in *NASA Technical Memorandum, Noise and Speech Interference Proceedings of Minisymposium,* W. T. Shepherd, Ed., NASA TM X-72696, 15 pages (Available from National Technical Information Service, Springfield, Va., 22151 and STIF/NASA Scientific and Technical Information Facility, College Park, Md., 20740, 1975).

Key words: aircraft noise; annoyance; noise; psychoacoustics; speech interference.

A method is proposed to measure both the interference of speech by noise and the annoyance caused by such interference. It is based upon a nonverbal preference procedure developed at the National Bureau of Standards called an "acoustic menu." Subjects listen to audible speech signals in a background of noise. At the same time the subjects are given a limited opportunity to select the background noise. By analyzing the preference structure for the various types of interfering noise, as well as the decrement in speech intelligibility suffered with each noise, information can be obtained on both annoyance and interference.

Mopsik, F. I., Broadhurst, M. G., **Molecular dipole electrets,** *J. Appl. Phys.* **46,** No. 10, 4204-4208 (Oct. 1975).

Key words: electret; dipoles; glass; piezoelectric; polarization; polyvinyl chloride; pyroelectric.

The total polarization due to molecular dipoles in a glassy electret is computed using an Onsager cavity approach. From this result, all the possible contributions to the piezoelectric and pyroelectric coefficients are considered. It is shown that there are major contributions from the variation in dielectric constant and, for pyroelectricity, from thermal motion. These results account well for experimental data for polyvinyl chloride.

Motz, J. W., Dick, C. E., **X-ray scatter background signals in transmission radiography,** *Med. Phys.* **2,** No. 5, 259-267 (Sept.-Oct. 1975).

Key words: image contrast; monoenergetic x-ray beams; optimum radiographic systems; transmission radiography; x-ray image signals; x-ray scatter.

With monoenergetic x-ray beams incident on polystyrene phantoms, the spectra of the transmitted x rays were measured with a scintillation spectrometer. The scattered and unscattered components of the transmitted x-ray fluence at a point on the beam axis were determined as a function of (i) the incident x-ray energy (18, 22, 32, 49, 58, 69, and 660 keV), (ii) the phantom thickness (5.3, 10, and 21 cm), (iii) the scatter solid angle determined by the exposed area of the phantom and the separation distance of the image plane (0.090, 0.31, 0.66, 1.8, 3.5, 4.3, 4.8, and 5.1 sr), and (iv) the beam diameter at the image plane (25, 17, and 10 cm). The results indicate that, as the incident x-ray energy *decreases* from 660 to 30 keV, the contribution of the scattered component to the transmitted fluence *increases* from approximately 50 to 90 percent for the 21-cm phantom and from 21 to 50 percent for the 5.3-cm phantom. For typical cases, the data show the effect of the scatter component on the ratio of the image to the background signals. In addition, the examples show that optimum conditions for maximizing this signal ratio may be obtained by a careful selection of the incident x-ray energy for low-, medium-, and high-contrast objects.

Mount, G. H., Ayres, T. R., Linsky, J. L., **A non-LTE analysis of the CN 3883 Å band head in the upper photosphere of Arcturus,** *Astrophys. J.* **200,** 383-391 (Sept. 1, 1975).

Key words: atomic abundances; CN spectra; non-LTE molecular spectra; photospheres, stellar; radiative transfer.

A detailed non-LTE study of the CN(0,0) 3883 Å band-head spectrum of Arcturus (K2 III) provides an accurate determination of the carbon, nitrogen, and oxygen abundances in Arcturus. Non-LTE effects are significant, and we find that the Ayres-Linsky model provides an adequate fit to the observations for $[C,N]_* = 1/3\,[C,N]_\odot$ and $[O]_* = 0.60\,[O]_\odot$, or for $[C,N,O]_* = 1/6\,[C,N,O]_\odot$, but the latter abundances are unlikely. The upper photospheric microturbulence is found to be 2.5 ± 0.2 km s^{-1}.

Mulholland, G. W., Zollweg, J. A., Sengers, J. M. H. L., **Liquid-vapor asymmetries in pure fluids,** *J. Chem. Phys.* **62,** No. 7, 2535-2549 (Apr. 1, 1975).

Key words: asymmetry; coexistence curve; compressibility; critical exponents; critical point; decorated lattice gas; hole-particle symmetry; law of corresponding states; liquid; Padé approximant; power law; slope of the coexistence curve diameter.

The coexistence curve and the compressibility-like quantity $(\partial\rho/\partial\mu)_T$ at the coexistence curve are calculated for Mermin's decorated lattice gas. We tabulate the Padé approximants to the Ising model properties which were used in these calculations. It is shown that for the proper choice of the adjustable parameter in the model the asymmetries in the coexistence curve and in $(\partial\rho/\partial\mu)_T$ over a large temperature range, $T_c/2 < T < T_c$, are qualitatively similar to those in real fluids. Also, similar correlations between the overall coexistence curve asymmetry and the amplitudes of divergences for the critical region occur in the model and in real fluids. Based on our model calculations, several predictions for fluid behavior near the critical point are listed: (1) The *asymptotic* asymmetry in the coexistence curve and in $(\partial\rho/\partial\mu)_T$ at the coexistence curve should be most observable for fluids with large overall asymmetry such as SF_6, NH_3, and H_2O; (2) the range of the asymptotic asymmetry for $(\partial\rho/\partial\mu)_T$ is expected to extend somewhat beyond $t = 1 - (T/T_c) = 0.1$ for such fluids; (3) in order to obtain an estimate for the compressibility exponent γ' that is within a few percent of the true asymptotic value, experiments will have to be confined to the range $t < 10^{-2}$. Recent experimental data for $(\partial\rho/\partial\mu)_T$ at the coexistence curve are found to be consistent with the model for $t > 10^{-2}$, but are inconclusive closer to the critical point.

Naimon, E. R., Ledbetter, H. M., Weston, W. F., **Low-temperature elastic properties of four wrought and annealed aluminium alloys,** *J. Mater. Sci.* **10,** No. 8, 1309-1316 (Aug. 1975).

Key words: aluminium; aluminium alloys; bulk modulus; compressibility; Debye temperature; elastic constants; elasticity;

Poisson ratio; pulse-echo method; sound velocity; Young's modulus.

The elastic properties of four annealed polycrystalline commercial aluminium alloys were studied between 4 and 300 K using a pulse-superposition method. Results are given for longitudinal sound velocity, transverse sound velocity, Young's modulus, shear modulus, bulk modulus (reciprocal compressibility), Poisson's ratio, and elastic Debye temperature. The elastic stiffnesses of the alloys increase 4 to 13 percent on cooling from room temperature to liquid helium temperature. The elastic constant-temperature curves exhibit regular behaviour.

Newbury, D. E., **Image formation in the scanning electron microscope,** Chapter IV in *Practical Scanning Electron Microscopy,* J. I. Goldstein and H. Yakowitz, Eds., pp. 95-148 (Plenum Press, New York, N.Y., 1975).

Key words: scanning electron microscope; SEM contrast formation; SEM image defects; SEM image formation; SEM image quality; signal processing.

The image formation process in the scanning electron microscope (SEM) is described in detail. The major components of the image formation system are the scan coils, scan generator, signal detectors, amplifiers, and the cathode ray tube display. Various types of signal detectors are described: the Everhard-Thornley detector for backscattered and secondary electrons, the solid state detector for backscattered electrons, specimen (absorbed) current detection, x-ray detectors, and cathodoluminescence detectors. Contrast formation is explained. The relationship between the image quality and the characteristics of the signal is detailed. For a given contrast level, a threshold beam current exists which must be exceeded to obtain a useful image. Various types of signal processing for image enhancement are described: black level suppression (differential amplification); gamma processing (non-linear amplification); time derivative signal transformation; and Y-modulation. The application of these signal processing techniques renders image details more readily visible to the human eye. Image defects are considered. Moiré effects can be obtained in images of periodic objects. If two contrast mechanisms are present in an image, one may dominate, requiring special signal processing techniques for detection of the weaker contrast.

Newbury, D. E., **Techniques of signal processing in the scanning electron microscope,** *Proc. 8th Symp. on Scanning Electron Microscopy, St. Louis, Mo., Apr. 7, 1975,* pp. 727-736 (IIT Research Institute, Chicago, Ill., Apr. 1975).

Key words: black level suppression; nonlinear amplification; scanning electron microscope; signal differentiation; signal processing; Y-modulation.

Signal processing applied during the formation of SEM images can greatly aid the microscopist in obtaining a maximum amount of information from a specimen. Signal processing is necessary in order to overcome basic limitations of the eye in extracting information from the SEM cathode ray tube display or from photographs of the display. The four most commonly encountered forms of signal processing are black level suppression (differential amplification), nonlinear amplification (gamma), signal differentiation, and Y-modulation. Black level suppression and gamma processing are useful in producing enhanced image contrast over a small range of input signal. Signal differentiation preferentially enhances high frequency components of the image and is therefore effective for emphasizing edges. Y-modulation is particularly sensitive to fine detail and enhances the effect of surface texture.

Newbury, D. E., **The origin, detection, and uses of electron channelling contrast,** *Proc. 7th Scanning Electron Microscopy Symp., Chicago, Ill., Apr. 8-11, 1974,* pp. 1047-1054 (IIT Research Institute, Chicago, Ill., 1974).

Key words: bend contours; contrast formation; crystalline materials; electron channelling contrast; electron channelling patterns; scanning electron microscope.

In the scanning electron microscope contrast can be obtained which is related to the crystallographic nature of a specimen through the mechanism of electron channelling. This contrast originates from the periodic arrangement of atoms in a crystal and depends on the angular relationship between the beam and the lattice. When the beam is caused to sweep through a range of angles greater than the Bragg angle while confined to a single crystal, a contrast pattern, called an electron channelling pattern (ECP), results. This pattern is uniquely related to the orientation of the crystal and it can therefore be used to orient a crystal relative to the beam. Instrument techniques have been developed to obtain useful ECP's from selected areas as small as 1 μm in diameter (selected area channelling patterns, SACP). Electron channelling contrast can also be used in conventional microscopy to reveal grains, twins, and other crystallographic features in polycrystalline microstructures.

This tutorial paper discusses briefly the origin of electron channelling contrast. The stringent electron-optical conditions required to detect the contrast are described. The formation of the ECP and the SACP technique are discussed. Finally, the use of electron channelling contrast in conventional micrograph operation and the types of information which can be obtained are described.

Newbury, D. E., Yakowitz, H., **Contrast mechanisms of special interest in materials science,** Chapter V in *Practical Scanning Electron Microscopy,* J. I. Goldstein and H. Yakowitz, Eds., pp. 149-210 (Plenum Press, New York, N.Y., 1975).

Key words: cathodoluminescence; electron beam induced conductivity contrast; electron channeling contrast; magnetic domain contrast; scanning electron microscope; voltage contrast.

This chapter considers several mechanisms of contrast formation in the scanning electron microscope (SEM). The physical origin of each mechanism is considered in detail. Electron channeling contrast results from effects of the periodic arrangement of atoms in a crystal on the penetration of the incident electrons. Type I magnetic contrast arises from effects of leakage fields outside the specimen on emitted secondary electrons. Type II magnetic contrast is related to effects of the internal magnetic field on the primary electrons as they undergo scattering in the specimen. Voltage contrast arises from the effect of surface potentials on the collection of emitted secondary electrons. Electron beam induced conductivity contrast (EBIC) occurs in certain semiconductors through the formation of electron-hole pairs, locally changing the conductivity from the interaction of the primary electrons. Cathodoluminescence results due to the emission of visible light when electron-hole pairs recombine. The characteristics of each contrast mechanism are related to the SEM operating parameters required for successful image formation.

Newbury, D. E., Yakowitz, H., **Specimen preparation, special techniques, and applications of the scanning electron microscope,** Chapter VI in *Practical Scanning Electron Microscopy,* J. I. Goldstein and H. Yakowitz, Eds., pp. 211-262 (Plenum Press, New York, N.Y., 1975).

Key words: scanning electron microscope; SEM applications; SEM dynamic experiments; SEM specimen preparation; SEM stroboscopy; stereomicroscopy.

Techniques of specimen preparation for scanning electron microscopy, including degreasing, electropolishing, and deposition of conductive coatings, are discussed. Stereomicroscopy, the technique of obtaining images with depth information, is described. Dynamic experiments conducted *in situ* in the scanning electron microscope (SEM) are considered. Examples of dynamic experiments, including tensile straining and the application of magnetic fields, are given.

Stroboscopy, the imaging of high frequency, cyclical events is described. Practical applications of the SEM to a range of materials science problems are described in detail. The problems include: (1) examination of fractured metals and composites; (2) investigation of lunar soil; (3) failure analysis of a corroded steam boiler; (4) recognition of mineral phases; (5) characterization of wear particles; (6) examination of human teeth; (7) orientation and crystal perfection analysis with electron channeling effects; (8) examination of magnetic recordings; (9) examination of magnetic domain structures; (10) operation of an integrated circuit; and (11) observation of ferroelectric domains.

Newman, M., Pierce, S., **Bounded matrix groups,** *Linear and Multilinear Algebra* **1,** No. 3, 251-256 (1973).

Key words: associated matrices; Burnside theorem; irreducible representations; matrix groups.

The principal result is that if G is any irreducible subgroup of $GL(n, C)$ (C the complex field) such that $|\mathrm{tr}(TA)|$ is uniformly bounded for all A in G and some fixed $n \times n$ nonzero matrix T, then G is equivalent to a unitary group. Similar results are proved for certain associated representations of G.

Nyyssonen, D., **Partial coherence in imaging systems,** *Opt. Eng.* **13,** No. 4, 362-367 (July-Aug. 1974).

Key words: coherence measurement; microdensitometry; optical imaging; partial coherence.

An improved method of measuring spatial coherence is described and some sources of measurement errors are discussed. Partial coherence in the image plane of an optical system is discussed and results of coherence measurements are given that demonstrate the scaling of the coherence function for coherence intervals large compared to the diameter of the Airy disk and the limiting value for the coherence interval equal to the diameter of the Airy disk. The application of these results to microdensitometry is discussed and results of coherence measurements in the source plane of currently-used classical microdensitometers are given.

O'Brien, J. T., Crannell, H., Kline, F. J., Penner, S., **Ionization loss for high-energy electrons in thin targets,** *Phys. Rev. C* **9,** No. 4, 1418-1429 (Apr. 1974).

Key words: energy loss; ionization loss; most-probable energy loss; target thickness.

The most-probable ionization loss has been measured for relativistic electrons passing through thin absorbers of carbon, aluminum, and copper. Incident energies of 50 and 100 MeV were used. Target thicknesses ranged from 48 to 614 mg/cm^2 and encompass the range of thicknesses most frequently used in electron scattering experiments at these energies. The measured values of the most-probable ionization losses are in good agreement with the theoretical predictions of Sternheimer. The techniques for using values of the ionization loss to determine the target thickness in electron scattering experiments are presented.

Olver, F. W. J., **Recent error analysis of asymptotic solutions of linear differential equations,** *Proc. Int. Conf. on Differential Equations, Los Angeles, Calif., Sept. 4-7, 1974,* pp. 636-645 (Academic Press, Inc., New York, N.Y., 1975).

Key words: approximation; asymptotics; asymptotic theory; error analysis; ordinary differential equations; turning points.

Considerable progress has been made during the past fifteen years in the error analysis of asymptotic solutions of linear ordinary differential equations. In addition to computational applications, realistic error bounds provide insight into the doubly asymptotic nature of many of the approximations, thereby avoiding the need for the somewhat unsatisfactory concept of generalized asymptotic expansions. The methods that have been developed for constructing error bounds have also led to the solution of some recalcitrant problems involving two or more turning points.

Ott, W. R., Behringer, K., **Absolute vuv radiometry with hydrogen arcs—comparisons with blackbody calibrations,** *Proc. XIth Int. Conf. on Phenomena in Ionized Gases, Prague, Czechoslovakia, Sept. 10-14, 1973, Paper 4.5.2.7,* pp. 412 (Czechoslovak Academy of Sciences, Prague, Czechoslovakia, 1973).

Key words: blackbody calibrations; hydrogen continuum; primary standard; radiometry; vacuum ultraviolet; wall-stabilized arc.

A hydrogen arc has been applied for the purpose of making spectral radiance calibrations in the wavelength region 1450 to 3600 Å. Absolute calibrations using the hydrogen continuum as a primary standard are presently possible with an estimated uncertainty of ±5 percent. Such accuracies are much better than can be obtained presently by any other source calibration method in the vuv. The hydrogen arc standard has been compared with two other calibration methods. Agreement with tungsten strip lamp calibrations in the visible and near uv and with the blackbody ceiling calibration in the vuv is within the combined experimental uncertainties associated with the various methods.

Ott, W. R., Behringer, K., Gieres, G., **Vacuum ultraviolet radiometry with hydrogen arcs. 2: The high power arc as an absolute standard of spectral radiance from 124 nm to 360 nm,** *Appl. Opt.* **14,** No. 9, 2121-2128 (Sept. 1975).

Key words: arc; calibrations; hydrogen; plasma; radiometry; spectral radiance; vacuum ultraviolet; wall-stabilized.

A wall-stabilized hydrogen arc can be utilized as a standard source of spectral radiance since the continuum emission coefficient is calculable to within a few percent. Previous efforts to apply this concept have been impeded by relatively large uncertainties associated with the plasma diagnostics. The present approach yields absolute intensities independent of other radiometric standards or the accuracy of any plasma diagnostics. The hydrogen arc is operated at high temperatures where the continuum emission coefficient reaches a broad, unique, and calculable maximum. Comparisons with other primary standards are consistent with the estimated uncertainty in the arc continuum intensities.

Pallett, D. S., **Force platform instrumentation system for the study of impact forces,** *Proc. Inter-Noise Conf., Sept. 30-Oct. 2, 1974,* J. C. Snowdon, Ed., pp. 89-92 (Noise Control Foundation, Poughkeepsie, N.Y., 1974).

Key words: building acoustics; force platforms; impact noise; instrumentation; mechanical impedance; noise.

Human footfall has long been recognized as an important source of impact noise in buildings, which in turn has been recognized as an important source of occupant dissatisfaction in multi-family dwellings. Very little is known of the dynamic characteristics of the footfall event. The instrumentation system described in this paper is intended for use in research dealing with the dynamic characteristics of footfall impact events. The data obtained in this research is directed toward the question of whether it is possible to reliably specify live walkers for use in impact noise studies. Force platform design considerations and description of related signal processing are presented. Preliminary calibration data indicate that the usable response of the force platform may extend from DC to nearly 2 kHz.

Pallett, D. S., **INCE laboratory measurements survey,** *Proc. Noise-Conf., Gaithersburg, Md., Sept. 15-17, 1975,* W. W. Lang, Ed., pp. 313-316 (Noise Control Foundation, Poughkeepsie, N.Y., 1975).

Key words: acoustical measurements; acoustics; impact noise; noise emission; reverberation rooms; sound transmission.

A detailed (eight-page) questionnaire dealing with "Laboratory Measurements of Noise Emission and of Acoustical Properties of

Building Elements and Materials" was developed by an INCE Measurement Survey Task Group. Copies of this questionnaire were distributed to more than 120 organizations believed to possess acoustical laboratory facilities. Since acoustical measurements are an integral element in the conduct of acoustical research, it is believed that the results of this survey will be important in the development of research priorities. This paper provides a qualitative description of the questionnaire in order to indicate its scope.

Pallett, D. S., **Noise and the national measurement system,** *Proc. Noise-Conf., Gaithersburg, Md., Sept. 15-17, 1975,* W. W. Lang, Ed., pp. 157-182 (Noise Control Foundation, Poughkeepsie, N.Y., 1975).

Key words: acoustical measurements; acoustics; national measurement system; noise; noise control; noise emission; sound.

This paper indicates the relationship of the acoustical measurements required for the effective implementation of noise abatement and control to the social system termed the National Measurement System. The relevant physical quantities being measured are described, and the infrastructure of the relevant acoustical standardization institutions is indicated. The interactions occurring between the participants in the system are specified, and the impacts, status and trends of the system in adapting to changing technology are discussed. Finally, the interactive role of NBS in the National Measurement System is briefly outlined.

Parkinson, J. S., **Studies of human factors in building design,** *Constr. Specifier* **27,** No. 11, 41-43 (Nov. 1974).

Key words: acoustics; human factors; human occupancy; illumination; interdisciplinary approach; physiology; psychology.

The human factors which affect design are not always known or understood. The Center for Building Technology of the National Bureau of Standards has mobilized an unusual aggregation of experts to study the human factors involved in building design and physical occupancy.

This interdisciplinary approach looks, for example, at the need for windows, the optimum level of illumination, individual's reactions to noise levels and human behavior during fires. They are also trying to find out how much can be learned from the occupants of the housing built under Operation Breakthrough by conducting interviews with the tenants, interrogating visitors, studying work orders, and asking for comments from those moving out of the developments.

The human factors approach is not new but psychological and physiological test techniques have improved a great deal in the past couple of decades so that designers and builders should now be able to provide more pleasant, comfortable and efficient environments for human occupancy.

Parrish, W. R., **An economic study of electrical peaking alternatives,** (Proc. Conf. Hydrogen Economy Energy, Miami Beach, Fla., Mar. 18-20, 1974), Paper R-889 in *Hydrogen Energy,* pp. 949-968 (Plenum Press, New York, N.Y., 1975).

Key words: energy storage; hydrogen utilization; power generation; synthetic fuels.

Results are given of a feasibility study of alternatives for producing peak power. Fuel cells, batteries, and superconducting magnetic storage are considered as well as gas turbines and pumped storage. The fuels considered are hydrogen, from coal or electrolysis, synthetic natural gas, and methanol. Fuel storage alternatives include liquid, compressed gas, and for hydrogen, metallic hydride.

Patel, P. R., Brown, W. E., **Thermodynamic solubility product of human tooth enamel: powdered sample,** *J. Dent. Res.* **54,** No. 4, 728-736 (July-Aug. 1975).

Key words: dental caries; hydroxyapatite; ion activity product; solubility; tooth enamel.

Solubility of human dental enamel in H_3PO_4 was studied in the pH range of 4.5 to 7.6. Thermodynamic solubility of the enamel mineral was calculated in terms of the ion activity product, $(Ca^{2+})^5(PO_4^{3-})^3(OH^-)$, for hydroxyapatite. The solubility product varied from 7.2×10^{-53} to 6.4×10^{-58} mol^9 $liter^{-9}$ depending on the cumulative amount of the dissolution of the solid in a series of repetitive sequences of solubility experiments.

Paule, R. C., **Calculation of complex equilibria involving vaporization into vacuum,** *High Temp. Sci.* **6,** No. 4, 267-275 (Dec. 1974).

Key words: Al_2O_3; chemical doping; complex equilibria; purification (evaporative); vacuum vaporization.

A simplified, direct approach is presented to the description of complex equilibria involving vaporization into vacuum. Emphasis is on the basic problem-solving process and on modification of existing techniques. Sequential solutions are presented to problems involving purification of a melt by vaporization into vacuum. The effects of concentration of melt and oxygen partial pressures on vaporization rates are demonstrated.

Pella, P. A., DeVoe, J. R., **Systematic error in tin ore assay by Mössbauer spectrometry,** *J. Radioanal. Chem. Short Commun.* **25,** No. 1, 185-188 (1975).

Key words: Mössbauer spectrometry; quantitative analysis; Stannic oxide; tin ores.

In this work, Mössbauer spectrometry was applied to the nondestructive, quantitative analysis of tin oxide in two NBS-SRM tin ore concentrates. Systematic errors of 10 to 25 percent were observed when these ore samples were measured versus calibrant samples prepared from A.R. tin oxide. The effect of heat treatment of the ores on the resonant absorption intensity is also discussed.

Pella, P. A., Diamondstone, B. I., **Stability of aqueous ethanol solutions stored in glass ampules,** *J. Forensic Sci. Tech. Note* **20,** No. 3, 537-538 (1975).

Key words: breath alcohol analyzers; dichromate oxidimetry; performance standards; reference ethanol solutions.

Stability studies were carried out on ampules samples of ethanol-water solutions. These solutions are used to measure performance capabilities of breath alcohol detection instruments.

Peterlin, A., **Dependence of diffusive transport on morphology of crystalline polymers,** *J. Macromol. Sci. Phys.* **B-11,** No. 1, 57-87 (1975).

Key words: crazing; crystalline polymer solid; diffusion; elastic deformation; permeability; plastic deformation; sorption.

The sorption and diffusion of low molecular weight penetrants proceeds almost exclusively through the amorphous component of the semicrystalline polymer solid. The diffusive transport properties and geometrical distribution of the amorphous component are substantially modified by mechanical and thermal treatment. Deformation of spherulitic material first loosens the structure and then transforms it into a densely packed fibrous structure with a great many taut tie molecules in the amorphous component. Annealing lets the crystals grow in thickness, removes crystal defects, sharpens the boundaries between crystalline and amorphous component, and relaxes the taut tie molecules. The resulting changes of transport properties cannot be described in a satisfactory manner by crystallinity and orientation but require a detailed consideration of morphology. The elastic tensile deformation enhances sorption and diffusion by reducing the density of amorphous component. The high anisotropy of diffusion and the drastic reduction of sorption and diffusion of fibrous material are the consequence of the microfibrillar morphology with the large fraction of highly aligned and closely packed taut tie molecules which eliminate many sorption sites, enormously reduce

the diffusivity, and increase its concentration dependence. The anisotropy may be reduced during plastic deformation of the fibrous material by the increased number of interfibrillar tie molecules.

Peterlin, A., **ESR investigation of chain rupture in mechanically strained crystalline polymer solids,** (Proc. Sixth Southeastern Magnetic Resonance Conf., Clemson, S.C., Oct. 1974), *J. Magn. Reson.* **19,** 83-98 (1975).

Key words: chain rupture; crystalline polymer; ESR investigation of radicals; fibrous structure; mechanical breakdown; microfibrillar structure; radical formation; tie molecules.

ESR detects radicals formed in a strained polymer sample as a consequence of chain rupture and, hence, for a while was considered the best method for investigation of molecular effects during tensile straining. It turned out that a sufficiently high number of radicals for ESR detection is only obtained in highly oriented material with well developed fibrous structure.

The primary end-of-chain radicals are too reactive and unstable so that, as a rule, they are not observable by ESR except at cryogenic temperatures. By proton transfer, more stable center-of-chain radicals are formed which are normally measured. They yield information about primary chain rupture. The much more easy rupture of bonds adjacent to center-of-chain radicals breaks less strained chains (secondary rupture), but does not produce any new radicals. Hence, the ESR information about chain rupture is rather incomplete and has to be supplemented by other methods as for instance IR which detects the unsaturated end groups formed during radical transfer and secondary chain rupture.

Since the broken chains are not exactly the same chains which before rupture were responsible for elastic modulus and tensile strength one has no direct correlation between the radical population and the load-elongation curve of the sample even if no secondary rupture is involved. It turns out that the specific morphology, in particular the presence of point defects of fibrous structure caused by the ends of microfibrils, is responsible for crack nucleation and growth to critical size which finally leads to sample failure. The chain rupture partially monitored by the radical population is a moderately reliable indicator of the effects leading to failure but not the cause of it.

Petersen, F. R., Evenson, K. M., Jennings, D. A., Wells, J. S., Goto, K., Jiménez, J. J., **Far infrared frequency synthesis with stabilized CO_2 lasers: Accurate measurements of the water vapor and methyl alcohol laser frequencies,** *IEEE J. Quantum Electron.* **QE-11,** No. 10, 838-843 (Oct. 1975).

Key words: absolute frequency measurements; laser frequency synthesis; water vapor laser.

A far infrared (FIR) frequency synthesis technique using saturated-absorption stabilized CO_2 lasers and a point-contact diode has been used to measure frequencies of a number of strong CW H_2O, D_2O, and CH_3OH laser lines. The first frequency measurements of the 79-μm H_2O, the 73- and 108-μm D_2O, and 11 CO_2-pumped CW $^{12}CH_3{}^{16}OH$ laser lines are reported. This measurement is the first demonstration of the general usefulness of CO_2 lasers for accurate synthesis of FIR frequencies.

Phillips, J. C., Wall, L. A., Aldridge, M. H., **Liquid (melt) heat capacities and heats of vaporization of oligomers of poly(hexamethylene sebacate),** *Polym. Eng. Sci.* **15,** No. 2, 73-78 (Feb. 1975).

Key words: alkanes; esters; heat capacity; heats of vaporization; oligomers; rates.

The liquid heat capacities and heats of vaporization of three linear esters of poly(hexamethylene sebacate) with hexyl-capped end groups (M(mol.wt.) = 370, 655, and 939) have been determined. The heats of vaporization of the oligomers measured at a mean temperature were corrected to 323.15 to 523.15 K by use of the experimental liquid (melt) heat capacities and the calculated gas heat capacities. The corrected heats of vaporization were fitted to the equation $\Delta H_v = S(T)M^{\alpha} + I(T)$, where the temperature dependence of the slope and intercept are represented, respectively, as $S(T) = C\ln T + K_0$ and $I(T) = aT + b_0$, and α is an exponent. The results indicate (at corresponding molecular weights and constant temperature) that the ratio of the liquid heat capacities of the oligomer ester and the n-alkane, and similarly the ratio of the heats of vaporization, depend on the number of carboxyl groups in the oligomer ester chain.

Pickart, S., Rhyne, J., Alperin, H., Savage, H., **Neutron diffraction study of sputtered and annealed Tb-Fe alloys,** *Phys. Lett.* **47A,** No. 1, 73-74 (Feb. 25, 1974).

Key words: amorphous alloys; amorphous magnetism; coercine magnetic force; magnetic structure; neutron diffraction; recrystallization; terbium-iron.

Sputtered alloys of composition $Tb_x Fe_{1-x}$, with $x = 0.118$, 0.45 and 0.75 were shown by neutron diffraction to be amorphous. Line-width measurements of an anealed sputtered sample with $x = 0.333$ indicate microcrystallinity with a particle size of ≈ 100 Å.

Piermarini, G. J., Block, S., **Ultrahigh pressure diamond-anvil cell and several semiconductor phase transition pressures in relation to the fixed point pressure scale,** *Rev. Sci. Instrum.* **46,** No. 8, 973-979 (Aug. 1975).

Key words: diamond-anvil pressure cell; fixed point pressure scale; high pressure; NaCl pressure scale; pressure measurement; ruby fluorescence; semiconductors; transition pressures.

A diamond-anvil type optical cell of improved design has produced static pressures in gasketed samples up to 500 kilobar as measured by the ruby fluorescence technique. The ruby R_1 line pressure shift is linear to 291 kilobar, and the maximum measured shift is extrapolated to 500 kilobar assuming continued linearity of the pressure dependence. The ultimate pressure capability of this diamond cell has not been established. Transition pressures in the semiconductors Si, ZnSe, ZnS, and GaP measured by the ruby method indicate that the revised 1970 fixed point scale and the ruby (NaCl) scale diverge above 135 kilobar and disagreement may be by as much as a factor of 2 in the 500 kilobar range with the ruby scale defining the lower pressure.

Prask, H., Trevino, S., Tsai, D. H., MacDonald, R. A., Kemmey, P., Yip, S., **Computer simulation studies of the microscopic behavior of shocked solids,** *Proc. Conf. on Mechanisms of Explosion and Blast Waves, Naval Weapons Station, Yorktown, Va., Nov. 13-15, 1973,* 1-21 (1974).

Key words: blast waves; computer simulation; interatomic potentials; lattice dynamics; molecular dynamics; shock waves.

The application of computer molecular dynamics (CMD) techniques to the understanding of blast wave phenomena in solids is discussed. Examples of CMD studies of simple systems undergoing plane shock waves are reviewed and the inadequacy of some of the assumptions made in the conventional continuum approach examined. Recent advances made in obtaining approximate interatomic potentials for complex solids from conventional lattice-dynamical studies are reviewed for NaN_3 and KN_3. These results are discussed in the context of extending the scope of CMD calculations.

Prince, E., **Dimethyl sulfone diimine, a neutron study,** *Acta Crystallogr. Short Structural Papers* **B31,** Part 10, 2536-2537 (1975).

Key words: alkyl sulfone; crystal structures; dimethyl sulfone diimine; hydrogen bonds; neutron diffraction; sulfone.

$(CH_3)_2S(NH)_2$, orthorhombic, $F2dd$ (No. 43), $a = 5.44$, $b = 10.59$, $c =$

16.13 Å, $Z=8$. The structure was refined from neutron diffraction data. The molecules lie on twofold axes, and are linked together by a three-dimensional network of N—H...N hydrogen bonds. The methyl groups are in an eclipsed conformation.

Prince, E., Mighell, A. D., Reimann, C. W., Santoro, A., **Hexakis(imidazole)cobalt(II) nitrate, $[Co(C_3H_4N_2)_6](NO_3)_2$,** *Cryst. Struct. Commun.* **1**, 247-252 (1972).

Key words: cobalt; complexes; hexakis(imidazole)cobalt(II) nitrate; imidazole, neutron: structure; x ray.

The structure of the title compound was determined by x-ray and neutron diffraction techniques. The hydrogen bonding in the structure was uniquely determined from the neutron data. Bond distances and angles obtained with the two techniques are compared.

Prince, E., Trevino, S. F., Choi, C. S., Farr, M. K., **A refinement of the structure of deuterium peroxide,** *J. Chem. Phys.* **63**, No. 6, 2620-2624 (Sept. 15, 1975).

Key words: crystal structure; deuterium peroxide; hydrogen bonds; hydrogen peroxide; neutron diffraction; structure refinement; thermal motion.

The structure of deuterated hydrogen peroxide, D_2O_2, at -15 °C was refined by least-squares methods from three dimensional neutron diffraction data. The data were fitted to two models, one with conventional anisotropic temperature factors and the other with the molecule treated as a rigid body except for torsional oscillations of the O—D groups about the O—O bond. The weighted agreement indices were 0.030 over 106 observed reflections for the conventional model and 0.032 over 102 reflections for the rigid body model. The structure is tetragonal, space group $P4_12_12$ or $P4_32_12$, with $a=4.035$ Å, $c=7.97$ Å, $Z=4$. Position parameters for the two models are essentially the same. The O—O distance in the molecule, 1.455(2) Å, is identical to that found in H_2O_2, but the O—D bond is about 0.015 Å shorter than the O—H bond, 0.993 Å as compared with 1.008 Å when corrected for thermal motion by the riding model. The O—O distance corrected for thermal motion in the rigid body model is 1.49 Å, in fair agreement with the value 1.48 Å found in the vapor phase.

Quintiere, J., **Some observations on building corridor fires,** *Proc. Fifteenth Symp. (International) on Combustion, Tokyo, Japan, Aug. 25-31, 1974*, pp. 163-174 (The Combustion Institute, Pittsburgh, Pa., 1974).

Key words: corridor; fire spread; flashover; floor covering; radiative heat transfer.

Full-scale corridor fire experiments designed to evaluate the potential fire hazard of floor covering materials exposed to a room fire are described. A phenomenological account of events leading to rapid fire propagation along the corridor is presented for one experiment. Mechanisms responsible for the rapid fire propagation, termed flameover, are explored through measurements and analysis of the data. Before flameover the corridor floor is heated by radiation which enables flames to spread into the corridor. On the wood floor considered, flame spread velocity accelerates from $\sim 10^{-2}$ ft/sec to ~ 1 ft/sec following flameover. Causative factors of flameover appear to be the increase in flame height of the floor fire, and a reduction of air supply to the burn room due to a change in flow pattern between the corridor and burn room. Calculations show that air flow to the burn room steadily drops as the corridor fire develops resulting in incomplete combustion for the room fire.

Radak, B. B., Kosanić, M. M., Sešić, M. B., McLaughlin, W. L., **A calorimetric approach to the calibration of liquid dose meters in high-intensity electron beams,** (Proc. Symp. on Biomedical Dosimetry, IAEA, Vienna, Austria, 1975), Chapter in *Biomedical Dosimetry*, pp. 633-641 (Int. Atomic Energy Agency, Vienna, Austria, 1975).

Key words: absorbed dose rate; calorimetry; chemical dosimetry; electron beams; gamma radiation; radiation dosimetry; radiochromic dyes.

A procedure for calibrating liquid dose meter systems in pulsed high-intensity electron beams is presented. The chemical change produced in solution by a totally absorbed collimated beam has been compared with the heat deposited in a calorimeter exposed to the same beam under identical conditions. Thin film dose meters containing radiochromic dyes, which were known to have a response that does not vary with absorbed dose-rate, were used to monitor the energy absorbed during irradiations. A quasi-adiabatic calorimeter and a cell of the same geometry for containment of the dosimetry solutions are described. The G-value for dye formation in 2-mmol/litre pararosaniline cyanide in 2-methoxy ethanol (O_2-saturated) has been determined in the range of dose-rates from 10^{12} to 10^{13} rad/s.

Radebaugh, R., Holste, J. C., Siegwarth, J. D., **Thermometric characteristics of some 1/8 W carbon resistors in the millikelvin range,** *Proc. Fifth Int. Cryogenic Engineering Conference, Kyoto, Japan, May 7-10, 1974*, Paper H11, pp. 253-255 (IPC Science & Technical Press, Kent, England, 1974).

Key words: carbon resistors; cryogenics; liquid helium; millikelvin; thermometry.

Gotoh and Awano have reported on the useful characteristics of 1/8 watt 100 Ω Matsushita carbon resistors (grade ERC-18GK) as thermometers for the region 0.4 and 4.2 K. We report here measurements on the resistance characteristics of this grade of resistors from 11 mK to 4 K. Nominal resistances of 56 Ω, 100 Ω and 220 Ω have been measured. We find that the 56 Ω resistor is useful as a thermometer down to at least 11 mK. Its sensitivity increases rather rapidly below 100 mK, which is a desirable feature because it is in this region where measuring power levels must be kept extremely small. At 20 mK the resistance of the 56 Ω resistor is about 4000 Ω, that of the 100 Ω resistor is about 5×10^5 Ω, and that of the 220 Ω resistor is about 10^8 Ω. A comparison of the resistance behavior of units immersed in dilute He^3-He^4 with those outside the liquid will also be made.

Radebaugh, R., Lawless, W. N., Siegwarth, J. D., **Semi-annual technical report on electrocaloric refrigeration for superconductors,** *ARPA Order 2535*, 17 pages (Available as AD-A008-852 from the National Technical Information Service, Springfield, Va., 1974).

Key words: cryogenics; dielectrics; electrocaloric; heat switches; polarization; refrigeration.

The most significant development in the project for the last six months was the discovery that $SrTiO_3$ glass ceramics showed only heating effects at 4 K for both polarization and depolarization. At the same time, the pitting problem for ceramming temperatures above 1100 °C was partially solved.

Several electrothermal measurements have been done on the $SrTiO_3$ glass-ceramic samples to try to understand why they behave as they do. In addition an apparatus for measurement of DC polarization and hysteresis was completed. The results from those measurements are consistent with the electrothermal measurements. Studies of several new materials have begun in order to better understand the electrocaloric effect near 4 K and in hopes of finding a satisfactory refrigerant material.

The gold-plated multiple leaf heat switch was shown to be useful for heat loads up to about 1 watt at 4 K. The magnetothermal conductivity measurements on single crystal beryllium indicate that it could be used for both the upper and lower switch. Further work on some details of the heat switches has been temporarily suspended in order to concentrate fully on solving the refrigerant material problem.

Radebaugh, R., Siegwarth, J. D., Holste, J. C., **Heat transfer between sub-micron silver powder and dilute He^3-He^4 solutions,** (Proc. 5th Int. Cryogenic Engineering Conf., Kyoto, Japan, May 7, 1974), Paper H6 in *5th International Cryogenic Engineering Conference*, K. Mendelssohn, Ed., pp. 242-245 (IPC Science and Technology Press, Surrey, England, 1974).

Key words: cryogenics; dilution refrigerator; heat transfer; helium 3; helium 4; Kapitza resistance; liquid helium; powder; silver.

The thermal resistance between copper cells lined with silver powder of 0.1—0.2 μm diameter and a dilute stream of He^3 in He^4 was measured between 15 and 250 mK. The results show that this powder can give an order of magnitude lower thermal resistance at 15 mK than an equal volume of copper powder of 1.8 μm diameter. The scientific and engineering significance of such a low resistance in a small volume is discussed. At the higher temperatures R is proportional to T^{-1}, which can be explained by a liquid thermal resistance and a resistance at the joint between the powder and the cell walls.

Radebaugh, R., Siegwarth, J. D., Oda, Y., Nagano, H., **Experiments with miniature heat exchangers for dilution refrigerators,** (Proc. 5th Int. Cryogenic Engineering Conf., Kyoto, Japan, May 7, 1974), Paper H3 in *5th International Cryogenic Engineering Conference, K. Mendelssohn, Ed., pp. 235-237 (IPC Science and Technology Press, Surrey, England, 1974).*

Key words: copper alloy; copper; cryogenics; dilution refrigerator; heat exchanger; Kapitza resistance; liquid helium; powder; silver.

This paper describes experiments done on three types of miniature heat exchanger for dilution refrigerators. These have liquid volumes on the order of 0.1 cm^3. The first is a continuous exchanger incorporating Cu(Cr) powder, the second is a continuous exchanger incorporating sub-micron silver powder, and the third is a discrete exchanger incorporating 1.8 μm copper powder. The first two were not successful and the reasons are not entirely clear. The third exchanger performed about as calculated and permits an order of magnitude reduction in liquid volumes from that normally used.

Reader, J., **Spectrum of Rb III observed with a pulsed-rf light source,** *J. Opt. Soc. Am.* **65,** No. 9, 988-990 (Sept. 1975).

Key words: rubidium; spectra; ultraviolet; wavelengths.

The spectrum of doubly ionized rubidium, Rb III, was observed with a pulsed-rf light source on two 10.7 m normal-incidence spectrographs at NBS. Wavelengths and classifications were obtained for 103 Rb III lines, 90 of which were newly observed. The three missing levels of the $4p^4 4d$ configuration, $(^3P)^4F_{9/2}$ and $(^1D)^2G_{7/2,9/2}$, and the one missing level of the $4p^4 5p$ configuration, $(^1S_0)\,[1]_{1/2}$, were located. The $4p^4(^1D)5d^2G_{9/2}$ level was also located. Improved values were determined for 13 excited levels.

Reneker, D. H., Martin, G. M., Broadhurst, M. G., **Search for correlations between dielectric relaxation and polymerization in trioxane crystals,** *J. Appl. Phys.* **45,** No. 10, 4172-4174 (Oct. 1974).

Key words: dielectric loss; dielectric relaxation; molecular motions; nuclear magnetic resonance absorption; polyoxymethylene crystals; solid state polymerization; trioxane crystals.

After exposure to ionizing radiation, trioxane polymerizes rapidly at temperatures between 50 and 60 °C. The nature of the molecular motions involved in this solid-state reaction is not clear. Line narrowing in nuclear magnetic resonance absorption has been reported as one indication of such motions. No related dielectric loss peaks were found in trioxane at temperatures from − 180 to 55 °C and frequencies from 1 to 10 000 Hz. Ionic conductivity is large above room temperature and it may play an important role in this polymerization reaction.

Reneker, D. H., Martin, G. M., Rubin, R. J., Colson, J. P., **Effect of polymeric structure on the permeation rate in standard reference material sulfur dioxide permeation tubes,** (Proc. Society of Plastics Engineers ANTEC Conf., San Francisco, Calif., May 1974), *Polym. Eng. Sci.* **15,** No. 1, 11-15 (Jan. 1975).

Key words: density; fluorocarbon copolymer; morphology; permeation; permeation tubes; polymer structure; sulfur dioxide.

Liquid SO_2 sealed into tubes made of a fluorocarbon copolymer permeates the walls of the tube at a temperature-dependent but accurately reproducible rate. Sulfur dioxide dispensers made in this way are called permeation tubes and are useful for calibrating instruments that measure SO_2 concentrations in air. The National Bureau of Standards calibrates SO_2 permeation tubes and makes them available as Standard Reference Materials. The permeation rate in a batch of nominally identical tubes varies enough that each Standard Reference Material tube must be individually calibrated. Changes in the length or radial dimensions of the tubes are much too small to explain most of this variation. An excellent (negative) correlation is found between the measured permeation rate and the density of the polymer (or weight per unit length). Since both the measured density and the permeation rate for this semi-crystalline polymer depend upon morphological factors, but in different ways, x-ray diffraction measurements of the thickness and orientation of the lamellar crystals were made and a mathematical model was set up to identify the morphological factors which can cause variations in the permeation rate.

Rhyne, J. J., Pickart, S. J., Alperin, H. A., **Magnetism in amorphous terbium-iron,** (Proc. 19th AIP Conf. on Magnetism and Magnetic Materials, Boston, Mass., Nov. 13-16, 1973), Chapter in *Magnetism and Magnetic Materials*, C. D. Graham, Jr., and J. J. Rhyne, Eds., pp. 503-577 (American Institute of Physics, New York, N.Y., 1974).

Key words: amorphous materials; magnetic materials; neutron diffraction; rare earths.

Neutron diffraction and magnetization measurements on a sputtered specimen of 33 percent terbium, 66 percent iron have confirmed the existence of long range magnetic order and an amorphous spatial distribution of atoms and spin sites. Elastic diffraction data taken above and below the 409 K Curie temperature have enabled the separation of nuclear and magnetic scattering contributions. The magnetic spin density function contains a very broad major peak, dominated by the Tb-Tb pair distribution function, with a maximum near 3.6 A. Longer range correlations are very much weaker. The principal features of the atomic structure can be accounted for by considering only near neighbor correlations between terbium and iron atoms in a random close-packed arrangement.

Inelastic scattering studies have revealed a significant shift in the magnetic density of states to lower energy in the amorphous material relative to the crystalline $TbFe_2$ counterpart. No discrete spin-wave excitations or critical scattering near T_c could be observed.

Robertson, B., **Evaluation of automotive fuel flowmeters,** *Proc. Automotive Energy Efficiency Program, Cambridge, Mass., Jan. 15-17, 1975, DOT-TSC-OST-75-31*, pp. 121-134 (National Technical Information Service, Springfield, Va., June 1975).

Key words: automotive fuel flowmeter environment; automotive fuel flowmeters; flowmeter evaluation; flowmeter evaluation test setup; flowmeters; gasoline flowmeter.

Fuel economy measurement procedures are being developed by the Transportation Systems Center. Flowmeters will be used to measure the gasoline consumed by the engine of an automobile either on the road or on a dynamometer. The role played by NBS in this work

is to survey commercially available meters and find which ones might be suitable, to determine the environment in which they will be ultimately used, and to measure their accuracy in a laboratory simulation of that environment.

A discussion will be given of: (1) the different kinds of possibly suitable flowmeters to measure gasoline flow to the carburetor, (2) the environment of the flowmeter in an automobile (.lowmeter temperature; fuel temperature, pressure, density, viscosity, color, opacity, flow pulsations, backflow, and swirl due to elbows; line voltage fluctuations; electromagnetic radiation from ignition; vehicle attitude with respect to the vertical; and vibration), and (3) plans for a test setup for evaluating and calibrating these meters in the laboratory under conditions simulating the automotive environment.

Roestamsjah, Wall, L. A., Florin, R. E., Aldridge, M. H., Fetters, L. J., **Degrading mixtures of monodisperse poly-α-methylstyrenes: Rates and anomalous molecular weight distributions,** *J. Polym. Sci. Polym. Phys. Ed.* **13,** 1783-1787 (1975).

Key words: mixtures; molecular weight distribution; monodisperse poly-α-methylstyrene; thermal degradation.

When a mixture of two monodisperse samples of poly-α-methylstyrene is thermally degraded, the components behave independently as a first approximation, as shown by GPC and rate of volatilization data. The ratio M_w/M_n, before approaching the ultimate value of 2.0, first goes through a minimum at a much lower value.

Rook, H. L., Moody, J. R., **Stabilization and determination of nanogram quantities of mercury in water,** (Proc. Second Int. Conf. on Nuclear Methods in Environmental Research, Univ. of Missouri, Columbia, Mo., July 29-31, 1974), Paper in *Nuclear Methods in Environmental Research,* J. R. Vogt and W. Meyer, Eds., CONF 740701, pp. 44-53 (Available from the National Technical Information Service, Springfield, Va., 1974).

Key words: mercury; stabilization; standard reference material; trace element; water standard.

The National Bureau of Standards has completed development work and analytical certification on two Mercury in Water Standard Reference Materials (SRM). SRM #1641 has a mercury content of 1.52 ± 0.05 μg Hg^{++} per gram of water and is intended as a "spike" standard for natural waters. SRM #1642 has a mercury content of 1.20 ± 0.05 ng Hg^{++} per gram of water and is intended as a benchmark trace standard used for analytical methods development.

These Standards have been stabilized using a new technique developed at NBS. Shelf life of the trace solutions has been demonstrated to be greater than one year with expectation of an even longer storage capability.

Rook, H. L., Suddueth, J. E., Becker, D. A., **Determination of iodine-129 at natural levels using neutron activation and isotopic separation,** *Anal. Chem.* **47,** No. 9, 1557-1562 (Aug. 1975).

Key words: improved limits of detection; iodine-129; isotopic separation; neutron activation.

Iodine-129 levels have been published for biological matrices that naturally accumulate iodine such as animal thyroid and kelp. However, published procedures have insufficient sensitivity to determine ^{129}I in other environmental and biological species. A unique procedure has been developed for the determination of ^{129}I which couples neutron activation with mass separation. The procedure results in a significant improvement in sensitivity, thus allowing analyses to be performed on a variety of matrices which heretofore had not been investigated. Method development and analytical procedures are presented and analytical results at the $10^{-13}-10^{-14}$ gram ^{129}I level are given.

Rosasco, G. J., Etz, E. S., Cassatt, W. A., **The analysis of discrete fine particles by Raman spectroscopy,** *Appl. Spectrosc.* **29,** No. 5, 396-404 (Sept.-Oct. 1975).

Key words: fine particles; laser Raman; micro-Raman; particle analysis; particulates; Raman spectroscopy.

A conventional laser Raman spectrometer has been modified and used to obtain useful Raman spectra from discrete solid particles as small as 0.7 μm in linear dimensions. Spectra obtained from single, micrometer-sized particles of several inorganic and organic compounds are reported. Simplified calculations are discussed which provide an estimate of detectability levels and other problems associated with these measurements. Certain parameters that must be considered in the design of an instrument especially intended for use in the chemical characterization of single fine particles are reviewed in the light of this work.

Rosenthal, R., **Accessing online network resources with a network access machine,** *Proc. IEEE Intercon 1975 Conf. Record on Access to Computer Networks, Session 25, New York, N.Y., Apr. 8-10, 1974,* 4 pages (Institute of Electrical and Electronics Engineers, Inc., New York, N.Y., 1974).

Key words: access procedures; command language; computer networks; macros; minicomputers; protocols.

While a large variety of computer resources is available to online users of computer networks, access to these resources is often complex and cumbersome. This paper describes a Network Access Machine (NAM) which acts as a network access point for a user at his terminal and assists the user through the automatic execution of access procedures.

Rosenthal, R., Watkins, S. W., **Automated access to network resources. A network access machine,** *Proc. 1974 Symp. on Computer Networks: Trends and Applications, Gaithersburg, Md., May 23, 1974,* pp. 47-50 (Institute of Electrical and Electronics Engineers, Inc., New York, N.Y., 1974).

Key words: automated computer access; computer networking; macro processor; minicomputer-based systems; operating systems.

A minicomputer based Network Access Machine to establish the access path between a user at a terminal and a computer network resource is described. The minicomputer maintains a file directory from which access procedures are referenced. Access procedures take the form of macros which expand to produce machine dependent dialogue. The dialogue consists of the messages to be sent to the computer network and the expected responses. Actual responses are compared with the expected response to ensure that resource access is proceeding normally.

Roth, R. S., Brower, W. S., Parker, H. S., Minor, D. B., Waring, J. L., **Alkali oxide-tantalum, niobium and antimony oxide ionic conductors,** *NASA CR-134869,* 76 pages (National Technical Information Service, Springfield, Va., 1975).

Key words: ionic conductivity; nonstoichiometry; potassium antimonate; rubidium niobate; rubidium tantalate; sodium antimonate; sodium antimonate fluoride.

The phase equilibrium relations of four systems were investigated in detail. These consisted of sodium and potassium antimonates with antimony oxide and tantalum and niobium oxide with rubidium oxide as far as the ratio $4Rb_2O{:}11B_2O_5$ (B = Nb, Ta). The ternary system $NaSbO_3$-Sb_2O_4-NaF was also investigated extensively to determine the actual composition of the body centered cubic sodium antimonate. In addition, various other binary and ternary oxide systems involving alkali oxides were examined in lesser detail. The phases synthesized were screened by ion exchange methods to determine mobility of the alkali ion within the niobium, tantalum or antimony

597-633 O - 76 - 9

oxide (fluoride) structural framework. Five structure types were found to be of sufficient interest to warrant further investigation. These structure types are (1) hexagonal tungsten bronze (HTB), (2) pyrochlore, (3) the hybrid HTB-pyrochlore hexagonal ordered phases, (4) body centered cubic antimonates and (5) $2K_2O{:}3Nb_2O_5$. Although all of these phases exhibit good ion exchange properties only the pyrochlore has so far been prepared with Na^+ ions as an equilibrium phase and as a low porosity ceramic. Unfortunately Sb^{+3} in the channel apparently interferes with ionic conductivity in this case, although relatively good ionic conductivity was found for the metastable Na^+ ion exchanged analogs of $RbTa_2O_5F$ and $KTaWO_6$ pyrochlore phases. Small crystals of the other phases can generally be prepared by flux techniques and ion exchanged with Na^+. However, in the one case where congruency allows large crystals to be pulled from the melt ($4Rb_2O{:}11Nb_2O_5$) ion exchange techniques up to ~ 450 °C are not sufficient to accomplish complete replacement with Na^+ ions.

Rowe, J. M., Price, D. L., Ostrowski, G. E., **Inelastic neutron scattering from a liquid ^{3}He-^{4}He mixture,** *Phys. Rev. Lett.* **31,** No. 8, 510-513 (Aug. 20, 1973).

Key words: lifetime of excitations; neutron scattering; perturbation of elementary excitations; quantum liquids; roton minimum; ^{3}He ^{4}He solutions.

We report inelastic-neutron-scattering measurements on liquid $^3He_{0.05}{}^4He_{0.95}$ in the Q region from 0.8 to 2.3 Å^{-1} at 1.6 K. The shifts and increases in natural linewidth of the single excitation peaks relative to pure ^{4}He at the same temperature were determined by a least-squares fitting procedure. The shifts vary from a small, possibly negative, value at the roton minimum to positive values around 0.5 K at both ends of the Q range. The full widths at half-maximum of the extra broadening vary from 0.5 to 1.5 K over the same range.

Rowe, J. M., Vagelatos, N., Rush, J. J., Flotow, H. E., **Acoustic modes of the phonon dispersion relation of NbD_x alloys,** *Phys. Rev. B* **12,** No. 8, 2959-2964 (Oct. 15, 1975).

Key words: alloy; electronic structure; interstitial; lattice dynamics; niobium deuteride; phonons.

The acoustic modes of the phonon dispersion relation in Nb, $NbD_{0.15}$, and $NbD_{0.45}$ have been measured at 473 K for phonons with wave vectors along the [100], [110], and [111] axes by coherent neutron scattering. The observed neutron groups for both alloys were well defined, with little or no apparent broadening. The results are compared to similar data for Nb-Mo alloys and with previous lattice-dynamics results for $PdD_{0.63}$. This comparison shows that despite differences in detail, the general features of the dispersion relations of NbD_x and Nb-Mo are similar after allowing for the differences in lattice parameters for the two alloys. The measured dispersion curves and derived phonon frequency distributions for the Nb-D alloys are quite different from the analogous results for $PdD_{0.63}$ in that the average acoustic phonon frequencies *increase* with increasing deuterium concentration and lattice parameter.

Rush, J. J., Livingston, R. C., de Graaf, L. A., Flotow, H. E., Rowe, J. M., **Study of hydrogen diffusion in tantalum hydrides by inelastic neutron scattering,** *J. Chem. Phys.* **59,** No. 12, 6570-6576 (Dec. 15, 1973).

Key words: activation energy; hydrogen diffusion; neutron scattering; quasielastic scattering; resonance time; tantalum hydrides; vibrational amplitude.

Neutron inelastic scattering spectra have been measured as a function of temperature and scattering angle for α-$TaH_{0.15}$ and for Ta_2H in its α and β_1 phases. The widths of the quasielastic peaks vs momentum transfer (Q) have been derived and compared with several models for hydrogen diffusion. The results suggest the dominance of tetrahedral jumps in the diffusion process, although no completely satisfactory theoretical fit was obtained. Residence times τ between 1.6 (340 °C) and 4.0 (148 °C) psec for $TaH_{0.15}$ and between 2.4 (300 °C) and 7 (153 °C) psec for Ta_2H were derived from the fit of the observed widths to the tetrahedral model. These results indicate a significant concentration dependence of the diffusion rates in α-TaH_x, with activation energies for diffusion of 10.4 ± 1.2 kJ/mol in $TaH_{0.15}$ and 15 ± 1.2 kJ/mol for Ta_2H. "Effective" mean square amplitudes of proton vibration of 0.02-0.04 Å^2 were obtained from the Q dependence of the quasielastic peak intensities, in reasonable agreement with the values predicted from relatively crude vibration frequency distributions obtained from our inelastic scattering spectra in the α phase. Our results are compared in detail with previous neutron results on VH_x and NbH_x. On the basis of this comparison it is tentatively concluded that the very high "Debye-Waller factors" obtained for VH_x and some other hydrides are related to high hydrogen diffusion rates.

Rybicki, G. B., Hummer, D. G., **A note on the "peaking effect" in spherical-geometry transfer problems,** *Mon. Not. Roy. Astr. Soc.* **170,** 423-427 (1975).

Key words: astrophysics; energy loss; radiative transfer; spectral line formation; stellar atmospheres.

This note presents evidence that the claims advanced by Wilson, Tung & Sen regarding the adequacy of Wilson & Sen's half-range moment method for treating the outward peaking of the radiation field in a spherical system are unjustified. In particular, the emergent intensity obtained by Wilson *et al.* is shown to be negative for $0 \leq \mu \lesssim 0.5$ and greatly in error for larger values of μ. A discussion is presented of the essential indeterminacy of the Wilson-Sen half-range method. It is suggested that the good values obtained by Wilson *et al.* for the mean intensity and the Eddington factor arise from their choice of the arbitrary function $A(r)$ to include the known asymptotic forms of the source function.

Saloman, E. B., **Time response of NBS windowless XUV radiometric transfer standard detectors,** *Appl. Opt.* **14,** No. 8, 1764 (Aug. 1975).

Key words: radiometry; rise time; temporal response; transfer standard detector; XUV photodiode.

For the spectral region between 200 Å and 1200 Å the NBS radiometric standard detector is a windowless photodiode with a 2.5 cm diameter cathode made of evaporated aluminum on whose surface a 150 Å thick Al_2O_3 layer has been anodized. A study has been made of the response of these diodes to pulsed radiation. A Garton-type flashlamp was modified to provide pulses of radiation with a duration of about 1 μsec. These pulses were passed through a half-meter Seya-Namioka vacuum monochromator and the zero order radiation was allowed to fall on the cathode of the diode. The emitted cathode current of the diode across a 50Ω load was displayed by an oscilloscope. Output pulses were observed with instantaneous amplitudes as high as 1 mA with no evidence of saturation. The rise time of the diode output pulses was on the order of 300 nsec which was the expected rise time of the flashlamp. In order to confirm that the rise time was flashlamp limited, a diode with a tungsten cathode was substituted for the Al_2O_3 diode. The temporal results were identical. Thus we are able to conclude that the NBS windowless Al_2O_3 radiometric transfer standard diodes have a rise time shorter than 300 nsec.

Sams, R. L., Lafferty, W. J., **High-resolution infrared spectrum of the $\nu_2+\nu_3$ band of $^{14}N^{16}O_2$,** *J. Mol. Spectrosc.* **56,** 399-410 (1975).

Key words: anharmonic constant; Coriolis resonance; high resolution; infrared spectrum; nitrogen dioxide; spin splitting.

The $\nu_2+\nu_3$ band of $^{14}N^{16}O_2$ has been recorded with resolution of 0.028 cm^{-1}. Ground state and upper state rotational constants have been obtained. The band center obtained, $\nu_0 = 2355.1517 \pm 0.0011$

cm^{-1} (error cited is 3σ), has been combined with the band centers recently determined for ν_3 and ν_2 to calculate $X_{23} = -11.348 \pm 0.020$ cm^{-1} where the uncertainty cited is based on reasonable estimates of the absolute frequency error.

Sarkes, L. A., Mann, D. B., **A survey of LNG technological needs in the U.S.A.—1974 to beyond 2000,** *Proc. 4th Int. Conf. on Liquefied Natural Gas, Algiers, Algeria, June 24-27, 1974, Session VII,* Paper 1, pp. 1-21 (Institute of Gas Technology, Chicago, Ill., 1974).

Key words: cryogenic; gas industry; liquefied natural gas; research; survey; technology.

A comprehensive analysis of near and long term research needs has been conducted by the U.S. Gas Industry covering operational areas of Production and Exploration, Synthetic Supply, Transmission, Distribution, Utilization, and LNG.

Identifiable research needs are reported for the area of LNG encompassing time frames of: 1974-1978 (in detail, year by year); 1979-1985 (in 5 year period); 1986-2000 (as specific as possible); beyond 2000 (as believed necessary).

A year by year examination of LNG research priorities for the first five years are considered vital to overcome the potential suppression of growth in the LNG industry that could result from lack of available technology. Assessments of technical LNG needs beyond 1978 cannot, of course, be too well defined and must be examined annually for purposes of updating.

The National Bureau of Standards Cryogenics Division has become the governmental focal point for LNG research. A survey of NBS LNG research and how these relate to the future technological growth of the LNG industry are discussed.

Scheide, E. P., Taylor, J. K., **Piezoelectric sensor for mercury in air,** *Environ. Sci. Technol.* **8,** No. 13, 1097-1099 (Dec. 1974).

Key words: air pollution; chemical analysis; industrial hygiene; mercury; piezoelectric detector; trace analysis.

A quartz piezoelectric crystal detector with gold evaporated onto the electrode as the sensor substrate has been developed for the detection of small mass changes caused by the selective adsorption of mercury vapor from an air sample. Incorporation of the crystal into a variable oscillator circuit and measurement of the change in frequency of the crystal due to the increase in mass allows a highly sensitive indication of the amount of mercury present in the air sample down to the subpart-per-billion level. Thus, the selectivity of mercury adsorption onto gold films and the sensitivity of the piezoelectric sensor are combined in this instrument. Calibration curves are obtained from part-per-million to subpart-per-billion concentrations of mercury. Reversibility is achieved by placing the sensor in an oven, raising the temperature to 150 °C, and flow switching a stream of clean, dry air over the detector. This detector has potential use both as an air pollution sensor and in industrial hygiene applications.

Scheps, R., Ottinger, C., York, G., Gallagher, A., **Continuum spectra and potentials of Li-noble gas molecules,** *J. Chem. Phys.* **63,** No. 6, 2581-2590 (Sept. 15, 1975).

Key words: lithium; molecules; noble gases.

The normalized emission spectrum of the Li($2p - 2s$) resonance transition has been measured in the presence of 10-1000 torr of noble gas. Fluorescence at 100-3000 Å from the atomic line, due to the *A-X* and *B-X* bands of Li-noble gas molecules, has been measured as a continuum with 1.5 nm resolution. The lithium is optically excited in a 670 K cell. The lithium is optically thin ($\sim 10^{-6}$ torr) so that the continuum emission per excited lithium atom is obtained from the normalized emission. The attractive *A*-state potentials for Li-Ar, Kr, and Xe have been constructed by analysis of the *A-X* band spectra in the limit of high and low noble-gas densities. At high densities each spectrum is due to an equilibrated vibrational distribution of *A*-state molecules, whereas at low densities only free collision states contribute. The ratio of the two spectra thus depends on the excited state potential and has been used to determine this potential where it is attractive. Absorption and stimulated emission coefficients for Li-noble gas vapors are also deduced from the data.

Schneider, S. J., Capps, W., Frederikse, H. P. R., Hosler, W. R., McDaniel, C. L., Plante, E. R., *Proc. US-USSR Colloquium on MHD Power Generation, Moscow, USSR, Feb. 25-27, 1974,* pp. 350-367 (Institute of High Temperatures, Moscow, USSR, 1975).

Key words: electrical conductivity; MHD materials; phase equilibrium; slag; vaporization; viscosity.

The National Bureau of Standards, under sponsorship of the Office of Coal Research, has initiated a program of materials research appropriate to open cycle, coal fired MHD. The program consists of several interrelated projects in the areas of vaporization, viscosity, electrical conductivity and phase equilibria. This paper is intended as a review of the progress achieved thus far. Initial work has concentrated on the behavior of coal slag in MHD environment since there is definite lack of data in this area. Slag specimens have been obtained under real MHD conditions and analyzed by a variety of techniques. For the most part slags are composed largely of Al_2O_3-FeO-Fe_2O_3-SiO_2 mixtures. The portions of each as well as the amount of glassy (liquid) or crystalline material vary depending upon the location sampled in the MHD system. From the data obtained on real slags, synthetic model slags were prepared for more systematic study. Viscosity-temperature relationships of both real and model slags indicate similar temperature coefficients but large differences in viscosity values at one given temperature (e.g, at 1500 °C viscosity range between 1.0 to 2.1 $\log_{10}$ poises). The electrical conductivity of a number of slags have also been determined to 1700 K in various environments. Electrical conduction is apparently caused by the transfer of electrons between Fe^{2+} and Fe^{3+} and is largely electronic rather than ionic. Vaporization studies have concentrated on the evaporation behavior of synthetic slags under their own vapor pressure. These data indicate the initial stages of evaporation are governed by a nonequilibrium process involving the decomposition of Fe_3O_4. Equilibrium, however, is achieved with respect to the evaporation of SiO_2 from the slag solution (activity of SiO_2 is near unity). Important also to MHD is the effect of seed reactions on insulators and electrodes. In this respect the phase equilibrium diagrams for the K_2SO_4-MgO and the K_2SO_4-$LaCrO_3$ system have been determined. Both systems (under their own vapor pressure) behave in a similar manner with melting beginning a few degrees below the melting point of K_2SO_4 (1069 °C).

Schooley, J. F., **Solid state phase transitions as thermometric fixed points,** *Inst. Phys. Conf. Ser. No.* **26,** Chapter 2, 49-56 (1975).

Key words: antiferromagnetism; ferroelectricity; solid-state transitions; superconducting temperature calibration; thermometric fixed points.

The general question of the usefulness of thermometric fixed-point devices based upon phase transitions in solids is examined. It appears that both the method of detection and the intrinsic character of the transition relate to thermometric precision and practical utility of such devices. Promising systems which are discussed are the AC mutual inductance detection of superconductive transitions and the AC heat capacity detection of antiferromagnetic and ferroelectric transitions.

Schooley, J. F., **The superconductive transition in cadmium,** (Proc. 13th Int. Conf. on Low Temperature Physics-LT 13, Boulder, Colo., Aug. 21-25, 1972), Paper in *Low Temperature Physics-LT 13,* K. D. Timmerhaus, W. J. O'Sullivan, and E. F. Hammel, Eds., **3,** 382-386 (Plenum Publishing Corp., New York, N.Y., 1974).

Key words: OSRM; pure cadmium; superconductive transition temperature; superconductive transition width; thermometric fixed point.

We have examined the superconductive transition of a single crystal of cadmium at temperatures from 0.1 K to its transition temperature, T_c, and in magnetic fields from 0-27 gauss. We have measured T_c as $0.515 \pm 0.002_5$ K on the T-62 scale. We have compared its transition width and its T_c with polycrystalline samples prepared for thermometric fixed-point devices. The single-crystal transition width is ~ 250 μK at H=0, compared to 2-6 mK for the polycrystalline samples. However, the T_c's of the polycrystalline samples agree within 0.5 mK with that of the single crystal. We have examined the width of the single-crystal transition as a function of applied field, and find a minimum width of about 25 μK for 0.5 gauss. These data will be discussed in terms of transition temperature theory.

Schutz, G. C., Clark, G. E., **Data communication standards,** *Computer* **7,** No. 11, 32-37 (Feb. 1974).

Key words: American National Standards Institute; Computer Society of the IEEE; Data Communication Standards; Electronics Industries Association; International Standards Organization; International Telecommunications Union.

This paper provides an overview description of a number of organizations that are involved in the development of industry, American national and international standards pertaining to data communications. The significant organizations include: the Computer Society of the Institute of Electrical and Electronic Engineers, the Electronics Industries Association, the American National Standards Institute, the International Standards Organization and the International Telecommunications Union. The functions and objectives of the pertinent committees, sub-committees and task groups sponsored by these organizations as well as various formal and informal interworking relationships among them are described. Timely information includes a discussion of presently unresolved technical issues being addressed by the data communication standards community as well as listings of the standards approved by each of the organizations described.

Sheingorn, M., **Poincaré series of polynomials bounded away from zero on a fundamental region,** *Amer. J. Math.* **XCV,** No. 4, 729-749 (Winter, 1973).

Key words: automorphic functions; Poincaré series; polynomial approximation.

The purpose of the present paper is to extend Knopp's Main Lemma to the case $q > 1$. Knopp's proof involves substantial use of the Bers' spaces of automorphic forms. Since the character of these spaces in the cases $q \geq 2$ and $1 < q < 2$ is vastly different, our proof bears only superficial resemblance to Knopp's. Indeed, the situation is this: If one replaces $q \geq 2$ by $q > 1$ at every stage of Knopp's proof, the proof turns out to be valid. However, verification of two of the resulting statements is quite hard and requires techniques far outside Knopp's paper.

Shih, A., **van der Waals forces between a Cs atom or a CsCl molecule and metal or dielectric surfaces,** *Phys. Rev. A* **9,** No. 4, 1507-1514 (Apr. 1974).

Key words: cesium beam; cesium chloride beam; gold surfaces; van der Waals forces.

The interaction potentials between a spherically symmetric atom (Cs) and a highly conducting surface (gold) or a dielectric surface (glass) are investigated by the atomic-beam-deflection technique. The observed beam profile is least-squares fitted to an r^{-3} potential. The derived interaction constant for the gold surface is 0.59 and 0.67 of the values predicted by Bardeen and Mavroyannis, respectively. A glass surface is found to have an interaction constant 0.65 that of gold. The measurements have also been obtained for a polar molecule (CsCl). With a gold surface the observed beam profile is almost identical to that for stainless steel (reported earlier) in spite of their difference in dc conductivity. Further, the observed constant for an insulator (glass surface) is 0.86 that of gold. With gold, the interaction constant obtained for a cesium-halide molecule, with a strong permanent dipole moment, is smaller than that for a Cs atom with zero dipole moment.

Simmons, G. L., Eisenhauer, C., Spencer, L. V., **Moments method calculations of neutron and gamma-ray penetration in bulk media,** *Proc. IVth Int. Conf. on Reactor Shielding, Paris, France, Oct. 9-13, 1972,* **2,** 268-283 (Oct. 1972).

Key words: adjoint; concrete; gamma-ray penetration; moments; neutron penetration; secondary gamma rays.

A system of computer codes using the moments method to calculate penetration of neutrons and gamma rays in bulk media is described. Results are presented for the penetration of fission neutrons incident at various angles on concrete. The use of adjoint procedures for calculating gamma-ray buildup factor data are also described and results are presented for the penetration of gamma rays from point sources emitting at various conical angles in a concrete medium. Finally, the two types of calculations are combined to produce data for penetration of gamma rays produced in concrete by a neutron source.

Simmons, J. D., Tilford, S. G., **Evidence for an accidental predissociation of CO,** *J. Mol. Spectrosc. Note* **49,** No. 1, 167-168 (Jan. 1974).

Key words: absorption spectrum; accidental predissociation; carbon monoxide; emission spectrum; perturbation; Rydberg state.

The perturbation in the $E-X(0-0)$ band of the CO absorption spectrum has been shown to be due to an unusual accidental predissociation. The intermediate predissociated state has not yet been identified.

Simpson, J. A., **Modernizing gage block calibrations: A case study in measurement assurance,** *Proc. 1974 Joint Measurement Conference, Gaithersburg, Md., Nov. 12-14, 1974,* pp. 153-157 (Instrument Society of America, Pittsburgh, Pa., 1975).

Key words: calibration; gage blocks; measurement assurance.

Recently the Optical Physics Division of the National Bureau of Standards was faced with a potentially serious set of problems in the gage block calibration laboratory; labor costs were escalating, metrication threatened to greatly increase the workload, and the system in use (interferometry) did not lend itself to providing a desired Measurement Assurance Program. The introduction of a new system that provides better accuracy, lower cost and the possibility of a MAP was undertaken. The methods used to insure compatibility, maintain performance, and to be economic both for the Bureau and its customers, provide an interesting case study which is applicable to many other situations in metrology.

Snyder, J. J., **Paraxial ray analysis of a cat's-eye retroreflector,** *Appl. Opt.* **14,** No. 8, 1825-1828 (Aug. 1975).

Key words: optical devices; optics, precision; reflector, cat's-eye; retroreflector, cat's eye.

The cat's-eye retroreflector is a passive optical system consisting of a secondary mirror placed at the focal point of a primary lens. We analyze the cat's eye using the paraxial ray matrix approach. The position of the equivalent reflecting surface and the angular field of view of a realizable cat's eye are functions of the radius of curvature of the secondary mirror. The field of view is maximum for a secondary mirror with a concave radius of curvature equal to the focal length of the primary lens. We further derive the general dependence of retroreflection errors on misadjustment of the secondary mirror.

Snyder, L. E., Buhl, D., Schwartz, P. R., Clark, F. O., Johnson, D. R., Lovas, F. J., Giguere, P. T., **Radio detection of interstellar dimethyl ether,** *Astrophys. J.* **191,** No. 2, Part 2, L79-L82 (July 15, 1974).

Key words: dimethyl ether; internal motion; interstellar molecules; Orion; radio astronomy.

Interstellar dimethyl ether, $(CH_3)_2O$, has been detected in emission from the direction of the Orion Nebula molecular cloud. The observed velocity of the $6_{06} \rightarrow 5_{15}$ transition 90.9 GHz is in excellent agreement with other molecules observed toward Orion. Observations of the $2_{20} \rightarrow 2_{11}$ transition at 86.2 GHz and the $2_{11} \rightarrow 2_{02}$ at 31.1 GHz support the dimethyl ether detection and indicate that either $(CH_3)_2O$ has two distinct velocity components in Orion or certain internal motion states are preferentially populated. This molecule has a large collisional cross-section and C_{2v} symmetry; hence it should be useful for future studies of molecular pumping models.

Somes, N. F., **Factors influencing structural safety,** Paper 48-7 in *Industrialization in Concrete Building Construction, ACI Publ. SP48,* pp. 177-189 (American Concrete Institute, Detroit, Mich., 1975).

Key words: buildings; codes; design criteria; regulatory system; safety; standards; structural loading.

The paper identifies and briefly discusses the factors that collectively influence the structural safety of a building. These include the probability of occurrence of extreme loading, the factors of design and construction process that determine the building's response, and the function of the building that influences both its design and the consequences of an extensive structural failure. Those factors within the sphere of influence and concern of individuals responsible for the design and supervision or regulation of construction are then discussed in further detail to point out deficiencies in current knowledge or practice. Finally, conclusions and recommendations are made with respect to these deficiencies.

Soulen, R. J., Jr., Gubser, D. U., **Superconducting properties of iridium,** (Proc. 13th Int. Conf. on Low Temperature Physics-LT 13, Boulder, Colo., Aug. 21-25, 1972), Paper in *Low Temperature Physics-LT* **13,** K. D. Timmerhaus, W. J. O'Sullivan, and E. F. Hammel, Eds., **3,** 498-502 (Plenum Publishing Corp., New York, N.Y., 1974).

Key words: critical field, fixed point; iridium; transition temperature.

The residual resistivity ratio, superconductive transition temperature, magnetization curves, and critical magnetic field data of several samples of iridium have been measured. It is found that the magnetic properties of superconducting iridium are highly dependent on the metallurgical state of the sample, whereas the transition temperature is relatively less sensitive. The use of iridium as a superconductive thermometric fixed point at 0.1 K is critically examined.

Soulen, R. J., Jr., Marshak, H., **The establishment of an absolute temperature scale using noise and nuclear orientation thermometry,** (Proc. 14th Int. Conf. on Low Temperature Physics, Otaniemi, Finland, Aug. 14-20, 1975), Paper in *Low Temperature Physics-LT 14,* **4,** 60-63 (Am. Elsevier Publ. Co., New York, N.Y., 1975).

Key words: dilution refrigerators; γ-ray anisotropy thermometry; Josephson junctions; noise thermometry; temperature.

We report on the present status of a comparison of the temperatures obtained from a Josephson junction noise thermometer and a ^{60}Co γ-ray anisotropy thermometer. The data reported here cover the range of 12 to 35 mK in 16 steps varying from ~ 0.5 to ~ 2 mK. Owing to improvements in: temperature stability of our dilution refrigerator, analysis of noise thermometer data, and the γ-ray data acquisition system, these new results have considerably less scatter than those reported previously. The overall agreement between both thermometers is about 1 percent.

Speller, L. C., Mendlowitz, H., **Characteristic electron energy losses in germanium,** *J. Phys. Chem. Solids* **36,** No. 11, 1229-1232 (1975).

Key words: electron energy loss; germanium; material structure; optical properties; scattering.

The characteristic electron energy loss spectrum of germanium was studied in a transmission type experiment as a function of the changes in structure due to electron bombardment. The structure of the material was characterized by electron micrograph and diffraction techniques. The electron energy loss spectrum of germanium was studied up to 45 eV, and loss peaks were observed at 15.7 eV and 31.6 eV as well as a 6 eV carbon loss. The positions of the most intense characteristic energy loss peak at 15.7 eV and its first multiple were constant for a large variation in the lattice parameters for the individual films.

Stampfl, P. P., Travis, J. C., Bielefeld, M. J., **Mössbauer spectroscopic studies of iron-doped rutile,** *Phys. Status Solidi A* **15,** No. 1, 181-189 (1973).

Key words: diffusion; doping; Fe-57; iron-doped; lattice distortion; Mössbauer spectroscopy; quadrupole splitting; temperature dependence.

Iron-57 Mössbauer spectra have been obtained of single crystal and powdered samples of rutile (TiO_2) doped to about one percent by weight in isotopically enriched iron. Spectral patterns found for powdered samples are consistent with theoretical expectations for substitutional doping with a uniform distribution of oxygen vacancies and impurity ions. The temperature dependence of the ferrous pattern indicates a slight shift in position of the neighboring oxygen ions to accommodate the relatively large size of the dopant ion. Spectral parameters from the single crystal samples differ radically from those of the powdered samples or the "ideal lattice" theory. Variations in stoichiometry, charge compensation mechanisms, or other diffusion-related phenomena are assumed to be responsible. Single crystal results do, however, furnish graphic evidence that trivalent iron diffuses faster in rutile than the larger divalent species.

Stark, J. P., Manning, J. R., **Correlated complete-path equations for diffusion in an electric field,** *Phys. Rev. B* **9,** No. 2, 425-434 (Jan. 15, 1974).

Key words: correlation factor; diffusion; drift mobility; electric field; random walk; symmetry plane; vacancy.

Diffusion of a substitutional solute in a face-centered-cubic metal is discussed in terms of the complete path of the defect giving rise to mass transport. For diffusion in the absence of an applied field, these results are equivalent to the matrix method of Howard for the calculation of the correlation factor. In an applied field, however, the possibility that during the lifetime of a defect it may cause a tracer atom to make a series of successive jumps in the positive field direction or alternatively a series of successive jumps antiparallel to the field can appreciably influence the form of the equations. The tracer can, with decreasing probability, find itself several or many jump distances from its original position. Previous descriptions of this process restricted the tracer to two adjacent planes perpendicular to the applied field. In the present paper, generalized equations are derived for diffusion in an applied field with successive jumps by the tracer in one direction being explicitly allowed. To illustrate the use of these equations, the diffusion of an isolated tracer by a single vacancy is evaluated for a case where successive jumps in one direction are allowed, and also for comparison it is evaluated with the assumption that arrival of the vacancy at the symmetry plane passing through the tracer normal to the diffusion direction returns the vacancy to equilibrium. The latter approach restricts the tracer to two adjacent planes in a sequence of correlated jumps but is shown to give the

same mobility. Thus use of the symmetry plane does not affect the results. In contrast to previous equations, the present treatment is applicable to situations where symmetry planes are not present. Thus, it will allow calculation of drift mobilities when the defect or crystal symmetry is more complex, as for diffusion via divacancies which can dissociate.

Stenbakken, G. N., Phillips, W. E., Bergsman, S. E., **Terms and definitions for intrusion alarm systems,** *LESP-RPT-0305.00*, 16 pages (U.S. Department of Justice, Law Enforcement Assistance Administration, National Institute of Law Enforcement and Criminal Justice, Washington, D.C., Oct. 1974).

Key words: alarms; burglar alarms; intrusion alarms; intrusion detection.

This document provides definitions in layman language of terms commonly used in the commercial intrusion alarm field.

Stiehler, R. D., **Measurement units in engineering and SI,** *Proc. Symp. on Standardization and Metric Conversion for Tunneling, Underground Construction, and Mining, Washington, D.C., May 21, 1974*, pp. 42-48 (Available from the National Technical Information Service, Springfield, Va., 1975).

Key words: International System of Units; measurement units; metric units; SI; systems of units; units of measurement.

Several systems of measurement units used in engineering are discussed. The multiplicity of units for the same quantity and the use of the same name for units of different quantities led to the adoption of the International System of Units (SI) in 1960. This system is *one* of the many metric systems that have been introduced since 1793. SI is a single, rational, coherent system consisting of seven base units, two supplementary units, and units derived from them, always with a factor of one relating them. In this sense, SI is a unitary rather than a decimal system. SI provides one and only one unit for each quantity and does not use the same name for units of two different quantities. Prefixes are provided for convenience in expressing decimal multiples and submultiples of SI units, but they are not essential to SI. The present confusion existing in units for quantities which relate to rotation or vectors is discussed. The inclusion of the radian in such units as moment of inertia, angular momentum, and torque is necessary. Some improvements needed in SI are mentioned. The simplicity and rational nature of SI should relieve the engineer from memorizing equations cluttered with conversion factors dependent on irrational units seldom understood.

Strobridge, T. R., **Feasibility study of a multipurpose refrigerator for a superconducting cable test facility,** *Paper EPRI* **282,** 52 pages (Electric Power Research Institute, Palo Alto, Calif., July 1975).

Key words: cryogenics; helium pump; power transmission; refrigeration; superconducting cables.

A major problem in simultaneously cooling a number of test sections of superconducting power transmission cables is the wide variation in cable operating pressures and temperatures. It is feasible to couple a single large refrigerator to the cables with individual pumped helium circulation circuits. The system is flexible in both pressure and temperature and in the temperature rise along the length of the cable. The total refrigeration capacity required for a test facility is derived from current estimates of cable characteristics. A single refrigerator is shown to be less expensive than individual refrigerators for each cable even when the penalties for pump work and heat transfer through large temperature differences are included. Sufficient process calculations are included to show that the system is practical, and a draft specification for the refrigerator is given.

Sugar, J., Kaufman, V., **Nuclear magnetic dipole moment of ^{181}Ta,** *Phys. Rev. C* **12,** No. 4, 1336-1339 (Oct. 1975).

Key words: ionization energy; nuclear moment; spectrum; tantalum.

The hyperfine structure of the $6s^2S_{1/2}$-$6p^2P_{1/2}$ line of Ta V at 1708 Å has been resolved using a 150 A sliding spark discharge. The $6p$-$8s$ multiplet was identified and the ionization energy was redetermined. With these new data a value for the nuclear dipole moment of ^{181}Ta of $(2.36 \pm 0.02)\mu_N$ is derived. New wavelengths are given for all previously classified lines.

Sugar, J., Kaufman, V., **Seventh spectrum of tungsten (W VII); resonance lines of Hf V,** *Phys. Rev. A* **12,** No. 3, 994-1012 (Sept. 1975).

Key words: hafnium; levels; spectra; tungsten; wavelengths.

Observations of W VII were carried out in the spectral range 100 to 2000 Å utilizing normal- and grazing-incidence spectrographs. The light source was a sliding spark operated at peak currents of 1000 to 3000 A. Eighty-five energy levels of $4f^13nl$ and $5p^5nl$ configurations were deduced for $nl = 5d$, $6s$, $6p$, $6d$, and $7s$. These are based on the classification of 310 lines in the range 130 to 1436 Å. Calculations of all observed configurations were carried out with configuration interaction (CI) for the purpose of fitting radial integrals and confirming the analysis. The strong CI between p^5nl and f^13nl configurations where $nl = 5d$, $6p$, $6d$ provided well-defined CI integrals in good agreement with Hartree-Fock values. A value of 984100 ± 500 cm^{-1} was derived for the ionization energy from the $4f^13ns$ series. The resonance lines of Hf V for $5p^6$-$5p^55d,6s$ are given. A revised value for the ionization energy of W VI is given.

Swanson, N., Celotta, R. J., Kuyatt, C. E., **Electron excitation of xenon near threshold,** (Proc. Int. Symp. on Electron and Photon Interactions w/Atoms, Univ. of Stirling, Stirling, Scotland, July 16-19, 1974), Chapter in *Electron and Photon Interactions with Atoms*, pp. 661-667 (Oct. 1975).

Key words: autoionizing states; electron excitation; energy loss; resonances; threshold; xenon.

An electron energy-loss spectrum and excitation functions for the four lowest excited states in Xe have been measured at a scattering angle of 45° in the near-threshold region (8–14 eV). Four peaks in the energy-loss spectrum above the $^2P_{3/2}$ ionization limit can be fitted to a $5p^5np'$ Rydberg series. The excitation functions for the two lowest states at 8.32 and 9.44 eV show large peaks due to decay of the $5p^56s^2(^2P_{1/2})$ resonance, as well as other resonance peaks which correlate well with previous transmission measurements.

Swanson, N., Celotta, R. J., Kuyatt, C. E., **Excitation of low-lying triplet states in ozone by electron impact,** (Proc. IX Int. Conf. on Physics of Electronic and Atomic Collisions, Seattle, Wash., July 24-30, 1975), Abstract in *Electronic and Atomic Collisions*, J. S. Risley, Ed., **2,** 128-129 (University of Washington Press, Seattle, Wash., 1974).

Key words: electron impact; energy loss spectra; oxygen; ozone; triplet states.

Energy loss spectra of ozone were measured at scattering angles of 45, 75, and 90° and incident energies below 10 eV to look for previously unobserved triplet states. A broad continuum between 1.3 and 2 eV energy loss was seen which we believe is due to excitation of these states.

Swing, R. E., **The case for the pupil function,** (Proc. SPIE Seminar on Image Assessment, Rochester, N.Y., May 20-22, 1974), Paper in *Image Assessment and Specification*, D. Dutton, Ed., **46,** 104-113 (Society of Photo-Optical Instrumentation Engineers, Palos Verdes Estates, Calif., 1974).

Key words: impulse response; lens aberrations; optical transfer function; partial coherence; pupil function; wave-front shearing interferometry.

The pupil function, a description of the wavefront errors associated with a lens (in terms of a phase distribution over its exit pupil), has long been used by lens designers since it is implicit in the determination of aberrations. Pupil functions require interferometry for measurement. The analysis of interferograms has been facilitated in modern times by the development of high-speed digital computers, automatic fringe scanners and laser sources and can be put on a routine, low-cost basis. When the theory of partial coherence is applied to the analysis of imaging systems, the pupil function is seen to be the fundamental measure of lens performance, because from this one description, the other measures of system behavior can be derived. Further, since the pupil function can be determined with great precision, a polynomial expansion can be curve-fitted in the computer to list the aberration coefficients out to orders whose height is a function of the size of the available computer core. It is thus practicable to provide not only transfer function but also a diagnosis of the lens ills, quantitatively. However, white-light response cannot be measured directly and must be synthesized from measurements at several wavelengths; the techniques for accomplishing this are well-known but are presently not implemented at NBS, where wave-front shearing interferometry has been utilized for measurement of the pupil function. Among the problems for which pupil function measurement is a solution are the cascading of lenses in imaging systems and the evaluation of microscope objective/eyepiece response.

Swing, R. E., **The sampling aperture for linear microdensitometry,** *Opt. Eng.* **13,** No. 5, 460-470 (Sept.-Oct. 1974).

Key words: impulse response; linear microdensitometry; microdensitometry; optics; slit imagery; transfer function.

In the development of modern linear microdensitometry, the trend of optical system design has been towards the condition of underfilling the efflux optics, with total collection of light after it passes through the sample. The system transfer function is therefore attributable to the influx optics, and the sampling aperture is the light distribution impinging on the sample, reduced from an illuminated slit or circular aperture through the influx optical system. The maximum frequency response of the system is obtained when the sample is illuminated with the impulse response of the influx optics. However, the theoretical impulse response can only be realized by imaging a delta-function and this is photometrically impossible. Similarly, because the system images an illuminated aperture onto the sample, scanning with a pure, geometrically-characterized slit or spot is not possible due to lens response and diffraction. These two problems are investigated, for both coherent and incoherent illumination.

For both impulse response and slit image, the MTF is investigated, and its deviation from the ideal is calculated. The results are characterized in terms of RMS-MTF differences over the spectrum for 10, 5, 2, and 1 percent levels. The controlling parameter is the ratio N/R, where R is the reduction factor employed for the influx optics, and N is the number of resolution elements contained within the nominal object slit width. The study shows that there are significant differences in these values for the same RMS difference level, with coherent and incoherent illumination, and that there are compromises to be made with both kinds of illumination. The results of this study facilitate calculation of system response for any configuration of object slit and influx optics (within the linear microdensitometer system), and defines limits on slit sizes for operation with impulse response and geometrically characterized slit images for the sampling aperture. The effects expected with the linear polarization associated with laser illumination (the most common source of high-energy, coherent radiation) is discussed, but not included in this scalar treatment.

Swyt, D. A., **National Measurement System: Microstudy of optics,** *Nat. Conf. Stand. Lab. (NCSL) Newsletter* **15,** No. 2, 13-17 (June 1975).

Key words: densitometry; lens evaluation; microdensitometry; microscopy resolution charts; National Measurement System.

Studies of the National Measurement System are currently in progress at the National Bureau of Standards. These studies are an attempt to understand the infrastructure and impact of measurement throughout our economy. One particular microstudy is entitled Optics. This brief article gives an overview of the developments to date; i.e., description of the infrastructure, identification of various users and the techniques of the study.

Taylor, J. K., **Electrochemical analysis,** *Med. Electron. Data,* pp. 39-42 (May-June 1972).

Key words: chemical analysis; coulometry; electrochemical analysis; ion-selective electrodes; polarography.

A brief review is presented, in popular style, of the various electrochemical techniques that are applicable to chemical analysis. Techniques described include polarography, coulometry and potentiometry employing ion-selective electrodes. The use of electrochemical sensors in titrimetry is also pointed out.

Thomson, R. M., **A review of nondestructive evaluation opportunities,** *ASTM Stand. News* **3,** No. 3, 8-14 (Mar. 1975).

Key words: materials reliability; nondestructive evaluation.

This paper is an abridged version of a recent report by a federal ad hoc working group on NDE. In the report, the NDE field is surveyed in order to foresee probable future growth areas and the technical developments which will be required to support this growth. Major NDE involvement is expected to continue in aerospace, to grow enormously along with the nuclear power industry, and to become a more important factor in ground transportation, general manufacturing, maintenance of machinery, and medical diagnosis. Technical issues and challenges are reviewed.

Tighe, N. J., **Examination of fracture interfaces in silicon nitride,** *Proc. 33d Annual Electron Microscopy Society of America, Las Vegas, Nev., Aug. 10-14, 1975,* G. W. Bailey, Ed., pp. 60-61 (Claitor's Publ. Div., Baton Rouge, La., 1975).

Tighe, N., **Microstructure of oxidized silicon nitride,** (Proc. 32d Annual Proc. Electron Microscopy Society of America, St. Louis, Mo., 1974), Paper in *32d Annual Proc. Electron Microscopy Society of America,* C. J. Arceneaux, Ed., pp. 470-471 (Claitor's Publ. Div., Baton Rouge, La., 1974).

Key words: β-cristobalite; electron microscopy; oxidation; silicon nitride; silicon oxynitride; Si_3N_4.

The reaction product layer produced on hot-pressed silicon nitride, Si_3N_4, during oxidation at temperatures from 1000 to 1400 °C was examined by transmission electron microscopy. The oxide was found to have at least two crystalline phases – silicon oxynitride Si_2ON_2 and β-cristobalite SiO_2, and two amorphous phases. The microstructure of the phases and of the silicon nitride near the reaction interface is discussed.

Tobler, R. L., Mikesell, R. P., Durcholz, R. L., Reed, R. P., **Low temperature fracture behavior of iron-nickel alloy steels,** (Proc. American Society for Testing and Materials Symp. on Properties of Materials for Liquefied Natural Gas Tankage, Boston, Mass., May 21-22, 1974), *Am. Soc. Test. Mater. Spec. Tech. Publ.* **579,** pp. 261-287 (1975).

Key words: crack propagation; cryogenics; fracture toughness; mechanical properties; nickel steels.

Fracture toughness tests over the interval 298 to 4 K and fatigue crack growth rate tests at 298, 111, and 76 K are reported on selected iron-nickel (Fe-Ni) alloys which are commercially available for potential use in storage or transportation of liquefied natural gas (LNG). These alloys include Fe-6Ni and Fe-5Ni in newly developed three-step heat treatments and Fe-9Ni in the quenched and tempered condition. Linear elastic fracture mechanics parameters (K_Q, K_{IC}) and J-integral (J_{IC}) test data are presented for 1.25-in.-thick compact

specimens. Discussion includes comparisons of fatigue crack growth rate and fracture data between alloys.

Tomuta, L., Mizushima, M., Howard, C. J., Evenson, K. M., **Rotational structure and magnetic g factors of $O_2(X^3\Sigma_g^-, v=0)$ from laser-magnetic-resonance spectra,** *Phys. Rev. A* **12,** No. 3, 974-979 (Sept. 1975).

Key words: effect; laser; magnetic resonance; oxygen; rotational structure; Zeeman.

Using the 108- and 84-μm D_2O laser lines, new laser-magnetic-resonance (LMR) spectra of the oxygen molecule in its ground state ($X^3\Sigma_g^-$, $v=0$) are observed and analyzed. The corresponding transitions are $n=15\rightarrow 17$ and $n=19\rightarrow 21$, respectively. Bauer, Kamper, and Lustig's values of the g factors are consistent with our results, but Hendrie and Kusch's values are not. Combining all LMR results with other results, we obtain rotational parameters $B_0=$ 43.1004608(75) GHz and $B_1=0.14520(20)$ MHz.

Torchia, D. A., Lyerla, J. R., Jr., Quattrone, A. J., **Molecular dynamics and structure of the random coil and helical states of the collagen peptide, α1-CB2, as determined by ^{13}C magnetic resonance,** *Biochemistry* **14,** No. 5, 887-900 (1975).

Key words: C-13 magnetic resonance; collagen; polymers; polypeptides; protein structure; relaxation times.

Carbon-13 chemical shifts, spin-lattice (T_1) and spin-spin (T_2) relaxation times, and ^{13}C-{^{1}H} nuclear Overhauser enhancements (NOE) have been determined for the random coil and triple helical states of the α1-CB2 fragment of rat skin collagen. Assignment of all aliphatic resonances of this 36 residue peptide in the random coil state (30°) has been achieved with the aid of model polypeptides containing pyrrolidine residues. The chemical shifts and intensities of the Pro and Hyp C^γ resonances show that $\gtrsim 90$ percent of the X-Pro and X-Hyp bonds are trans in both helix and coil conformations. From T_1 measurements rotational correlation times (τ_{eff}) of *ca.* 0.45 nsec are calculated for interior C^α carbons in the coil, while τ_{eff} values of the side chain and near terminal carbons are found to be 2-9 times smaller. These results along with the narrow natural line widths (3-5 Hz) and maximal NOE values (2.8 ± 0.3) demonstrate the high degree of backbone mobility, due to segmental motion, in the unordered state of the peptide. By contrast, the broad lines (50-90 Hz) and small NOE values (1.3 ± 0.3) for the α carbons in the helical state (2°) suggest much slower motion. The line widths and NOE values together with the C^α T_1 values (0.025-0.040 sec) correspond to correlation times which are in reasonable agreement with those calculated for an axially symmetric rigid ellipsoid, undergoing rotational diffusion, having dimensions approximating those of a collagen-type triple helical aggregate of three α1-CB2 chains. A satisfactory computer simulation of the experimental 2° spectrum is obtained by assigning the narrow aliphatic resonances in the spectrum (line widths 5-40 Hz) to (a) carbons in the small amounts of α1-CB2 (3 mol %) and α1-CB1 (2.5 mol %) random coil conformations, (b) carbons in the flexible terminal triplets of the helix, and (c) Ala, Leu, and Phe methyl and phenyl carbons. The side chain carbon line widths obtained from the simulation—when compared with side chain line widths calculated for a rotating rigid ellipsoid with internal motion—indicate rapid axial reorientation of methyl and phenyl groups. With the exception of the Hyp residue the line widths suggest local motion for at least some carbons in most other side chain moieties. The Hyp C^β and C^γ line widths indicate the presence of little if any rapid Hyp ring motion.

Treu, S., **Interactive command language design based on required mental work,** *Int. J. Man-Mach. Stud.* **7,** No. 1, 135-149 (1975).

Key words: association links; command language design; interactive user; language transformation; mental work.

Although the definition of "mental work" remains elusive, systematic means/methods should be considered for gaining evidence about interactive language features requiring more/less effort of the human mind. The suggested approach employs a structuring of the user's conceptual reference spaces into sets of "action primitives," peculiar to the type of computer-aided task involved. An interactive command language can then be regarded as the range of some transformation on the user's set of action primitives. The nature and efficiency of that transformation, in conjunction with the inherent number of mental association links, are hypothesized to have direct relationships to the level of required mental work. The user's delay or "think time," expended immediately preceding command utilization, is one measurable quantity that should be useful as a work level indicator.

Troy, T. N., **Working hand in hand with government,** (Proc. 36th Annual National Packaging Forum, Chicago, Ill., Oct. 7-9, 1974), *Packaging Report F-7432,* 10 pages (The Packaging Institute, U.S.A., New York, N.Y., 1974).

Key words: consumer activism; control proliferation; industry; interaction; package quantity standards; voluntary standards; working with government.

Consumer activism and concomitant opening-up of agency activities means industries must reevaluate their strategies for working with government. NBS, short on regulatory authority but holding a strong suit in technology, is sensitized to economic realities and encourages interaction. Getting your story told early and often, can lead to effective voluntary standards and perhaps draw praise from enlightened consumer advocates. Since inflation and metrication portend another effort to control the proliferation of the number of package sizes, industry may want to reconsider their package quantity standards.

Utton, D. B., **Nonchemical applications of NQR,** *Proc. Second Int. Symp. on Nuclear Quadrupole Resonances Spectroscopy, Viareggio, Italy, Sept. 3-7, 1973,* pp. 341-350 (A. Vallerini, Pisa, Italy, 1975).

Key words: applications; material detection; nuclear quadrupole resonance; piezometry; thermometry.

Since the early work on NQR over twenty years ago it has been suggested that the temperature dependence of NQR frequencies can be used as a thermometer. A natural extension of this idea is to use an NQR frequency to measure pressure. A review is given of the work that has been done to investigate these applications of NQR. The criteria for the choice of material and measurement technique are discussed with emphasis on chlorine compounds since they have received the most attention. As an example, the accuracy and precision obtainable with the Cl^{35} NQR in $KClO_3$ (for which accurate measurements are available) will be described.

There has been some renewed interest in using characteristic NQR frequencies to detect the presence of specific materials. As an example, estimates are given for the signal to noise ratio to be expected for nitrogen compounds when the material is not located within the detector coil.

Utton, D. B., Soulen, R. J., Jr., Marshak, H., **Intercomparison of temperature scales using low transition-temperature superconductors,** (Proc. 14th Int. Conf. on Low Temperature Physics, Otaniemi, Finland, Aug. 14-20, 1975), Paper in *Low Temperature Physics-LT 14,* **4,** 76-79 (Am. Elsevier Publ. Co., New York, N.Y., 1975).

Key words: copper NMR thermometer; γ-ray thermometer; noise thermometer; superconductive transition temperatures; temperature.

Recent studies of several superconductors (W, Be, $Ir_{80}Rh_{20}$, Ir, $AuAl_2$, and $AuIn_2$) showed them to provide useful temperature reference temperatures below 0.5 K. Samples of each material were used to intercompare the temperature scales obtained from noise, γ-

ray, and copper NMR thermometers from 0.024 to 0.208 K. The results of this intercomparison are given in tabular form.

Van Brunt, R. J., Kieffer, L. J., **Angular distribution of N^+ from dissociative ionization of N_2 near threshold,** *J. Chem. Phys.* **63,** No. 8, 3216-3221 (Oct. 15, 1975).

Key words: electrons, ions; molecules; nitrogen.

Translational kinetic energy and angular distributions of N^+ from dissociative ionization of N_2 have been measured at electron energies close to threshold. For electron energies above 50 eV the energy distributions agree favorably with earlier measurements of Kieffer and Van Brunt. The ion energy distributions at electron energies below 50 eV are dominated by a feature peaked at a kinetic energy below 1 eV in agreement with recent measurements of Locht *et al.* For electron energies closest to threshold the angular distribution of N^+ associated with this feature is consistent with the previously proposed mechanism involving excitation of the $C^2\Sigma_u^+$ state followed by predissociation. At higher electron energies the degree of anisotropy increases and then rapidly decreases suggesting a significant contribution from direct excitation to the $^4\Sigma_g^+$ repulsive state of N_2^+ leading to fragments in their ground states.

VanderHart, D. L., **Study of molecular reorientation: Pressure and temperature dependence of deuterium relaxation in liquid $CDCl_3$,** *J. Chem. Phys.* **60,** No. 5, 1858-1870 (Mar. 1, 1974).

Key words: chloroform; deuterium; NMR; pressure dependence; relaxation; reorientation; temperature dependence.

Deuterium NMR spin-lattice relaxation measurements have been performed on the neat liquid $CDCl_3$ over the range 28 °C $< T <$ 165 °C and at pressures up to 5 kbar (5×10^8 N/m^2). These measurements enable one to determine $\tau_{\theta,2}$, the correlation time for molecular reorientation about the axes perpendicular to the symmetry axis. The data are presented as a function of all three state variables, P, V, and T. An attempt is made to describe the data in terms of various simple models for reorientation including activation and free volume models. Each of these models predicts certain aspects of the data but fails in other areas. In particular, the activation model fails to predict the correct behavior at constant temperature and the free volume theories generally fail to predict the constant volume experiments. Deviations from the Debye and microviscosity theories are also noted. The mean time between collisions τ_{coll} was calculated from $\tau_{\theta,2}$ assuming both Gordon's J-diffusion model and the equivalence of τ_{coll} and τ_J, the angular momentum correlation time. These values of τ_{coll} were then compared with the predictions of the cell model for liquids in which τ_{coll} is simply the mean free path divided by the mean velocity. Generally, the data did not fit the cell model; however, at constant pressure, the cell model did predict the changes in τ_{coll} quite well. Qualitative suggestions are made to account for the discrepancies. Finally, the possibility that H-bonding exists in $CHCl_3$ and affects the generality of these results by changing the quadrupole coupling constant and disturbing the dynamics of the system is discussed. It is concluded that these effects are small if they exist at all.

Velapoldi, R. A., Travis, J. C., Cassatt, W. A., Yap, W. T., **Inorganic ion-doped glass fibres as microspectrofluorimetric standards,** *J. Microsc.* **103,** Part 3, 293-303 (Apr. 1975).

Key words: europium ions; fluorescence; fluorescence standards; inorganic ion-doped fibers; microspectrofluorimetry; uranyl ions.

Uranyl and europium ion-doped fibres of 5-45 μm diameter were prepared which emit in the green and red spectral regions, respectively. Measurements were made of fluorescence flux as a function of fibre length, dopant concentration, slit shape and fibre diameter. The flux was found to be proportional to fibre length and fluorophor concentration and proportional to the square of the fibre radius. In addition, the fluorescence flux as a function of aperture size and shape and fibre position has been measured experimentally and compared to computer generated fluorescence flux envelopes. It is suggested that inorganic ion-doped fibres are suitable for use as microspectrofluorimetric standards.

Vickers, A., Krasny, J., Tovey, H., **Some apparel fire hazard parameters,** *Proc. Seventh Annual Meeting of the Information Council on Fabric Flammability, New York, N.Y., Dec. 5, 1973,* pp. 205-226 (1975).

Key words: apparel fires; burn injury severity; fabric flammability; FFACTS; garments.

The effect of three parameters, fiber content, fabric content, fabric burn time (a function of ease of ignition and rate of flame spread), and garment configuration and fit, on frequency of involvement in accidental garment fires and on the extent of resulting injury was investigated using fabrics and data from the National Bureau of Standards Flammable Fabric Accident Case and Testing System (FFACTS). Cellulose-containing fabrics are overrepresented in FFACTS though this may be, in part, the result of biases in the data base. The extent of injury appears to be more closely related to garment configuration and fit than to fiber content and fabric burn time.

Wagner, G. A., Reimer, G. M., Carpenter, B. S., Faul, H., Van der Linden, R., Gijbels, R., **The spontaneous fission rate of U-238 and fission track dating,** *Geochim. Cosmochim. Acta* **39,** No. 9, 1279-1286 (1975).

Key words: fission track dating; neutron flux; neutron irradiation; plateau annealing; uranium glasses; U-238 fission decay constant.

The rate of spontaneous fission decay of uranium-238 (λ_f^{238}) was determined in 4π-geometry by the fission track method. Uranium glasses of known age of manufacture were used. Spontaneous tracks have accumulated since the time of manufacture and induced tracks to determine the uranium content were produced by thermal neutron irradiations. Spontaneous tracks in all glasses were found to be partially annealed. By correcting for this annealing effect, a $\lambda_f^{238} = 8.7 \pm 0.6 \times 10^{-17}$ yr^{-1} was obtained. Uncertainty in the neutron dose is the largest source of error.

Wang, F. W., **Dynamics of block-copolymer molecules in dilute solution,** *Macromolecules* **8,** No. 3, 364-371 (May-June 1975).

Key words: bead-spring model; block-copolymers; dilute solutions; dynamics; limiting viscosity number; solution properties; viscoelasticity; Zimm theory.

A theory for the dynamics of block-copolymer molecules in dilute solution has been developed by modifying the bead-spring model theory of Zimm to take into account the existence of dissimilar segments in block copolymers. The eigenvalue equation encountered in the theory has been solved numerically by extending the method of Lodge and Wu. The applications of the theory have been illustrated with calculations for the viscoelastic properties of poly(styrene-*b*-methyl methacrylate) solutions and poly(styrene-*b*-*cis*-1,4-isoprene) solutions. It is found that, for some block copolymers in solution, the calculated values of the viscoelastic properties deviate significantly from the values for the parent homopolymers toward the values predicted by the free-draining case.

Wassermann, I., Samuel, D., Yuwiler, A., Carpenter, B. S., **Location of catecholamines in the brain using the $^{17}O(n, \alpha)^{14}C$ reaction,** *ANS Trans.* **18,** 85 (1974).

Wehrli, R., **Metrication and the construction industry: Potential problems and promising opportunities,** *AIA J.*, pp. 50-54 (May 1974).

Key words: building industry; conversion; engineering; human and modular standards; metrication; product-dimensions.

Conversion to the metric system, now nationally underway but still unorganized, challenges the building industry especially to plan promptly for hard conversion (metrication's approaching later stages). Why planning now is needed to accomplish competent hard conversion is examined in relation to standards. Because the building industry will need new dimensional standards for products to achieve a successful, final conversion, three types of hard conversion standards should be fixed upon to avoid haphazard pitfalls as conversion advances. The three standards briefly examined are engineering, modular, and human and their possible interrelationships.

Weston, W. F., Ledbetter, H. M., **Low-temperature elastic properties of a nickel-chromium-iron-molybdenum alloy,** *Mater. Sci. Eng. Short Commun.* **20,** 287-290 (1975).

Key words: bulk modulus; compressibility; Debye temperature; elastic constants; nickel-base alloys; Poisson's ratio; shear modulus; sound velocity; Young's modulus.

The elastic properties of a nickel-chromium-iron-molybdenum alloy were determined between room temperature and liquid-helium temperature by measuring both the longitudinal and transverse sound-wave velocities in a polycrystalline material. These properties include: the longitudinal modulus, Young's modulus, the shear modulus, the bulk modulus (reciprocal compressibility), and Poisson's ratio. Except for a small anomaly in the bulk modulus, this material exhibits regular elastic-constant/temperature behavior.

Weston, W. F., Ledbetter, H. M., Naimon, E. R., **Dynamic low-temperature elastic properties of two austenitic nickel-chromium-iron alloys,** *Mater. Sci. Eng.* **20,** 185-194 (1975).

Key words: bulk modulus; compressibility; Debye temperature; elastic constant; nickel-chromium-iron alloys; Poisson's ratio; shear modulus; sound velocity; Young's modulus.

The zero-magnetic-field low-temperature elastic properties of two polycrystalline nickel-chromium-iron alloys were determined ultrasonically between 4 and 300 K. Results are given for: longitudinal and transverse sound velocities, Young's modulus, shear modulus, bulk modulus, Poisson's ratio and elastic Debye temperature. Effects of alloying are discussed. The elastic property changes due to additions of chromium and iron to nickel are reviewed comprehensively.

Weston, W. F., **Low-temperature elastic constants of a superconducting coil composite,** *J. Appl. Phys.* **46,** No. 10, 4458-4465 (Oct. 1975).

Key words: bulk modulus; composite; compressibility; elastic compliance; elastic stiffness; piezoelectric oscillator; Poisson's ratio; shear modulus; Young's modulus.

A resonant piezoelectric oscillator method for measuring elastic moduli was applied to composite materials. The complete set of elastic compliances of a superconducting coil composite was determined semicontinuously between 4 and 300 K. Also, two moduli of a layered fiber-glass-epoxy composite were determined; this composite is essentially the matrix material of the coil composite. The Young's moduli, shear moduli, Poisson ratios, and elastic stiffness coefficients are also reported. Results agree closely with elastic data obtained by conventional testing methods.

Weston, W. F., Naimon, E. R., Ledbetter, H. M., **Low temperature elastic properties of aluminum 5083-0 and four ferritic nickel steels,** (Proc. American Society for Testing and Materials Symp. on Properties of Materials for Liquefied Natural Gas Tankage, Boston, Mass., May 21-22, 1974), *Am. Soc. Test. Mater. Spec. Tech. Publ.* **579,** pp. 397-420 (1975).

Key words: aluminum alloy; bulk modulus; compressibility; Debye temperature; elastic constant; nickel steels; Poisson's ratio; shear modulus; sound velocity; Young's modulus.

The low-temperature elastic properties have been determined for five commercial alloys that have possible structural applications at cryogenic temperatures. The alloys are 5083-0 aluminum and four ferritic steels: 3.5, 5, 6, and 9 percent nickel. An ultrasonic (10 MHz) pulse-superposition method was used to measure longitudinal and transverse wave velocities. Using the velocities and the mass density as input, the following elastic constants were calculated: longitudinal modulus, Young's (tensile) modulus, shear (rigidity) modulus, bulk modulus (reciprocal compressibility), and Poisson's ratio. Measurements were made semicontinuously from 300 to 4K. The room-temperature composition dependence of iron-nickel alloys is reviewed comprehensively up to 12 percent nickel. Debye temperatures were calculated from the elastic constants. A discussion is given of the temperature dependences of the elastic constants and differential relationships among the elastic constants.

White, H. J., Jr., **Data centers and data evaluation,** *Proc. Conf. on Thermodynamics and National Energy Problems, Warrenton, Va., June 10-12, 1974,* pp. 372-382 (National Academy of Sciences, Washington, D.C., 1975).

Key words: data center; data compilation; data evaluation; energy program, thermodynamics; transport properties.

The expected uses for numerical data in the national energy program are discussed. The uses and activities of mission-oriented data centers and discipline-oriented data centers in mission-oriented tasks are also discussed. It is concluded that both types of activities will be needed for the effective carrying out of currently proposed energy initiatives. A listing of existing discipline-oriented data centers in the area of thermodynamics and transport properties that could make a contribution to a national energy program is given.

Whittaker, J. K., **A signal processing system for a semiconductor detector ladder,** *Proc. IEEE Thirteenth Scintillation and Semiconductor Counter Symp., Washington, D.C., Mar. 1-3, 1972,* pp. 444-452 (June 1972).

Key words: computer; detector-ray; discriminator; emitter-couple; integrated circuit; signal processor.

The resolution of the NBS high resolution electron spectrometer has been improved recently by installing a new 48 channel detector array at its focal plane, in place of the original channel array that has been in use for some time. This has necessitated the design and construction of a new electronics system to accommodate the increased amount of information from the detectors. The new detector system digitally processes the signals from the detectors after amplification and discrimination. It is coupled on line to a computer which accumulates and manipulates the processed data.

An effective and economical solution has been found for the construction of a large logic network for nuclear data accumulation. The functions provided are those normally found only in modular form; e.g., coincidence, with the necessary time resolution. Time differences for simultaneous signal paths have been restricted to ± 1 ns maximum with a minimum pulse width of 5 ns for any pulse input. The entire system is dc coupled and the pulse pair resolution, measured during construction, is 10 ns.

Wiederhorn, S. M., Evans, A. G., **A new method for the design of structural ceramic components,** *Nav. Res. Rev.* **XXVII,** No. 2, 18-25 (Feb. 1974).

Key words: crack growth; fracture; fracture mechanics; porcelain; strength; structural ceramics.

A new method in design of structural ceramic components is discussed. The method is based on an understanding of crack growth in these materials and provides a means of estimating the time to failure under load.

Wiederhorn, S. M., Johnson, H., **Effect of zeta potential on crack propagation in glass in aqueous solutions,** *J. Am. Ceram. Soc.* **58,** No. 7-8, 342 (July-Aug. 1975).

Key words: crack propagation; fracture; glass; zeta potential.

In this paper the effect of zeta potential on crack propagation in glass is studied. Results indicate that in aqueous environments the zeta potential has no effect on crack growth. Reasons for this null effect are discussed.

Wiederhorn, S. M., **Reliability, life prediction and proof testing of ceramics,** (Proc. Second Army Materials Technology Conf., Hyannis, Mass., Nov. 13-16, 1973), Chapter 29 in *Ceramics for High-Performance Applications,* pp. 633-663 (Army Materials and Mechanics Research Center, Watertown, Mass., 1974).

Key words: ceramics; crack propagation; delayed failure; fracture; proof testing; Weibull analysis.

Proof testing is discussed as a design method for assuring the reliability of structural components. The advantages of proof testing over the statistical approach used for design lies in the insensitivity of the proof testing method to the detailed history of handling or processing of structural components. Methods are presented for developing and using proof test diagrams that assure minimum lifetime after proof testing. Procedures of proof testing and precautions that must be followed during proof testing are discussed. Provided these precautions are followed, proof testing offers a general method for assuring the reliability of structural components under stress.

Wiederhorn, S. M., **Strength of glass—A fracture mechanics approach,** (Proc. 10th Int. Congress on Glass, Kyoto, Japan, July 8-13, 1974), Paper in *Tenth International Congress on Glass,* pp. 11-1/11-15 (The Ceramic Society of Japan, Kyoto, Japan, July 1974).

Key words: crack growth; fracture; glass; static fatigue; strength.

After a brief review of those factors that determine the strength of glass (brittleness, surface flaws, susceptibility to stress corrosion cracking), a discussion will be given of how fracture mechanics techniques can be used to understand the physics and chemistry of glass strength. In this paper we assume that the strength of glass is limited by the growth of cracks that are always present in normal glass surfaces. Fracture mechanics techniques can be used to characterize the crack growth and to relate the growth to experimental parameters such as temperature, environment, and glass composition. Crack growth data obtained in this manner can be used to develop a deeper understanding of fracture mechanisms, and to develop charts that can be used for the design of glass structural components. Examples of both applications are given in the paper.

Wiese, W. L., **Experimental progress on plasma broadening of hydrogen lines,** *Proc. Invited Lectures given at the 7th Yugoslav Symp. and Summer School on the Physics of Ionized Gases, Rovinj, Yugoslavia, Sept. 16-21, 1974,* V. Vujnovic, Ed., pp. 637-673 (Institute of Physics, University of Zagreb, Yugoslavia, 1974).

Key words: Balmer lines; hydrogen plasma; ion motion; line shapes; reduced mass; Stark broadening.

Recent experimental investigations on the Stark broadening of hydrogen Balmer lines in high density plasmas are described. The review is principally devoted to the finer details of the line shapes, such as their central structure, asymmetries, shifts, and the decay in the line wings. Recently detected variations in the line shapes with the reduced mass of the radiator-perturber system are discussed, comparisons with theory are presented, and some preliminary conclusions are drawn.

Wiese, W. L., Martin, G. A., **Oscillator strength distributions in the lithium isoelectronic sequence,** (Proc. Invited Lectures 7th Yugoslav Symp. and Summer School on the Physics of Ionized Gases, Rovinj, Yugoslavia, Sept. 16-21, 1974), Paper in *Physics of Ionized Gases,* V. Vujnovic, Ed., pp. 675-700 (Institute of Physics, University of Zagreb, Zagreb, Yugoslavia, 1974).

Key words: f-sum rule; f-values; lithium sequence; oscillator strength distribution; oscillator strengths; systematic trends.

A recent study on the oscillator strength distributions of several spectral series throughout the lithium isoelectronic sequence is described. In this work critically compiled oscillator strength data for discrete and continuum transitions have been subjected to four principal constraints: (a) to fit into systematic trends along the lithium isoelectronic sequence, (b) to fit into systematic trends within spectral series, (c) to comply with the requirement of continuity across the spectral series limit, and (d) to adhere to f-sum rules. The best available data require only minor modifications to adhere closely to all these constraints, which gives these data—for which several illustrative examples are presented—a very high degree of reliability.

Wyatt, D. M., Gray, R. C., Carver, J. C., Hercules, D. M., Masters, L. W., **Studies of polymeric bond failure on aluminum surfaces by x-ray photoelectron spectroscopy (ESCA),** *Appl. Spectrosc.* **28,** No. 5, 439-445 (Sept.-Oct. 1974).

Key words: adhesion failure; cohesive failure; polymeric bond failure; scanning electron microscopy (SEM); x-ray photoelectron spectroscopy (ESCA).

X-ray photoelectron spectroscopy (ESCA) has been used to identify very thin layers of polymeric species remaining on aluminum plates after the polymer was cured and stripped from the aluminum. Two polymers were studied. In one, the residual polymeric carbon was used as the tracing signal; in the other, the polymeric silicon was used. In both cases, the polymeric species was partially sputtered from the aluminum surface by an argon ion gun. A reduction in the polymeric signal relative to a standard signal was noted. The results of this study show that, when the polymers studied were mechanically pulled from the aluminum substrate, the failure was a cohesive separation within the polymer, rather than failure at the polymer-aluminum interface. Scanning electron microscopy was used to show that the residual polymer does not remain on the surface as "clumps" or "islands," but rather as a smooth surface a few atomic layers thick.

Yakowitz, H., **Computational schemes for quantitative x-ray analysis: On-line analysis with small computers,** Chapter X in *Practical Scanning Electron Microscopy,* J. I. Goldstein and H. Yakowitz, Eds., pp. 373-400 (Plenum Press, New York, N.Y., 1975).

Key words: empirical methods; minicomputers; on-line analysis; quantitative electron probe microanalysis; scanning electron microscopy; SRM-480.

This chapter deals with rapid means to perform data reduction for quantitative electron probe microanalysis with the aid of small computational devices (desk calculator to 8K machine). Included will be a complete discussion of a ZAF program packaged for on-line data reduction and the basis for use of the hyperbolic approximation on-line. For the laboratory which only does occasional quantitative analysis, a brief discussion is given of how to obtain an analysis with a desk calculator in a reasonable time—about two hours for a six component system or 30 minutes for a binary starting from scratch is needed. Solved examples are included.

Yakowitz, H., Goldstein, J. I., **Practical aspects of x-ray microanalysis,** Chapter XI in *Practical Scanning Electron Microscopy,* J. I. Goldstein and H. Yakowitz, Eds., pp. 401-434 (Plenum Press, New York, N.Y., 1975).

Key words: crystal spectrometers; elemental distribution; elemental identification; energy dispersive spectrometers; microanalysis; specimen preparation.

Element identification and distribution as determined by electron probe microanalytical techniques is explained. Both energy dispersive systems and curved crystal spectrometers are considered from the point of view of ease and accuracy of identification and distribution determination. A series of examples including minerals, meteorites, composite materials, superalloys and tool steel is

discussed in terms of solution of practical problems by elemental identification and distribution.

For accurate quantitative electron probe microanalysis, specimen preparation plays a crucial role. Therefore, effects of specimen preparation are evaluated in terms of surface roughness, instrumental design and nature of the specimen. The role of standards in the analysis is outlined. Finally a series of examples involving compositional analysis is presented.

Yakowitz, H., **Methods of quantitative x-ray analysis used in electron probe microanalysis and scanning electron microscopy,** Chapter IX in *Practical Scanning Electron Microscopy*, J. I. Goldstein and H. Yakowitz, Eds., pp. 327-372 (Plenum Press, New York, N.Y., 1975).

Key words: electron probe microanalysis; empirical methods; Fe-Si alloys; Monte Carlo methods; quantitative analysis; scanning electron microscopy.

Quantitative microprobe analysis is considered from the classical point of view as well as the so-called empirical approach. The relations used to convert raw data to mass fractions are discussed and scrutinized with respect to sources of error in the final analysis. Histograms depicting the typical spread of results are used to show what can be expected. By way of illustration, the complete planning and execution of the analysis of binary silicon-iron alloy is described in detail. Brief mention is made of special specimen geometrics such as thin films or fracture surfaces and means to obtain analyses from them. An extensive reference list is appended.

Yakowitz, H., **Use of divergent-beam x-ray diffraction to measure lattice expansion in LiF as a function of thermal-neutron dose up to 6×10^{16} nvt,** *J. Appl. Phys.* **43,** No. 11, 4793-4794 (Nov. 1972).

Key words: Kossel diffraction; lattice expansion; LiF; NBS reactor; radiation damage; thermal neutrons.

The lattice expansion of LiF was measured by means of the divergent-beam (Kossel) x-ray diffraction method at three levels of thermal-neutron dose, 0.45, 2, and 6×10^{16} nvt, respectively. The lattice parameter of LiF increases due to the production of Frenkel defects resulting from the $Li^6(n,\alpha)H^3$ reaction. At 6×10^{16} nvt, the lattice expansion was found to be 0.13 ± 0.02 percent which is in good agreement with previously reported values.

Yates, J. T., Jr., **Catalysis,** *Chem. Eng. News* **52,** No. 34, 19-22, 24-29 (Aug. 26, 1974).

Key words: adsorption; Auger spectroscopy; catalysis; infrared spectroscopy; kinetics; photoelectron spectroscopy.

A survey of a number of modern methods of surface science is given. The objective is to provide the reader with a general appreciation of the new advances in surface science which relate to fundamental thinking about heterogeneous catalysis.

Yates, J. T., Jr., Erickson, N. E., **X-ray photoelectron spectroscopic study of the physical adsorption of xenon and the chemisorption of oxygen on tungsten (111),** *Surface Sci.* **44,** No. 2, 489-514 (1974).

Key words: chemisorption; ESCA; oxygen; physical adsorption; tungsten; xenon.

X-ray photoelectron spectroscopy (ESCA) has been used to study the physical adsorption of Xe and the chemisorption of oxygen by W (111). An ultrahigh vacuum ESCA spectrometer has been modified such that thermal desorption behavior from the W (111) crystal can be directly compared with ESCA spectra of the adsorbed species. In addition, since the work function of a W (111) crystal covered with one monolayer of Xe is accurately known from previous work, the binding energy of the $Xe(3d_{5/2})$ adsorbate level can be accurately compared to the gaseous $Xe(3d_{5/2})$ level.

When Xe is physisorbed to 1 monolayer the Xe $(3d_{5/2})$ level exhibits a binding energy (relative to the vacuum level) which is 2.1 eV below that found for Xe (g). At lower Xe coverages the shift becomes monotonically greater, approaching 2.6 eV at a Xe coverage of 0.05. This 0.5 eV shift downward is accompanied by an increase of only 0.05 eV in adsorption energy as coverage decreases, and may be partially caused by the presence of ~ 10-20 percent of extraneous adsorption sites other than W (111) which adsorb Xe with higher adsorption energy. The adsorption energy of Xe may also be increased by coadsorption of oxygen and the Xe $(3d_{5/2})$ binding energy exhibits a corresponding shift downward as adsorbed oxygen coverage is increased to $\theta_o = 0.5$. Electronic relaxation processes affecting the final state are dominant factors in determining the magnitude of the chemical shift upon adsorption, in agreement with the predictions of Shirley. The magnitude of the relaxation effect seems to be very sensitive to small changes in Xe adsorption energy. Similar effects have been seen for chemisorption of CO.

The adsorption of O_2 at 120 K by W (111) yields a single broad O(1s) peak whose linewidth decreases with increasing coverage. The final spectra at $\theta_o = 1$ monolayer are very similar to those obtained at temperatures of 300 K or above on polycrystalline tungsten.

Yokel, F. Y., Dikkers, R. D., Fattal, S. G., **Strength of load-bearing masonry walls,** *J. Structural Div. Proc. ASCE ST5*, 948-950 (May 1973).

Key words: bricks; buckling; deflection; loads (forces); masonry; moments; slenderness ratio; stability; structural engineering; walls.

This is a closure of the American Society of Civil Engineers Proceedings Paper 8143, published in May 1971.

Yokel, F. Y., **Reply to a question on connections between bearing walls and precast floor panels,** *Civ. Engr. Engineers' inquiry box*, 60-61 (Dec. 1974).

Key words: design standards; earthquake load; masonry construction; precast concrete construction; progressive collapse; structural connection; structural design; wind load.

The design of ties between masonry bearing walls and precast concrete floor panels is discussed.

Yokel, F. Y., **Reply to question on the design of unreinforced masonry load-bearing walls,** *Civ. Engr. Engineers' inquiry box*, p. 79 (Nov. 1973).

Key words: codes; masonry; standards; structural design.

Provisions of present U.S. Code and Design Standards are clarified and interpreted in response to a question by a reader of *Civil Engineering* magazine.

Yokel, F. Y., **Stability and load capacity of members with no tensile strength,** *J. Structural Div. Proc. ASCE ST4*, 788-789 (Apr. 1973).

Key words: buckling; compression members; concrete; cracking; deflection; eccentricity; equilibrium; loads (forces); masonry; stability; stress distribution; structural engineering.

This is a closure of the discussion of ASCE Proceedings Paper 8253 by Felix Y. Yokel.

Yokel, F. Y., **The Operation Breakthrough evaluation, an experience in the application of performance criteria,** *Industrialization Forum* **6,** No. 1, 27-33 (1975).

Key words: building codes; building standards; housing; performance criteria.

The testing and evaluation of Operation Breakthrough housing

systems relied heavily on a special set of performance criteria developed especially for the program. Valuable experience was gained in this application of performance criteria.

The Breakthrough program is assessed with respect to how effectively the criteria were formulated, the level of guidance and information provided, whether all the criteria were used and implemented, and the problems and difficulties encountered. The experience indicates that performance criteria should not be used as a substitute for specific standards and should be reserved for guiding and evaluating innovative schemes. Performance criteria are rarely simple and can be successfully implemented only in situations where compliance can be objectively measured. Particular difficulties arise in the assessment of durability. Performance criteria can provide valuable guidance in areas outside the domain properly regulated by codes and standards. Inflexible application in such areas, however, could inhibit the evolution of new concepts.

Yonemura, G. T., **An image quality criterion for the identification of faces,** *Photogr. Sci. Eng.* **19,** No. 4, 223-227 (July-Aug. 1975).

Key words: acutance; identification (faces); image quality; Modulation Transfer Functions.

The performance required of imaging devices should be based on the needs of the user. In analyzing these needs, three psychophysical levels of visual task performance must be considered; detection, recognition, and identification. The experimental data base for these levels of performance is very uneven. Many detection studies have been performed, fewer have addressed problems of recognition, and rarer still are investigations associated with identification. This study determined experimentally the observer's perception of the image quality required for the identification of faces, as determined by two criteria: (1) the average observer and (2) 90 percent of the population. The subjective response from the human observer was then transformed into a physical descriptor amenable to direct measurement by instruments. The Modulation Transfer Function is recommended as the physical correlate for subjective facial identification.

Young, J. P., **Codeposition of particulate matter with chromium,** *Plat. Surf. Finish. Tech. Brief* **62,** No. 4, 348-34 Apr. 1975).

Key words: cermet; chromium plating; codeposition, composite coating; dispersion plating; electroplating; hard particles; wear-resistance; wear-tests.

Particles were included in a chromium deposit with the addition of a monovalent cation, e.g., thallium nitrate, in a small amount to the sulfate chromic acid bath. Using these additives, hard particles, lubricating particles, and metal powders were incorporated in a chromium matrix on vertical surfaces. When even less than 1 wt % of hard particles such as diamond, boron carbide or silicon carbide were codeposited with the chromium, resistance to wear was increased up to threefold over that of a hard, bright chromium deposit as measured by an abraser type wear-testing device.

Young, R. D., **National Measurement System micro study,** *Natl. Conf. Stand. Lab. (NCSL) Newsletter* **13,** No. 2, 20-21 (Aug. 1973).

Key words: calibration; economic dimensions; National Measurement System: surface finish; surface roughness.

A brief description of the National Measurement System for Surface Finish is given together with a descriptive block diagram. The economic dimensions of the measurement system are discussed briefly. A biographical sketch of the author is included.

Young, R. D., Teague, E. C., **The measurement and characterization of surface finish,** Chapter 2 in *Properties of Electrodeposits Their Measurement and Significance,* R. Sard, H. Leidheiser, and F. Ogburn, Eds., pp. 22-49 (Electrochemical Society, Princeton, N.J., 1975).

Key words: characterization; instruments; measurement, statistical surface parameters; surface finish; surface parameters.

The surface microtopography of an electrodeposit is determined by a variety of parameters, particularly the physical and chemical character of the initial substrate. Modern instrumentation for quantitative measurement of substrate and electrodeposit surface microtopography are reviewed. Statistical parameters associated with measured surface profiles which permit concise geometrical characterization of height distributions, periodicities along the surface, etc., are defined and discussed. Illustrative examples based on measurements of electrodeposited surfaces are reported together with appropriate characterizing parameters.

Zahn, J. P., **The dynamical tide in close binaries,** *Astron. Astrophys.* **41,** No. 314, 329-344 (July 1975).

Key words: binary; gravity modes; nonadiabatic; oscillations; resonances; stellar.

The nonadiabatic oscillations of a star, driven by an outer rotating gravitational field, have been studied by the use of matched asymptotic expansions. The interior and envelope solutions in this procedure are derived in Sections 2 and 3. The results apply to stars which have a convective core and a radiative envelope, and they are discussed in Section 4.

We find that the resonances of the free gravity modes are damped by radiative dissipation, which operates in a relatively thin region below the surface of the star. Due to that dissipation, some properties of the dynamical tide have observable consequences in close binary systems: i) A torque is applied to a binary component; this serves to make it corotate with its companion in a time which can be short compared to its nuclear life. ii) Before that synchronization is achieved, the brightness distribution over the surface of the star is in general phase shifted relative to the external driving potential.

U. S. GOVERNMENT PRINTING OFFICE : 1976 O - 597-633

NBS TECHNICAL PUBLICATIONS

PERIODICALS

JOURNAL OF RESEARCH reports National Bureau of Standards research and development in physics, mathematics, and chemistry. It is published in two sections, available separately:

• Physics and Chemistry (Section A)

Papers of interest primarily to scientists working in these fields. This section covers a broad range of physical and chemical research, with major emphasis on standards of physical measurement, fundamental constants, and properties of matter. Issued six times a year. Annual subscription: Domestic, $17.00; Foreign, $21.25.

• Mathematical Sciences (Section B)

Studies and compilations designed mainly for the mathematician and theoretical physicist. Topics in mathematical statistics, theory of experiment design, numerical analysis, theoretical physics and chemistry, logical design and programming of computers and computer systems. Short numerical tables. Issued quarterly. Annual subscription: Domestic, $9.00; Foreign, $11.25.

DIMENSIONS/NBS (formerly Technical News Bulletin)—This monthly magazine is published to inform scientists, engineers, businessmen, industry, teachers, students, and consumers of the latest advances in science and technology, with primary emphasis on the work at NBS. The magazine highlights and reviews such issues as energy research, fire protection, building technology, metric conversion, pollution abatement, health and safety, and consumer product performance. In addition, it reports the results of Bureau programs in measurement standards and techniques, properties of matter and materials, engineering standards and services, instrumentation, and automatic data processing.

Annual subscription: Domestic, $9.45; Foreign, $11.85.

NONPERIODICALS

Monographs—Major contributions to the technical literature on various subjects related to the Bureau's scientific and technical activities.

Handbooks—Recommended codes of engineering and industrial practice (including safety codes) developed in cooperation with interested industries, professional organizations, and regulatory bodies.

Special Publications—Include proceedings of conferences sponsored by NBS, NBS annual reports, and other special publications appropriate to this grouping such as wall charts, pocket cards, and bibliographies.

Applied Mathematics Series—Mathematical tables, manuals, and studies of special interest to physicists, engineers, chemists, biologists, mathematicians, computer programmers, and others engaged in scientific and technical work.

National Standard Reference Data Series—Provides quantitative data on the physical and chemical properties of materials, compiled from the world's literature and critically evaluated. Developed under a world-wide program coordinated by NBS. Program under authority of National Standard Data Act (Public Law 90-396).

NOTE: At present the principal publication outlet for these data is the Journal of Physical and Chemical Reference Data (JPCRD) published quarterly for NBS by the American Chemical Society (ACS) and the American Institute of Physics (AIP). Subscriptions, reprints, and supplements available from ACS, 1155 Sixteenth St. N. W., Wash. D. C. 20056.

Building Science Series—Disseminates technical information developed at the Bureau on building materials, components, systems, and whole structures. The series presents research results, test methods, and performance criteria related to the structural and environmental functions and the durability and safety characteristics of building elements and systems.

Technical Notes—Studies or reports which are complete in themselves but restrictive in their treatment of a subject. Analogous to monographs but not so comprehensive in scope or definitive in treatment of the subject area. Often serve as a vehicle for final reports of work performed at NBS under the sponsorship of other government agencies.

Voluntary Product Standards—Developed under procedures published by the Department of Commerce in Part 10, Title 15, of the Code of Federal Regulations. The purpose of the standards is to establish nationally recognized requirements for products, and to provide all concerned interests with a basis for common understanding of the characteristics of the products. NBS administers this program as a supplement to the activities of the private sector standardizing organizations.

Federal Information Processing Standards Publications (FIPS PUBS)—Publications in this series collectively constitute the Federal Information Processing Standards Register. Register serves as the official source of information in the Federal Government regarding standards issued by NBS pursuant to the Federal Property and Administrative Services Act of 1949 as amended, Public Law 89-306 (79 Stat. 1127), and as implemented by Executive Order 11717 (38 FR 12315, dated May 11, 1973) and Part 6 of Title 15 CFR (Code of Federal Regulations).

Consumer Information Series—Practical information, based on NBS research and experience, covering areas of interest to the consumer. Easily understandable language and illustrations provide useful background knowledge for shopping in today's technological marketplace.

NBS Interagency Reports (NBSIR)—A special series of interim or final reports on work performed by NBS for outside sponsors (both government and non-government). In general, initial distribution is handled by the sponsor; public distribution is by the National Technical Information Service (Springfield, Va. 22161) in paper copy or microfiche form.

Order NBS publications (except NBSIR's and Bibliographic Subscription Services) from: Superintendent of Documents, Government Printing Office, Washington, D.C. 20402.

BIBLIOGRAPHIC SUBSCRIPTION SERVICES

The following current-awareness and literature-survey bibliographies are issued periodically by the Bureau:

Cryogenic Data Center Current Awareness Service

A literature survey issued biweekly. Annual subscription: Domestic, $20.00; foreign, $25.00.

Liquefied Natural Gas. A literature survey issued quarterly. Annual subscription: $20.00.

Superconducting Devices and Materials. A literature survey issued quarterly. Annual subscription: $20.00. Send subscription orders and remittances for the preceding bibliographic services to National Bureau of Standards, Cryogenic Data Center (275.02) Boulder, Colorado 80302.

Electromagnetic Metrology Current Awareness Service Issued monthly. Annual subscription: $24.00. Send subscription order and remittance to Electromagnetics Division, National Bureau of Standards, Boulder, Colo. 80302.

U.S. DEPARTMENT OF COMMERCE
National Bureau of Standards
Washington, D.C. 20234

OFFICIAL BUSINESS
Penalty for Private Use, $300

POSTAGE AND FEES PAID
U.S. DEPARTMENT OF COMMERCE
COM–215

SPECIAL FOURTH-CLASS RATE
BOOK

[illegible]

JOURNAL OF RE
A. Physics and C

Vol. 80A, No. 6 Jan.–Feb. 1976

Contents

Page

Line strengths and lifetimes of levels in neutral uranium. C. H. Corliss. 1

Optical properties of nuclear matter. J. S. O'Connell. 9

A study of the polarization of fluorescence of ordered systems with application to ordered liquid crystals. E. D. Cehelnik, K. D. Mielenz, and R. B. Cundall. 15

PVT and vapor pressure measurements on ethane. G. C. Straty and R. Tsumura. 35

Functional equations for the enhancement factors for CO_2-free moist air. Lewis Greenspan. 41

Experimental values for the elastic constants of a particulate-filled glassy polymer. Jack C. Smith. 45

Heat capacities of polyethylene IV. High molecular weight linear polyethylene. Shu-Sing Chang. 51

Computer simulation of metastable fluid states in the Lennard-Jones system. Harold J. Raveché and W. B. Streett. 59

Relative enthalpy of solid beryllium aluminate (chrysoberyl), $BeO{\cdot}Al_2O_3$, from 1175 to 2025 K, and of liquid beryllium aluminate from 2170 to 2350 K. S. Ishihara and E. D_t West. 65

Publications of the National Bureau of Standards. 75

Library of Congress Catalog Card Number: 62–37059

For sale by the Superintendent of Documents, U.S. Government Printing Office, Washington, D.C. 20402. (Order by SD Catalog No. C 13.22/sec.A:80/1). Single copy price varies. Subscription price: $17.00 a year; $4.25 additional for foreign mailing.

UNITED STATES GOVERNMENT PRINTING OFFICE, WASHINGTON : 1976